Università Degli Studi Di Milano-Bicocca
Facoltà di Scienze Matematiche, Fisiche e Naturali
Doctorate in Materials Science

Artificial Photosynthesis:

Molecular Approaches for Photocatalytic Hydrogen Production

Ph.D. thesis of:

Bianca Cecconi

Supervisor:

Prof. Alessandro Abbotto

Dean of the Doctorate:

Prof. Gianpaolo Brivio

9 February 2016

XXVIII Cycle

TABLE OF CONTENTS

ABSTRACT

The humankind today needs to face an epochal transition from a fossil fuel to a renewable source-based economy. Renewable sources are our chance to build a clean world with unlimited and widespread energy. Nowadays renewable energies could be properly harvested to produce electricity, while the development of a future clean fuel is less advanced. Since our energetic consumption is made essentially of fuels we need to build devices to transform renewable energy, such as solar radiation, into chemical energy of bonds. A promising future fuel is hydrogen since its carbon footprint is zero and it can be obtained from an abundant source such as water. Nature, through the photosynthesis, could inspire us to build our feed in the form of fuels. In this research project DSSC (dye-sensitized solar cells) have been modified to produce chemical energy instead of electricity. Attention has been focused on hydrogen production semi-reaction, thus the use of a sacrificial electron donor has been adopted. Such system is composed of TiO_2 nanoparticles covered by a reduction catalyst and a metal-free organic sensitizer to harvest the visible spectrum of solar radiation.

The aim of this research has been the development of molecular approaches to provide efficient light harvesting systems and reduction catalysts. Molecular design allowed a fine tuning of materials properties and a deep understanding of structure/performances relationships.

The first part of the project has focused on designing push-pull structures to harvest visible light portion of solar spectrum. Fine molecular tuning of metal-free dyes afforded enhanced performances depending on the kind of modification. We modified a known phenothiazine dye in the donor, spacer and acceptor units in order to derive structure/performances relationships. Enhanced light harvesting properties and photo-stability have been afforded through π-spacer modification with various mono- and polycyclic simple and fused thiophene derivatives, while decoration of the donor core with glycolic or sugar chains gave better hydrophilicity and surface wettability. Lastly, hydroxamic acids have been introduced as alternative anchoring groups to give stronger ester bonds on TiO_2 surface and prevent hydrolysis in aqueous media.

The second part of the research has concerned the study of cobaloximes as alternative noble metal free reduction catalysts. Starting from a mini-library of

cobaloximes bearing various equatorial bridges, axial ligands, and starting oxidation numbers, molecular structure/efficiency studies have been done, while UV/Vis spectroscopy has been used to investigate the nature of the eventual Co(I) species transiently formed. For cobaloximes a Co(I) species is hypothesized but not confirmed in photocatalytic experiments and optimization of efficiency and stability of new catalysts needs a deep understanding of the catalytic cycle in order to intervene in the critical intermediates.

LIST OF PAPERS

This thesis has been based on the following papers:

- ⇨ Norberto Manfredi, Bianca Cecconi, Alessandro Abbotto*
  "**Multi-Branched Multi-Anchoring Metal-Free Dyes for Dye-Sensitized Solar Cells**"
  Microreview for Eur. J. Org. Chem., **2014**, 7069.

- ⇨ Grigory Smolentsev,* Bianca Cecconi, Alexander Guda, Murielle Chavarot-Kerlidou, Jeroen A. van Bokhoven, Maarten Nachtegaal, Vincent Artero
  "**Microsecond X-ray Absorption Spectroscopy to Identify Co(I) Intermediates of Cobaloxime-Catalized H_2 Evolution**"
  Chem. Eur. J., **2015**, *21*, 15158.

- ⇨ Bianca Cecconi, Norberto Manfredi, Riccardo Ruffo, Tiziano Montini, Ismael Romero Ocaña, Paolo Fornasiero,* Alessandro Abbotto*
  "**Tuning Thiophene-Based Phenothiazines for Stable Photocatalytic H_2 Production**"
  ChemSusChem, **2015**, *8*, 4216.

- ⇨ Norberto Manfredi, Bianca Cecconi, Valentina Calabrese, Alberto Minotti, Francesco Peri, Riccardo Ruffo, Matteo Monai, Ismael Romero-Ocaña, Tiziano Montini, Paolo Fornasiero,* Alessandro Abbotto*
  "**Dye-Sensitized Photocatalytic Hydrogen Production: Enhanced Activity in a Glucose Derivative of a Phenothiazine Dye**"
  In preparation for Chem. Commun.

- ⇨ Bianca Cecconi, Norberto Manfredi, Tiziano Montini, Paolo Fornasiero, Alessandro Abbotto*
  "**Dye-Sensitized Solar Hydrogen Production: the Emerging Role of Metal-Free Organic Sensitizers**"
  Microreview in preparation for Eur. J. Org. Chem.

Chapter 1

ENERGETIC ISSUE AND ARTIFICIAL PHOTOSYNTHESIS

Introduction and brief overview of Natural Photosynthesis

You'll be happy and wholesome again

when the city clears and the sun ascends

Winter Winds

Mumford and Sons

1.1 ENERGETIC ISSUE

Fossil fuels played a fundamental role from the industrial revolution till nowadays to ensure high quality life, especially in rich countries. Despite of the beneficial effects of this epoch, drawbacks of the fossil fuels exploitation have begun to arise in the last years. The main limitations of fossil fuels are the non-renewability, the uneven geographical dislocation of the sources that has been the reason of many disparities of the modern times, and the environmental pollution arising from their exploitation.[1]

Many scientists agree in believing that the non-renewable epoch is coming to the end and that humanity has to deal with an energetic transition from a fossil fuel to a renewable sources based economy. Renewable energies are able to solve at least the problem of durability, since no "peak" is envisaged for those sources. The geographical distribution of renewable energies is more fair than fossil fuels and even in geographical regions where one source is lacking, another one is generally exploitable. In principle the environmental pollution problem could be solved with the use of renewable energies since carbon dioxide emissions of those sources is zero. It should be taken into account the energy cost and pollution for production of devices as well as; used materials that could be rare, expensive or toxic, and cause other problems maybe not forecast at the moment. Amongst all the renewable sources, solar energy plays the prominent role since it is the only source that alone is able to answer to the energy demand of the whole Earth (Figure 1.1). That does not mean that all the other sources will be embedded by solar energy and are destined to disappear. The future society should be differentiated in energy forms and every geographical region should be as independent as possible to limit human disparities that are at the basis of wars and the current migratory fluxes.[2]

Renewability is defined as the possibility of an energy source to be unlimited in quantity in time or not, typical non-renewable sources are oil, coal, and natural gas, while renewable sources are solar energy, wind, hydroelectric, geothermic, and other more limited sources. Nuclear energy is considered in the middle between the two categories not having the peculiar features of fossil fuels but it has many issues due to non-endlessness of the fissile material and high toxicity of radioactive wastes, giving many problems associated with their manipulation. Nuclear fusion could solve almost all the problems correlated to energy supply, but nowadays no forecast can be done since a breakthrough is necessary and it could be possible that no contribution will be given by that technology.

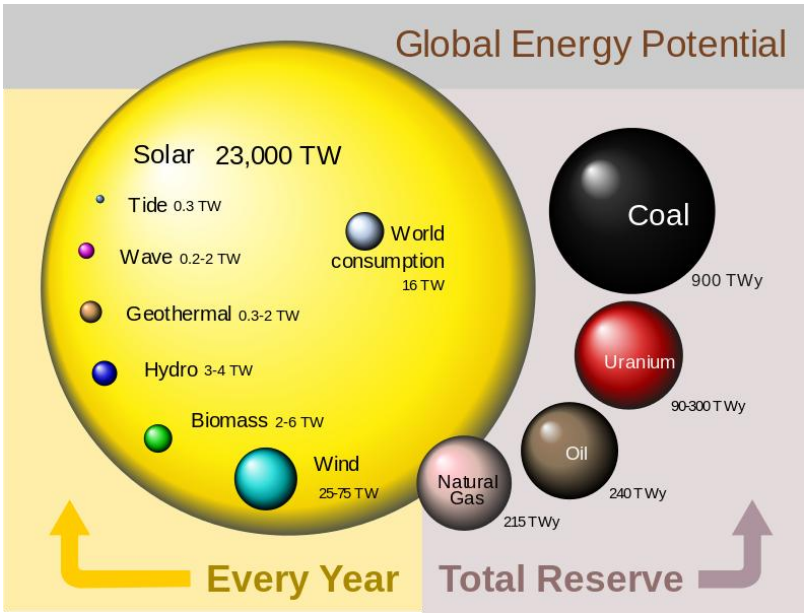

Figure 1.1: Global energy potential.[3]

An important problem of modern society is disparity, even in energetic terms, between developed and developing countries. Impressive analyses can be obtained calculating the amount of toe (tons of oil equivalent) per capita per year in various countries. Canada is the leader with 9.4 toe per capita per year, followed by Saudi Arabia and USA (7.8 and 7.2 toe respectively). When these data are compared with some values as 0.05 toe per year per capita in Ethiopia, disparities are evident. Remarkable matching between energy consumption and life quality can be obtained, meaning that there is a net improvement of some human development indexes (such as infant mortality) with the increase of energy consumption till a threshold, while a further increase is then detrimental. This threshold is quite high and it is 2.8 toe per year per capita that is the value for Italy and not so lower than the EU mean value (3.2 toe). Even though many developed countries should lower energy consumption, the contribution of poor countries reaching such a value corresponds to twice the amount of energy used nowadays. This concept clearly explains why the reduction of energy levels in developed countries is not enough to solve the energetic issue. All the developing countries deserve to reach acceptable quality of life and their growth will be much higher in energetic terms than the eventual decrease of the over-energetic countries. The shift to a renewable energy society is thus necessary, and it is not only an ethical choice as some politicians and economists are affirming.[4]

Unlike common sense, renewable energies are gaining in importance and could not be considered of irrelevant contribution especially in the electric energy supply. If attention is given to the global supply of commercially traded primary energy from BP analysis, the total energy supplied by fossil fuels covered the 87%, while renewable energies are responsible for almost 10% that is a remarkable percentage.[5] Such energy supplies are graphically represented in Figure 1.2.

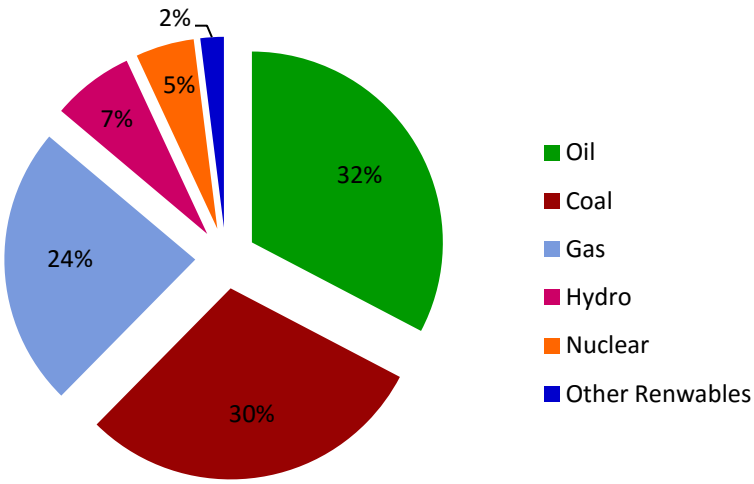

Figure 1.2: Global supply of commercially traded primary energy, from REF.5.

This increment has been largely helped by government aid in different taxation of renewable energies through incentives. It should be noted that if "externalities"[a] are considered in the evaluation of the cost of an energy source, renewable supply is already competitive in the market without subsidies. Amongst the renewable sources hydroelectric is one of the most used nowadays but the most promising one in terms of energy power is solar energy. As it can be easily seen from Figure 1.1 solar energy is by far the most abundant source and it is fairly distributed on Earth surface.

For example in 2014 Italy produced 7.9% of its annual electricity need through photovoltaics being at the first place in Europe followed by Greece and Germany that

[a] "Externalities" include all the measurements needed to solve problems connected to the energy source. For example all the medical expense are not directly considered in the price of energy but should be included especially in the case in which the government pays for medical treatments.

covered 7.6 and 7.0% respectively.[6] Italy, Germany and Spain reached the grid parity for electricity produced through photovoltaics in 2013 and opened the road to many other countries that are now reaching such a goal. A last comment about general features of renewable energies regards the possibility of offering many new job places thanks to their development. 1.2 million of new jobs in EU have been created thanks to renewable energies market, in striking contrast with the trend of job market after the economical crisis.[7]

Photovoltaics has the advantage of a shift from a GW to a TW scale both on-grid and off-grid and this is the reason why, even though many other renewable energies are more appealing nowadays in terms of efficiency and stability, PV is necessarily the choice of the future. Photovoltaic technology was born in 1950 in Bell Laboratories with silicon based devices and is still the current technology used in almost all the commercially available solar cells. The working principle is based on light-induced charge separation at p-n junctions of two slices of semiconductor materials, such as silicon, doped in a different way. There is a second generation of photovoltaic devices that is the field of thin films that have the aim of reducing the amount of active material to prevent energy losses and reduce manufacturing costs. Such devices are now on the market but silicon supremacy is still far from being replaced by other technologies. Advantages and disadvantages of first and second generations cells have been largely revised.[8,9,10,11]

A third generation of solar cells have been proposed, based on a different mechanism from the photovoltaic effect in semiconductors and partially inspired by the working mechanism of natural photosynthesis. These devices are based on organic or organometallic molecules and, after a first promising trend in development, they are still almost at the laboratory level and they are not expected to replace silicon market. Thanks to some advantages over the first generation devices, such as good performances in non-standard conditions of diffused and low intensity light, and lower requirements in terms of quality and quantity of raw materials, they will probably complement the current technology in building integration and in applications in which the performances of silicon PV are not satisfactory. The main drawback of those devices is the limited efficiency and lower stability compared to the silicon based one. Dye-Sensitized Solar Cells (DSSC) and Organic Photovoltaics (OPV) are the main examples of technologies belonging to this class, certified efficiencies for DSSC are 11.9 ± 0.4% (1 cm^2 cell) and 8.8 ± 0.3% at the submodule scale (400 cm^2), while for OPV the actual certified efficiency is 11.0 ± 0.3%

(1 cm^2 cell) and 9.7 ± 0.3% at the minimodule scale (26 cm^2).[12] A third class of devices is gaining interest and it is the one of Perovskite Solar Sells (PSC) that was first reported in 2009[13] as a modification of a liquid DSSC structure where the sensitizer was replaced with a lead perovskite crystal. Further improvements by the groups of Snaith[14] and Grätzel[15] transformed the structure of the cells getting a solid state device that has been able to reach 21.02% as certified efficiency.[16] A deeper analysis of DSSC working principles and components will be given in paragraph 2.1 since these devices have been the starting point to generate the hydrogen evolving system studied in this thesis. Finally it has to be stressed that the less promising properties of some of the third generation PV should not be translated in setting aside those technologies, since we need to have a diversified energy portfolio, thus complementary technologies should be preferred to the supremacy of only one.

There are many limitations in the use of renewable energies, but one of the most important is that all the renewable sources are able to produce electricity but not fuels. This will be a great limitation in the future because, even if the society evolves to a more "electrified" one, there are some needs that are necessarily depending on fuels. If Figure 1.3 is analyzed, it can be seen that nowadays consumes are made of electricity for only the 18% of the total energy consumption, while more than the 60% of the overall consumption is in the form of a fuel.[17]

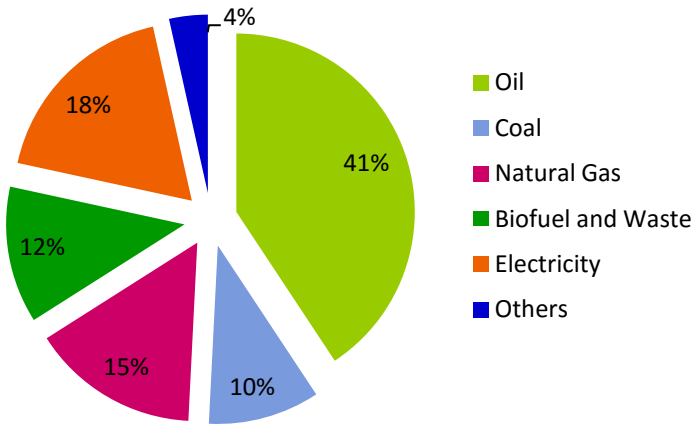

Figure 1.3: World energy consumption from REF. 17.

That issue opens to the need of a future fuel that should be clean when burnt, easy to store, safe, non-toxic, and that has many other desirable features. Amongst all the candidates, hydrogen is considered a promising choice since it produces water when

it is burnt, thus its carbon footprint is zero, and it can be obtained from water that is largely abundant. Unfortunately hydrogen mines are not present on Earth; thus it must be obtained from other sources, such as water, through molecular splitting. Such a reaction is thermodynamically and kinetically disfavored and renewable energies could be used to overcome such a limit (Figure 1.4). Energetically water splitting requires a free energy ΔG° of 237 kJ mol^{-1} or 2.46 eV per mol of hydrogen produced.

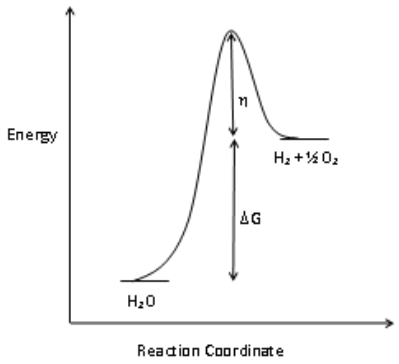

Figure 1.4: Energetic profile for water splitting.

Hydrogen is not a primary form of energy as oil, coal, or natural gas since it has to be "manufactured" starting from another form of energy. For that reason hydrogen is considered a secondary form or vector of energy and could be intended as a way to store electricity alternative to batteries. Hydrogen has not only advantages but a lot of limitations that are strongly containing its diffusion and the construction of a hydrogen-based economy. Scientific technologies to produce hydrogen are still at the laboratory scale and are considered uneconomical right now, moreover there are problems related to the storage and transportation of such a gas that is not an easy task as for natural gas. The risks of leakages are high and eventual losses could be really dangerous. Moreover, even if hydrogen has the highest energy density by weight (33.3 kWh kg^{-1} compared to gasoline with 12.4 kWh kg^{-1}, and to 13.9 kWh kg^{-1} of liquefied natural gas), it has a much lower energy density by volume (2.5 kWh L^{-1} compared to 8.07 kWh L^{-1} of gasoline and 10.9 kWh L^{-1} of diesel) meaning that tanks containing hydrogen would be very big causing stocking problems, e.g. in vehicles. In addition, for safety reasons the hydrogen tanks should be cylindrical and could not have the more convenient shape depending on the vehicle. Discussion about detailed advantages and disadvantages of hydrogen storage and transportation is beyond the

scope of this introduction and of this thesis, thus a review is referred for a deeper analysis.[18]

Concerning the way to produce hydrogen from water splitting, the main difficulties arise from the necessity of coupling one-photon reactions to multi-electrons processes, thus a deep research on catalysts for reduction and oxidation is at the basis of the success of water splitting. There are two approaches: not integrated systems such as PV coupled with electrolyzer (Figure 1.5), and integrated systems that comprehend photocatalytic technologies (PC) and photoelectrochemical cells (PEC), including dye-sensitized photoelectrochemical cells (DSPEC). The last class of technologies (integrated systems) is at a laboratory scale and at the beginning of the investigation, while PV and electrolizers are more mature technologies, thus an evaluation of costs can be done. Hydrogen is now produced from natural gas reforming that is the cheapest way, while electrolysis is chosen only if high purity hydrogen is needed. The actual cost of hydrogen from methane reforming is 1 € kg^{-1}, while in the case of electrolysis is 2.6 € kg^{-1}.[19] Even though the difference does not seem high it should be considered that PV and electrolizers are already at good working efficiencies and moreover 2.4 of the 2.6 € kg^{-1} are the electricity costs, thus the only effect in lowering the price will be given by an unlikely much lower price of electricity from renewable energies. Of course an alternative possibility could be an increment of the price of natural gas, but nowadays no hypothesis could be done in this direction.

Figure 1.5: DSSC submodule coupled with electrodes to perform water electrolysis.

For that reason PEC, dye-sensitized PEC (DSPEC), and photocatalysis are considered promising since energy from the solar radiation is directly converted in chemical energy of bonds skipping the electricity production step, thus in principle they are more promising techniques. These devices are composed of a material, or a multi-material, that is able to absorb light, separate and transport charges, and run oxidation and reduction catalysis. Materials that are suitable for all these requirements are hard to find, thus multi-materials are investigated, especially the ones where the catalytic role and light harvesting are played by different components. The efficiency record for a PEC device is 16% (η_{STH}).[20] The main limitation of these systems is the difficulty to find the suitable material able to light harvest and to well separate and transport charges, thus the idea of introducing a sensitizer that is responsible for light absorption only has been done in DSPEC. A deeper detailed analysis on the photocatalytic systems will be given in paragraphs 2.2 and 2.3, since development of dyes for TiO_2 semiconductor nanoparticles catalyst has been the aim of this research. A cost evaluation for integrated devices is currently unavailable since these techniques are still at the early stages but scientists agree in thinking that these solutions could be the most cost-effective ones over a long period.[4]

The following paragraph is a brief description of the basic principles of natural photosynthesis and some parallelisms are made with artificial systems in order to highlight the fundamental features that scientists need to mimic to create artificial devices. Compared to natural photosynthesis the artificial one should not be too complicated since there is no need to keep an organism alive and this could be reflected in higher performances since photosynthesis has a quite low efficiency in biomass generation (around 0.1 – 1%).[21]

This thesis is organized in Chapter 2 where an overview on DSSC technology and the transformation of such devices into photocatalytic systems to run the hydrogen reduction half reaction will be given. Special attention will be done to light harvesting systems known in the literature and their design principles, since in Chapter 3 the research projects about developed organic dyes will be explained, with detailed information about the synthetic plans and the characterization strategies. Finally the role of reduction catalyst is explained in Chapter 4, where cobaloximes as proton reduction catalysts are illustrated together with the experiments run at the CEA in Grenoble to try to isolate and characterize the Co(I) species that is hypothesized as a key catalytic intermediate of the cycle.

1.2 LEARNING FROM NATURE: BASIC WORKING PRINCIPLES OF PHOTOSYNTHESIS

Nature is a great source of inspiration for the mankind and scientific world, thus mimicking nature could give us a help in finding solutions to solve the energetic problem. Many bacteria and all the green plants actually transform solar radiation in the chemical energy of their feeding every day. It is straightforward to try to mimic a process that already exists and that has been improved over thousands of years of evolution. Moreover, it is definitively "simpler" to try to reproduce and modify a method that is on Earth from thousands of years than starting from scratching something more similar to science fiction than reality. At the same time I would like to point out many doubts advanced by researchers in the path of trying to mimic nature. Natural photosynthesis is a highly complex system that works in restricted conditions and has an overall efficiency below 1% (apart from rare exceptions) in energy conversion.[21] Such a percentage is too low to try to feed energetic demand of the world, thus nature should be a source of inspiration for the working mechanism and the hints proposed to solve problems, but we need to keep in mind that our purpose is to develop a highly simple system with a high efficiency. A meticulous reproduction of nature is not our goal since the natural molecular assembly requires multiple and complex synthetic pathways that are not viable on large scale. Moreover, joining the knowledge of scientists expert in different fields of science (biology, chemistry, physics, engineering et cetera) could give the basis to build a modular system in which each component has a role and is the best performing one. In that way the integration of all the optimized components opens the pathway to future solutions to the energetic problem. Beside the advice of "*keep it simple*" it is deeply true that we have to learn many tricks and solutions from nature and to develop our artificial photosynthetic systems we need to know in details all the secrets of nature.[22] The basic principle that drives all the photosynthetic transformations in nature is the photo-induced electron transfer, which is able to produce a charge separation state.[23] The potential energy of this state could then be used to build high-energy molecules that are the feeding for the living organisms.

Indeed, even sweeping from different organisms, the main strategy for photosynthesis is the same, i.e. solar radiation is absorbed by antenna systems, energy is then transferred to reaction centre proteins where the charge separation occurs and the reduction or oxidation equivalents are used to drive chemical reactions.[24] Antenna systems have been largely differentiated during evolution so there are thousands of examples where adaptation of the organism to peculiar

environmental conditions pushed the development for *ad hoc* pigments composition. The light intensity and the spectral photons distribution strongly depend on the environment, thus various pigments are present in different composition in photosynthetic cells. As illustrated in Figure 1.6 every pigment has a different range of absorption, thus "calibration" of their concentration depends on the external environment. For example sea algae are rich in β-carotenoids because blue-green light is the most intense portion of the spectrum in seabed.

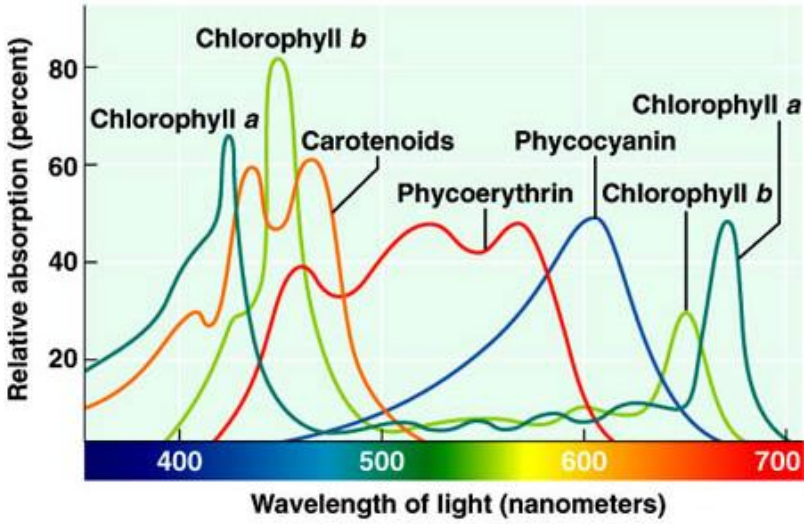

Pigment	Chlorophyll A	Chlorophyll B	β-carotene	Phycoerythrin	phycocyanin
λ_{max} (nm)	430, 680	463, 660	450	550	620

Figure 1.6: Absorption spectra of chlorophylls and other accessory pigments and respective absorption maxima.

A brief overview on bacterial and green plants photosynthesis will be now given, reminding that the second one is an evolution of the first and simplest one, thus the basic principles of photo-induced electron transfer are the same.

Photosynthesis in Bacteria

We need to start from the observation of how the photosynthetic system is made in nature and X-rays crystallography is a useful tool for this purpose. The scientific world started from the interpretation of the simplest living systems that are bacteria, before facing complex structures such as green plant cellules. The first antenna

system studied is the one from the purple bacteria *Rhodopseudomonas acidophila*[25] and it is composed of light harvesting complexes (LH) where bacteriochlorophylls are disposed in a precise manner to have the best and complementary light absorption properties. Moreover the presence of solvent molecules and the different chemical environment that is around each LH cluster is responsible for slightly dissimilar visible range coverage, bringing to a total large absorption spectrum of the solar emission. All the light harvesting complexes are connected together and the energy migration amongst the units is quite fast (~300 fs).[26] Figure 1.7 represents how the energy collected from the LH2 antenna is then transferred directionally to LH1 antenna (~3 ps) that surrounds the reaction centre (RC). The reaction centre is responsible for charge separation and the energy transfer from LH1 and RC is much longer than the previous ones (~35 ps). X-rays crystallographic analysis gave high resolution images of LH2, while for LH1 the quality of the information is lower, in any case it is a bigger complex than LH2 and it is probably very similar to LH2 as structure.[27] This is the first teaching coming from nature: the building of well-working antenna systems needs ultrafast energy transfers amongst almost iso-energetic subunits of a single complex, followed by fast energy transfer to a lower energy complex with minimal losses. An energetic gradient is what we need to have directionality in the energy transfer.

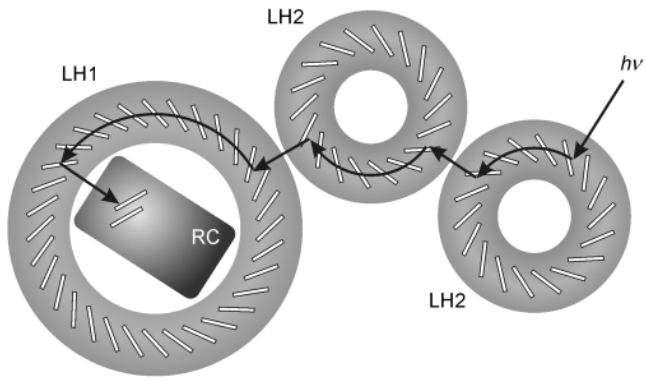

Figure 1.7: Schematic representation of the antenna system in a photosynthetic bacteria, from Ref.23.

Such a detailed description for photosynthetic systems in green plants is not known nowadays, but it is likely that the basic structure is the same as the one just described.[28,29,30,31]

The reaction centre structure is known in details for many bacteria, in all the cases it is a protein fixed in a lipid bilayer membrane. The structure of the reaction centre is

not simple and many molecules actively participate and are necessary for generating the charge separation state.[32,33] The most important components are a bacteriochlorophyll "special pair" (P), a bacteriochlorophyll monomer (BC), a bacteriopheophytin (BP), a quinone (Q_A), and a four-heme c-type cytochrome (Cyt). The geometric disposition of these molecules is schematically represented in Figure 1.8-left, while the energy transfer path is illustrated in Figure 1.8-right. As it can be easily seen from the picture, the final result of this electron transfer is the spatial separation of charges, with the positive charge situated on the cytochrome and the negative charge on the quinone. Those two components, apart from being spatially separated by 50 Å, are located on opposite sides of the lipid membrane, making back charge-recombination really slow.[34] If the driving force of this energy transfer was several eV smaller, the quantum efficiency of the whole system would have been lower, suffering from strong recombination. On the contrary if the driving force for the charge separation was increased, the efficiency of the whole reaction would have been lower.

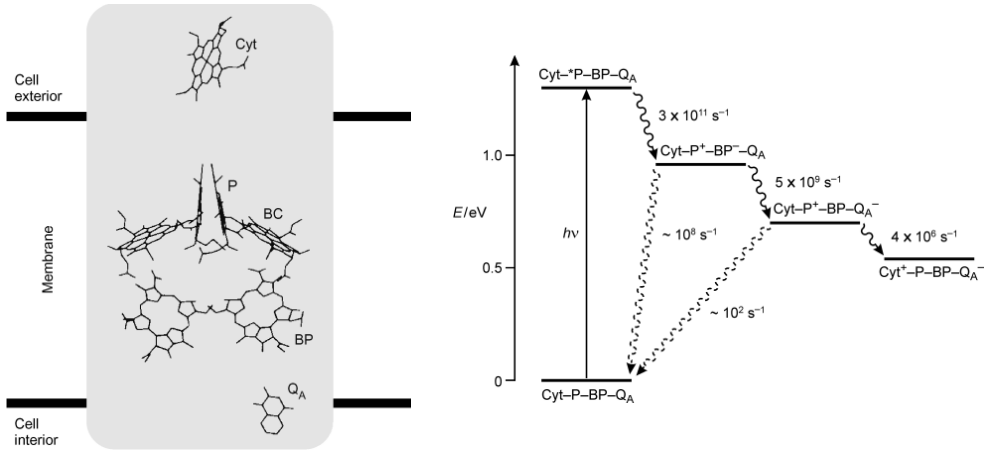

Figure 1.8: Schematic representation of the reaction centre for Rhodopseudomonas viridis (left) and the energetic levels of the molecular components (right), from Ref.23.

After the transfer on Q_A, the process continues with the energy transfer to a second quinone Q_B. Then a second photon is absorbed and transferred in the same way to Q_B that is reduced to the hydroquinonic form by picking two protons from the cytoplasm of the cell and a series of electrons and protons transfers and molecules migration have the final goal of producing ATP starting from ADP and inorganic phosphate (P_i).[35,36,37]

Photosynthesis in Green Plants

Bacterial photosynthesis is very interesting to pose the basis of the mechanism, but a deep understanding of the working mechanism in green plants is needed as well. Photosystem II (PS II) is the core of the photosynthesis in green plants and it contains all the components needed for light harvesting, energy transfer, charge separation, and charge stabilization. In addition, it is able to use water as reductant of the quinone, meaning that it is able to reach and handle very high potentials to run the reaction and couple a one-photon system to a four-electrons reaction handling four positive charges near enough to run the oxidation of water to oxygen (that is the side product of the photosynthesis). The key features of PSII are a triad of chlorophylls (P_{680}), a redox-active tyrosine residue (Y161) and an oxygen evolving complex (OEC) that is a Mn_4Ca cluster.[38,39] The first steps of light harvesting are more or less the same as in the bacteria systems: P_{680} is responsible for light absorption and energy transfer occurs till the quinones Q_A and Q_B, located on the opposite site of the membrane. P_{680}^+ is thus generated and it is rapidly reduced by the tyrosine residue which is nearby a histidine aminoacid that transforms the electron transfer into a proton-coupled electron transfer (PCET), as illustrated in Figure 1.9. PCET is a key factor for the strategy of electron transfer since it lowers the Gibbs energy (advantage of 9.5 kcal/mol compared to the simple electron transfer) of the reaction, making it possible in a faster way, without generating highly unstable radical intermediates.[40,41] The working efficiency of PSII is really high, with 200 water molecules oxidized per second.

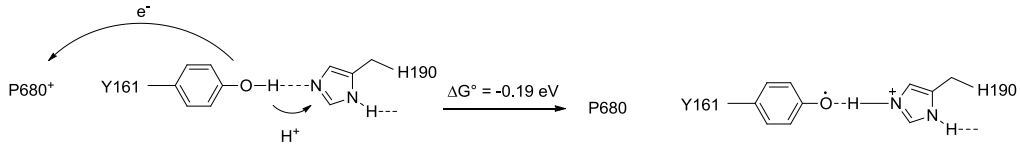

Figure 1.9: PCET mechanism of reduction of P_{680}^+.

Water oxidation takes place in the Kok cycle where manganese cluster plays the pivotal role. Mn_4Ca cluster is positioned nearby the tyrosine residue and four oxidation equivalents are transferred stepwise. Manganese atoms are peculiar because they have many contiguous oxidation states with low energy differences, moreover the cluster contains Mn-O bonds that are very strong and up to four water molecules on the external coordination sphere that induce high substrate

concentration nearby the catalytic centre. When the cluster reaches the most oxidized state O_2 is evolved. The structure of Mn_4Ca cluster has been investigated for a long time since it has the key to correctly design a powerful oxidation catalyst for water that is nowadays one of the major limitations in overall water splitting. The working mechanism based on a 4-electrons mechanism has been largely hypothesized,[42] while the high resolution images of the cluster have been collected only in 2011, paving the way to the deep understanding of the working mechanism.[43] Nowadays the structure of the cluster is known but not all the catalytic intermediates have been characterized, leaving some obscure points in the correct interpretation of the catalytic cycle. It is sure that the Mn_4Ca has a flexible structure thanks to the surrounding protein that is responsible for the high activity of that catalyst, moreover assisted protons and electrons transfers mediated by aminoacid residues are fundamental to avoid the formation of high-energy species.

Artificial Strategies

After this brief description of the working mechanisms of natural photosynthesis in bacteria and plants, I would like to focus on some interesting hints that can be picked as "take-away" advices from nature. The main property of the illustrated systems is the presence of a high number of molecules that are in the right position and work in the right moment thanks to a supramolecular organization, so that the right energy transfer occurs mainly because of the optimal disposition of all the components. Thus in developing an artificial photosynthetic system supramolecular chemistry should be considered a good tool to manage molecules. Nature teaches us which are the main components needed for an artificial leaf: an antenna for light harvesting, a centre for charge-separation, catalysts that are able to manage multi-electronic processes, and a membrane to separate reduction from oxidation products. Fortunately, the artificial system does not need to be as complicated as the natural one, since it is not dealing with living organisms and the high ordered structures that nature builds can be re-created by molecular engineering employing directional covalent or hydrogen bonding. An original solution to mimic nature in the light harvesting antenna can be found in dendrimer chemistry, since a nanometric control of the residues position can be obtained.[44,45,46,47,48] Moreover, the structure of a dendrimer itself reminds a tree (from Greek "dendron" that means tree) and resembles well an antenna system with branches able to catch light from different directions. Furthermore, the high degree of control of dendrimer synthesis allows the construction of systems with a preferential flow for energy, gaining the right energy

transfer. As dendrimers could be employed as antenna systems there are some artificial reaction centers as well. The main and simplest mimicry of the natural reaction center is a dyad composed of parts with different electronic nature: an acceptor and a donor unit, to generate charge separation. It is necessary that one of the two moieties has a light harvesting property as well. The main drawback of such systems is the fast recombination, since there is no large spatial separation of the two charges and the recombination rates are more or less in the same order of time as the separation occurs. Recombination occurs depending on the overlapping extent of the orbitals representing the positive and negative charges, thus if the donor and acceptor orbitals are close and highly overlapping a fast recombination takes place. Nature solved the problem of rapid recombination through the introduction of fast energy transfers with the final goal of having two charges separated in space with long distances. In that way a special separation of the charges and consequently of the orbitals limit the undesired back transfer. For that reason the obvious extension of a dyad is a triad (where the central unit has the role of spacing spatially the two charges), tetrad, pentad, and so on.[49] Figure 1.10 represents an example of triad investigated in the literature.[50]

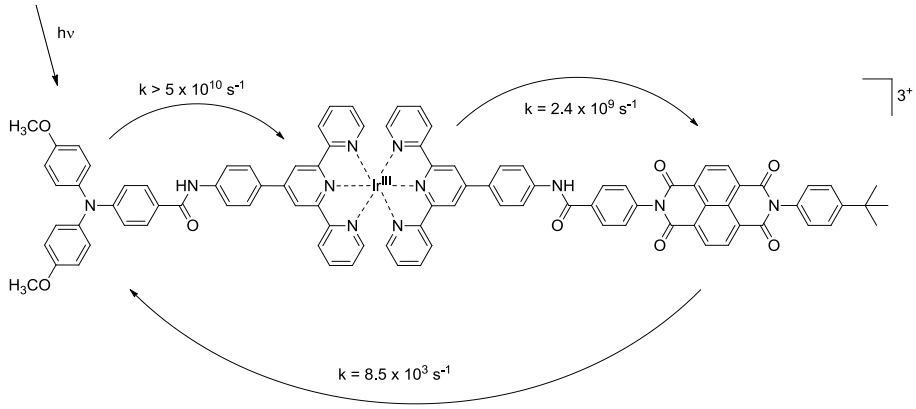

Figure 1.10: Example of a triad.[50]

The working mechanism for charge separation is the following one: the donor core (triphenylamine) or the Ir complex are excited by a photon and a charge separation takes place with the final result of a positive charge on the triphenylamine unit and a negative charge on the naphthalene-bisimide moiety with 10% efficiency in 400 ps. The recombination rate in a deareated acetonitrile solution is 120 μs, meaning that charge recombination is largely suppressed in the time scale of charge separation.

Many complex systems have been studied to try to mimic the energetic cascade that occurs in the reaction centre of natural photosynthesis, gaining both in efficiency and longer lifetime of the charge separation.[51,52,53]

Finally, a comparison between natural photosynthesis and DSSC (explained in more details in paragraph 2.1) needs to be done, since, even though apparently the working mechanisms are quite different, there are many shared analogies.[23] First of all, DSSC technology is based on photo-induced charge separation that, as illustrated at the beginning of the chapter, is the reaction of choice in nature. Moreover comparing DSSC to triads, the former ones are heterogeneous pseudo-triads where the molecular structure is implemented with the semiconductor acting as primary acceptor of the energy transfer. The main difference is that the charge separation is employed to generate an electric current instead of chemical energy. The main drawback reactions that occur in DSSC, limiting the performances, are actually correlated to the right charge separation, all the back electron transfers contribute negatively to the generated current, as in nature all the back electron transfers do not produce any new bond.

An eclectic solution could be mixing together all the best properties of the artificial systems, such as antenna for light harvesting,[54] triads for optimal charge separation,[55] and semiconductors to generate photo-accumulated charge. This could be a good research even though there is always the risk of getting too complex systems that could be too expensive to be widespread all over the world. It is anyway remarkable that efforts in this fields gave at least very elegant scientific solutions to the energetic problem.

Photo-protection

I would like to end this short excursus on natural photosynthesis with the description of the self healing systems in nature. Carotenoids are the nature's choice for protecting the photosynthetic apparatus from highly reactive radical species. As a matter of fact carotenoids are present in the LH2 cluster having the function of both light harvesting (since they have conjugated structures) and quenching the singlet oxygen species that form. In this way LH2 is protected from photo-degradation reactions that could lead to the permanent damage of the systems. Photo-degradation occurs in high irradiation conditions when the S1 levels of the chlorophylls are highly populated because of a strong photons absorption. When the saturation of S1 level occurs, the T1 level starts to be populated and at that level

electron transfer to O_2 could occur, generating highly reactive singlet oxygen species that are strong oxidants. One of the photo-protection mechanisms is given by carotenoids that are able to quench the triplet state of chlorophylls without undergoing the same kind of tranfer, meaning that the triplet state of carotenoids is not able to generate radical oxygen species but energy is dissipated in the form of heat (Figure 1.11). Thus saturation of the S1 level is suppressed and photo-protection takes place.[56,57,58] Alternatively, it is known that carotenoids are able to directly quench the singlet oxygen species when their distance from chlorophyll molecules is too far away to have direct triplet-triplet energy transfer (within the van der Waals radius).

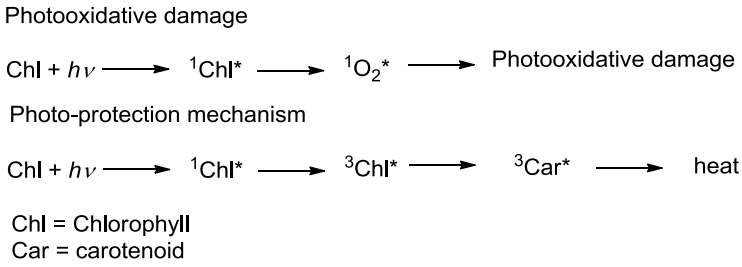

Figure 1.11: Cascade reactions that occur in the absence or presence of carotenoid photo-protection.

For that reason the use of carotenoids in triad system is highly investigated, since the dual role of light harvesting and photo-protection of the artificial system can be mimicked. Figure 1.12 represents an example of triad bearing a carotenoid unit as donor core.[59]

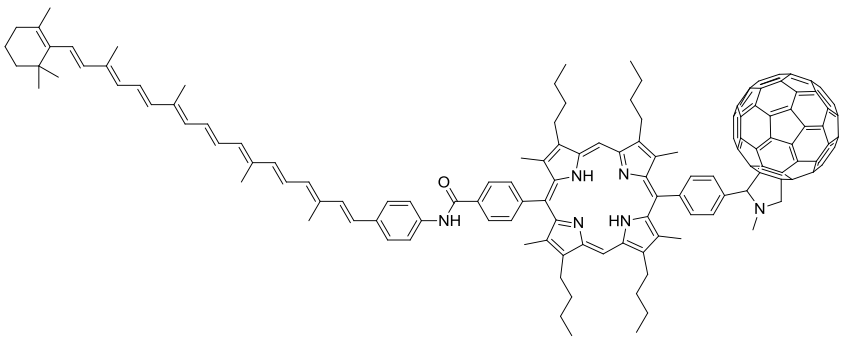

Figure 1.12: Carotenoid containing triad: light harvesting and photo-protection combined in the same residue.

1.3 BIBLIOGRAPHY

1. N. Armaroli, V. Balzani, Energy for a Sustainable World, **2011**, Wiley-VCH Edition.
2. N. Armaroli, V. Balzani, *Angew. Chem. Int. Ed.*, **2007**, *46*, 52.
3. Image taken from http://commons.wikimedia.org/wiki/
4. N. Armaroli, V. Balzani, *Chem. Eur. J.*, **2015**, *22*, 32.
5. British Petroleum, BP Statistical Review of World Energy 2015, http://www.bp.com.
6. A Snapshot of Global PV (**1992-2014**), IEA – International Energy Agency, http://www.iea-pvps.org/ , ISBN 978-3-906042-32-9.
7. REN 21—Renewable Energy Policy Network for the 21 st Century, Renewables 2015 Global Status Report **2015**, http://www.ren21.net/.
8. M. A. Green, Silicon Solar Cells: Advanced Principles and Practice, Bridge Printery, Sydney **1995**
9. M. A. Green, K. Emery, Y. Hishikawa, W. Warta, E. D. Dunlop, *Prog. Photovolt. Res. Appl.*, **2012**, *20*, 12.
10. Thin-Film Silicon Solar Cells, A. V. Shah, **2010**, EPFL Press.
11. Chalcogenide Photovoltaics: Physics, Technologies, and Thin Film Devices, R. Scheer, H.-W. Schock, **2011**, Wiley-VCH
12. M. A. Green, K. Emery, Y. Hishikawa, W. Warta, E. D. Dunlop, *Prog. Photovoltaics,* **2015**, *23*, 805.
13. A. Kojima, K. Teshima, Y. Shirai, T. Miyasaka, *J. Am. Chem. Soc.*, **2009**, *131*, 6050.
14. M. M. Lee, J. Teuscher, T. Miyasaka, T. N. Murakami, H. J. Snaith, *Science*, **2012**, *338*, 643.
15. H. S. Kim, C. R. Lee, J. H. Im, K. B. Lee, T. Moehl, A. Marchioro, S. J. Moon, R. Humphry-Baker, J. H. Yum, J. E. Moser, M. Grätzel, N. G. Park, *Sci. Rep.*, **2012**, *2*, 591.
16. EPFL Achieves 21% Efficiency for Perovskites, *Dyesol Laboratories*, 8 December **2015**.
17. International Energy Agency Key World Energy Statistics **2014**, www.iea.org .
18. N. Armaroli, V. Balzani, *ChemSusChem*, **2011**, *4*, 2.
19. S. D. Ebbesen, S. H. Jensen, A. Hauch, M. B. Mogensen, *Chem. Rev.*, **2014**, *114*, 10697.
20. O. Khaselev, A. Bansal, J. A. Turner, *Int. J. Hydrogen Energy*, **2001**, *26*, 127.
21. J. Barber, *Chem. Soc. Rev.*, **2009**, *38*, 185.
22. J. J. Concepcion, R. L. House, J. M. Papanikolas, T. J. Meyer, *PNAS*, **2012**, *109*, 15560.
23. V. Balzani, A. Credi, M. Venturi, *ChemSusChem*, **2008**, *1*, 26.
24. R. E. Blankenship, *Molecular Mechanisms of Photosynthesis*, Blackwell Science, Oxford, **2002**.

25. G. McDermott, S. M. Prince, A. A. Freer, A. M. Hawthornthwaite-Lawless, M. Z. Papiz, R. J. Cogdell, N. W. Isaacs, *Nature*, **1995**, *374*, 517.
26. T. Pullerits, V. Sundstrcm, *Acc. Chem. Res.*, **1996**, *29*, 381 *and references therein.*
27. S. Karrash, P. A. Bullough, R. Ghosh, *EMBO J.*, **1995**, *14*, 631.
28. W. Kühlbrandt, D. N. Wang, Y. Fujiyoshi, *Nature,* **1994**, *367*, 614.
29. E. Formaggio, G. Cinque, R. Bassi, *J. Mol. Biol.*, **2001**, *314*, 1157.
30. A. N. Melkozernov, V. H. R. Schmid, S. Lin, H. Paulsen, R. E. Blankenship, *J. Phys. Chem. B*, **2002**, *106*, 4313.
31. H. Rogl, R. Schodel, H. Lokstein, W. KZhlbrandt, A. Schubert, *Biochemistry,* **2002**, *41*, 2281.
32. J. R. Norris, M. Schiffer, *Chem. Eng. News,* **1990**, *68*, 22.
33. V. Balzani, F. Scandola, *Supramolecular Photochemistry*, Horwood, Chichester,**1991**, Ch. 5.
34. P. L. Dutton, J. S. Leigh, R. C. Prince, D. M. Tiede, *Tunneling in Biological Systems* (Eds.: B. Chance, D. C. DeVault, H. Frauenfelder, R. A. Marcus, J. R. Schrieffer, N. Sutin), Academic Press, New York, **1979**.
35. J. E. Walker, *Angew. Chem. Int. Ed.*, **1998**, *37*, 2308.
36. D. Stock, A. G. W. Leslie, J. E. Walker, Science 1999, 286, 1700.
37. P. D. Boyer*, Angew. Chem. Int. Ed.*, **1998**, *37*, 2296.
38. B. A. Dinner, G. T. Babcock, *Oxygenic Photosynthesis: The Light Reactions* (Eds.: D. R. Ort, C. F. Yocum), Kluwer, Dordrecht, **1996**.
39. R. Danielsson, M. Suorsa, V. Paakkarinen, P.-N. Albertsson, S. Styring, E.-M. Aro, F. Mamedov, *J. Biol. Chem.*, **2006**, *281*, 14241.
40. J. H. Alstrum-Acevedo, M.K. Brennaman, T. J. Meyer, *Inorg. Chem.*, **2005**, *44*, 6802.
41 . D. N. Beratan, J. N. Onuchic, J. R. Winkler, H. B. Gray, *Science*, **1992**, *258*, 1740.
42. C. Tommos, G. T. Babcock, *Acc. Chem. Res.*, **1998**, *31*, 18.
43. Y. Umena, K. Kawakami, J.-R. Shen, N. Kamiya, *Nature*, **2011**, *473*, 55.
44. A. Nantalaksakul, D. Raghunath Reddy, C. Thayumanavan, *Photosynth. Res.*, **2006**, *87*, 133.
45. V. Balzani, S. Campagna, G. Denti, A. Juris, S. Serroni, M. Venturi, *Acc. Chem. Res*., **1998**, *31*, 26.
46. P. E. Froehling, *Dyes Pigm.,* **2001**, *48*, 187.
47. Y. Zeng, Y.-Y. Li, J.Chen, G. Yang, Y. Li, *Chem. Asian J.*, **2010**, *5*, 992.
48. X. Zhang, Y. Zeng, T. Yu, J. Chen, G. Yang, Y. Li, *J. Phys. Chem. Lett.*, **2014**, *5*, 2340.
49. O. S. Wenger, *Coord. Chem. Rev.*, **2009**, *253*, 1439.
50. L. Flamigni, E. Baranoff, J.-P. Collin, J.-P. Sauvage, *Chem. Eur. J.*, **2006**, *12*, 6592.

51. F. Barigelletti, L. Flamigni, *Chem. Soc. Rev.*, **2000**, *29*, 1.
52. P. D. Frischmann, K. Mahata and Fr. Wurthner, *Chem. Soc. Rev.*, **2013**, *42*, 1847.
53. Q. Yan, Z. Luo, K. Cai, Y. Ma, D. Zhao, *Chem. Soc. Rev.,* **2014**, *43*, 4199.
54. R. Amadelli, R. Argazzi, C. A. Bignozzi, F. Scandola, *J. Am. Chem. Soc*., **1990**, *112*, 7099.
55. J. Warnan, F. Buchet, Y. Pellegrin, E. Blart, F. Odobel, *Org. Lett.*, **2011**, *13*, 3944.
56. B. Loll, J. Kern, W. Saenger, A. Zouni, J. Biesiadka, *Nature*, **2005**, *438*, 1040.
57. A. Telfer, *Photochem. Photobiol. Sci.*, **2005**, *4*, 950.
58. A. Krieger-Liszkay, C. Fufezan, A. Trebst, *Photosynth. Res.*, **2008**, *98*, 551.
59. P. A. Liddell, D. Kuciauskas, J.P. Sumida, B. Nash, D. Nguyen, A. L. Moore, T. A. Moore, D. Gust, *J. Am. Chem. Soc.*, **1997**, *119*, 400.

Chapter 2

FROM DSSC TO DYE-SENSITIZED PHOTOCATALYTIC HYDROGEN PRODUCTION

Look at the frequencies at which I vibrate

I'm going to light up the world

Peace

Depeche Mode

2.1 DSSC: DYE-SENSITIZED SOLAR CELLS

2.1.1 Introduction, Working Mechanism, and Main Cell Parameters

The breakthrough that introduced dye-sensitized solar cells as they are known nowadays has been given by O'Regan and Grätzel in 1991[1]. The basic principles were already known in the literature[2] but the innovative idea was the introduction of high surface nanocrystalline semiconductor as basis for the attachment of the light harvesting systems. After an initial optimism in the success of DSSC technology, the enthusiasm vanished since no breakthrough in the performances arrived and the average efficiency of the best devices was steady around 10%, definitively incomparable with the silicon technology. Nonetheless there are some properties, maybe less appealing in the first years of the run to the higher efficiency, that came out and posed DSSC technology as complementary to the silicon PV rather than in replacing its market. DSSC have the main advantage of a potential low cost in fabrication (and an alternative market for raw materials), they work in diffuse light conditions and even when the devices are inclined not with the right matching angle with the striking solar radiation. For that reason they are good candidates to cover many applications, from indoor and portable devices to outdoor building integration.[3,4,5,6,7] After the first enthusiasm in DSSC, a steady and continuous growth of the market of this technology followed and is currently going on.[8]

As it has already been presented in paragraph 1.2, the basic principle of the dye-sensitized solar cells is inspired by natural photosynthesis. The main components of these devices are illustrated in Figure 2.1 and they are

1. a conductive support, such as conductive glass FTO (fluorine doped SnO_2);
2. a wide band gap mesoporous and nanorystalline semiconductor oxide, such as TiO_2;
3. a sensitizer that is able to absorb the visible (and/or IR) portion of the solar spectrum (the wide band gap semiconductors typically absorb in the UV region that is a limited portion of the solar emission);
4. a redox shuttle that has the role of transferring electrons from the counter electrode to the oxidized sensitizer;
5. a counter electrode made of conductive glass (FTO) covered by a catalyst as platinum or carbon.

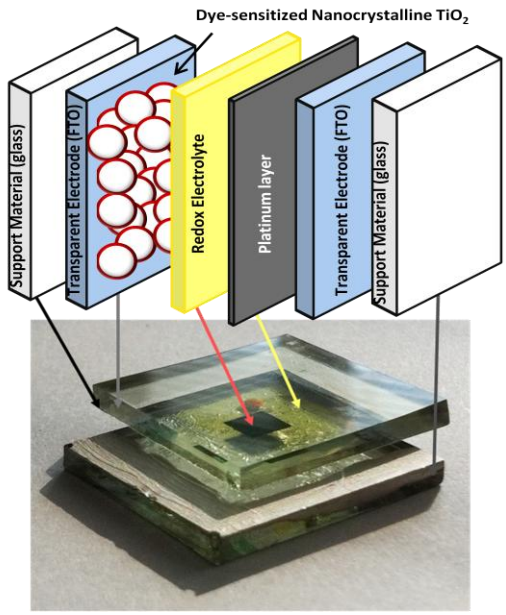

Figure 2.1: DSSC components in parallel with a real device.

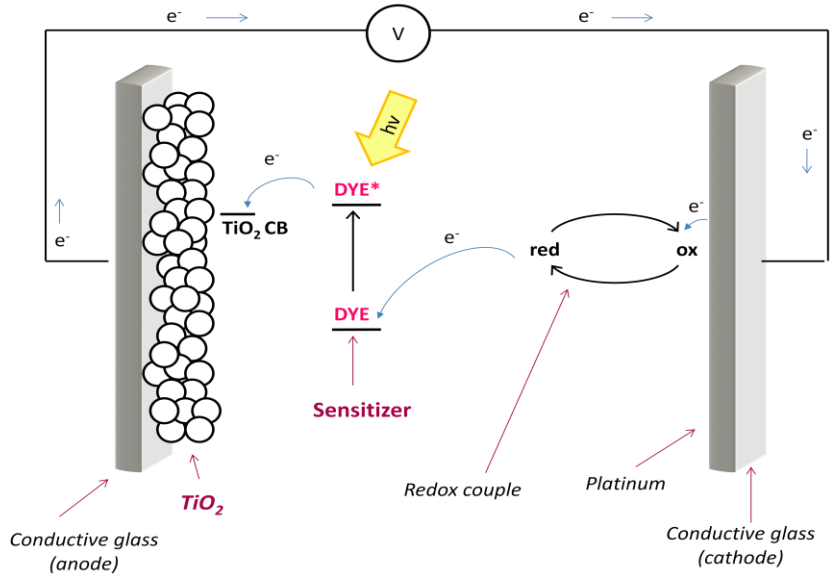

Figure 2.2: DSSC working mechanism.

The working mechanism is illustrated in Figure 2.2 and it starts with the absorption of a photon by the sensitizer that is thus excited and able to inject an electron in the

conduction band (CB) of the semiconductor oxide. The electron in the CB migrates to the FTO support and then into the external circuit where it is transferred to the oxidized form of the redox couple through the counter electrode. The reduced form of the redox shuttle interacts with the oxidized form of the sensitizer and regenerates it. The overall result of such a mechanism is the generation of an electric current without any permanent modification of any component, moreover, theoretically from each incident photon that is absorbed, an electron is generated in the external circuit.[9] The working mechanism points out the main difference for this kind of cells compared to the previous generations' ones: the functions of light harvesting and charge transport are carried out by different components, so that a fine optimization of the performances can be done separately.

To have comparable data, the cell performances have been standardized in the procedure of production and measurement.[10] Through the use of a calibrated solar simulator, the main cell parameters can be obtained in the form of efficiency curves. These parameters are contained in two curves: the J/V (photocurrent vs. photo-voltage) graph, and the IPCE (Incident Photon-to-Current Efficiency) that are illustrated as examples in Figure 2.3. From the J/V curves parameters as J_{sc} (mA/cm^2, photocurrent in the case of zero potential, meaning in short circuit conditions), V_{oc} (mV, photo-voltage in case of null photocurrent, meaning in open circuit conditions), *ff* (fill factor that gives an idea of the cell fabrication quality) and PCE (Photon-to-Current Efficiency) can be obtained. The mathematical expression that connects these four values is illustrated in Equation 2.1. In standard conditions the light intensity (P_{in}) is 1000 Wm^{-2} and the graphical representation of presented parameters is illustrated in Figure 2.3-left.

$$PCE\ (\eta) = \frac{ff\ \times J_{sc}\ \times V_{oc}}{P_{in}}$$

Equation 2.1: PCE equation

The V_{oc} is the potential difference between the Fermi level of TiO_2 and the redox potential of the electrolyte in open circuit conditions. It depends on E_{CB} (charge surface of TiO_2) and n_c (free electron density) that takes into account the balance between electrons injected and recombined.

The fill factor is obtained by Equation 2.2.

$$ff = \frac{P_{max}}{J_{sc} \times V_{oc}}$$

Equation 2.2: Fill factor equation.

where P_{max} can be calculated as the product of the data V_{max} and J_{max} extrapolated from the J/V curve. As it can be deduced from Figure 2.3-left, the *ff* is graphically the ratio between the areas of the two drawn rectangles thus it is much higher (close to 100%) when the J/V curve has a rectangular shape.

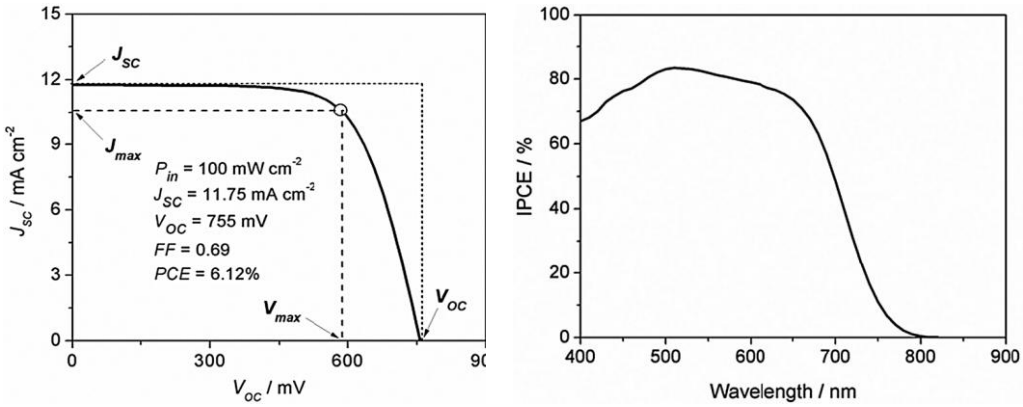

Figure 2.3: Cell parameters and their graphical representation in J/V curves (left) and IPCE (right).

The IPCE corresponds to the photocurrent density that is obtained when a monochromatic irradiation is selected divided by the photon flux and a scan over the spectral range is done. It gives an idea of the ability of the cell in transforming photons in electrons with dependence on the wavelength of the striking photons. Such a parameter is strongly correlated with the number of sensitizer molecules absorbed of the surface and the charge collection efficiency, but it also takes into account the light harvesting properties of the sensitizer, e.g. if the absorption spectrum of the sensitizer is zero at 800 nm, IPCE in that region will be zero as well. An example of IPCE curve is depicted in Figure 2.3-right while the mathematical expression of IPCE is reported in Equation 2.3.

$$IPCE\ (\%) = \frac{1240\ (eV\ nm) \times J_{ph}\ (mA\ cm^{-2})}{\lambda\ (nm)/I\ (mW\ cm^{-2})}$$

Equation 2.3: IPCE formula (J_{ph} is the photocurrent density in short circuit conditions when a monochromatic light of wavelength λ and intensity I are used).

Perovskite Solar Cells (PSC) were born as a branch of the DSSC technology[11] but they are differentiating day by day from the DSSC, so they can be considered out of the field of this thesis dissertation, although they are surely promising devices with 21.02% as record certified efficiency.[12]

Sensitizers have a pivotal role in DSSC technology since they are the first interface of the device towards solar radiation, thus their optimization is the first step in building high performances devices. Moreover, as it has been illustrated in the parameters part, they have a crucial role being the core of the device, interacting with both the semiconductor and the redox couple. They influence both J_{sc}, V_{oc}, IPCE, and not least the stability of the whole device. Long term stability is a fundamental property in building commercial devices since the durability of the current technology is quite high. Thus photostability and thermostability are key points that must be taken into account when designing new sensitizers. Fortunately the development of new sensitizers is a huge field in which the contribution of many scientists has allowed a rationalization of the structure-performance correlations that are essential for the improvement of the technology.

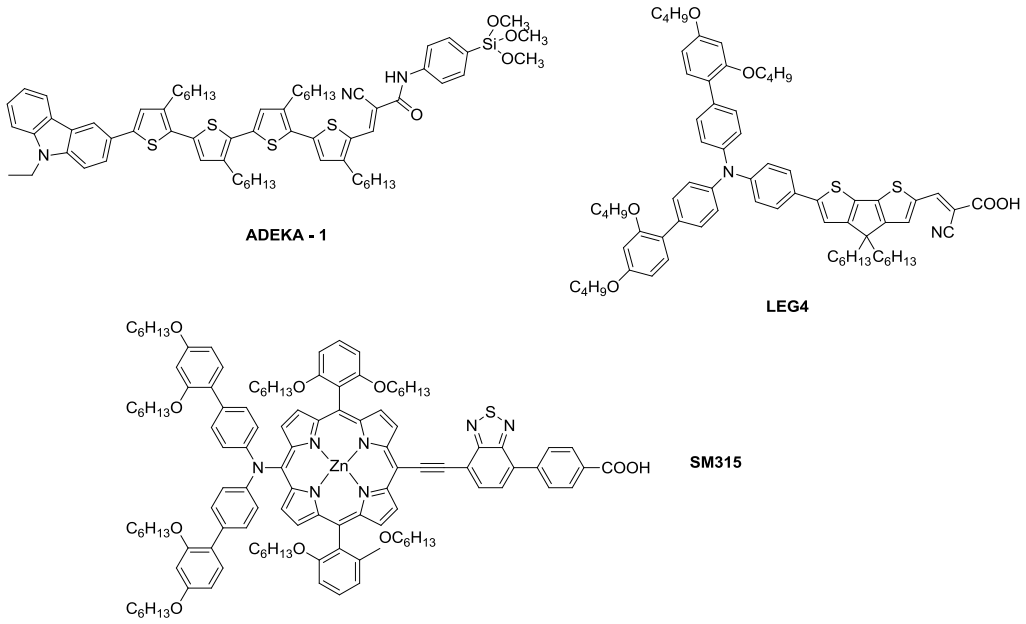

*Figure 2.4: Dyes with record efficiencies, 13% for **SM315**, and 14.3% for a co-sensitization of organic dyes **ADEKA-1** and **LEG4**.*

Sensitizers could be classified into three categories depending on their nature: metallorganic complexes (in particular ruthenium),[13,14,15,16] porphyrins (and elaborated cores starting from natural dyes),[17,18,19,20,21] and organic dyes. For many years the efficiency record in DSSC was of the ruthenium complex N719,[22] while in recent years porphyrinic and organic dyes are under the spotlight and posed two new records: 13% for a modified porphyrins **SM315**[23] and over 14% for a combination of two organic dyes (**ADEKA-1** and **LEG4**),[24] all the molecular structures are reported in Figure 2.4.

The principal properties that a good sensitizer should possess are 1) a broad absorption spectrum able to cover the solar emission spectrum and high absorption coefficients that are compatible with the use of thin layer of semiconductor; 2) the LUMO of the dye should lie at more negative potential than the conduction band of the semiconductor to have electron injection; 3) the HOMO of the dye should be more positive than the redox potential of the electrolyte to guarantee a fast regeneration; 4) the dye should have anchoring units to ensure the attachment on semiconductor surface and electronic communication; 5) the dye should have steric properties to suppress as much as possible all the recombination pathways that contribute to the dark current, and 6) a high photo- and thermo-stability to ensure long life devices. The literature that concerns sensitizers is considerable and the detailed description of all the developed systems is out of the interest of this thesis, thus attention will be focused only on the class of organic dyes since they have been developed in this research activity.

2.1.2 Metal-free Organic Sensitizers

Many excellent reviews give comprehensive reports of the state of the art of many organic dyes systems.[25,26,27] Organic dyes are considered promising candidates as sensitizers as they can overcome many of the limitations of the other two categories, especially the metal complexes. Amongst the advantages of this class of sensitizers, it must be highlighted the potential low cost of organic molecules compared to metal complexes (especially the most active ones that are made of quite rare elements), high absorption coefficients necessary for satisfactory light harvesting (visible absorption arises from an ICT rather than a MLCT as in metal complexes), and high tunability of performances through organic synthesis. Even though it is not always an easy task, the application of a modular approach to these systems allows the right rationalization of structure-properties relationships. The main strategy to build organic dyes is through a D-π-A skeleton that is able to give a push-pull structure

where an ICT (intra-molecular charge transfer) from the electron donating unit to the accepting one is the starting step before electron injection.

These structures are characterized by the presence of three "components": an electron-donor group (D), a π spacer (π), and an electron-withdrawing/anchoring group (A). The donor group is characterized by electron donating ability and should lie as far as possible from the TiO_2 surface and as close as possible to the redox electrolyte; π spacers are generally polarizable conjugated groups that are able to transfer charge. The A group is composed of an electron-withdrawing group that attracts electrons from the donor unit and an anchoring moiety that is able to strongly bind the dye on TiO_2 surface. To ensure such characteristics, molecular orbital disposition must be the right one. The most important orbitals, in terms of reactivity, are usually the LUMO and the HOMO. Even if both the orbitals should be diffused in the whole molecule to ensure electronic communication, LUMO should be mostly localized on the acceptor/anchoring unit because it represents the injection "precursor", lying as close as possible to TiO_2 to have proper electron injection. Instead HOMO represents the dye in the radical cation form, so it should lie mostly on the donor core, far away from TiO_2 surface to avoid charge recombination and close to the electron donating agent. Energetically LUMO should be higher (more negative) than conduction band (Fermi level) of TiO_2 to perform electron injection and HOMO should be lower (more positive) than redox potential of the electrolyte to have regeneration. Theoretical calculations are able to predict orbitals shape and their energies, so that a sorting on designed dyes can be done before synthesizing and testing them. Experimentally HOMO and LUMO energies can be detected electrochemically. Oxidation and reduction waves in cyclic voltammetry can be used to calculate such levels.

The main limitation of the structure-properties investigations is that the modification of even a little part of one of the moieties could affect many parameters and could yield to many variations at the same time.

A brief introduction on the principal strategies to modulate D, π, and A moieties is now given, with a special focus on phenothiazines as donor cores and di-branched structures (paragraph 2.1.4), because they are the scaffolds that have been developed in this research.

Donor core

The most detailed investigation in push-pull structures regards without any doubt the donor core: most of the articles and the modifications interest the donor core with hundreds of alternative approaches.[26] The second more modified moiety is the π-spacer and definitively few examples regarding the anchoring unit have been reported. Amongst the donor cores, arylamines are the typical choice, they have been satisfactory employed in other fields as hole transporting materials or light emitters, such as OLED, NLO, and OPV. [28,29,30,31] A list of donor arylaminic cores is depicted in Figure 2.5. The main limitations about dyes bearing such cores are principally the null absorption in the NIR region, charge recombination at the semiconductor surface, dyes aggregation and eventual mismatch of the energy levels between dye, semiconductor and electrolyte. Organic chemistry could intervene in this field to modulate the properties and solve partially or completely those drawbacks. The simplest arylamine core is the triphenylamine (TPA) one that is surely the most investigated and the one that has the most comprehensive investigation of structure-efficiency relationships. Modification of the triphenylamine core gives birth to the substituted TPA where alkyl chains are used to reduce molecule aggregation, while further donor cores are introduced to enhance the light harvesting.[32,33]

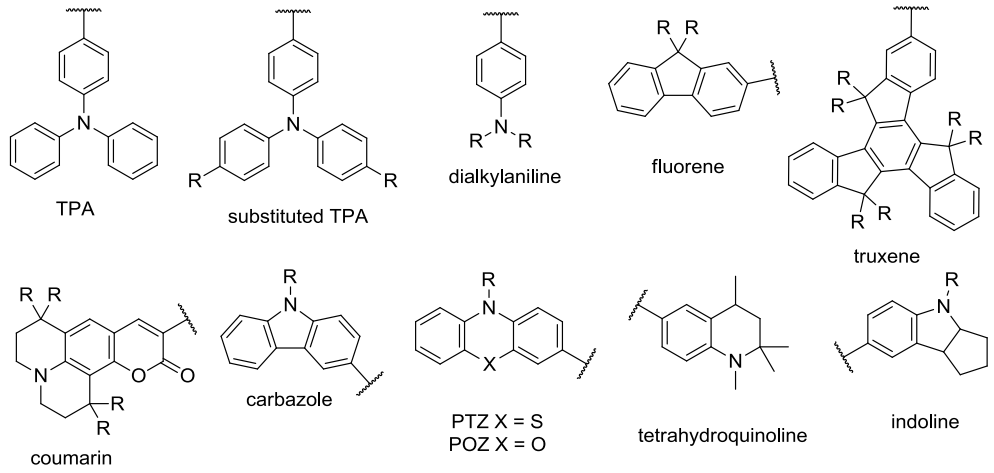

Figure 2.5: Common donor cores in organic dyes.

Through the introduction of symmetric additional donor cores, starburst or branched structures (that remind the antenna systems in natural photosynthesis) can be obtained, in which the de-aggregating property is achieved with the spatial

distribution of the non-planar disposition of the conjugated groups. Such modification to D-D-π-A structures cause a bathochromic shift of the absorption spectra, ε enhancement, and usually high thermal stability.[34,35] All the other donor cores have been less investigated than the triphenylamine one, thus sometimes limited library of dyes can be found, nonetheless some of them have appealing properties and each of them has singular features that are unique or seldom reproducible by other cores. Fluorene is an interesting alternative donor core since it is highly photo- and thermo-stable, moreover it is able to block the access of water molecules to the semiconductor surface that could induce the hydrolysis of the ester bond between the dye and the semiconductor; so it is a promising choice for long term stability devices.[36,37] Truxenes are more complicated that fluorene moieties but they possess the same durability properties, moreover the high hindrance of this core allows a great tunability of the de-aggregating properties between dye molecules.[38,39] Indolines,[40,41] tetrahydroquinolines,[42] coumarines,[43,44] and dialkylanilines[45] have been tested as well, they showed promising efficiency with impressively high photocurrents, but much lower photo-voltages than the other cores. The low conjugation extent of those cores needs high manipulation of the π-spacer moiety to balance the low starting light harvesting features. The use of carbazole as donor core is highly investigated since the full planar structure of this moiety ensures a complete electronic communication with the rest of the molecule, on the other hand the planar structure allows high π-π stacking amongst molecules, thus the use of de-aggregating alkyl chains or co-adsorbents in the fabrication of the cells is necessary.[46] The current efficiency record in DSSC belongs to a mixture of two organic dyes, one of which has carbazole as donor unit that has an efficiency of 12.5%[47] (14.3%[24] together with the other dye). Phenothiazines (PTZ) and phenoxazines (POZ) are gaining interest as donor cores since they have peculiar features: first of all they have a butterfly conformation of the core in the ground state that is in between the propeller-like structure of triphenylamine and the completely planar carbazole.[48] Secondly the radical cation arising after electron injection is highly stable, hampering charge recombination and thus allowing the right dye regeneration.[49] Thirdly it has been demonstrated that the aggregation and the formation of intermolecular excimers is partially limited by such geometry.[50] Moreover they contain electron-rich sulfur/oxygen heteroatoms in addition to nitrogen that could improve the donating effect. Dyes bearing phenothiazines as donor core showed good performances even in quite simple structures, indicating the great hole-transporting properties of this core. The first example of

phenothiazine dye has been given by Hagfeldt *et al.* demonstrating the cheap and easy synthesis of these dyes.[51] Some interesting insights have been outlined by Kim *et al.* that correlated the torsion angles of the phenothiazine core to the DSSC performances, since the use of different π-spacers induced different torsion angles affecting PCE.[52] The phenothiazine nitrogen can be decorated with aromatic or alkyl moieties, the general trend is that all the modifications that force the PTZ core to be flat are detrimental in terms of aggregation, thus the highest distortion from planarity could bring to highest performances. Comparison between PTZ and POZ showed that their properties are comparable, so a deeper investigation in POZ as donor core is needed, since they have been scantily studied till now.[53]

π-spacers

The π-spacer is the second component of the push-pull structure, it has the aim of keeping the electronic communication between the donor and the acceptor/anchoring units, the most common spacers are illustrated in Figure 2.6.

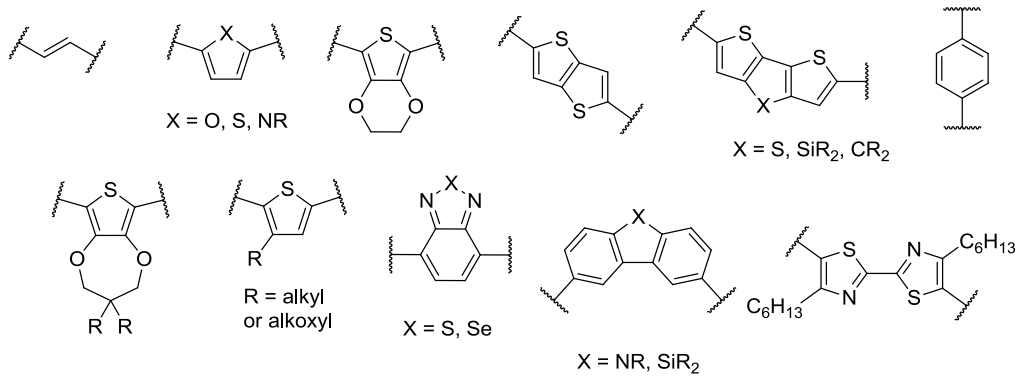

Figure 2.6: Common π-spacers in organic dyes.

Even though it could seem that the main properties are determined by the other two moieties, the rationalization of the effects in the spacer modification is probably the most challenging task. One of the first organic dye reported in the literature was spacer-free and the introduction of simple moieties such as vinyl groups revealed their fundamental role.[54] Moreover the real breakthrough could be considered the introduction of heteroaromatic cores that paved the way for light harvesting optimization. The first heteroaromatic core was introduced by Hagfeldt *et al.* and it has been followed by many modifications aimed at enhancing the light harvesting properties, or lowering the detrimental recombination rates.[55] The resonance energy

could give a hint for the interpretation of the performances in the case of comparison of furan (16 kcal/mol), thiophene (29 kcal/mol), and benzene (36 kcal/mol), since the order in performances is furan>thiophene>benzene.[56] Multiple, fused and highly extended π-spacers give better light harvesting properties (necessary for ssDSSC or thin film devices) that sometimes are not translated in higher efficiency because of high recombination rates. It is supposed that specially sulfurated heterocycles could interact with I_3^- (oxidized form of the most used electrolyte) and create some kind of tunnels that bring electrolyte molecules in contact with the semiconductor surface lowering the V_{oc}. To overcome this limit the same strategy of the donor core can be applied with the introduction of alkyl or alkoxyl chains that act as de-aggregating agents and hinder the semiconductor surface.[57,58] Furthermore alkoxyl chains have an electron donating character that can partially suppress the recombination rates not only because of the steric hindrance but also thanks to the electronic character. At the same time introduction of very long chains is irrelevant on the donor core, but could be detrimental in the spacer because of lowering of dye loading due to steric effects (thus lowering the photocurrent). In addition the presence of many bulky chains, one next to the other, could suppress the planar structure of the dye, limiting the conjugation of the system and thus suppressing the light harvesting properties.[59] **MK2** (Figure 2.7) has been taken as example to study the effect of steric hindrance on dye coverage of the semiconductor surface and on recombination rates and it came out that a balance between de-aggregation and high dye sensitization is needed to have good performances.[60]

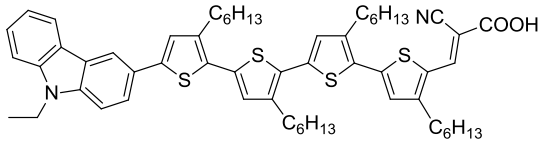

MK2

Figure 2.7: Carbazole dye MK2.

The introduction of electro-withdrawing systems in the π-spacer has been controversial since a better light harvesting property is generally achieved, but together with the drawbacks of having high electronic recombination rates and suppression of electron injection. Thus opposite results can be obtained depending on the kind of group, its position, and the whole structure of the dye. A good

compromise is the introduction of electron withdrawing groups together with alkyl/alkoxyl chains that are able to balance the electronic properties and limit charge recombination.[61,62] It is highly important that the spacer is photo- and thermo-stable to build durable devices, and Katoh *et al.* pointed out the superior stability of heterocyclic spacers compared to vinyl moieties introducing them in coumarin dyes.[63]

Anchoring/Acceptor Units

Special attention will be given to the illustration of the anchoring groups since they have a critical role in shifting from organic DSSC to aqueous dye-sensitized hydrogen production. Stability and good electronic communication are the basis of a good anchoring moiety.[64] There are many experimental tools to evaluate the efficiency in electronic communication by mean of the electron injection kinetics, while techniques as FTIR , Raman Spectroscopy or PES (Photo-Electron Spectroscopy) are able to give information about the nature of the linkage between the sensitizer and the semiconductor metal oxide surface. There are many kinds of bonds that might be employed for anchoring, for example covalent bonds, hydrogen bonds, van der Waals interactions, coordination et cetera. One of the first examples of semiconductor oxide sensitization employed physisorption of sensitizers on the surface, but it was immediately clear that anchoring units were necessary for breakthrough.[65] Therefore covalent bonding is now the preferred way to strongly anchor a dye on TiO_2 surface, anyway the presence of auxiliary H-bonds could not be excluded thanks to the presence of OH pending moieties from TiO_2 surface. Covalent attachment has plenty of advantages over other anchoring bonds since it guarantees high surface monolayer coverage (while through physisorption the number of layers is hardly controlled and less homogeneous), high stability, minimal dye losses because of desorption, and good electronic coupling between the dye and the semiconductor levels. Interesting studies regarding the development of linkers (flexible, rigid or tripods) to separate the anchoring unit from the chromophore have been reviewed;[66] anyway the use of linkers to study the kinetics of electron injections is typical for metallorganic complexes. Amongst organic dyes the anchoring and acceptor units could be performed by the same moiety or by two different parts of the molecule. The first step in developing and characterizing a new anchoring group is the understanding of the binding geometry that is sometimes not straightforward. FTIR (and in particular ATR-FTIR) plays a fundamental role in the interpretation of the binding mode by mean of the variation of vibrational frequencies from the free

molecule to the bonded one, but DFT calculations could have a fundamental role when the experimental data are not straightforward. Changing the anchoring group means intervening on all fronts, so careful characterization must be performed. The most widespread group for anchoring is the carboxylic acid that together with a nitrile group constitutes the cyanoacrylic ending moiety that is by far the most recurrent group in dyes.[9] The right balance between electron injection rate, strength of anchoring and electron withdrawing character gives to the cyanoacrylic moiety the prominent role in dyes. Nonetheless such a group has some limitations, but the modification by insertion of different groups could generate better properties from one point of view and collapse from other sides. Figure 2.8 represents the 6 possible coordination geometries for a carboxylic group, while the bidentate bridging and the chelating modes are the main contributions, probably all of them in some extent contribute to the binding mode.

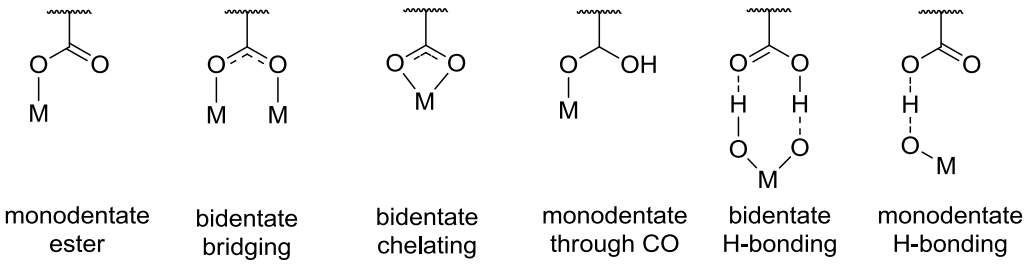

Figure 2.8: Possible coordination geometries for carboxylic anchoring groups.

Many research groups endeavored to develop alternative anchoring moieties, and some of them gave promising results (Figure 2.9).

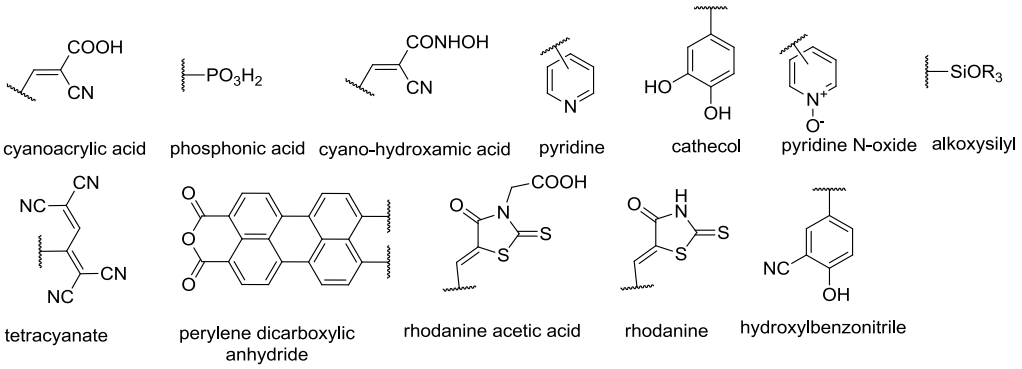

Figure 2.9: Anchoring groups for organic dyes.

Amongst the most promising alternative groups, phosphonic acids are considered highly stable system (up to one or two order of magnitude) with negligible detachment from TiO_2 even in water, unfortunately the electronic communication is worse because of the tetragonal geometry of phosphorous, thus electron injection is less efficient giving lower performances in DSSC. Since the anchoring stability is so strong in water, a good strategy is the combination of phosphonic moieties together with carboxylic ones as it has been proposed for a ruthenium complex.[67] Pyridine as been tested as well and the efficiencies are still low but promising since the binding mode is alternative to the other groups: coordination occurs on the Lewis acid sites instead of the Brønsted basic sites as in covalent bonds. Dye loading is lower but a perpendicular mode for coordination is proposed, which is fundamental to have good electron injection; a co-sensitization of pyridine and cyanoacrylic acid dyes could be an interesting strategy for those groups since they do not compete for the same anchoring points.[68] Hydroxamic acids are proposed to be more stable upon hydrolysis than the carboxylic counterparts, but few examples are described in the literature, where stability is actually higher but the results in efficiencies are controversial.[69,70] Other examples of anchoring groups are tetracyanates,[71] perylene dicarboxylic acid anhydrides,[72] hydroxylbenzonitriles,[73] pyridine N-oxides,[74] tetrazoles,[75] rhodanines,[76] and rhodanine acetic acids.[77] Alkoxysilyl moieties have been investigated because of the strong covalent bond that they could give with TiO_2 surface. The results are quite promising since the electronic communication seems to be satisfactory and the actual efficiency record has been measured with **ADEKA-1** (Figure 2.4), a dye with carbazole as donor unit and an alkoxysilyl anchor.[47] Dyes bearing cathecols as anchoring units belong to the type II sensitizer; for these molecules a different electron injection mechanism is envisaged. Common dyes belong to the type I category meaning that absorption of a photon causes the electron excitation from HOMO to LUMO and a subsequent electron injection step into the CB of TiO_2. For cathecols the molecular orbitals are intimately connected so that a direct transition from the HOMO of the dye to the CB is favored. These dyes exhibit low efficiencies till now because of strong electron recombination but interesting development could be forecast.[78,79]

2.1.3 Electrolytes

The electrolyte is another key factor for the optimization of performances in DSSC. Indeed it is fundamental for fast dye regeneration to avoid degradation of the sensitizer, and its redox potential is correlated to the output photo-voltage. The

redox couple I^-/I_3^- has been by far the most employed one, since it is highly reproducible and works with almost all the sensitizers, thus it is ideal for testing performances of new dyes. Unfortunately there are some drawbacks associated with this redox couple, such as highly corrosion towards most of the metals and sealing materials, challenging the large scale diffusion; moreover its redox potential limits a maximum of photo-voltage to ~0.7-0.8 V even when the performing dye could give higher V_{oc}. The supposed bonding with the electron rich heterocyclic moieties of the π-spacers is detrimental for recombination rates (illustrated in π-spacer part of paragraph 2.1.2), moreover it absorbs competitively to the dye a portion of the visible range. For that reason the need of finding an alternative electrolyte has centered most of the efforts in the last years and the cobalt polypyridyl complexes are now promising candidates. Such complexes could lead in principle to high photo-voltage (up to ~1 V) without losing in *ff*, moreover since they are quite bulky and they do not interact with the π-spacer moieties, the photo-voltage shows the trend forecasted for the increasing of π-length. Increasing the number of thiophene rings in the spacer the performances are enhanced, without any loss in V_{oc}, since no intercalation occurs, the longer is the molecule the more distant is the electrolyte from the semiconductor surface.[80] By the use of such electrolyte many dyes that were not overperforming other sensitizers with I^-/I_3^- showed to be the best ones, e.g. when very high molar absorption coefficients were achieved, a further improvement of the light harvesting properties were not translated in higher PCE, while with the cobalt polypyridyl complexes the difference was perceptible. The first example of polypyridyl complexes of cobalt yielded to low PCE because of the slow mass transport and increased recombination of the injected electrons, thus the use of thin layer of TiO_2 is fundamental to have high performances with the new redox shuttle.[81,82] The actual record in DSSC efficiency for a porphyrin dye has been measured with cobalt polypyridyl complexes as redox shuttle, confirming the superior skills of that electrolyte.[24,47]

2.1.4 Multi-Anchoring Organic Dyes

To conclude this paragraph an illustration of multi-anchoring dyes will be given since they are the structures that have been developed during this research. Even though metal-free dyes are appealing for the easiness and cheapness of the synthesis and the likable possibility of tuning performances through dye engineering, their efficiencies are usually lower that the ruthenium complexes, apart from some exceptions. A comparison between the peculiarities of the two classes of structures

might bring out the winning strategy to develop high performance metal-free dyes. Literature was full of branched structures on the donor and spacer moieties but all the examples were bearing only one anchoring unit. Thus multi-anchoring dyes have been introduced by Abbotto *et al.* with the aim of mimicking metal complexes that were the most performing ones.[83] Apart from the presence of a metal center, all those complexes show at least two (usually up to four) anchoring units, while the organic sensitizers presented only one anchoring point to TiO_2. The manipulation of a known dye in the literature brought to the first di-anchoring dye that showed promising properties, such as great light harvesting, cell photocurrent, power conversion efficiency and long-term stability thanks to a tighter contact of the dye with TiO_2. From that article many research groups showed interest in this approach when developing new sensitizers, thus quite a large number of articles appeared in the literature in last five years, and we wrote a microreview to try to sort them.[84] Multi-branched dyes can be classified into two broad categories: 1) the D–(π–A)$_n$ structures (Figure 2.10), and 2) multi-donor multi-anchoring interconnected architectures (donor cores or π-spacers linked through conjugated or saturated linker, π-bridge-interconnected dyes), more complicated structures such as X- and Y-shaped dyes, and other multi-anchoring systems.

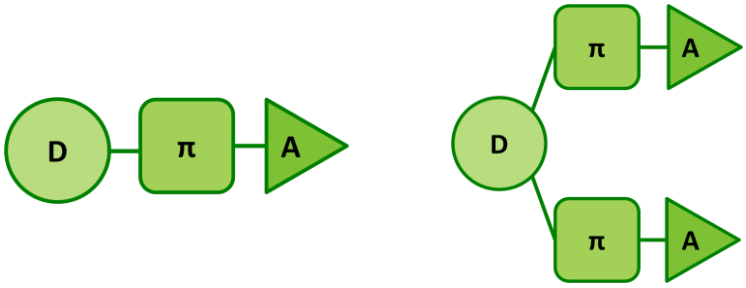

Figure 2.10: Comparison between a mono-anchoring sensitizer (left) and a D-(π-A)$_2$ type (right).

The optical properties have been largely enhanced reaching 530 nm as maximum of absorption and 140 000 $M^{-1}cm^{-1}$ as molar extinction coefficient;[85] high photocurrent up to 15 $mAcm^{-2}$ and PCE over 7% have been achieved.[86,87,88,89,90] The higher photocurrents of multi-branched systems compared to the mono-branched analogues might be ascribed to a better light harvesting and electron-injection efficiency derived from the more intimate connection with TiO_2. Concerning stability of the linkage between dye and semiconductor surface, a cooperative effect of the

two anchoring groups might be hypothesized. Figure 2.11 represents such hypothesis: if one anchoring unit detaches from the surface because of hydrolysis, the dye will still be attached allowing electron injection and a possible restoration of the broken bond.

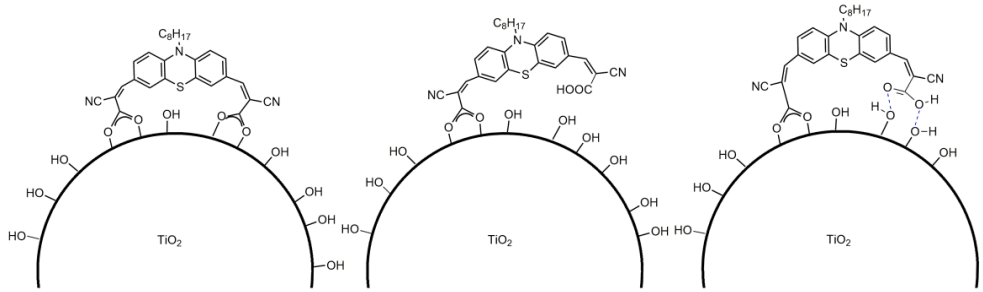

Figure 2.11: Hypothesized mechanism of cooperation among the anchoring units.

Although right now efficiencies of multi-branched structures are usually slightly higher or comparable with the mono-branched analogues, the main limitation is the lower photo-voltage because charge recombination is faster in multi-branched structures. For that reason a future appropriate investigation on the branched structures could generate high performances dyes, because, as it has been previously demonstrated, organic chemistry could help in finding the right balance and compromise to gain the best activities. Furthermore till now the rational modification on these dyes has followed faithfully the strategies of the mono-branched dyes, but it is not sure that the introduction of a known moiety has the same effect in mono- and di-branched dyes; also mono-branched systems are full of opposing results (e.g. the effect of electron withdrawing units in the π-spacer), thus a deeper research in multi-branched structures could hopefully show unexpected and pleasant results.

2.2 EVOLUTION OF TITANIUM DIOXIDE-BASED PHOTOCATALYSTS

In 1972 Honda and Fujishima published an article on water splitting using TiO_2 nanoparticles loaded with metallic platinum as catalytic active material.[91] Such experiment used UV irradiation and a little electric bias applied to ensure both H_2 and O_2 evolution. From the following years till nowadays research strongly studied semiconductors' chemistry and physics to discover materials suitable for water splitting application. Many photocatalysts have been developed, reaching the number of 130 semiconductors, including oxides, sulphides, nitrides and hydroxides.[92] A record quantum efficiency (QE) of 56% in H_2 production has been recorded for $NiO/NiTaO_3$ under deep UV irradiation.[93] However such a good system suffers for easy deactivation upon irradiation. A very long list of photocatalysts has been studied, but amongst them TiO_2 still plays a prominent role even if its activity and quantum efficiency are lower than many other materials. Some advantages, such as photostability, low impact on the environment, the low cost and the easy availability, must be considered during the development of a material that should be diffused worldwide.[94,95,96,97]

2.2.1 Mechanisms for Photocatalytic Water Splitting on Semiconductors

The working mechanism for photocatalytic water splitting is the same for all the semiconductors. Figure 2.12 represents schematically the principle of water splitting on TiO_2. E_g is defined as the energy gap between the lowest empty energy band (conduction band, CB) and the highest occupied energy band (valence band, VB). To be able to reduce protons to give molecular hydrogen, the CB potential must be more negative than the H^+/H_2 potential (0.0 V at pH = 0). Whereas to be able to oxidize water the semiconductor VB potential must be more positive than redox potential of the couple O_2/H_2O (1.23 V at pH = 0). From such values, a minimum energy gap of 1.23 eV/photon (or 237.11 kJ mol^{-1} corresponding to two electrons) is necessary and it could be generated by photons with $\lambda < 1000$ nm. Thus theoretically the 70% of solar photons could be employed for water splitting reaction;[98] but even in the best conditions some energy losses and overpotential must be accounted, thus a higher energy minimum could be envisaged. Most of the semiconductors show a larger bandgap than the minimum necessary to run the water splitting reaction. The working mechanism starts with the absorption of a photon with energy equal or higher than the energy gap, such absorption causes the formation of a e^-/h^+ couple; the charge separation (e^- in the CB and H^+ in the VB) is then followed by the charge

migration from the bulk to the surface and finally the real water splitting reaction can take place.

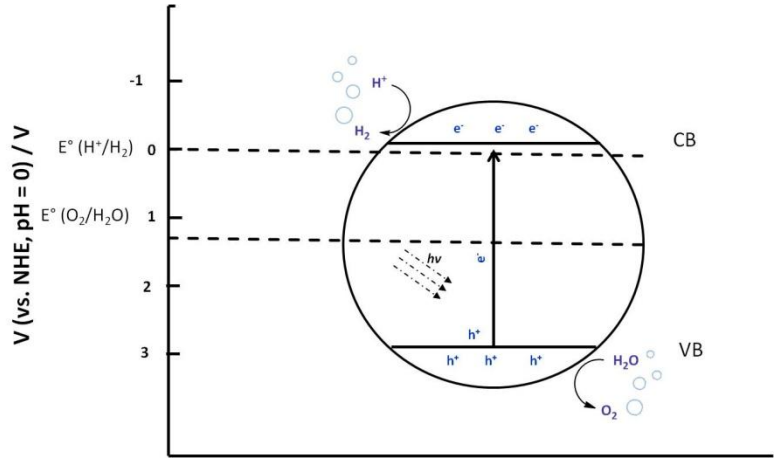

Figure 2.12: Water splitting mechanism on semiconductors.

Charge transport is a critical step and it is influenced by the crystallinity and the crystal structure of TiO_2: crystals with few defects reduce the probability of charge recombination, instead little particles have shorter paths for electrons to reach surface from the bulk. Thus little particles with high crystallinity should be the best choice, even though crystallinity affects activity more than particle size. A high surface area is desirable because more active sites are available, but at the same time photostability of the catalyst is negatively affected by high surface area because of destabilization due to high photo-charging, so a balance should be found.[99] Amongst different crystal structures of TiO_2, anatase and rutile are the most investigated ones, in the bulk energy gaps are 3.2 eV for anatase and 3.0 eV for rutile, corresponding to threshold wavelengths of 390 nm and 415 nm respectively. Even if optically rutile should be better thanks to a larger portion of solar spectrum absorbed, it is less active than anatase for "kinetic" reasons.[100] A more detailed explanation is given by electronic levels distribution, since the valence band of both anatase and rutile is situated at ca 3.0 V and it is originated from O2p orbital; instead the conduction band potential is mainly due to Ti3p and it is nearby NHE potential for rutile, while it is 0.2 V cathodically shifted for anatase, thus there is a higher driving force for water reduction for anatase. Moreover photocharges are found to be less mobile in rutile than anatase.[101] Figure 2.13 shows energy gaps of common semiconductors and a focus on anatase and rutile is given on the left.

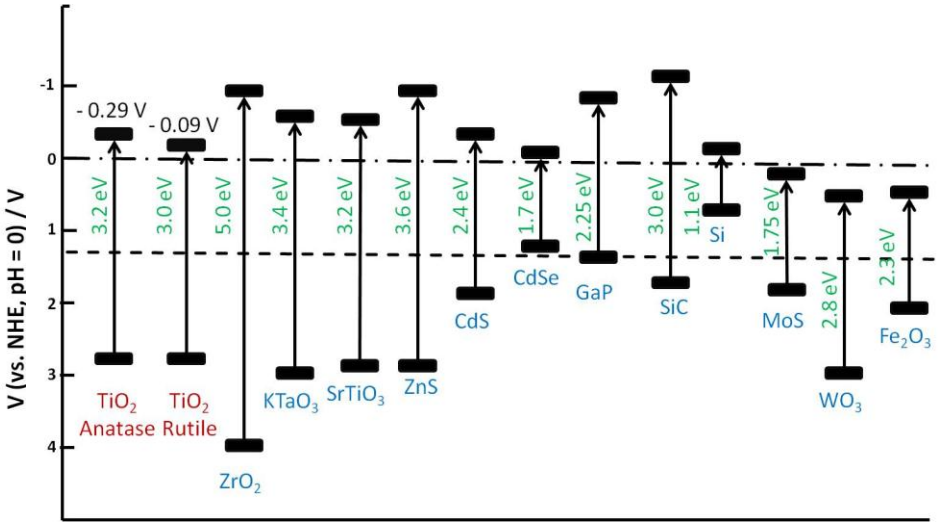

Figure 2.13: Energy bandgaps for the most common semiconductors studied for hydrogen production.

2.2.2 Limitations and Drawbacks of TiO_2 Alone

There are at least four disadvantages associated with the use of TiO_2: 1) TiO_2 has a large overpotential as water splitting catalyst, thus reaction on pure TiO_2 proceeds very slowly and with low yields;[102] 2) rapid charge recombination e^-/h^+ takes place, studies found that 90% of the photo-generated charges are bound to recombine;[103] 3) thermal backreaction between H_2 and O_2 to give H_2O is highly favored;[104] 4) TiO_2 is unable of absorbing visible light, only UV can be used so that a slight part of the solar spectrum can be harvested (UV covers 4-5% of the solar spectrum, while visible photons, 400 nm < λ < 700 nm, are 50%).[98] Many modifications have been developed to enhance TiO_2 activity and solve or limit its drawbacks. Not all the aspects will be covered by this thesis, only the ones related to the research developed will be considered. The three following paragraphs focused on the use of sacrificial electron donors or acceptors, noble metal loading to reduce overpotential, and sensitization as a way to enlarge the absorbed spectrum, with most of the attention dedicated to dye-sensitization.

2.2.3 Use of Sacrificial Electron Donor/Acceptor

Overall water splitting has been performed over many semiconductors but there are some drawbacks. First of all the two gases (H_2 and O_2) are produced in the same reactor, therefore gas separation is needed as additional treatment. Moreover in the

development of new systems, catalysts or sensitizers, it is useful to focus on one part of the overall reaction avoiding any dependence on kinetics and thermodynamics of the other semi-reaction. To do that, sacrificial electron donors or acceptors are largely used. In the presence of a sacrificial electron donor the photo-generated holes in the valence band of the semiconductor oxidized permanently the sacrificial agent instead of running the water oxidation, as can be seen in Figure 2.14. An analogous mechanism could be envisaged for the oxidation semi-reaction.[94]

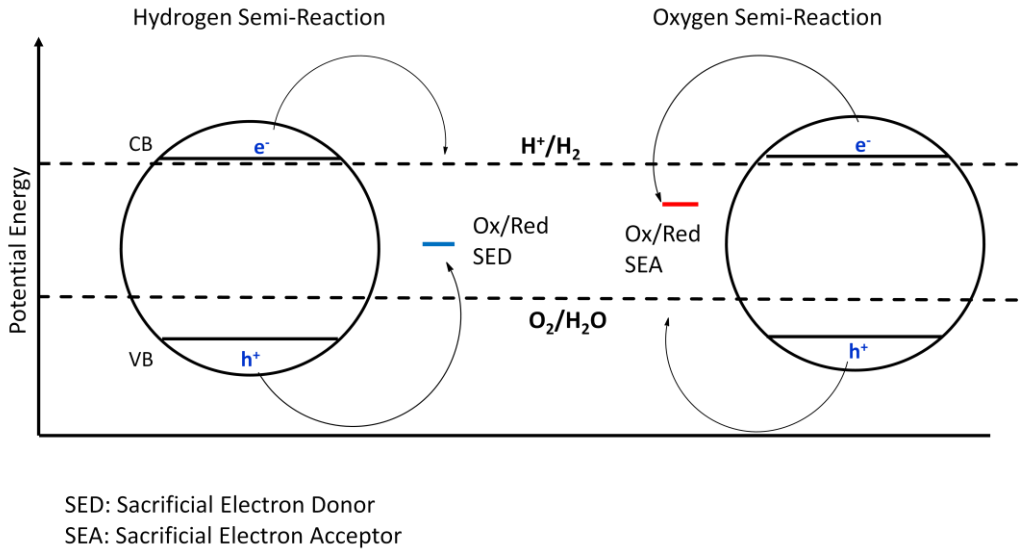

Figure 2.14: Sacrificial electron donor and acceptor mechanism.

It is important that the sacrificial agent is not able to thermally run the studied reaction and that after electron transfer in undergoes to a series of reactions that lead to the production of inert molecules. Attention will be focused on the sacrificial electron donors that can be classified into two categories: inorganic and organic molecules.[105] Amongst inorganic sacrificial electron donors S^{2-}, SO_3^{2-}, Fe^{2+}, Ce^{3+}, I^-, Br^-, and CN^- are the most used ones. Upon oxidation S_n^{2-}, SO_4^{2-}, Fe^{3+}, Ce^{4+}, I_3^- (in acid conditions otherwise IO_3^- in basic media), Br_2, and OCN^- are thus formed. H_2S could be considered an interesting option since, if bubbled in water solution (especially if basic), it generates protons for hydrogen production and S^{2-} that is a sacrificial electron donor of the reaction, and sulfidric acid could come from desulfuration process of petrochemical plants, therefore it could be considered a recycle of a side product of the oil refinery industry. This concept has attracted many research groups since the use of sacrificial donors could couple two beneficial effects, hydrogen

production as solar fuel and decomposition of polluting reagents.[106] This concept is even more important for the second class of sacrificial electron donors, organic molecules. Many alcohols (methanol, ethanol, isopropanol et cetera), aldehydes (formaldehyde, acetaldehyde et cetera), organic acids (formic acid acetic acid et cetera), amines (TEA and TEOA), or a combination (as in EDTA) could be employed in hydrogen production systems, allowing to couple fuel production to organic waste degradation in polluted water, if the final product of the sacrificial electron donor decomposition is CO_2. This is a side reason why we are interested in developing semi-reaction systems and not only the overall water splitting reaction. Methanol is by far the most investigated alcohol as electron donor and its first intermediate upon oxidation is formaldehyde that is more easily reduced to formic acid and finally to CO_2.[107] This concept opens the way to the use of biomass and other industrial wastes to produce clean hydrogen and simultaneously reclaiming waste water.[108,109,110,111] There is a connection between hydrogen production efficiency and the choice of the sacrificial electron donor, since studies in the literature highlighted the strong dependence of performances on the kinetics and thermodynamics of the sacrificial electron donor oxidation. For example TEOA is considered one of the best sacrificial donor since the kinetics of the transfer is fast thanks to an hypothesized interaction of the three OH groups with TiO_2 surface, while ascorbic acid, that should be a better sacrificial electron donor from the potential point of view, is instead of lower activity probably because of repulsion between ascorbate in solution and the partially negative charged surface of TiO_2.[112] Therefore the influence of the sacrificial electron donor is not only governed by the reduction potential but also on the kinetic barrier of the electron transfer process.

The two semi-reactions could be coupled in a Z-scheme manner (Figure 2.15) that reminds the natural photosynthetic approach. The two gases form in different positions (for example thanks to a membrane) with the advantage that no final gas separation is needed. Moreover through Z-scheme the coupling of the two semi-reactions is easier since there are less problems arising from the coupling of the two components and back electron transfers. The Z-scheme could imply the use of a redox shuttle to connect the two semi-reactions and amongst the possible couples the most promising ones are Fe^{2+}/Fe^{3+},[113] Ce^{3+}/Ce^{4+},[114] I^-/IO_3^-,[115] since they have the right potential to run both the semi-reactions in a proper way. Some examples avoiding the use of the redox couple are present in the literature, but the efficiency is quite lower hinting a pivotal role of the shuttle in the Z-scheme.[116]

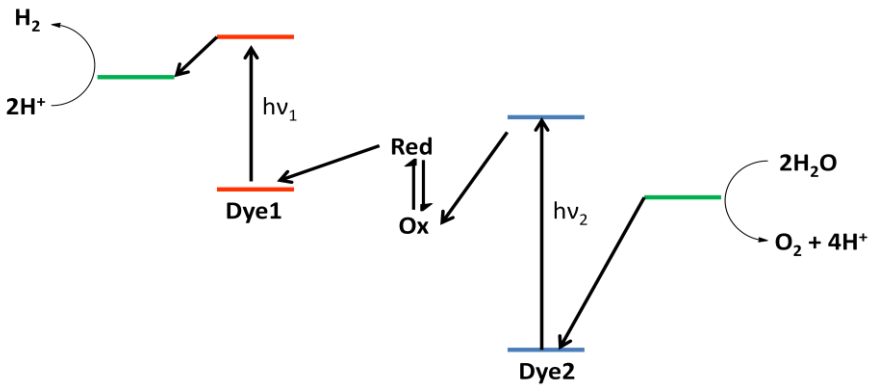

Figure 2.15: Z-Scheme for dye sensitized overall water splitting.

Many of the articles on dyes investigations, that will be illustrated in paragraph 2.3, reported how pH variations, dye concentration on TiO_2 surface, and suspension concentration of the overall composite affect the hydrogen production efficiency. pH is directly connected to both the stability of the system and the availability of protons on the surface to run proton reduction at the platinum center. The best pH for Pt/TiO_2 with TEOA as sacrificial electron donor seem to be around neutral, since acidic media could cause the detachment of the dye from the surface and protonation of the sacrificial electron donor (detrimental for the regeneration step since TEOA is no more a SED in the protonated form), on the contrary basic media affect stability of the ester bond between the dye and TiO_2 in the same way as acidic media and limit the concentration of protons available for reduction. This simple result is really important for future developments, when oxidation catalysts should be implemented since the final water splitting system should work well in neutral pH for simplicity reasons. The same behaviour has been found for dye concentration on nanoparticles surface, with an increase of efficiency increasing dye loading to reach a maximum of saturation of the active sites on the surface and then a decrease probably due to competition in light absorption and energy transfer. Moreover high concentration of dye on the surface could imply strong detrimental intermolecular energetic exchanges (detailed experimental investigations are reported in Refs. 150, 153, 155, 159, 160 of paragraph 2.3). Depending on dye structure and dimension, different optimal dyes concentrations have been found. Concerning the suspension concentration of nanoparticles, the same concept as dye loading can be applied, the maximum corresponds to a compromise to high light harvesting properties without

the limitation of light shielding and reduction of penetration depth typical of highly concentrated systems.

2.2.4 Noble Metal Loading: Platinum

Many noble metals can be used to lower the reaction overpotential and increase activity.[117] Amongst them platinum is the most used, showing the lowest overpotential and the best H_2 production activity.[118] Usually noble metals are even capable of reducing e^-/h^+ recombination, because they have Fermi levels that are lower than the one of TiO_2, thus electrons in the CB of TiO_2 are transferred to metals on the surface while holes stay in the TiO_2 VB.[119] The lowering of the overpotential for H_2 generation can be explained by analyzing work functions that are high in the case of noble metals, with Pt as the highest one (5.65 eV), while in the case of TiO_2 is only 4.2 eV.[120] Upon noble metal loading a Schottky barrier forms at the M/TiO_2 interface that pushes electrons from the bulk TiO_2 to the metal till thermodynamic equilibrium is reached (thus till the two Fermi levels are aligned).[102] Clearly the larger is the difference in work functions the stronger is the formed Schottky barrier. With a further exposition to light, photo-generated electrons cause a shift of the TiO_2 Fermi level generating a quasi-Fermi level, thus equilibrium is destroyed and electrons continue flowing to the metal.[121] Figure 2.16 shows a TiO_2 particle modified with both Pt as reduction catalyst and Ru_2O as example of oxidation catalyst.

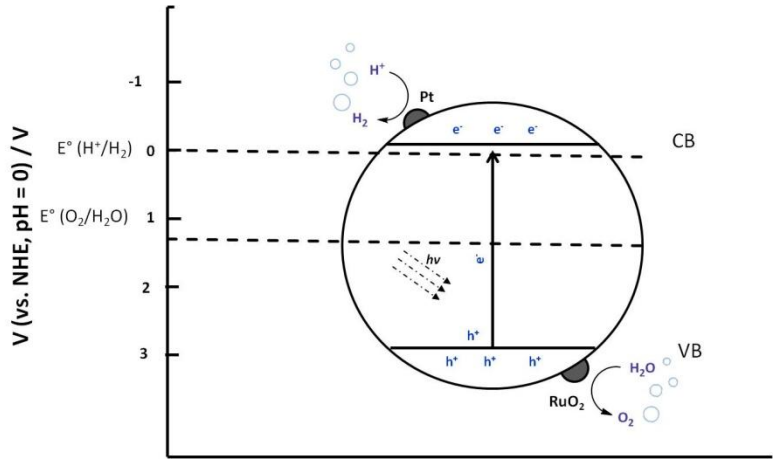

Figure 2.16: Water splitting process with noble metal loading (Ru_2O is an oxidation catalyst).

There are many methods for noble metal deposition, the most used ones can be classified in impregnation[122,123] and photodeposition methods.[124] Usually methods

belonging to the second class give better results in terms of activity, moreover they have other advantages such as less number of reaction steps, better control of particle size and dispersion (usually photodeposition is done at room temperature). Higher activities are associated to better surface contact between TiO_2 and the metal, while disadvantages of such a method are long terms irradiation with UV light at high intensity. Studies on activity showed that the best platinum loading is around 1.0%,[125] higher loading values interfere with the UV absorption of TiO_2, can deform the potential field of TiO_2, bringing h^+ near to the Pt/TiO_2 junction favoring thermal recombination to give water.[126] Regarding Pt particle size and dispersion it has been found that in the 0.5 – 10% range of loading values, particle sizes are more o less the same, even if theoretically smaller and highly dispersed particles should be more active.[127,128]

2.2.5 TiO_2 Sensitization

There are mainly two strategies to harvest visible light with TiO_2: band gap engineering by doping TiO_2 with metals and non-metals, so that the resulting E_g is lower than 3.0 – 3.2 eV, or surface sensitization with small bandgap semiconductors, dyes and noble metal nanoparticles. A brief focus on the second technique is here given, while review references are suggested for details on the first technique.[94,96] Small bandgap semiconductors and dyes sensitization work with the same mechanism (Figure 2.17 illustrates the energy levels requirements for a dye sensitized system). The strict condition is that conduction band of semiconductors should be at a more negative potential than the one of TiO_2, whereas for dyes the same requirement is valid for the LUMO level. The most used small bandgap semiconductor is CdS, that is used in combination with S^{2-} as sacrificial electron donor to avoid photo-corrosion of the material because of displacing S^{2-} with O^{2-}.[129,130,131] A detailed analysis of dyes will be given in paragraph 2.3.

An alternative sensitization technique is the use of Ag or Au nanoparticles to decorate TiO_2 surface. Such metals show surface plasmon absorption (SPA).[132] Depending on the size and the shape of the nanoparticles, different regions of the solar spectrum can be harvested, till potentially having the whole visible range covered.[133,134,135] Compared to the other sensitizers, such systems are more stable (no problem of photodegradation) and seem to be more powerful. Anyway noble metals utilization should be avoid in developing new materials, because their cost would hamper their diffusion.

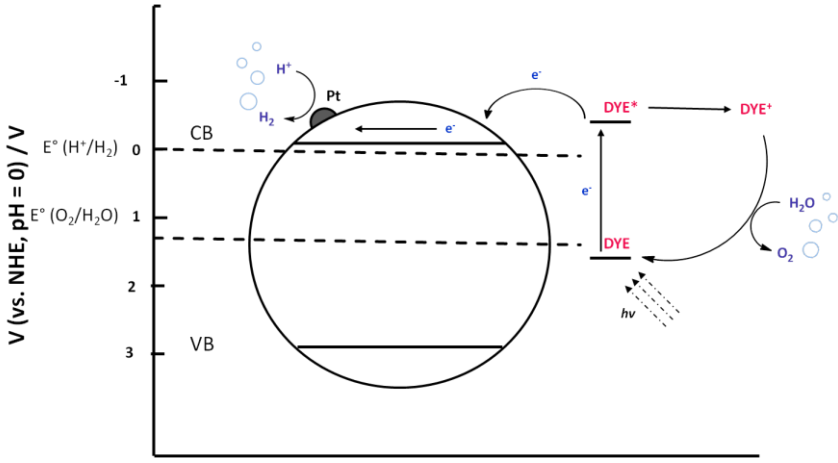

Figure 2.17: Dye-Sensitized TiO_2.

2.2.6 Evaluation of Performances: Efficiency Parameters

Performances in the case of hydrogen measurements are evaluated in a different way than in PV field.[94] The amount of hydrogen is typically measured and plotted vs. time, or elaborated in the form of rate of hydrogen production. The shape of hydrogen production graph gives an idea of stability of the system since, if the trend is different from the linear one, it means that there in an induction period for first hours of irradiation or deactivation pathways occur. This trend is even more evident if rate is calculated since the graph is not a line parallel to x-axis. There are some examples, especially when dye-sensitized composites are compared, in which it is convenient to normalize the amount of evolved gas or the evolution rate to the weight of the catalytic composite (e.g. $\mu mol\ h^{-1}\ g^{-1}$), taking care of comparing catalysts with similar loadings of dye (that is, active sites).

Compared to PV, all the parameters are referred to irradiation times because of the different nature of the measurements (efficiency values for tests over 2 h or 20 h could not be compared). The first parameter to evaluate the ability of a photocatalytic system to efficiently produce hydrogen is taken from the field of catalysis and it is Turnover Number (TON). Equation 2.4 illustrates the mathematical definition of the parameter and its “translation” in processable and measurable quantities; it is evident that TON should be higher than 1, since the amount of evolved hydrogen should be higher than the moles of dye molecules to have catalysis.

$$TON = \frac{number\ of\ reacted\ electrons}{number\ of\ active\ sites} = \frac{2\ \times moles\ of\ produced\ hydrogen}{moles\ of\ dye\ on\ the\ nanoparticles}$$

Equation 2.4: Turnover Number definition.

As already illustrated TON should be referred to irradiation period since it is dependent on the irradiation time (e.g. TON(5 h)). TON is also clearly related to the experimental arrangement, depending on the intensity of light source and the emission spectrum of the lamp (or the eventual presence of wavelength filters), thus the quantum yield (QY) becomes the actual parameter to compare different catalytic systems. The TON formula is modified to get the external (apparent) quantum yield (AQY) definition where the number of catalytic sites is replaced by the number of striking photons (Equation 2.5). As for the TON formula, the definition can be manipulated to get a correlation to measurable quantities, commonly used in photocatalytic experiments. This parameter is called Apparent Quantum Yield since not all the incident photons are actually absorbed and available for catalysis, and it can be interpreted as the equivalent of the external quantum efficiency in photovoltaics (also known as IPCE in the DSSC community).

$$AQY = \frac{number\ of\ reacted\ electrons}{number\ of\ incident\ photons} = \frac{2\ \times number\ of\ hydrogen\ molecules}{number\ of\ incident\ photons}$$

Equation 2.5: Apparent quantum yield definition.

Experimentally the number of incident photons must be measured, for instance by using a silicon photodiode placed in the photoreactor position. An additional advantage of this parameter is that it can be evaluated in case of monochromatic light (single wavelength irradiation) or when a portion of the spectrum is selected (band-pass filters). Thus it allows a proper comparison when dyes with different light harvesting properties are under investigation, usually a set of wavelengths or only the maximum in the Vis absorption spectrum are selected.

To overcome the problem of distinguishing the number of striking photons and the absorbed ones, the intrinsic or internal quantum yield (IQY) has been introduced (Equation 2.6), where the absorbed photons are used in place of the striking ones of AQY. The corresponding parameter in DSSC field for IQY is the APCE. Unfortunately the evaluation or measurement of the real absorbed photons is not an easy task because of light scattering of heterogeneous photocatalytic mixtures, thus this parameter is rarely used.

$$IQY = \frac{number\ of\ reacted\ electrons}{number\ of\ absorbed\ photons}$$

Equation 2.6: Internal quantum yield definition

It is evident that the measured AQY should be lower or at least equal (in the case of all the striking photons absorbed by the system) to IQY.

Another important parameter is Solar-to-Hydrogen Efficiency (STH) that is the analogue of PCE in DSSC field. STH is the efficiency of the system in converting the incoming solar energy into chemical energy of the hydrogen molecules (Equation 2.7).

$$STH\ (\%) = \frac{output\ energy\ as\ H_2\ (free\ Gibbs\ energy)}{input\ solar\ energy}$$

Equation 2.7: Solar to hydrogen efficiency definition.

An alternative and slightly different parameter to evaluate overall performances is the Light-to-Fuel Efficiency (LFE) expressed by Equation 2.8.

$$LFE\ (\%) = \frac{F_{H2} \times \Delta H°_{H2}}{S \times A_{irr}}$$

Equation 2.8: Light-to-Fuel Efficiency definition.

where F_{H2} is the flow of H_2 produced (mol s^{-1}), $\Delta H°_{H2}$ is the enthalpy associated with H_2 combustion (285.8 kJ mol^{-1}), S is the total incident light irradiance, (W cm^{-2}) and A_{irr} is the irradiated area (cm^2).

Regrettably STH and LFE are only rarely calculated in articles, while PCE is commonly reported for PV efficiency evaluation. A second drawback of STH over PCE is that it is dependent on the irradiation time (as all the other illustrated parameters), while PCE is univocally defined for a PV device. This disadvantage limits the ability of results comparisons that are meaningless unless the same irradiation time is used. Moreover typical reported values of STH are below (in most cases much below) 1%, although comparable to the low efficiency of the natural photosynthesis (<1%).[136] Comparison of very low values is probably the main reason why TON is generally the preferred parameter when describing the photocatalytic activity of these systems.

2.3 DYE-SENSITIZED HYDROGEN PRODUCTION: SENSITIZERS

Enhancement of visible light absorption through dyes has attracted attention of many research groups. Mainly because dye sensitization is at the basis of the working mechanism of DSSC (discussed in paragraph 2.1), thus exportation of all the know-how of that field into the H_2 production one seems to be an appealing plan. The working mechanism resembles the DSSC one as well with the exception that electrons in the TiO_2 conduction band are not transferred to an external circuit (electric energy), but to a catalyst able to generate H_2 (chemical energy). Figure 2.18 illustrates the two working mechanisms, shared features have been pointed out in violet.

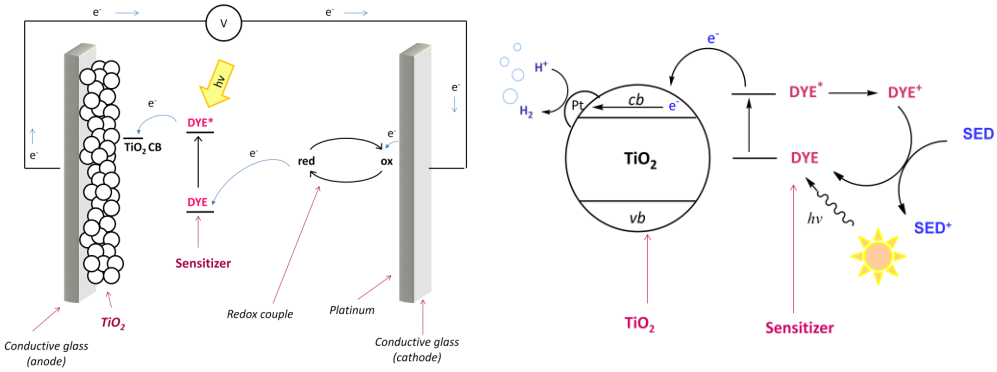

Figure 2.18: Comparison between the working mechanisms for electric and chemical energy production.

The reactions involved in H_2 production through dye-sensitized Pt/TiO_2 composite are described by the following processes:

$$Pt/TiO_2/Dye \xrightarrow{h\nu} Pt/TiO_2/Dye^* \quad (1)$$

$$Pt/TiO_2/Dye^* \longrightarrow Pt/TiO_2(e^-)/Dye^{+\cdot} \quad (2)$$

$$Pt/TiO_2(e^-)/Dye^{+\cdot} + SED \longrightarrow Pt/TiO_2(e^-)/Dye \quad (3)$$

$$Pt/TiO_2(e^-)/Dye \longrightarrow Pt(e^-)/TiO_2/Dye \quad (4)$$

$$Pt(e^-)/TiO_2/Dye + H^+ \longrightarrow Pt/TiO_2/Dye + 1/_2\ H_2 \quad (5)$$

$$Pt/TiO_2/Dye^* \longrightarrow Pt/TiO_2/Dye + h\nu \quad (6)$$

$$Pt/TiO_2(e^-)/Dye^{+\cdot} \longrightarrow Pt/TiO_2/Dye \quad (7)$$

Dye is responsible for light harvesting and it goes to an excited state upon the absorption of a photon **(1)**, a subsequent electron injection into the conduction band of TiO_2 takes place generating a charge separation **(2)**. To have an efficient process and high durability of the dye, fast regeneration from the sacrificial electron donor (SED) must take place **(3)** bringing the dye to the starting redox state. Electrons in the conduction band of TiO_2 are accumulated on Pt present on the surface **(4)** that is able to transform protons into molecular hydrogen **(5)**. Many other paths could be envisaged in the whole process, with two main steps responsible for loss in activity: relaxation of the dye that releases excitation energy without electron injection **(6)** or hole-electron recombination between TiO_2 and dye because of slow H_2 generation or dye regeneration **(7)**. Especially these two last reactions are responsible for most of the inefficiency of the whole process, thus their minimization is the aim to get high performances and durability of the system. Compared to DSSC field, dyes library is still very reduced, with few sensitizers tested, anyway a similar classification can be done, in fact dyes can be divided into three categories: metallorganic complexes (mainly ruthenium), dyes from natural cores and metal-free organic dyes.

Amongst metallorganic dyes, ruthenium complexes play the prominent role.[137,138,139,140,141] The high performances in DSSC pushed many researchers in testing them in H_2 production. In spite of the high performances in DSSC field, when applied in hydrogen production all the tested ruthenium complexes showed limited activity. Moreover when tested in comparison with organic dyes, usually less active than the ruthenium family in DSSC, the results are opposite with good activities for organic sensitizers, indicating that, even if the working mechanism is quite the same, the role of water and the whole system have different insights.

Few natural cores have been investigated,[142] with special attention given to the study on phtalocyanines made by Zang *et al.*[143,144] aimed at improving the ability of dyes at absorbing in the IR region. Such results should be underlined because promising H_2 production and dye stability have been recorded. The winning strategy is to synthesize asymmetric phtalocyanines, **Zn-*tri*-PcNc** (Figure 2.19), with a push-pull structure that is able to better generate charge separation compared to the symmetrical **Zn-*tetra*-Nc**. For this reason such dyes can be considered belonging to both the natural cores family (phtalocyanine core is very similar to porphyrinic one that is at the basis of chlorophyll molecules) and the organic dyes. As a matter of fact push-pull structures and directional electron transfer are typical features of this latter category even if no metal is present.

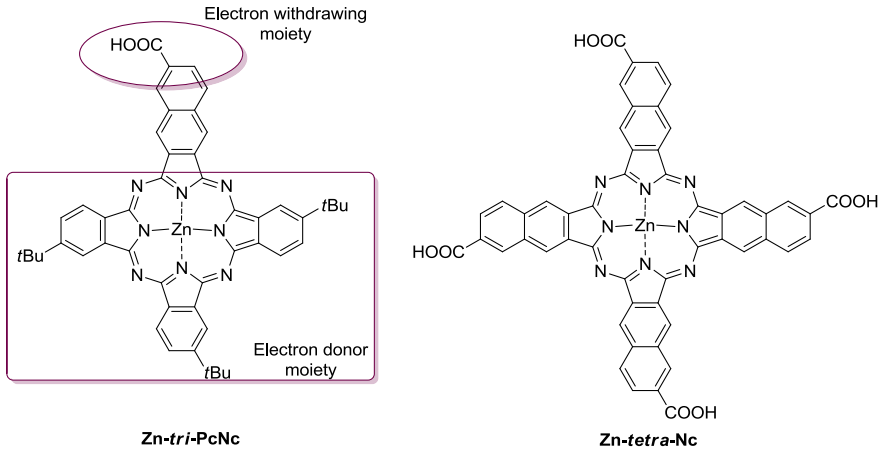

*Figure 2.19: Structure of phtalocyanine dye **Zn-tri-PcNc** compared to the symmetric tested one **Zn-tetra-Nc**, push-pull structure is outlined in violet .*

Amongst organic dyes the push-pull structure is the most common one. As known from DSSC (see paragraph 2.1), this skeleton is able to better generate charge separation. A more detailed discussion on organic dye structures tested will be given since dyes developed during this research belong to that class. But before going into details of push-pull structures, the emissive dyes will be illustrated first (Figure 2.20), with particular interest on the fluorescein eosin Y. Two working mechanisms have been proposed, one in which the dye accepts an electron while it is excited and then injects it into the CB of TiO_2 (i.e. thionine, nile blue A, and methylene blue) and the one in which the dye gives an electron upon excitation and goes to the oxidized form (i.e. eosin Y, rhodanine B, and safranin O).[145] Sensitizers belonging to the second class are found to be more active. The major limitation of emissive dyes is their low photo-stability because xanthenes rings can be easily hydrogenated in the H_2-Pt/TiO_2 environment leading to inactive unconjugated molecules. *Ortho*-dihydroxyl-antraquinone[146] derivatives such as Alizarin and Alizarin Red showed higher stability compared to the more common dyes eosin Y[147,148,149] and coumarin 343[146] in the strongly reducing environment present during irradiation. For these scaffolds the undesired hydrogenation reaction of the conjugated core leads to the formation of AQH_2 species that are inactive in anaerobic environment but they are able to recover the active form AQ by contact with oxygen, thus a temporary deactivation is achieved instead of a permanent degradation as in the case of eosin Y and coumarin 343.

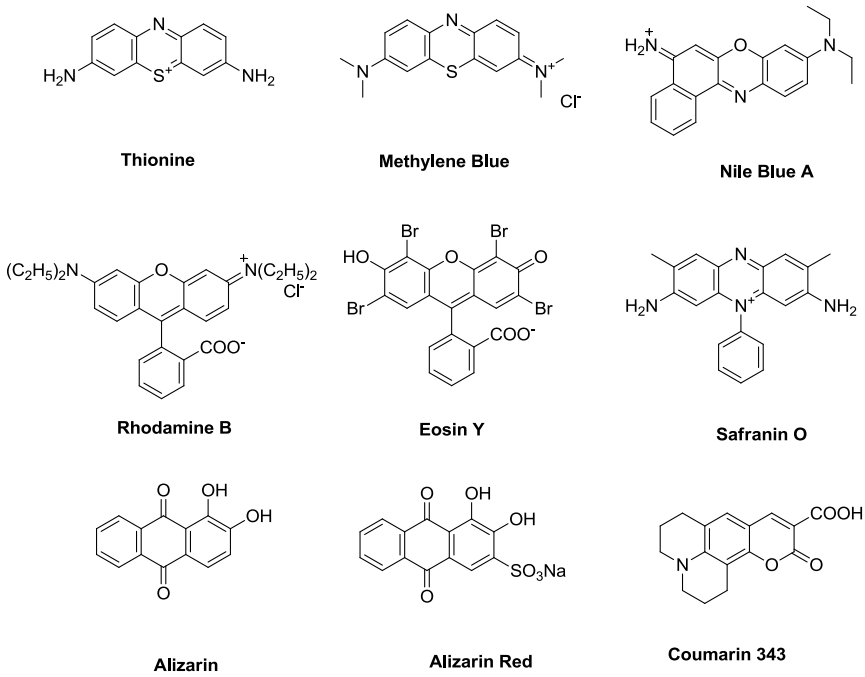

Figure 2.20: Emissive dyes.

Aside the fluoresceins case most of the organic dyes have a push-pull structure. The design approach of these dyes is the same as in the DSSC field, thus the rules are the ones already illustrated in paragraph 2.1.2. An overview on the more important papers on organic dyes tested over Pt/TiO_2 composite is now given.

In 2009 Park *et al.*[150] published a paper on triphenylamine dyes where the effect of the *para*-substituent of phenyl groups was studied. Being the aqueous medium the main difference from DSSC technology, hydrophilic chains of various lengths have been studied. As a matter of fact, most of the organic dyes are intrinsically hydrophobic, thus poor miscibility with water could influence conformation or behavior of the dye and consequently electron transfer and chemical steps involved in the whole process. They compared hydrophilic glycolic chains with different lengths, from hydrophobic H to hydrophilic CH_2-$(OCH_2CH_2)_3$-OCH_3 (Figure 2.21). The results showed an enhancement in performances increasing the length of the chain till **DEO1**-**DEO2** and a following decrease for **DEO3**, probably due to steric effects. Long chains indeed could also interfere in dye regeneration, shielding the core from the right interaction with the sacrificial donor. A second study with a similar approach tested the effects of changing hydrophilic chain position from the donor to

the spacer: **MO4D** (methoxymethyl groups both on donor group and on π spacer) has been investigated.[151] Chains on the spacer had a detrimental effect on activity, probably because solvent molecules organization around the dye is fundamental in the regeneration step and hydrophilic chains on spacer affect such phenomenon. When charge recombination times have been investigated through transient absorption spectra on TiO_2 films, this hypothesis has been confirmed. Except these two articles all the other tested dyes are hydrophobic.

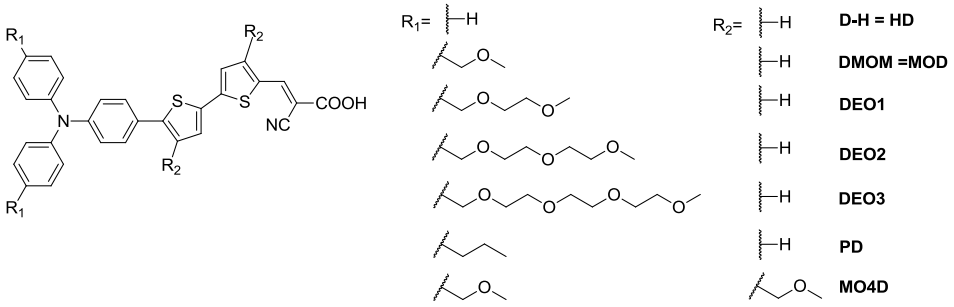

Figure 2.21: Hydrophilic dyes known in literature for H_2 production.

Phenothiazine core represent one of the most studied donor in the literature. Compared to other donor cores, phenothiazine is highly stable in the form of radical cation, paving the way for a good mono-electronic oxidation process, which is at the basis of photo-injection. The pioneer work by Son *et al.* investigated the influence on activity for various chain lengths (Figure 2.22).[152] Hydrophobic chains on phenothiazine nitrogen have been tested and better performances have been found for longer chains, probably thanks to the limitation of detrimental π-stacking of almost flat phenothiazine cores. In the ESI of the same article better activities of di-branched structures have been measured, compared to the mono-branched analogues, confirming the important role of good electron communication in the whole process. A second work dealing with the investigation of the chain length influence showed the same results, with the hexyl chain being the most beneficial in terms of hydrogen production compared to pentyl and butyl groups (Figure 2.22).[153] The beneficial effect of alkyl chains has been explained in both the role of de-aggregating groups, in lowering charge recombination rates and in driving molecules to the right orientation on TiO_2 surface. Benzo[b]phenothiazines, not so different cores from simple phenothiazines, have been used as well in mono-branched dyes to study the effect of π-spacer length on efficiency (Figure 2.22).[154] It is known from DSSC that longer π-spacers usually give better optical performances, and the higher

light harvesting properties could be translated to better photovoltaic performances, because spacer contributes to well separate donor and acceptor groups. Actually the best H_2 production performances have been measured for the dye bearing the longest π-spacer (**3**), moreover kinetic decay profiles showed a real high stability of such dyes in the radical cation form.

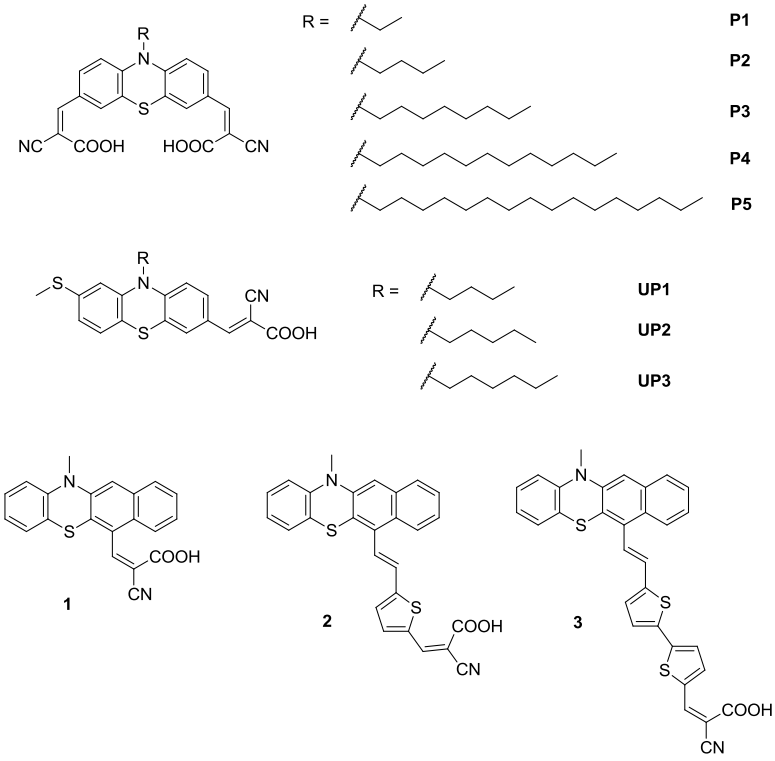

Figure 2.22: Phenothiazine dyes known in literature for H_2 production.

However, a part from the peculiar interest in phenothiazine dyes, one of the most investigated core is the triphenylaminic one as in DSSC field. Pal *et al.* studied the combined effects of modifying the π-spacer together with the donor core both in conjugation length and in the presence of de-aggregating butoxyl chains (Figure 2.23).[155] Butoxyl chains on the donor core have both the role of enhancing the donor character, de-aggregating dye molecules, and protecting the TiO_2 surface from the sacrificial electron donor, this modification has already been reported in the literature from Hagfeldt *et al.* in DSSC technology.[156] In their article Pal *et al.* found out a strong correlation between the light harvesting properties, the hydrogen production efficiencies, and good stability for **DN-F05** in recyclability tests.

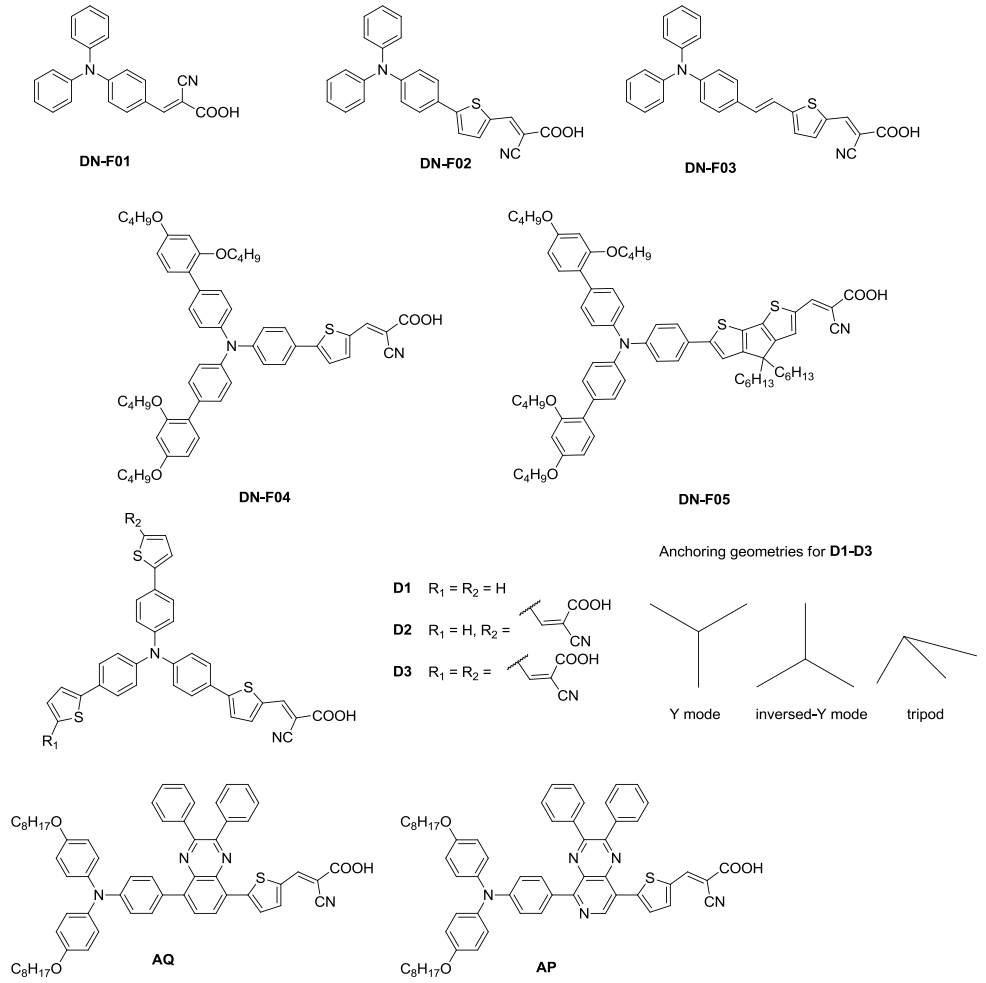

Figure 2.23: Triphenylamine dyes known in literature for H_2 production.

In the series **D1-D3** comparison between anchoring geometries (illustrated in Figure 2.23) and efficiency are screened.[157] The mono-branched dye resulted as the less active one with only one anchoring geometry (Y), while **D2** is able to be attached both in the Y mode and in the inversed-Y mode. The ratio between the two geometries for **D2** seems to be due to the kind of sacrificial electron donor used (TEOA favors the inversed Y, while EDTA competes in the anchoring and favors the binding with only one cyanoacrylic moiety). The most active dye is **D3** for which three anchoring geometries are possible (Y, inversed-Y, or tripod even though the last is unlikely), such flexibility is translated to the best performances of the series. Furthermore an original solution to enhance charge separation in triphenylamine dyes has been proposed by Tian *et al.*: modification of the ordinary D-π-A skeleton

has been performed by introducing an additional electron withdrawing group, such as quinoxaline (**AQ**) or pyrido[3,4-b]pyrazine (**AP**), resulting in a D-A-π-A sequence (Figure 2.23).[158] The additional acceptor group is supposed to stabilize the oxidized state of the dye and enhance light harvesting properties. Both dyes showed high stability and irradiation was continued till 10 h. **AQ** gave the best performances both in H_2 production and in DSSC, hinting that the knowledge about DSSC is still valid for H_2. Carbazole is a highly investigated donor core in DSSC literature but scantily in hydrogen production. The only example is from Pal *et al.* where a very simple structure as **AM** is compared to the DSSC highly performing **MK2** that bears four hexyl-thiophene moieties that have the role of both enhancing light harvesting and de-aggregating (Figure 2.24). [159] The results in hydrogen production confirmed **MK2** as better performing than **AM**, but the latter one is not so bad considering the easiness and cheapness of its synthesis. As a matter of fact they hypothesized a drawback for **MK2** dye that could suffer from some steric hindrance on TiO_2 surface that hampers the right protons flux on Pt nanoparticles to produce hydrogen.

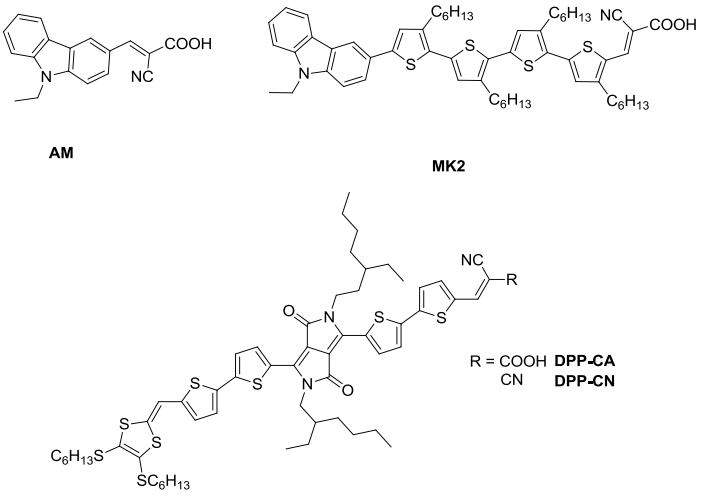

Figure 2.24: Carbazole dyes and DPP dyes know in literature for H_2 production.

The last example is a dithiafulvalene (DFT) donor together with diketopyrrolopyrrole (DPP) spacer derivative, a quite complex structure compared to all the other dyes reported in the literature (Figure 2.24).[160] The choice of DPP has been made for its high thermo- and photo-stability, necessary properties for hydrogen generation, while DFT is a good performing donor core in DSSC.[161,162] Singh *et al.* introduced malononitrile group as an alternative anchoring unit than cyanoacrylic acid, discovering that even if the interaction between TiO_2 and malononitrile is weaker (no

ester bond or other covalent bond can be formed) the electron injection occurs and the performances are better than the cyanoacrylic counterpart thanks to the higher electron withdrawing ability.

A prominent contribution in organic dyes investigation for hydrogen generation has been given by Abe *et al.* in the study of coumarin dyes (Figure 2.25) for overall water splitting system with a Z-scheme. They used $Pt/H_4Nb_6O_{17}$ as substrate for proton reduction and Ir_2O-Pt/WO_3 as substrate for oxygen evolution, together with I^-/I_3^- as redox shuttle to guarantee electrons circulation.[163] Their first tests focused on hydrogen generation and the best performing dyes were tested for the overall reaction (**NKX-2677** and **NXK-2697**). The investigated system is quite different from the Pt/TiO_2 composite present in the articles previously reported but, if attention is focused on the deduced information on organic dyes structures, significant results can be elaborated. The best performing dyes are the ones bearing the longer oligo-thiophene spacers that induced higher activity and stability in water. Such property can be investigated through electrochemical analysis such as CV run in water. Higher stability can be confirmed in CV spectra when a reversible current peak in the reverse cathodic scan in present, denoting that the oxidized state has a lifetime long enough to be regenerated by the redox couple. Such a property is not found in **C343**, **NKX-2311** and **NKX-2587**, meaning that their oxidized forms strongly react with water (or oxygen in overall water splitting experiments) giving photo-inactive species and pointing out the importance of designing the right π-spacer. Oligo-thiophenes seem to be one of the best choice with high photo-stability in water and high tolerance to O_2 due to their ability of delocalizing the positive charge of the oxidized form in the spacer, making the dye unreactive towards water and O_2.

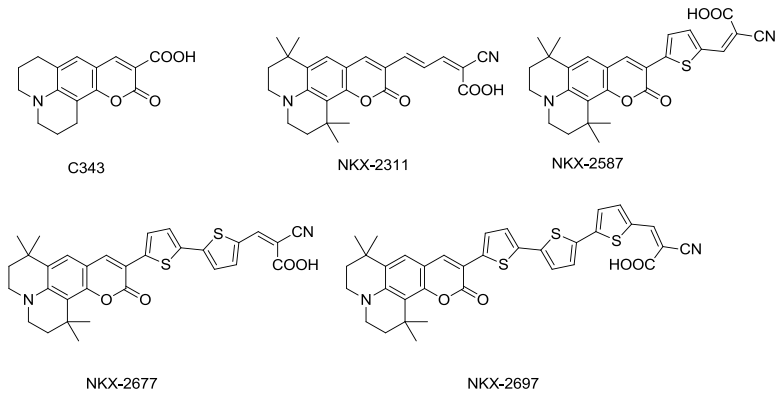

Figure 2.25: Coumarin dyes investigated for water splitting.

Table 2.1 summarizes all performances of organic dyes tested in literature. Since there is not always homogeneity in reported parameters, when possible, some data have been elaborated adapting general procedure elsewhere presented (such calculated data are indicated with *).

Table 2.1: Summary of dye performances in H_2 production from literature.

Name	Amount of dye (µmol/100 mg catalyst)	TON	SED	pH	Ref.
Zn-tri-PcNc	50	7565 (5 h) [a]	EDTA	3.6-3.8	143
Zn-tetra-PcNc	50	3153 (5 h)[a]	EDTA	3.6-3.8	143
Thionine	17.6	318 (20 h)[a]	TEOA	7	145
Methylene Blue	7.5	320 (20 h)[a]	TEOA	7	145
Nile blue A	7.9	462 (20 h)[a]	TEOA	7	145
Eosin Y	15.6	1773 (20 h)[a]	TEOA	7	145
Rhodamine B	11.1	1117 (20 h)[a]	TEOA	7	145
Safranine O	14.8	622 (20 h)[a]	TEOA	7	145
Alizarin	0.25	6326 (92 h)	TEOA	9	146
Alizarin Red	0.25	6342 (80 h)	TEOA	9	146
Eosin Y	0.25	104 (2 h)	TEOA	9	146
Coumarin 343	0.25	127 (2 h)	TEOA	9	146
D-H	1	270 (5 h)*[b]	EDTA	3	150
DMOM	1	570 (5 h)*[b]	EDTA	3	150
DEO1	1	730 (5 h)*[b]	EDTA	3	150
DEO2	1	800 (5 h)*[b]	EDTA	3	150

[a] Photocatalytic tests have been done on TiO_2 without Pt.
[b] TON values have been roughly elaborated from the graph reported in the article since no table with the precise data was present.

DEO3	1	530 (5 h)*[b]	EDTA	3	150
HD	10	8 (4 h)	EDTA	3	151
PD	10	5.4 (4 h)	EDTA	3	151
MOD	10	17 (4 h)	EDTA	3	151
MO4D	10	15 (4 h)	EDTA	3	151
P1	3	380 (5 h)	TEOA	7	152
P2	3	440 (5 h)	TEOA	7	152
P3	3	606 (5 h)	TEOA	7	152
P4	3	800 (5 h)	TEOA	7	152
P5	3	1026 (5 h)	TEOA	7	152
UP1	15	860 (10 h)	TEOA	7	153
UP2	15	1250 (10 h)	TEOA	7	153
UP3	15	1397 (10 h)	TEOA	7	153
1	1.95[c]	483 (16 h)	TEOA	7	154
2	2.75[c]	3510 (16 h)	TEOA	7	154
3	2.90[c]	4460 (16 h)	TEOA	7	154
DN-F01	10	954 (6 h)	TEOA	7	155
DN-F02	10	1400 (6 h)	TEOA	7	155
DN-F03	10	1432 (6 h)	TEOA	7	155
DN-F04	10	1466 (6 h)	TEOA	7	155
DN-F05	10	1864 (6 h)	TEOA	7	155
D1[d]	-[d]	60 µmol (90 min) [d]	TEOA	10	157

[c] Dye loading has been calculated through absorption spectra difference prior and after dye loading.

D2	-[d]	98 µmol (90 min) [d]	TEOA	10	157
D3	-[d]	111 µmol (90 min) [d]	TEOA	10	157
AQ	-[d]	~30 µmol (10 h)[d]	CH_3OH	-[e]	158
AP	-[d]	~13 µmol (10 h)[d]	CH_3OH	-[e]	158
AM	1[f]	6751 (6 h)	TEOA	7	159
MK2	1[f]	9051 (6 h)	TEOA	7	159
DPP-CA	2.5	6720 (10 h)	TEOA	7	160
DPP-CN	2.5	9664 (10 h)	TEOA	7	160

[d] There is no reference to the amount of photocatalyst or dye loading in the text. TON calculation is thus not possible, moles of evolved hydrogen have been reported for comparison.
[e] No reference to pH in the text.
[f] Nafion coated TiO_2/Pt nanoparticles have been used for hydrogen tests.

2.4 BIBLIOGRAPHY

1. B. O'Regan, M. Grätzel, *Nature*, **1991**, *353*, 737.
2. H. Gerischer, F. Willig, *Top. Curr. Chem.*, **1976**, *61*, 31.
3. C. M. Elliott, *Nat. Chem.* **2011**, *3*, 188.
4. M. D. McGehee, *Science,* **2011**, *334*, 607.
5. M. Grätzel, *Acc. Chem. Res.* **2009**, *42*, 1788.
6. B. E. Hardin, H. J. Snaith, M. D. McGehee, *Nature Photon.* **2012**, *6*, 162.
7. M. K. Nazeeruddin, E. Baranoff, M. Grätzel, *Sol. Energy* **2011**, *85*, 1172.
8. IDTechEx Research report "Dye Sensitized Solar Cells (DSSC/DSC) 2013–2023: Technologies, Markets, Players" (www.IDTechEx.com/dssc).
9. A. Hagfeldt, G. Boschloo, L. Sun, L. Kloo, H. Pettersson, *Chem. Rev.*, **2010**, *110*, 6595.
10. K. Kalyanasundaram, Dye-Sensitized Solar Cells, EPFL Press¸2010.
11. A. Kojima, K. Teshima, Y. Shirai, T. Miyasaka, *J. Am. Chem. Soc.*, **2009**, *131*, 6050.
12. EPFL Achieves 21% Efficiency for Perovskites, *Dyesol Laboratories*, 8 December **2015**.
13. P. G. Bomben, K. C. D. Robson, B. D. Koivisto, C. P. Berlinguette, *Coord. Chem. Rev.,* **2012**, *256*, 1438.
14. M. K. Nazeeruddin, C. Klein, P. Liska, M. Grätzel, *Coord. Chem. Rev.,* **2005**, *249*, 1460.
15. J.-F. Yin, M. Velayudham, D. Bhattacharya, H.-C. Lin, K.-L. Lu, *Coord. Chem. Rev.,* **2012**, *256*, 3008.
16. A. Abbotto, N. Manfredi, *Dalton Trans.*, **2011**, *40*, 12421.
17. A. Kay, M. Grätzel, *J. Phys Chem.*, **1993**, 97, 6272
18. M. Kimura, H. Nomoto, H. Suzuki, T. Ikeuchi, H. Matsuzaki, T. N. Murakami, A. Furube, N. Masaki, M. J. Griffith, S. Mori, *Chem. Eur. J.*, **2013**, *19*, 7496.
19. M.-E. Ragoussi, J.-J. Cid, J.-H. Yum, G. de la Torre, D. Di Censo, M. Grätzel, M. K. Nazeeruddin, T. Torres, *Angew. Chem. Int. Ed.*, **2012**, *51*, 4375.
20. M.-E. Ragoussi, J.-H. Yum, A. K. Chandiran, M. Ince, G. de la Torre, M. Grätzel M., M.K. Nazeeruddin, T. Torres, *ChemPhysChem*, **2014**, *15*, 1033.
21. T. Higashin, H. Imahori, *Dalton Trans.*, **2015**, *44*, 448.
22. M. K. Nazeeruddin, F. De Angelis, S. Fantacci, A. Selloni, G. Viscardi, P. Liska, S. Ito, B. Takeru, M. Grätzel, *J. Am. Chem. Soc.,* **2005**, *127*, 16835.
23. S. Mathew, A. Yella, P. Gao, R. Humphry-Baker, B. F. E. Curchod, N. Ashari-Astani, I. Tavernelli, U. Rothlisberger, M. K. Nazeeruddin, M Grätzel, *Nature Chem.,* **2014**, *6*, 242.
24. K. Kakiage, Y. Aoyama, T. Yano, K. Oya, J. Fujisawa, M. Hanaya, *Chem. Commun.*, **2015**, *51*, 15894.
25. Y. Ooyama, Y. Harima, *Eur. J. Org. Chem.*, **2009**, 2903.

26. M. Liang, J. Chen, *Chem. Soc. Rev.,* **2013**, *42*, 3453.
27. P. Kumaresan, S. Vegiraju, Y. Ezhumalai, S. Lin Yau, C. Kim, W.-H. Lee, M.-C. Chen, *Polymers*, **2014**, *6*, 2645.
28. H. Yan, P. Lee, N. R. Armstrong, A. Graham, G. A. Evmenenko, P. Dutta, T. J. Marks, *J. Am. Chem. Soc*., **2005**, *127*, 3172.
29. Organic Light-Emitting Materials and Devices, Second Edition, Edited by Z. R. Li, CRC Press, **2015**, Pages 309–488, doi: 10.1201/b18540-4.
30. Y. Shirota, *J. Mater. Chem.*, **2005**, *15*, 75.
31. Y Lin, Y. Li, X. Zhan, *Chem. Soc. Rev.*, **2012**, *41*, 4245.
32. G. L. Zhang, Y. Bai, R. Z. Li, D. Shi, S. Wenger, S. M. Zakeeruddin, M. Grätzel, P. Wang, *Energy Environ. Sci*., **2009**, *2*, 92.
33. S. Haid, M. Marszalek, A. Mishra, M. Wielopolski, J. Teuscher, J.-E. Moser, R. Humphry-Baker, S. M. Zakeeruddin, M. Grätzel, P. Bauerle, *Adv. Funct. Mater*., **2012**, *22*, 1291.
34. Z. J. Ning, Q. Zhang, W. J. Wu, H. C. Pei, B. Liu, H. Tian, *J. Org. Chem.*, **2008**, *73*, 3791.
35. J. Tang, J. Hua, W. Wu, J. Li, Z. Jin, Y. Long,H. Tian, *Energy Environ. Sci.*, **2010**, *3*, 1736.
36. S. Kim, J. K. Lee, S. O. Kang, J. Ko, J. H. Yum, S. Frantacci, F. D. Angelis, D. D. Censo, M. K. Nazeeruddin, M. Grätzel, *J. Am. Chem. Soc.,* **2006**, *128*, 16701.
37. H. Choi, I. Raabe, D. Kim, F. Teocoli, C. Kim, K. Song, J. H. Yum, J. Ko, M. K. Nazeeruddin, M. Grätzel, *Chem.–Eur. J.*, **2010**, *16*, 1193.
38. Y. Sun, K. Xiao, Y. Liu, J. Wang, J. Pei, G. Yu, D. Zhu, *Adv. Funct. Mater*., **2005**, *15*, 818.
39. M. Lu, M. Liang, H. Han, Z. Sun, S. Xue, *J. Phys. Chem. C*, **2011**, *115*, 274.
40. T. Horiuchi, H. Miura, K. Sumioka, S. Uchida, *J. Am. Chem. Soc*., **2004**, *126*, 12218.
41. B. Liu, Q. B. Liu, D. You, X. Y. Li, Y. Naruta, W. H. Zhu, *J. Mater. Chem.*, **2012**, *22*, 13348.
42. R. Chen, X. Yang, H. Tian, X. Wang, A. Hagfeldt, L. Sun, *Chem. Mater.*, **2007**, *19*, 4007.
43. K. Hara, M. Kurashige, Y. Dan-oh, C. Kasada, A. Shinpo, S. Suga, K. Sayama, H. Arakawa, *New J. Chem.*, **2003**, *27*, 783.
44. Z. S. Wang, Y. Cui, Y. Dan-Oh, C. Kasada, A. Shinpo, K. Hara, *J. Phys. Chem. C*, **2008**, *112*, 17011.
45. K. Hara, M. Kurashige, S. Ito, A. Shinpo, S. Suga, K. Sayama,H. Arakawa, *Chem. Commun.*, **2003**, 252.
46. Z. S. Wang, N. Koumura, Y. Cui, M. Takahashi, H. Sekiguchi, A. Mori, T. Kubo, A. Furube, K. Hara, *Chem. Mater.*, **2008**, *20*, 3993.
47. K. Kakiage, Y. Aoyama, T. Yano, T. Otsuka, T. Kyomen, M. Unno, M. Hanaya, *Chem. Commun.*, **2014**, *50*, 6379.
48. *Comprehensive Heterocyclic Chemistry* (Eds.: A. R. Katritzky, C. W. Rees), Pergamon, Oxford, UK, **1984.**

49. L. Levy, T. N. Tozer, L D. Tuck, D. B. Loveland, *J. Med. Chem.*, **1972**, *15*, 898.
50. C. J. Yang, Y. J. Chang, M. Watanabe, Y. S. Hon, T. J. Chow, *J. Mater. Chem*., **2012**, *22*, 4040.
51. H. Tian, X. Yang, R. Chen, Y. Pan, L. Li, A. Hagfeldt, L. Sun, *Chem. Commun.*, **2007**, 3741.
52. S. H. Kim, H. W. Kim, C. Sakong, J. W. Namgoong, S. W. Park, M. J. Ko, C. H. Lee, W. I. Lee, J. P. Kim, *Org. Lett*., **2011**, *13*, 5784.
53. H. Tian, X. C. Yang, J. Y. Cong, R. K. Chen, J. Liu, Y. Hao, A. Hagfeldt, L. C. Sun, *Chem. Commun*., **2009**, 6288.
54. T. Kitamura, M. Ikeda, K. Shigaki, T. Inoue, N. A. Anderson, X. Ai, T. Q. Lian, S. Yanagida, *Chem. Mater.*, **2004**, *16*, 1806.
55. D. P. Hagberg, T. Edvinsson, T. Marinado, G. Boschloo, A. Hagfeldt, L. C. Sun, *Chem. Commun.*, **2006**, 2245.
56. J. T. Lin, P. C. Chen, Y. S. Yen, Y. C. Hsu, H. H. Chou, P. M. C. Yeh, *Org. Lett*., **2009**, *11*, 97.
57. Y. M. Cao, N. Cai, Y. L. Wang, R. Z. Li, Y. Yuan, P. Wang, *Phys. Chem. Chem. Phys.*, **2012**, *14*, 8282.
58. C. Baldoli, S. Bertuolo, E. Licandro, L. Viglianti, P. Mussini, G. Marotta, P. Salvatori, F. De Angelis, P. Manca, N. Manfredi, A. Abbotto, *Dyes Pigm.*, **2015**, *121*, 351.
59. J. I. Nishida, T. Masuko, Y. Cui, K. Hara, H. Shibuya, M. Ihara, T. Hosoyama, R. Goto, S. Mori, Y. Yamashita, *J. Phys. Chem. C*, **2010**, *114*, 17920.
60. G. A. Sewvandi, . Chen, T. Ishii, T. Kusunose, Y. Tanaka, S. Nakanishi, Q. Feng, *J. Phys. Chem. C*, **2014**, *118*, 20184.
61. H. H. Chou, Y. C. Chen, H. J. Huang, T. H. Lee, J. T. Lin, C. T. Tsai, K. Chen, *J. Mater. Chem.*, **2012**, *22*, 10929
62. Z. M. Tang, T. Lei, K. J. Jiang, Y. L. Song, J. Pei, *Chem.–Asian J*., **2010**, *5*, 1911.
63. R. Katoh, A. Furube, S. Mori, M. Miyashita, K. Sunahara, N. Koumura, K. Hara, *Energy Environ. Sci.*, **2009**, *2*, 542.
64. L. Zhang, J. M. Cole*, ACS Appl. Mater. Interfaces*, **2015**, *7*, 3427.
65. E. Borgarello, K. Kiwi, E. Pelizzetti, M. Visca, M. Grätzel, *Nature*, **1981**, *289*, 158.
66. E. Galoppini, *Coord. Chem. Rev.*, **2004**, *248*, 1283.
67. D. G. Brown, P. A. Schauer, J. Borau-Garcia, B. R. Fancy, C. P. Berlinguette, *J. Am. Chem. Soc.*, **2013**, *135*, 1692.
68. Y. Ooyama, S. Inoue, T. Nagano, K. Kushimoto, J. Ohshita, I. Imae, K. Komaguchi, Y. Harima, *Angew. Chem. Int. Ed.,* **2011**, *123*, 7567.
69. W. R. McNamara, R. L. Milot, H. Song, R. C. Snoeberger, V.S. Batista, C. A. Schmuttenmaer, G. W. Brudvig, R. H. Crabtree, *Energy Environ. Sci.*, **2010**, *3*, 917.

70. C. Koenigsmann, T. S. Ripolles, B. J. Brennan, C. F. Negre, M. Koepfl, A. C Durrell, R. L. Milot, J. A. Torre, R. H. Crabtree, G. W. Brudvig, J. Bisquert, C. A. Schmuttenmaer, *Phys. Chem. Chem. Phys.*, **2014**, *16*, 16629.
71. T. Michinobu, N. Satoh, J. Cai, Y. Li, L. Han, *J. Mater. Chem. C*, **2014**, *2*, 3367.
72. T. Edvinsson, C. Li, N. Pschirer, J. Schoneboom, F. Eickemeyer, R. Sens, G. Boschloo, A. Herrmann, K. Mullen, A. Hagfeldt, *J. Phys. Chem. C*, **2007**, *111*, 15137.
73. S.-F. Li, X.-C Yang, M. Cheng, J.-H. Zhao, Y Wang, L.-C. Sun, *Tetrahedron Lett.*, **2012**, *53*, 3425.
74. L. Wang, X. Yang, S. Li, M. Cheng, L. Sun, *RSC Adv.*, **2013**, *3*, 13677.
75. J. Massin, L. Ducasse, T. Toupance, C. Olivier*, J. Phys. Chem. C*, **2014**, *118*, 10677.
76. J. Mao, N. He, Z. Ning, Q. Zhang, F. Guo, L. Chen, W. Wu, J. Hua, H. Tian, *Angew. Chem. Int. Ed.*, **2012**, *51*, 9873.
77. S. Ito, H. Miura, S. Uchida, M. Takata, K. Sumioka, P. Liska, P. Comte, P. Péchy, M. Grätzel, *Chem. Comm.*, **2008**, 5194.
78. B.-K An, W. Hu, P. L. Burn, P. Meredith, *J. Phys. Chem. C*, **2010**, *114*, 17964.
79. Y. Ooyama, T. Yamada, T. Fujita, Y. Harima, J. Ohshita, *J. Mater. Chem. A,* **2014**, *2*, 8500.
80. M. Zhang, J. Y. Liu, Y. H. Wang, D. F. Zhou, P. Wang, *Chem. Sci.*, **2011**, *2*, 1401.
81. S. M. Feldt, E. A. Gibson, E. Gabrielsson, L. Sun, G. Boschloo, A. Hagfeldt, *J. Am. Chem. Soc.*, **2010**, *132,* 16714.
82. J. -H. Yum, E. Baranoff, F. Kessler, T. Moehl, S. Ahmad, T. Bessho, A. Marchioro, E. Ghadiri, J. E. Moser, C. Yi, M. K. Nazeeruddin, M. Grätzel, *Nat. Commun.*, **2012**, *3*, 631.
83. A. Abbotto, N. Manfredi, C. Marinzi, F. De Angelis, E. Mosconi, J. H. Yum, X. X. Zhang, M. K. Nazeeruddin, M. Grätzel, *Energy Environ. Sci.* **2009**, *2*, 1094.
84. N. Manfredi, B. Cecconi, A. Abbotto, *Eur. J. Org. Chem.* **2014**, 7069 *and references therein*.
85. H. Zhang, J. Fan, Z. Iqbal, D.-B. Kuang, L. Wang, H. Meier, D. Cao, *Org. Electron.,* **2013**, *14*, 2071.
86. J. Liu, J. Zhang, M. Xu, D. Zhou, X. Jing, P. Wang, *Energy Environ. Sci.,* **2011**, *4*, 3021.
87. G. Wu, F. Kong, Y. Zhang, X. Zhang, J. Li, W. Chen, W. Liu, Y. Ding, C. Zhang, B. Zhang, J. Yao, S. Dai, *J. Phys. Chem. C,* **2014**, *118*, 8756.
88. R. Y.-Y. Lin, F.-L. Wu, C.-H. Chang, H.-H. Chou, T.-M. Chuang, T.-C. Chu, C.-Y. Hsu, P.-W. Chen, K.-C. Ho, Y.-H. Lo, J. T. Lin, *J. Mater. Chem. A,* **2014**, *2*, 3092.
89. S. S. Park, Y. S. Won, Y. C. Choi, J. H. Kim, *Energy Fuels,* **2009**, *23*, 3732.
90. W.-I. Hung, Y.-Y. Liao, C.-Y. Hsu, H.-H. Chou, T.-H. Lee, W.-S. Kao, J.-T. Lin, *Chem. Asian J.,* **2014**, *9*, 357.
91. A. Fujishima, K. Honda, *Nature*, **1972**, *238*, 37.
92. F. E. Osterloh, *Chem. Mater.***, 2008**, *20*, 35.

93. H. Kato, K. Asakura, A. Kudo, *J. Am. Chem. Soc.,* **2003**, *125*, 3082.
94. X. Chen, S. Shen, L. Guo, S. S. Mao, *Chem. Rev.,* **2010**, *110*, 6503 *and references therein*.
95. A. Kudo, Y. Miseki, *Chem. Soc. Rev.*, **2009**, *38*, 253 *and references therein*.
96. D. Y. C. Leung, X. Fu, C. Wang, M. Ni, M. K. H. Leung, X. Wang, X. Fu, *ChemSusChem*, **2010**, *3*, 681 *and references therein*.
97. Y. Ma, X. Wang, Y.Jia, X. Chen, H. Han, C. Li, *Chem. Rev.*, **2014**, *114*, 9987.
98. R. M. Navarro Yerga, M. Consuelo Àlvarez Galvàn, F. della Valle, J. A. Villoria de la Mano, J. L. G. Fierro, *ChemSusChem*, **2009**, *2*, 471.
99. X. Chen, S. S. Mao, *Chem. Rev.*, **2007**, *107*, 2891 *and references therein*.
100. M. V. Rao, K. Rajeshwar, V. R. P. Verneker, J. DuBow, *J. Phys. Chem.*, **1980**, *84*, 1987.
101. Y. V. Kolen'ko, B. R. Churagulov, M. Kunst, L. Mazerolles, C. Colbeau-Justin, *Appl. Catal. B.: Environ*., **2004**, *54*, 51.
102. A. L. Linsebigler, G. Q. Lu, J. T. Yates, *Chem. Rev.*, **1995**, *95*, 735.
103. D. E. Skinner, D. Philipp Colombo, J. J. Cavaleri, R. M. Bowman, *J. Phys. Chem.*, **1995**, *99*, 7853.
104 K. Yamaguti, S. Sato, *J. Chem. Soc. Faraday Trans. 1*, **1985**, *81*, 1237.
105. For detailed information about the literature tested sacrificial electron donors please refer to articles cited in paragraph 6.1 of REF. 94.
106. R. M. Navarro, M. C. Sanchez-Sanchez, M. C. Alvarez-Galvan, F. del Valle, J. L. G. Fierro, *Energy Environ. Sci*., **2009**, *2*, 35 *and references therein*.
107. C. R. López, E. P. Melián, J. A. O. Méndez, D. E. Santiago, J. M. D. Rodríguez, O. González Díaz, *J. Photochem. Photobiol. A: Chemistry*, **2015**, *312*, 45.
108. Y. Li, G. Lu, S. Li, *Chemosphere,* **2003**, *52*, 843.
109. T. Kawai, T. Sakata, *Nature*, **1980**, *286*, 474.
110. T. Kawai, T. Sakata, *Chem. Lett.*, **1981**, 81.
111. D. I. Kondarides, V. M. Daskalaki, A. Patsoura, X. E. Verykios, *Catal. Lett.*, **2008**, *122*, 26.
112. U. Pal, S. Ghosh, D. Chatterjee, *Transition Met. Chem.*, **2012**, *37*, 93.
113. T. Arai, M. Yanagida, Y. Konishi, H. Sugihara, K. Sayama, *Electrochemistry*, **2008**, *76*, 128.
114. E. A. Kozlova, T. P. Korobkina, A. V. Vorontsov, *Int. J. Hydrogen Energy*, **2009**, *34*, 138.
115. R. Abe, K. Sayama, K. Domen, H. Arakawa, *Chem. Phys. Lett.*, **2001**, *344*, 339.
116. Y. Sasaki, H. Nemoto, K. Saito, A. Kudo, *J. Phys. Chem. C*, **2009**, *113*, 17536.
117. R. Baba, S. Nakabayashi, A. Fujishima, K. Honda, *J. Phys. Chem.*, **1985**, *89*, 1902.
118. Y. Z. Yang, C. H. Chang, H. Idriss, *Appl. Catal. B: Environm.*, **2006**, *67*, 217.
119. M. Anpo, M. Takeuchi, *J. Catal.*, **2003**, *216*, 505.
120. H. B. Michaelson, *J. Appl. Phys.*, **1977**, *48*, 4729.

121. J. Bisquert, A. Zaban, P. Salvadors, *J. Phys. Chem. B,* **2002**, *106*, 8774.
122. J.-J. Zou, C.-J. Liu, K.-L. Yu, D.-G. Cheng, Y.-P. Zhang, F. He, H.-Y. Du, L. Cui, *Chem. Phys. Lett.*, **2004**, *400*, 520.
123. X. Fu, J. Long, X. Wang, D. Y. C. Leung, Z. Ding, L. Wu, Z. Zhang, Z. Li*, Int. J. Hydrogen Energy*, **2008**, *33*, 6484.
124. H. Yoshida, K. Hirao, J. I. Nishimoto, K. Shimura, S. Kato, H. Itoh, T. Hattori, *J. Phys. Chem. C*, **2008**, *112*, 5542.
125. X. J. Zheng, L. F. Wei, Z. H. Zhang, Q. J. Jiang, Y. J. Wei, B. Xie, M. B. Wei, *Int. J. Hydrogen Energy*, **2009**, *34*, 9033.
126. B. Sun, A. V. Vorontsov, P. G. Smirniotis, *Langmuir*, **2003**, *19*, 3151.
127. P. Pichat, M. N. Mozzanega, J. Disdier, J. M. Herrmann, *Nouv. J. Chim.*, **1982**, *6*, 559.
128. J. J. Zou, H. He, L. Cui, H. Y. Du, *Int. J. Hydrogen Energy*, **2007**, *32*, 1762.
129. J. S. Jang, S. H. Choi, H. G. Kim, J. S. Lee, *J. Phys. Chem. C*, **2008**, *112*, 17200.
130. H. Park, W. Choi, M. R. Hoffmann, *J. Mater. Chem.*, **2008**, *18*, 2379.
131. J. S. Jang, W. Li, S. H. Oh, J. S. Lee, *Chem. Phys. Lett.*, **2006**, *425*, 278.
132. P. V. Kamat, *J. Phys. Chem. B*, **2002**, *106*, 7729.
133. J. Yu, G. Dai, B. Huang, *J. Phys. Chem. C*, **2009**, *113*, 16394.
134. R. Jin, Y. Cao, C. Mirkin, K. Kelly, G. Schatz, J. Zheng, *Science*, **2001**, *294*, 1901.
135. E. Kowalska, R. Abe, B. Ohtani, *Chem. Commun.*, **2009**, 241.
136. J. Barber, *Chem. Soc. Rev.*, **2009**, *38*, 185.
137. W. J. Youngblood, S.-H. A. Lee, Y. Kobayashi, E. A. Hernandez-Pagan, P. G. Hoertz, T. A. Moore, A. L. Moore, D. Gust, T. E. Mallouk, *J. Am. Chem. Soc.*, **2009**, *131*, 926.
138. W. J. Youngblood, S.-H. A. Lee, K. Maeda, T. E. Mallouk, *Acc. Chem. Res.*, **2009**, *42*, 1966.
139. X. Zhang, U. Veikko, J. Mao, P. Cai, T. Peng, *Chem. Eur. J.*, **2012**, *18*, 12103.
140. E. Bae, W. Choi, J. Park, H. Suk Shin, S. Bin Kim, J. Sung Lee, *J. Phys. Chem. B*, **2004**, *108*, 14093.
141. Y. Gao, X. Ding, J. Liu, L. Wang, Z. Lu, L. Li, L. Sun, *J. Am. Chem. Soc.*, **2013**, *135*, 4219.
142. E. A. Malinka, G. L. Kamalov, S. V. Vodzinskii, V. I. Melnik, Z. I. Zhilina*, J. Photochem. Photobiol. A: Chemistry*, **1995**, *90*, 153.
143. X. Zhang, L. Yu, C. Zhuang, T. Peng, R. Li, X. Li, *RSC Adv.*, **2013**, *3*, 14363.
144. X. Zhang, L. Yu, C. Zhuang, T. Peng, R. Li, X. Li, *ACS Catal.*, **2014**, *4*, 162.
145. D. Chatterjee, *Cat. Commun.*, **2010**, 336.
146. Q. Li, Y. Che, H. Ji, C. Chen, H. Zhu, W. Ma, J. Zhao, *Phys. Chem. Chem. Phys.,* **2014**, *16*, 6550.

147. R. Abe, K. Hara, K. Sayama, K. Domen, H. Arakawa, *J. Photochem. Photobiol. A: Chemistry*, **2000**, *137*, 63.

148. Q. Li, Z. Jin, Z. Peng, Y. Li, S. Li, G. Lu, *J. Phys. Chem. C,* **2007**, *111,* 8237.

149. Z. Yan, X. Yu, Y. Zhang, H. Jia, Z. Sun, P. Du, *Appl. Cat. B*, **2014**, *160*, 173.

150. S.-H. Lee, Y. Park, K.-R. Wee, H.-J. Son, D. W. Cho, C. Pac, W. Choi, S. O. Kang, *Org. Lett.,* **2010***, 12*, 460.

151. W.-S. Han, K.-R. Wee, H.-Y. Kim, C. Pac, Y. Nabetani, D. Yamamoto, T. Shimada, H. Inoue, H. Choi, K. Cho, S. O. Kang, *Chem. Eur. J.,* **2012**, *18*, 15368.

152. J. Lee, J. Kwak, K. C. Ko, J. H. Park, J. H. Ko, N. Park, E. Kim, D. H. Ryu, T. K. Ahn, J. Y. Lee, S. U. Son, *Chem. Commun.*, **2012**, *48*, 11431.

153. A. Tiwari, I. Mondal, U. Pal, *RSC Adv.*, **2015**, *5*, 31415.

154. M. Watanabe, H. Hagiwara, A. Iribe, Y. Ogata, K. Shiomi, A. Staykov, S. Ida, K. Tanakaab, T. Ishihara, *J. Mater. Chem. A*, **2014**, *2*, 12952.

155. A. Tiwari, U. Pal, *Int. J. Hydrogen Energy*, **2015**, *40*, 9069.

156. X. Jiang, K. M. Karlsson, E. Gabrielsson, E. M. J. Johansson, M. Quintana, M. Karlsson, L. Sun, G. Boschloo, A. Hagfeldt, *Adv. Funct. Mater.,* **2011**, *21*, 2944.

157. S. K. Choi, H. S. Yang, J. H. Kim, H. Park, *Appl. Cat. B: Environ.*, **2012**, *121*, 206.

158. X. Li, S. Cui, D. Wang, Y. Zhou, H. Zhou, Y. Hu, J.-G Liu, Y. Long, W. Wu, J. Hua, H. Tian, *ChemSusChem,* **2014**, *7*, 2879.

159. A. Kumari, I. Mondal ,U. Pal, *New J. Chem.*, **2015**, *39*, 713.

160. K. Narayanaswamy, A. Tiwari, I. Mondal, U. Pal, S. Niveditha, K. Bhanuprakash, S. P. Singh, *Phys. Chem. Chem. Phys.*, **2015**, *17*, 13710.

161. K. Guo, K. Yan, X. Lu, Y. Qiu, Z. Liu, J. Sun, F. Yan, W. Guo and S. Yang, *Org. Lett*., **2012**, *14*, 2114.

162. Z. Wan, C. Jia, Y. Duan, X. Chen, Y. Lin and Y. Shi, *Org. Electron.*, **2013**, *14*, 2132.

163. R. Abe, K. Shinmei, K. Hara, B. Ohtani, *Chem. Commun.*, **2009**, 3577.

Chapter 3

ORGANIC DYES FOR PHOTO-CATALYTIC H_2 PRODUCTION:

TUNING PERFORMANCES THROUGH DYE DESIGN

Effect of Molecular Design on Donor, Spacer or Acceptor units

on Phenothiazine Dyes

Something about you,

you're like a diamond in the way you catch the light

The way you catch the light

Donavon Frankenreiter

3.1 OBJECTIVES OF THE RESEARCH

The central task of this PhD research has been the investigation of structure/activity relationships of phenothiazine dyes in photocatalytic production of hydrogen. Phenothiazine dyes have attracted the attention of many research groups in the DSSC field[1,2,3,4] and in hydrogen production as well (as illustrated in paragraphs 2.1.2 and 2.3). Phenothiazine is a peculiar donor core amongst the arylamine moieties, with a butterfly and non-planar conformation bent along the N-S axis. This feature is fundamental in avoiding planar geometries that are at the basis of detrimental intermolecular quenching mediated by the aggregates on the TiO_2 surface. Phenothiazines are considered promising donor cores thanks to the high stability of their radical cation form compared to the widespread triphenylamine derivatives.[5] High stability of the dye in the oxidized form is a necessary prerequisite for photocatalytic hydrogen production since the research is currently addressed to the reduction semi-reaction but the oxidation semi-reaction should be joined in a overall water splitting system in the future; therefore a stable radical cation is necessary to be interfaced with "slow" oxidation catalysts (in comparison with sacrificial electron donors). Moreover the symmetric structure of phenothiazine is ideal to develop di-branched dyes through functionalization of the two benzene rings, while the nitrogen atom could be functionalized with moieties able to tune conjugation or other properties of the dye, e.g. de-aggregating, peculiar solubility in specific media, or affinity to bio-inspired molecules.

The research started from a reference compound, **PTZ1** (named P3 in REF.6), used as standard to observe the effect of structural modification on dye skeleton. **PTZ1** has been taken as reference amongst dyes known in the literature because it has a simple and di-branched structure. Molecular modifications regarding almost all the parts of the dye have been investigated, synthetic approaches to reach the desired structures have been followed by optical and electrochemical characterization to screen the potential light harvesting properties of dyes as well as the energetic levels. DSSC characterization has been additionally carried out to try to sort out some general rules to compare photovoltaic performances to hydrogen production to see if common assumptions for the former category could be exported to the emerging field of solar hydrogen. In case of mismatching between cell performances and photocatalytic hydrogen production, hypotheses could anyway be elaborated pointing out the main differences between the two fields of application. The molecular design started with the observation of the strength and limiting features of

the reference dye, all the modifications on the molecular design are depicted in Figure 3.1. The dye skeleton is simple giving large possibility of improvement on the light harvesting properties, it is composed of the minimum moieties to have a dipolar molecule, a donor and an acceptor. From the DSSC field we know that the presence of π-spacers has key role in light absorption, charge separation and dye stability (see paragraph 2.1). Therefore the first kind of modification has been the introduction of well widespread π-spacers bearing thiophene units. Secondly the donor core is highly hydrophobic because of the aromatic structure and the presence of an octyl chain that could be a limitation for the performances in aqueous media such as the TEOA mixture used in hydrogen production; thus one of spacer-developed dyes (**PTZ2**) has been modified through the introduction of hydrophilic moieties to improve surface wettability in aqueous media. Lastly the anchoring unit has been modified with hydroxamic acid instead of the widespread carboxylic one to improve stability in TiO_2 anchoring toward hydrolysis in the presence of water.

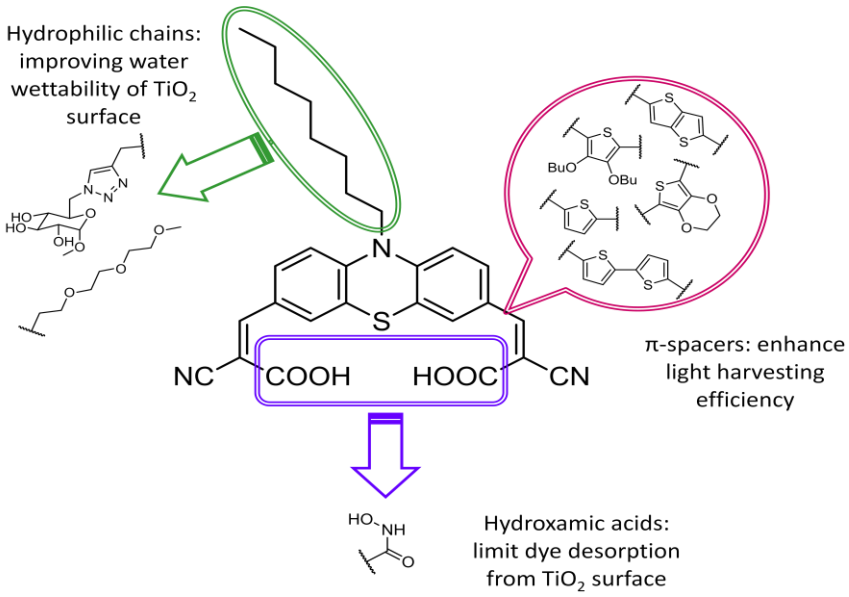

*Figure 3.1: Modifications on the reference dye **PTZ1** developed in this thesis.*

All the investigated changes will be illustrated in details in the following paragraphs with a detailed overview on the kind of modification, the synthetic routes and the eventual troublesome steps, optical and electrochemical characterization, DSSC screening of performances, and hydrogen production tests (unfortunately still in progress for the hydroxamic acid derivative). Depending on the kind of investigated

performances, additional characterizations (such as dye photostability upon irradiation, water contact angles, desorption measurements of dye stability towards hydrolysis) will be presented. Collaborations with different research groups have been necessary for a complete characterization, therefore electrochemical measurements have been performed in collaboration with Prof. Riccardo Ruffo from the University of Milan Bicocca, while hydrogen measurements have been done in collaboration with the group of Prof. Paolo Fornasiero from the University of Trieste. Concerning the synthetic issues we collaborated with the group of Prof. Francesco Peri from the University of Milan Bicocca for the introduction of hydrophilic moieties, while we collaborated with the group of Dr. Alessandro Mordini from the University of Florence and CNR Department in Florence (ICCOM) for the development of water stable anchoring groups.

3.2 ENHANCING OPTICAL PROPERTIES AND PHOTOSTABILITY: Π-SPACER

The first modification interested the central π-spacer core of the dye since the reference system **PTZ1** has no conjugated moiety separating the donor from the acceptor unit. Mono- and poly-cyclic simple and fused thiophene derivatives have been systematically introduced in between phenothiazine core and cyanoacrylic group. Since barely investigation regarding the π-spacer is currently available for dyes employed in dye-sensitized hydrogen production, we decided to investigate further. One of the most interesting articles regarding dye photo-stability in hydrogen production pointed out the supreme role of thiophene rings as stabilizers of the positive charge arising after electron injection.[7] The choice of the spacers have been done following the most widespread choices in the DSSC literature. Sulfur-containing spacers, particularly if deriving from thiophene ring, are promising candidates thanks to their peculiar structural and electronic condition, due to the π-excessive heteroaromatic nature. Indeed the resonance energy of thiophene ring is lower than in benzene, therefore easy charge transfer is supposed to occur across these rings, moreover they are stable and have a high structural versatility and easiness of manipulation in comparison to other five-membered heterocycles (e.g. furan or pyrrole).[8,9] Hydrophobic octyl chain has been kept on the phenothiazine nitrogen that is supposed to prevent intermolecular aggregation, and cyanoacrylic acid as anchoring and acceptor unit. The introduction of a spacer has two effects, the first one is an enhancement of visible light harvesting, while the second one is the improvement of photo-stability, a feature regrettably still scantly investigated in dyes for photocatalytic hydrogen production. In order to evaluate the eventual photo-stability of the new designed dyes, irradiation and hydrogen measurements have been kept till 20 h contrary to the widespread 5 h or little longer times typically reported.[6,10,11,12,13,14,15,16] Moreover an investigation on the reasons of the decrease of hydrogen activity has been done since many articles showed that problem without going further in the investigation.

The first designed dye is **PTZ2** bearing a simple thiophene ring that could be a good candidate to enhance light harvesting by both red-shifting and enhancing the absorption, still keeping the synthetic pathway easy, short, and cheap. The inclusion of more elaborated heteroaromatic moieties such as the rigid and cyclofused thienothiophene (**PTZ3**) or bisthiophene (**PTZ4**) has been done to see if further tuning of the optical properties was possible and the eventual beneficial presence of a highly stable group as thienothiophene.[17,18,19] Further modifications did not regard

the conjugated path in the π-spacer but the decoration of the thiophene ring with electron-rich oxygenated groups, in order to study eventual influence in electronic communication of the dye with TiO_2, such as electron injection efficiency. Moreover de-aggregating effects have been studied through the introduction of alkyl chains that are known to suppress molecular π-stacking that leads to detrimental intermolecular energy transfers. As a matter of fact phenothiazines could easily stack up one on the other. For that purpose butoxyl chains have been introduced on **PTZ2** in order to get **PTZ5**, where the cumulative effect of oxygenated and bulky chains can be investigated,[20,21] while the oxygen effect without any contribution from de-aggregating chains has been studied with **PTZ6**.[22] The designed dyes are depicted in Figure 3.2.

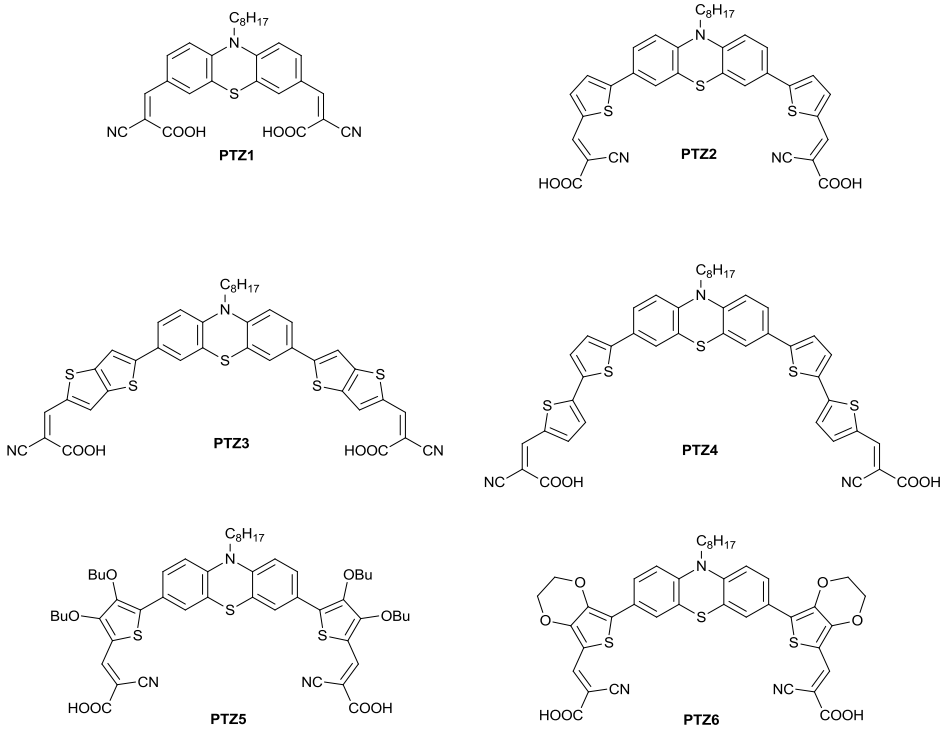

Figure 3.2: Designed dyes to improve optical properties.

3.2.1 Synthetic Strategy

Reference dye **PTZ1** has been synthesized according to the literature procedure starting from 10*H*-phenothiazine that is commercially available (Scheme 3.1).[6] Alkylation on the phenothiazine nitrogen is performed under basic conditions thanks

to NaH and bromo-octane is used as alkylating agent to get molecule **1**. Formylation under Vilsmeier-Haack conditions gave aldehyde **2** that is transformed into the cyanoacrylic acid through Knoevenagel condensation in basic conditions.

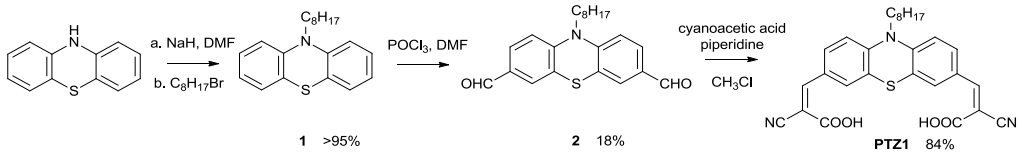

*Scheme 3.1: Synthetic route to afford **PTZ1**.*

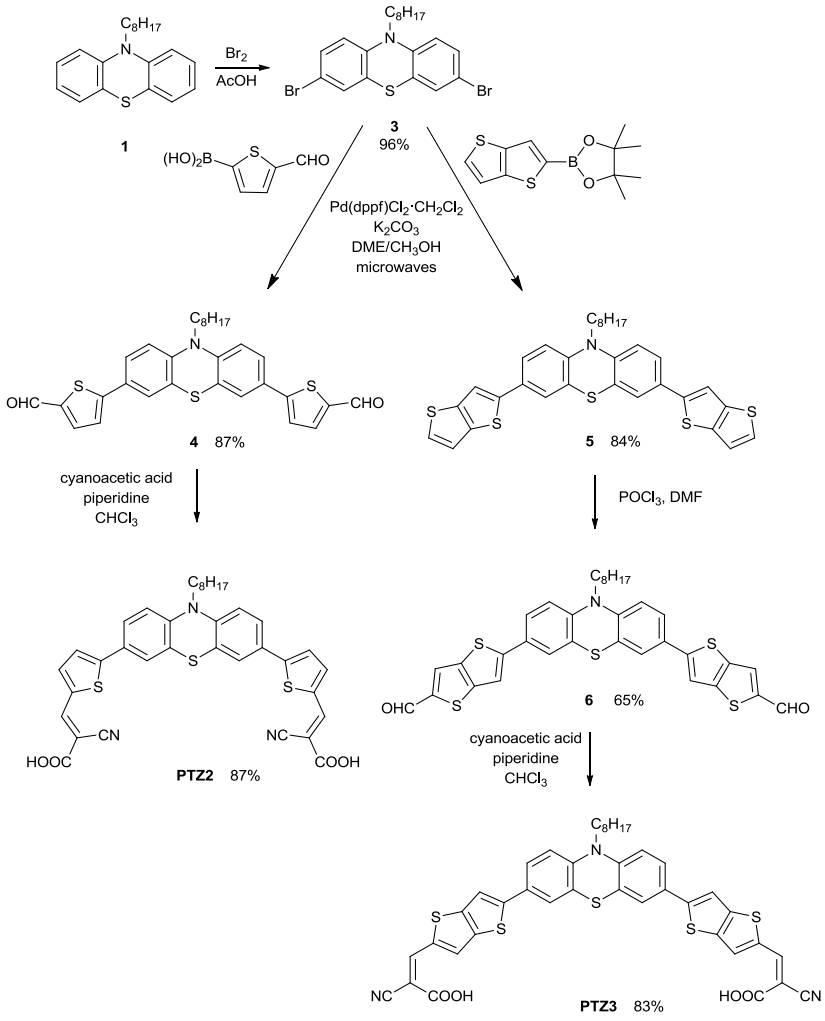

*Scheme 3.2: Synthetic routes to afford **PTZ2-3**.*

For the synthesis of the designed dyes **PTZ2-6**, dibromo-derivative **3** is the central intermediate. Bromination with N-bromosuccinimide (NBS) gave very low yields probably because of the radical mechanism that is hampered by radical stabilization of the phenothiazine core, while bromination with Br_2 in acetic acid gave the desired product in high yield.[23,24] The synthetic pathways for **PTZ2** and **PTZ3** consist in a Suzuki-Miyaura cross coupling reaction[25,26] (catalytic cycle in Annexes) between molecule **3** and 5-formyl-2-thienylboronic acid, or 4,4,5,5-tetramethyl-2-(thieno[3,2-b]thiophen-2-yl)-1,3,2-dioxaborolane respectively. The dioxaborolane of thienothiophene has been synthesized according to literature conditions with *n*BuLi.[27] In the case of the simple thiophene unit the intermediate has already the formyl group, while for **PTZ3**, formylation of **5** is done in Vilsmeier-Haack conditions. The final Knoevenagel condensation in basic conditions because of piperidine gave **PTZ2-3** with good overall yields. The synthetic routes are illustrated in Scheme 3.2.

In the case of **PTZ4-6** the spacer moieties were not currently commercially available or of easy synthesis, thus a semi-convergent method has been employed introducing the boronic ester groups on the phenothiazine core while the spacers containing both formyl group and halogen for coupling were prepared independently.

In that way the double steps necessary to develop di-branched structures are limited to the Suzuki-Miyaura cross-coupling and the Knoevenagel condensation. Boronic functionalities were introduced on phenothiazine core through lithium-halogen exchange with *n*BuLi and quench with 2-isopropoxy-4,4,5,5-tetramethyl-1,3,2-dioxaborolane giving the intermediate **11**.[28] The spacer precursors **7**, **9**, and **10** have been synthesized following literature procedures in the case of bithienyl[29] and EDOT,[30] while for the dibutoxyl intermediate an adapted procedure from the one of EDOT has been employed. A first trans-etherification reaction occurs between 3,4-dimethoxythiophene and butanol in the presence of *p*-toluensulfonic acid,[31] formylation in position 2 is done with *n*BuLi addition and DMF quench, followed by bromination with NBS to introduce the halogen atom in position 5. All the corresponding intermediates have been treated in microwave assisted Suzuki-Miyaura cross coupling together with boronic ester **11**. The resulting aldehydes have been transformed into the corresponding cyanoacrylic acids under Knoevenagel condensation with cyanoacetic acid and piperidine. The synthetic routes are illustrated in Scheme 3.3, while the experimental details of the synthesis are reported in paragraph 3.5.

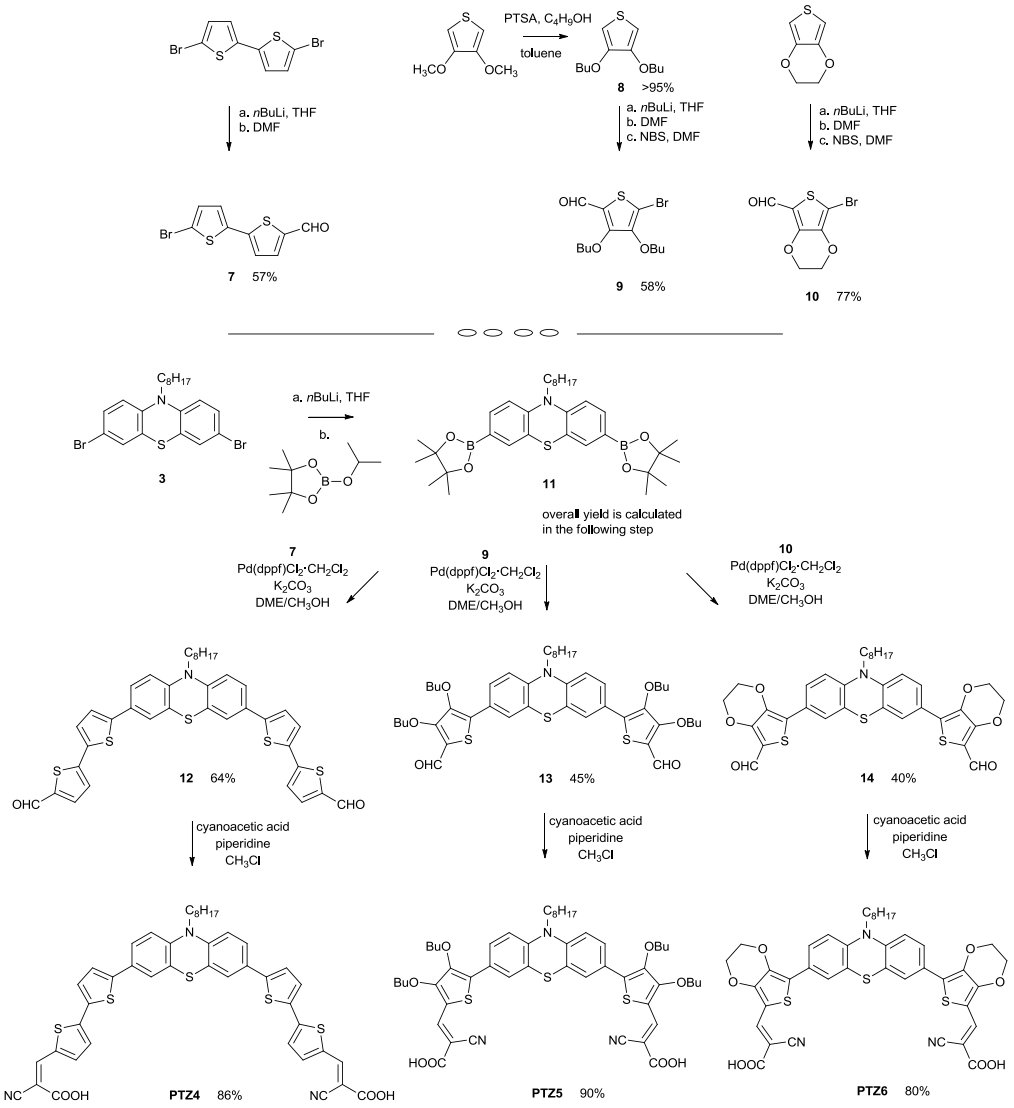

*Scheme 3.3: Synthetic routes to afford **PTZ4-6**.*

3.2.2 Optical and Electrochemical Characterization

Optical spectroscopy is the first step of dye characterization and it is performed recording UV/Vis and fluorescence spectra. The used solutions contain a known concentration of dye so that Lambert-Beer law might be applied to calculate the molar extinction coefficient (ε).

$$A = \varepsilon \times b \times c$$

Where *A* is the measured absorbance, *b* is the cell path (in cm) and *c* is the concentration expressed in molarity. There are two parameters that directly indicate the light harvesting properties of a dye: the maximum of absorption (λ_{max}) and the molar extinction coefficient (ε). The second parameter is directly related to the amount of photons that the dye is able to absorb and that could be potentially be transformed into electrons by injection in the TiO_2 CB. Moreover, high ε indicates a species that is able to absorb a higher amount of photons compared to a less performing dye (in terms of ε) at the same concentration and it is compatible with the use of thinner layer of TiO_2 that is necessary for the development of solid state DSSC.[32,33] In such devices the thickness of the semiconductor layer should be as thinner as possible to maximize electron transfers, but a thinner layer of TiO_2 means a lower loading of dye, thus high ε are necessary to keep a good photon absorption. A further important parameter is the wavelength of the maximum of absorption (λ_{max}) that is related to the range in the visible spectrum where the dye is more active in photon absorption. The solar radiation that strikes the Earth has a strong component in the visible range but in a different composition for various wavelengths as illustrated in Figure 3.3. The best dye (or mixture of dyes) should cover the solar spectrum as much as possible, thus one of the aim in dye development is the red-shift of the maximum of absorption where the solar radiation has its maximum (around 500 nm). This is not the only purpose when developing dyes, absorption in the near-IR region as well as panchromatic absorption (black dye) are two other important goals.

Fluorescence spectra are generally recorded because from the intersection between the normalized absorption and fluorescence spectra the optical band gap (E_{gap}^{opt}) can be evaluated. There are some cases in which molecules exhibit low fluorescence (very noisy spectra) or with strange shapes because of aggregation or intermolecular energy exchange phenomena. In these cases the intersection measurement is not reliable thus the absorption spectrum only is used for E_{gap}^{opt} evaluation using Tauc plot for determination.[34]

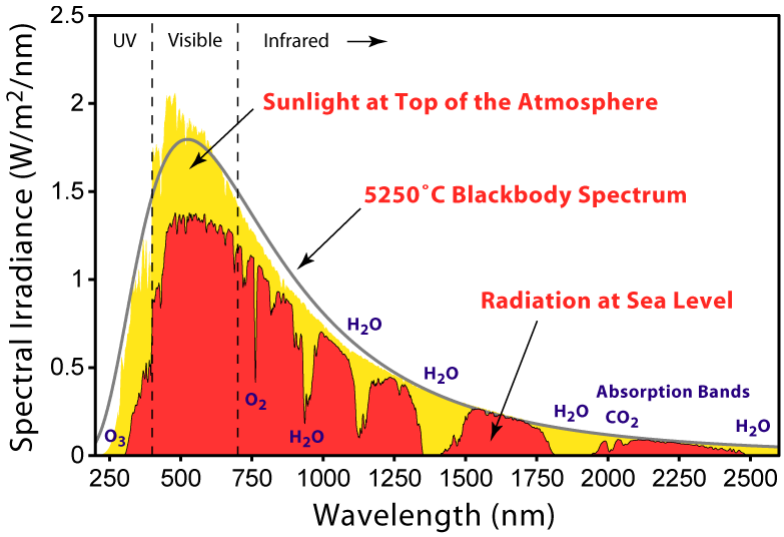

Figure 3.3: Solar radiation spectrum on Earth.

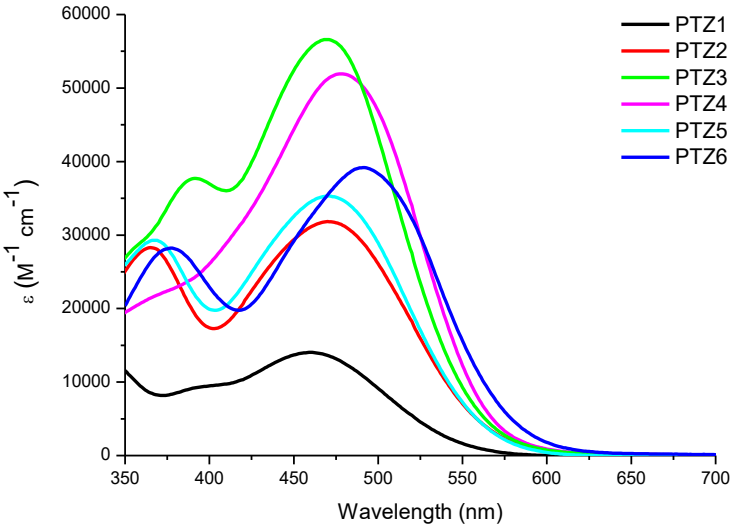

*Figure 3.4: Absorption spectra of dyes **PTZ1–6** in 10^{-5} M solutions in THF normalized to ε.*

Some of the dyes **PTZ1-6** showed limited solubility in ethanol or chlorinated solvents even at low concentrations, thus optical characterization have been performed in THF to ensure the solubility of all the molecules. UV/Vis spectra have been recorded in order to measure the maximum wavelength of absorption (λ_{max}) and the molar

extinction coefficient (ε) using 10^{-5} M solutions of each dye. Collected data are reported in Table 3.1.

Table 3.1: Optical parameters

Dye	λ_{max} (nm)	ε (M^{-1} cm^{-1})	λ_{onset} (nm)	E_{gap}^{opt} (eV)
PTZ1	460	13700 ± 300	590	2.10
PTZ2	471	34000 ± 1800	608	2.04
PTZ3	470	57800 ± 2900	596	2.08
PTZ4	478	56200 ± 2200	598	2.07
PTZ5	477	35400 ± 1300	598	2.02
PTZ6	490	39200 ± 600	654	2.01

The spectroscopic behavior of the dyes is typical of dipolar molecules with the main absorption band in the visible range that can be assigned to an intramolecular donor-to-acceptor charge-transfer (ICT). Theoretical studies support this assignment in many organic dyes as well as in phenothiazines.[35] When thienyl spacers are introduced a second absorption band at higher energies appears and it is generally attributed to a local thiophene π-π* transition. We verified the presence of such a band for all the modified phenothiazine dyes **PTZ2-6**.[4] Recorded UV/Vis spectra are depicted in Figure 3.4 with the absorption normalized to the ε coefficient for easy comparison. Overall higher light harvesting properties have been recorded for all the designed dyes with significantly red-shifted absorption peaks and/or enhanced ε compared to **PTZ1**.

It is evident that the optical properties of the reference dye **PTZ1** were limited and the improvement in light absorption is highly remarkable through the spacer modification. In **PTZ2** the introduction of only a thiophene unit allowed to have a red-shift of the maximum of absorption of 11 nm (bathochromism) and a hyperchromism, meaning a higher molar extinction coefficient that is more than twice in comparison to the reference (from 13 700 $M^{-1}cm^{-1}$ of **PTZ1** to 34000 $M^{-1}cm^{-1}$ in **PTZ2**). Shifting from the simple thiophene to the higher conjugated polycyclic fused system of **PTZ3**, the main effect is a remarkable hyperchromism that allowed

to reach very high ε (nearby 60 000 $M^{-1}cm^{-1}$), while in the case of polycyclic bithienyl **PTZ4**, a combination of bathochromism and hyperchromism is revealed resulting in a combination of red-shifting and high ε, comparable to **PTZ3**. Switching to the analysis of UV/Vis spectra belonging to **PTZ5** and **PTZ6**, it is evident that since there is no increase in the conjugated path in comparison to **PTZ2** the ε are of the same order of magnitude. However the presence of electron rich oxygenated moieties (auxochrome groups) on the thiophene ring allowed to afford good red-shift up to 490 nm for **PTZ6** that is 30 nm higher than the reference compound **PTZ1**. The fluorescence spectra of the investigated dyes were considered not reliable for optical band gap evaluation since their shape was quite different from the absorption band and with very low intensities, therefore Tauc plots have been used to evaluate the zero–zero energies and the absorption onset wavelengths (Figure 3.5 and Table 3.3). The optical band gaps showed that the reference dye **PTZ1** has the highest energy difference amongst frontier orbitals, while **PTZ5** and **PTZ6** seem to be the most promising ones having the lower optical bandgap. It is worth nothing that the enhancement of optical properties is remarkable for molecules that are quite simple in structure and synthesis. This is not a secondary issue for the development of new sensitizers, since several synthetic steps and low yields to achieve complicated molecules is not the best condition to interface academic research with industrial world.

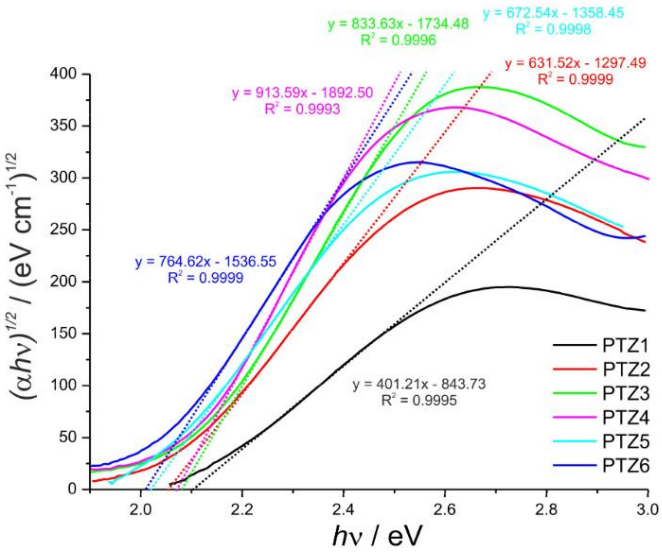

Figure 3.5: Tauc plots of the investigated dyes.

The main reaction at the basis of the working mechanism of DSSC and of dye-sensitized hydrogen production is a redox, therefore electrochemistry could help us in understanding if the new sensitizers are suitable for such application. The measurement of the oxidation and reduction potentials allowed the determination of the frontier orbital energies (HOMO and LUMO). Such energetic levels should be in the right position to have electron injection in TiO_2 CB and fast regeneration by the redox couple in DSSC or by the sacrificial electron donor in hydrogen production. Moreover the shape and reversibility of the cathodic or anodic waves give an idea on the nature of the electronic process.

Electrochemical characterization has been performed by measuring cyclovoltammetry (CV) of saturated solutions of each dye in CH_2Cl_2 in the presence of a supporting electrolyte (0.1 M tetrabutylammonium perchlorate, $TBAClO_4$), the CV traces are reported in Figure 3.6. All dyes traces show a quasi-reversible behavior at positive potentials and several irreversible reduction waves for lowest negative potentials (< −1.0 V). In such a negative range of potentials, electrolyte decomposition could be the main contribution to current raising, as confirmed by scanning the electrolyte together with 10 mM of ferrocene as internal standard (for potentials more negative than −2.0 V).

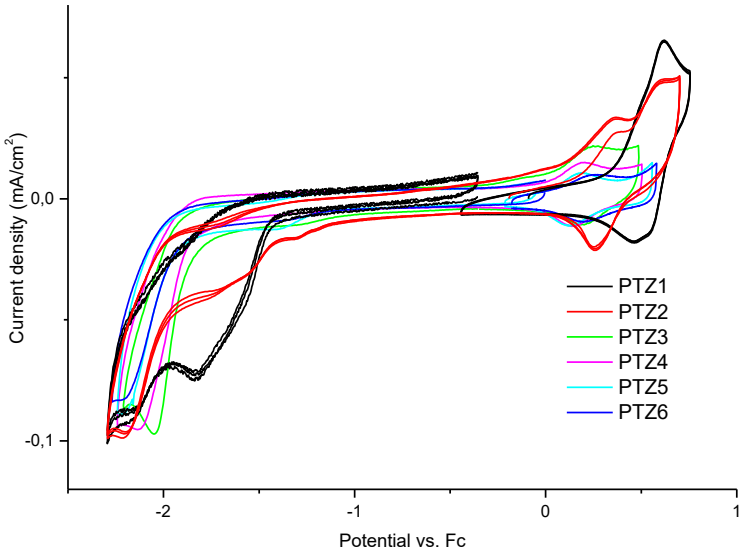

*Figure 3.6: CV traces for **PTZ1-6**.*

Due to this limitation for CV analysis, differential pulse voltammetry (DPV) has been preferred since it allows a minimum decomposition of the supporting electrolyte and a more precise estimation and attribution of the oxidation and reduction potentials to evaluate HOMO and LUMO levels. The DPV traces are shown in Figure 3.7. Oxidation processes are composed of two evident waves for all the dyes, even though in the case of **PTZ1** it is a shoulder of the main wave. All of the new dyes were found easier to oxidize by 120-240 mV in comparison with the reference **PTZ1**, probably because of the slight donor character of the thiophene moieties as already reported in the literature.[30] Moreover the measured oxidation potentials for **PTZ2-6** are similar to each other (within a range of 120 mV), as foreseen by the presence of the same donor core, the phenothiazine unit and similar thienyl groups. Therefore no great contribution to the HOMO energy level is expected in differentiating the **PTZ2-6** behavior. Anyway particularly low oxidation potentials have been registered for **PTZ2, PTZ5**, and **PTZ6**; in the case of **PTZ5-6** such a contribution could arise from the electron-rich oxygenated moieties. The main differences amongst dyes have been localized in the cathodic region, where all the designed dyes are more easily reduced than the reference **PTZ1**. In the case of **PTZ1** and **PTZ2** the cathodic region is characterized by two broad current profiles and two reduction waves, hinting the presence of more than one occurring reduction process. This could be ascribed to reductive chemisorption of acidic protons onto the electrodes surface and to the electron injection in the LUMO orbital.[36] As a matter of fact a simple washing step with organic solvent is not enough to detach the dye from the electrode surface, indicating a strong interaction between the molecules and the glassy carbon electrode during the reduction step. This multi-wave and complex structure of the cathodic traces for **PTZ1** and **PTZ2** did not allow a reliable evaluation of reduction potentials for these dyes, thus optical band gap together with the HOMO energies were used for the estimation of the LUMO levels. In the case of **PTZ3-6** the traces in the cathodic region are more regular, thus reliable evaluation of the reduction potentials is possible. All the LUMO energies are higher for the new dyes in comparison with the reference **PTZ1**, with a net increase from **PTZ2** to **PTZ5** and **PTZ6** that is explainable with the presence of electron-rich oxygenated groups. All the LUMO energies are higher than the TiO_2 CB so that electron injection is expected to be efficient. Table 3.2 reports all the electrochemical data and Figure 3.7 illustrates the HOMO and LUMO levels in comparison to the TiO_2 CB and the potential of the redox couple.

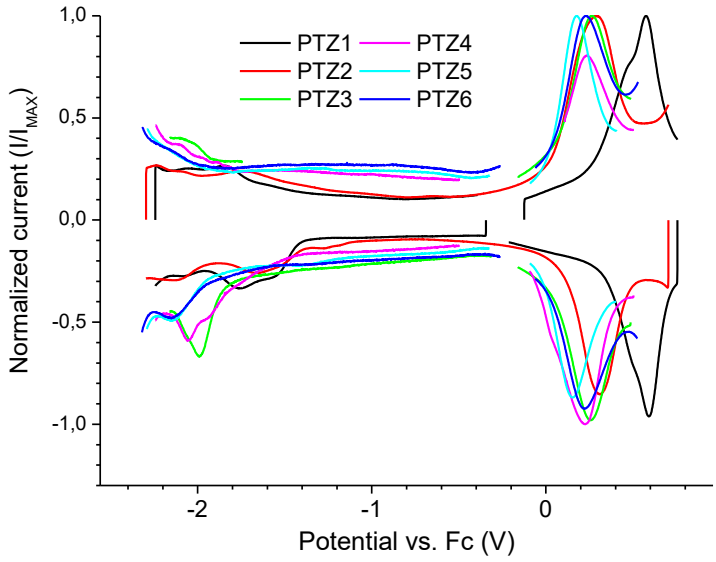

*Figure 3.7: DPV traces for **PTZ1-6**.*

*Table 3.2: Electrochemical data for dyes **PTZ1-6**.*

Dye	E_{ox} (V) ± 5 V	HOMO (eV) ± 50 meV	E_{red} (V) ± 5 V	LUMO (eV) ± 50 meV
PTZ1	0.39	−5.62	-	−3.52[a]
PTZ2	0.15	−5.38	-	−3.33[a]
PTZ3	0.26	−5.49	−1.99	−3.25
PTZ4	0.27	−5.50	−2.06	−3.17
PTZ5	0.16	−5.39	−2.15	−3.08
PTZ6	0.22	−5.45	−2.16	−3.07

[a] Calculated from electrochemical HOMO energies and optical bandgaps.

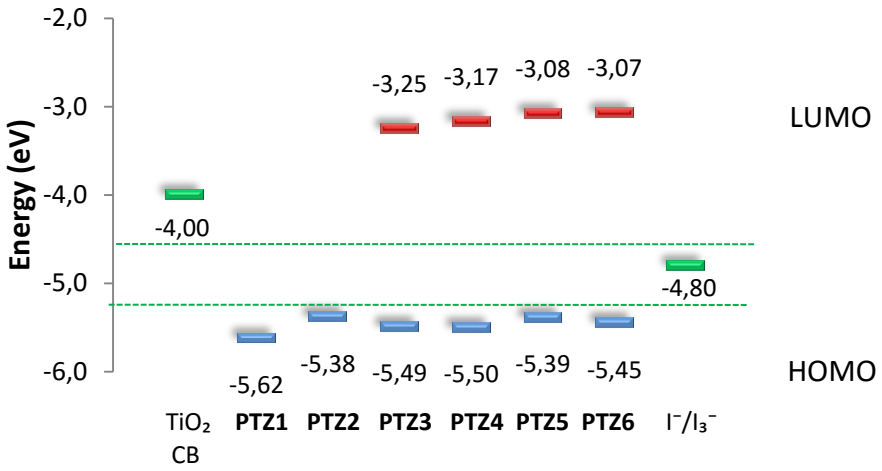

*Figure 3.8: Electrochemical measured HOMO and LUMO levels for **PTZ1-6**.*

3.2.3 DSSC Performances

DSSC performances have been measured in order to further characterize the new sensitizers. DSSC is a precious tool to investigate structure/activity relationships and to find in molecular design some answers to different activities. Since dye-sensitized hydrogen production is a new field, recovering structural connections to activities is more difficult. We therefore performed DSSC characterization to see if a similar behavior in activity can be found between the two analyses, otherwise differences could be compared and ascribed to the dissimilar environmental situations. Standard cells have been prepared and no particular optimization has been performed since the DSSC data were not the final goal of the research. Moreover, hydrogen tests have been performed in very simple and standard conditions, without addition of other agents as it generally happens in the DSSC field, thus optimization by mean of exotic electrolyte compositions or TiO_2 pastes was beyond the scope of the work. Chenodeoxycholic acid (CDCA) has been added in dye absorbing solutions (1:1) to prevent dye aggregation that is known to happened in phenothiazine dyes because of their almost planar structure. A single layer film of TiO_2 (10 µm) blend of anatase consisting of active 20-nm up to 450-nm scattering nanoparticles has been used as semiconductor layer. Z960 (1.0 M dimethyl imidazolium iodide, 0.03 M I_2, 0.05 M LiI, 0.1 M guanidinium thiocyanate and 0.5 M 4-*t*-butylpyridine in acetonitrile/valeronitrile 85/15) has been used as liquid electrolyte.[37] The recorded J/V curves are illustrated in Figure 3.9, and it is evident that better light harvesting

properties, highlighted by optical characterization, are reflected in DSSC performances for all the new dyes apart from **PTZ6** that seems to suffer from aggregation on TiO_2 surface.

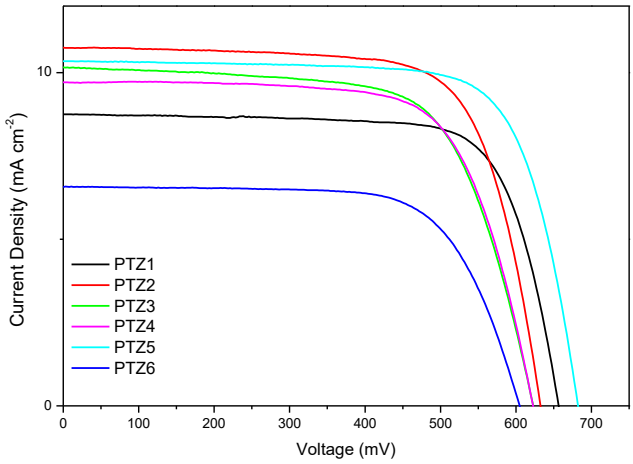

Figure 3.9: J/V traces.

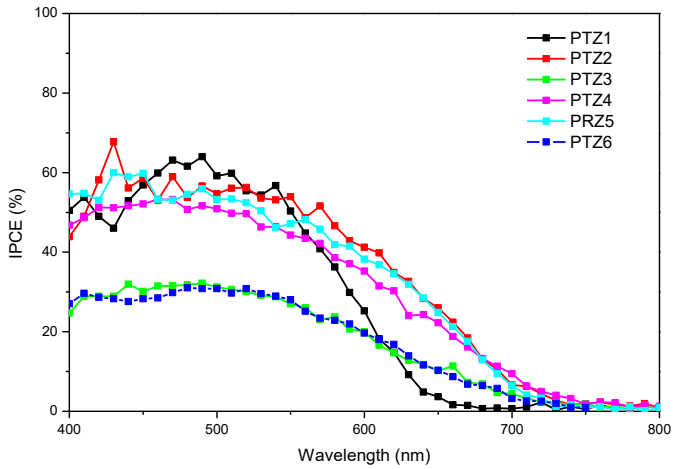

Figure 3.10: IPCE curves.

The main advantage of the new dyes is reflected in higher generated photocurrents as it was predictable from better photons absorption. Photovoltages do not follow a precise trend with the chemical structure, but the highest photovoltage is the one of **PTZ5**. De-aggregating effect of the butoxyl chains is probably at the basis of such good performances, suggesting that a cooperative effect of better light harvesting

together with de-aggregating moieties could be a promising strategy in the development of new phenothiazine dyes. IPCE curves are reported in Figure 3.10 and it is clear that the reference dye has a limited activity for long wavelength (600-700 nm) while all the investigated dyes have activities till 700 nm thanks to the superior light harvesting efficiencies. In the case of **PTZ3** and **PTZ6** the IPCE curves are quite low probably because of detrimental aggregation of the dyes that damage cell performances.

To further compare DSSC performances, particularly to explain differences in photovoltages, electrochemical impedance spectroscopy (EIS in Figure 3.11) has been performed and analyzed in terms of Nyquist plots with the imaginary part of the impedance plotted as a function of the real part over a range of frequencies. An equivalent circuit model can be used to describe the cell impedance where the different cell components and the corresponding interfaces are considered as discrete electrical elements. An illustration of the equivalent circuit is given in the inset of Figure 3.11. The measurement starts with illumination in open circuit conditions to achieve null direct current and force the cell to mainly describe recombination phenomena. Properties of the interface TiO_2/redox electrolyte can be derived from the main arc in terms of recombination resistance (R_{rec}) and chemical capacitance (C_μ) that is dependent on the density states in the bandgap of TiO_2. By mean of these two parameters, electron lifetime (τ_n), graphically the angular frequency at the top of the middle arc of the Nyquist plot, can be estimated through the formula $\tau_n = R_{rec} \times C_\mu$. Table 3.3 reports these three parameters that are related to the detrimental back-charge transfer phenomena between the injected electrons and the oxidized form of the electrolyte, which are considered the main limitation in cell photovoltage according to Shockley-Quiesser model. There is a good agreement between the photovoltages and the τ_n trends, e.g. **PTZ5** that is the best performing in cell photovoltage has the highest electron lifetime, suggesting slow back-charge recombination, on the contrary the worst performing dyes such as **PTZ3**, **PTZ4**, and **PTZ6** have the shortest lifetimes. It is important to analyze the two components of the electron lifetime, R_{rec} and C_μ, to see which is the main contribution to the overall parameter. **PTZ5** has a superior activity thanks to the high chemical capacitance, therefore structural molecular modifications such as the presence of alkyl chains suppress charge recombination as already reported in the literature.[3,38,39,40] A special attention is given to the position of the alkyl chains in the thiophene spacers (instead of in donor core only) hinting that central position is positive in terms of recombination suppression.[41,42]

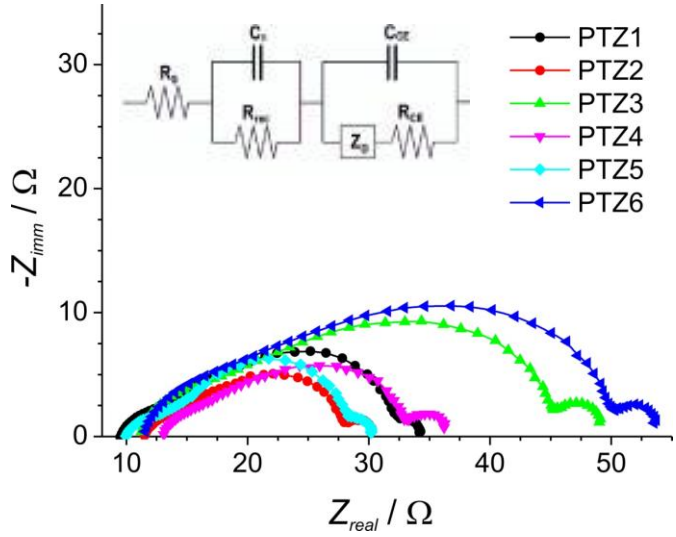

Figure 3.11: Nyquist plots of the cells, equivalent circuit is represented in the inset.

*Table 3.3: Photovoltaic characteristics of DSSCs containing **PTZ1-6** dyes (AM 1.5 solar light).*[a]

Dye[b]	J_{sc} (mAcm^{-2})	V_{oc} (mV)	ff (%)	PCE (%)	R_{rec} [Ω]	C_μ x 10^4 [F]	τ (ms)
PTZ1	8.76 (11.1)	656 (667)	74 (74)	4.3 (5.5)	20	16	3.1
PTZ2	10.8 (13.4)	632 (649)	72 (70)	4.9 (6.1)	13	20	2.6
PTZ3	10.2 (13.1)	622 (632)	67 (66)	4.3 (5.5)	30	6	1.8
PTZ4	9.71 (12.7)	622 (632)	70 (67)	4.2 (5.3)	18	12	2.2
PTZ5	10.3 (12.0)	682 (690)	74 (74)	5.2 (6.1)	14	37	5.0
PTZ6	6.58 (9.00)	604 (614)	69 (68)	2.8 (3.7)	35	5	1.7
N719[c]	14.7 (17.4)	768 (753)	73 (71)	8.3 (9.3)			-

[a] Values without a black mask on the top of the cell are listed in brackets.
[b] Dye solution of 2 x 10^{-4} M in EtOH with 1:1 CDCA; electrolyte Z960 (see text), single TiO_2 layer (10 µm); surface area 0.20 cm^2.
[c] Dye solution of 5 x 10^{-4} M in EtOH solution with 1:1 CDCA; electrolyte A6141 (0.6 M *N*-butyl-*N*-methyl imidazolium iodide, 0.03 M I_2, 0.10 M guanidinium thiocyanate, and 0.5 M 4-*t*-butylpyridine in acetonitrile/valeronitrile 85:15).

3.2.4 Dye-Sensitized Hydrogen Production

The Pt/TiO_2 support to perform photocatalytic tests has been prepared by photodeposition of platinum nanoparticles from a Pt^{2+} solution on TiO_2 surface. Commercial TiO_2 Degussa P25 was suspended in a water/ethanol mixture of $Pt(NO_3)_2$ and irradiation in the UV/Vis allowed the photodeposition following a similar mechanism as the working principle of the photocatalyst without dyes on the surface. UV photons are absorbed by TiO_2 and conduction band of the semiconductor becomes populated, thus Pt^{2+} is reduced on the surface while ethanol in solution is responsible for neutralization of the holes in the valence band. Pt/TiO_2 composite has been prepared in collaboration with the group of Prof. Fornasiero and it has been characterized in details.

Figure 3.12 illustrates the TEM characterization of such nanoparticles and it is evident that platinum (black spots) seems to be homogeneously deposited on the surface of TiO_2, size distribution of Pt nanoparticles is around 2.4 nm. A full and complete characterization of these nanoparticles has not been the objective of this thesis, therefore we recall the corresponding reference article for powder X-ray diffraction (PXRD) analysis to determine crystallites composition and dimension, textural analysis through N_2 physisorption (BET and BJH analyses) to evaluate active surface and pores dimension, TEM and HAADF-STEM images.[43]

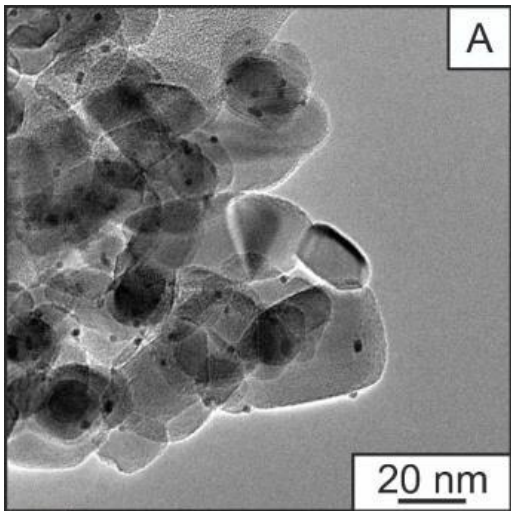

Figure 3.12: TEM image of the Pt/TiO_2 composite, black spots on the surface are Pt nanoparticles.

Pt/TiO_2 composite has been sensitized with the corresponding dye from ethanolic staining solutions, after dye anchoring the remaining solutions were colorless indicating a quantitative adsorption of dyes on the composite. The Pt/TiO_2/dye photocatalyst has been tested in aqueous TEOA (10% v/v) at pH 7 as sacrificial electron donor solution and it has been irradiated through solar simulator cutting the UV range at $\lambda < 420$ nm, after having the solution degassed from oxygen. Hydrogen evolved has been measured by mean of a gas-chromatograph equipped with TCD detector. The irradiation time has been 20 h that is a long irradiation range compared to the general procedures reported in the literature (see references in paragraph 2.3). Such long irradiation measurements have been necessary to study medium range photostability of the system that was one of the purpose of the research. The limit of 20 h has been set as compromise to avoid considerable changes in the photocatalytic mixture, since lowering of the concentration of sacrificial agent together with accumulation of the decomposition products and evaporation of the solvent used in the flow reactor could not be neglected after 20 h. Figure 3.13 illustrates the hydrogen curves measuring hydrogen produced per mass of composite during the whole irradiation period. Unfortunately, all the new developed dyes are considerably lower in activity compared to the reference molecule **PTZ1**, apart from **PTZ5** that showed comparable activity. **PTZ2-4** and **PTZ6** showed lower activity and they are comparable one to each other. These results are in contrast with the efficiencies obtained through DSSC, therefore the explanation of such behavior needs to be correlated to the different environment in hydrogen production. Our hypothesis is that sulfur atom in the spacer could interact with Pt nanoparticles poisoning the catalyst for hydrogen production, or thiophene spacers could hinder the catalytic sites from protons approach. It is known that sulfur is a poison for platinum catalyst but this is the first time, for the best of our knowledge, that such an effect has been verified in these photocatalytic conditions. Phenothiazine as well contains a sulfur atom and no detrimental effect has been reported, a probable influence from the position and the number of sulfur atoms could be hypothesized, being the spacer much closer to the composite surface than the donor core. Moreover the use of di-branched structures leads to a double amount of sulfur units compared to the mono-branched dyes. Such hypothesis would be verified with the introduction of sulfur free spacers that is currently under development in our research laboratory. In the case of **PTZ5** this effect seems to be partially balanced by the de-aggregating alkyl chains that might limit the interaction of thiophene moieties with platinum catalyst.

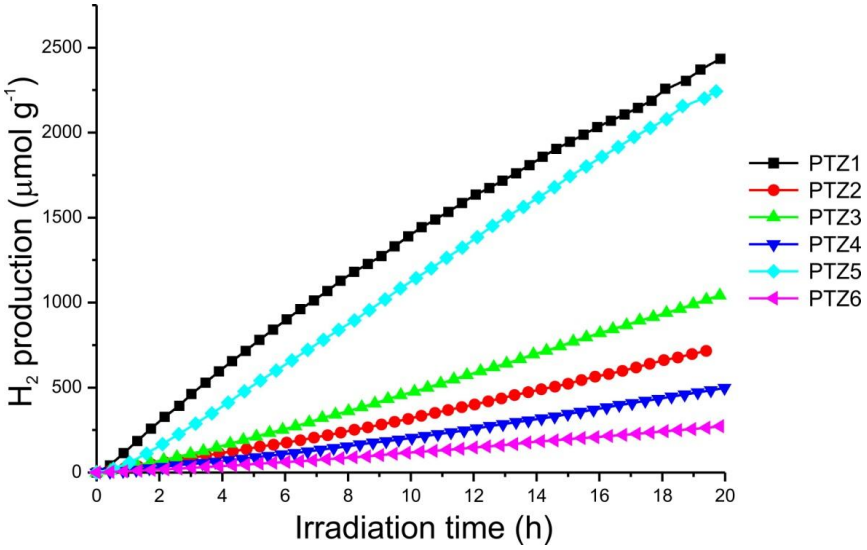

Figure 3.13: Hydrogen produced in photocatalytic tests.

Therefore the first deduction from this analysis is that better light harvesting properties are not necessarily translated into better activities in hydrogen production as in DSSC field. Activity is one of the fundamental parameters to evaluate overall efficiency of a system, a second parameter is durability in the photocatalytic conditions. Such a parameter is fundamental for real application of the tested systems.

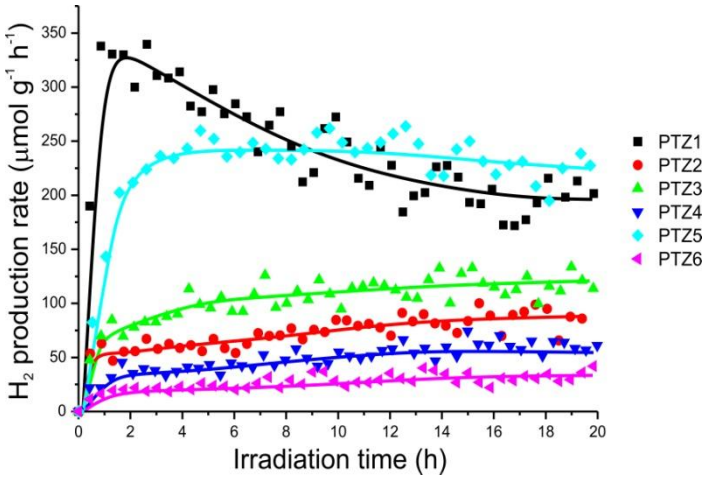

Figure 3.14: Hydrogen production rates in photocatalytic tests.

Aside from the higher activity of **PTZ1**, it is slightly evident that the curve for the reference dye is not exactly a straight line, while **PTZ5** (and all the other dyes) showed a more linear behavior. To stress such a difference we reported in graph the rate in hydrogen production vs. time as illustrated in Figure 3.14, where it is clear that the behavior of the reference dye is completely different from the new dyes that have an "induction period" of 4-6 h after which a constant rate in hydrogen production is achieved.

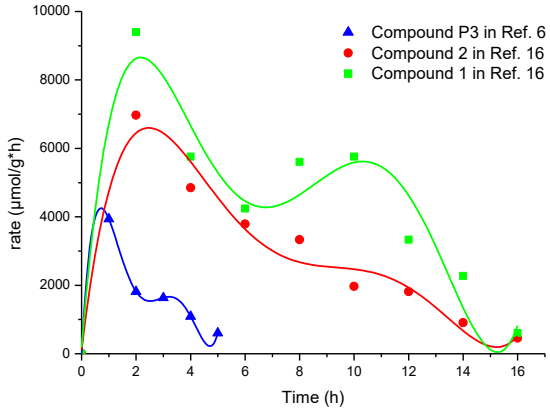

Figure 3.15: Hydrogen production rates for data elaborated from literature reports.

Instead, after the first two hours, when the reference system is highly active, a progressive deactivation of the **PTZ1** system takes place as suggested by the reduction of the evolved hydrogen amount. This is in line with the data reported in the literature for the reference dye and similar systems, as showed in Figure 3.15, in which the deactivation was not completely highlighted since data were not elaborated in the corresponding rates and irradiation was stopped after 5 h in the case of reference **PTZ1**.[6] As a matter of fact **PTZ5** is less active than the reference system for short irradiation times but it surpasses **PTZ1** performances after 8 h of irradiation. All the other dyes showed the same behavior of **PTZ5** with lower efficiencies but the same shape of hydrogen production rate curves. To better compared efficiencies, turnover numbers (TON), which indicates the number of photo-generated electrons available for catalysis, have been calculated and they pointed out the comparable efficiency of **PTZ1** and **PTZ5**. Secondly we calculated light-to-fuel efficiencies (LFE) after 3 and 20 h of irradiation to evaluate stability properties. Table 3.4 shows all the measured and calculated parameters in

photocatalytic hydrogen production, LFE are particularly interesting since after 3 h the supremacy of **PTZ1** in hydrogen production is evident, as well as the deactivation highlighted by the LFE_{20} value.

Table 3.4: Hydrogen measurements under photocatalytic conditions.

Dye	Dye loading (μmol/50 mg)	H_2 (μmol)	TON (20 h)	LFE_{03} (%)	LFE_{20} (%)
PTZ1	2.97	121.7	82	0.144	0.090
PTZ2	2.98	35.8	24	0.026	0.039
PTZ3	3.01	52.1	35	0.037	0.048
PTZ4	2.99	24.9	17	0.017	0.027
PTZ5	2.98	111.6	75	0.104	0.0103
PTZ6	2.98	13.6	9	0.010	0.014

In contrast all the other dyes showed more constant values, especially in the case of **PTZ5** that has noticeably higher LFE_{20} compared to **PTZ1**. Considering the TON values it is evident that from comparison with reported data we had significantly lower numbers even for **PTZ1** that has already been tested in the literature.[6] Thus it is necessary to stress that the relative and comparative studies are till now of main importance since efficiencies depend strongly on the kind and power of irradiation source, the reactor geometry, dye loading on the catalyst, and catalyst composition both in platinum and in TiO_2. There is no standard procedure to evaluate hydrogen produced in this way thus comparison should be done only in the same experimental conditions with reference systems from the literature.

3.2.5 Dye Photo-Stability Tests

Starting from hydrogen production rates graph we decided to investigate further the reason of the progressive deactivation that **PTZ1** was suffering from. We decided to evaluate the amount of dye that was still on the composite surface after different irradiation times under the same conditions of hydrogen photocatalytic production. We therefore prepared the Pt/TiO_2/dye composite, suspended it in TEOA aqueous solution and irradiated it with visible light. After 7, 14 and 20 h aliquots were taken

from the photocatalytic mixture and after centrifugation of the suspension the liquid phase has been analyzed to evaluate eventual dye desorbed in the solution, while the solid component was immersed in a basic solution to have dye desorption. None of the liquid phases after centrifugation showed the presence of any dye, hinting that detaching of the dye from the surface was not occurring. Desorbing solutions have been analyzed at the UV/Vis spectrophotometer and the obtained results are reported as graph in Figure 3.16. The ratio of the starting dye molecules on the surface and the survived dyes for different irradiation times are reported in the vertical axis. It is evident that the decrease in hydrogen production in the case of **PTZ1** is ascribed to photo-instability of the system in the used conditions, since only ~30% of the dyes survived on the composite surface after 20 h of irradiation. It is not sure if detachment from the surface and subsequent degradation occur, but there are no traces of dye in solution and it is probable that degradation is mediated by platinum catalysis or TiO_2. All the other dyes suffer from photo-degradation as well, apart from **PTZ5** that survived in more that 95% extent after 20 h of irradiation. The extent of photo-degradation for **PTZ2-4** and **PTZ6** was between ~35-70%. That analysis pointed out the insufficiency of literature data with 5 h of irradiation since no information about medium-term stability could be studied, moreover curves behavior reported in Figure 3.15 calculated from literature tests hint a possible photo-instability of those systems, therefore further investigation would be necessary. Short irradiation tests give a partial view of the overall performances, without taking into consideration other intrinsic properties of the system apart from hydrogen production activity, giving partially and potentially misleading information about the structure/efficiency correlations. While we do not know the reason of the higher stability for the new sensitizers compared to the reference dye, it is evident that it should be connected to the presence of the spacers since it is the common feature of **PTZ2-6**. We proposed two hypotheses to explain the higher stability of the new dyes: the first one is that stronger interaction of the dyes and the Pt/TiO_2 composite, mediated by the sulfur atoms, partially inhibits catalyst efficiency both in hydrogen production (as clear from efficiency results) and in dye degradation reaction, the second one is that the thiophene spacer has a fundamental role in stabilizing the oxidized form of the dye after photo-injection as it has already been reported in the literature.[7]

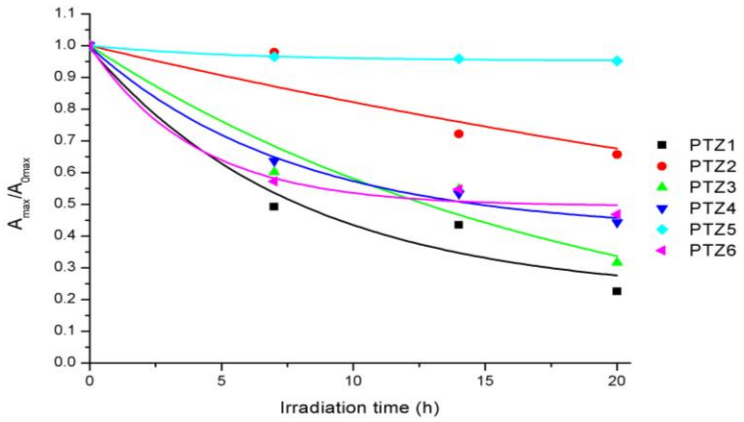

*Figure 3.16: Degradation plots of the **PTZ1-6** dye-sensitized Pt/TiO_2 catalysts under visible light.*

3.2.6 Conclusions

Introduction of thiophene π-spacers as modification of the reference dye **PTZ1** allowed to enhance the optical properties both in red-shifting of the maximum of absorption and in molar extinction coefficients. All the dyes have higher light harvesting properties with benchmarking for **PTZ3** and **PTZ4** that reached ε values that are more than 4 times than the reference one, while **PTZ6** is the most performing one in terms of bathochromism with a shift of 30 nm towards the red wavelengths. DSSC performances are in good agreement with better light harvesting properties, apart from **PTZ6** that seems to suffer from detrimental dye-aggregation. Considering that light harvesting is not the only property that contributes to high efficiency, the presence of alkyl chains in the spacer unit in **PTZ5** pointed out the importance of de-aggregating moieties in dyes especially in almost flat molecules as phenothiazine core. Even though performances in cell of **PTZ2** and **PTZ5** are comparable, the latter one has a good behavior in terms of impedance spectroscopy that suggests a strong limitation of detrimental recombination pathways for this dye. Photocatalytic hydrogen production seems to be less dependent, in terms of amount of evolved gas, on the light harvesting properties compared to the DSSC performances, hinting that the photocatalytic system has a more complex structure than photovoltaic cells. The introduction of the spacer did not affect the amount of evolved hydrogen but the stability for medium-long term irradiation. For the first time we irradiated for quite long times in order to investigate dyes photostability and we pointed out photo-instability of the reference dye that has never been reported.

The results are very promising, especially for **PTZ5** that showed a good balance between efficiency and stability giving a constant rate of hydrogen production when steady state is reached, giving an overall promising efficiency. **PTZ5** has the higher activity amongst the new dyes as well as the higher photo-stability in agreement with the results in DSSC. This result is in agreement with the EIS data and points out the importance of reducing the detrimental electron recombination pathways that seems to be even more relevant in hydrogen production, since they seem to be at the basis of dye stability. Such promising properties would probably be not related to the bis-butoxyl-thiophene core itself but for sure the superior performances should be ascribed to the alkyl chains since they are the only molecular difference compared to the other dyes. The superior performances seem not to be connected to the presence of electron-rich oxygen atoms, since **PTZ6** has no gained photo-stability or activity compared to the other dyes of the group. Higher photo-stability is probably not due to bis-alkoxythiophene moiety since other spacers, such as thienothiophene, are considered more stable thanks to the rigid structure.[44,45,46] Concerning the lower performances in comparison to the reference dye, the hypothesis of sulfur poisoning seems to be the more likely, even though no direct proof has been collected. A possible way to confirm our hypothesis is the synthesis of sulfur-free analogous dyes that is currently in progress in our laboratory. Lower activity is well balanced with high stability in the case of **PTZ5** that has promising properties for long-term applications. It should be highlighted that TON and more particularly LFE at various irradiation times are at the basis of dye stability evaluation, since constant LFE values are peculiar of stable systems.

3.3 HYDROPHILIC CHAINS TO IMPROVE SURFACE WETTABILITY

The second modification to the molecular structure interested the chain attached on the phenothiazine nitrogen. In the reference dye and all the new dyes developed in paragraph 3.2 the chain has an hydrophobic nature being an octyl group. This could be a limitation for photocatalytic hydrogen production, inducing possible surface wettability problems in aqueous media. For that reason other research groups developed hydrophilic dyes bearing glycolic units on the donor or spacing moieties to investigate the effect on hydrogen production performances.[11,14] Inspired by those articles we decided to develop the same kind of modification on **PTZ2**, which has been chosen instead of **PTZ1** because of the higher photo-stability as already illustrated in paragraph 3.2.5. The choice of **PTZ2**, instead of the most promising **PTZ5**, was due to easiness of synthesis, since we decided to introduce a glycolic chain, as already reported in the literature for DSSC with phenothiazine dyes,[47] but we went further introducing a carbohydrate moiety such as glucose derivative. We chose **PTZ2** since the number of synthetic steps was lower and with high overall yield (> 70%) compared to **PTZ5** (< 40%), since a good synthetic route was necessary for the coupling with carbohydrate chemistry. The glycolic functionality could be beneficial for surface wettability properties in the aqueous media, without any other advantage, such as self-assembly properties, limiting the eventual future development of this category of dyes. A further tuning of properties might be done with more sophisticated groups such as carbohydrates. Actually carbohydrates could give additional advantages being good acceptors and donors for hydrogen bonds, therefore effects in dye-assembly on TiO_2 surface mediated by the sugar moiety could not be excluded. Sugars have been largely applied in biomedical materials reaching promising results[48] and lately *D*-glucose has been incorporated into materials to achieve self-aggregation properties,[49] therefore it seems a promising substrate to be tested in dye-sensitized photocatalytic hydrogen production as well. The goal of the research has been to see if the modification on the hydrophilicity affected performances, eventual development of higher performing dyes has been forecast in case of positive effect of the introduction of the carbohydrate moiety. The designed modifications should not affect the conjugated structure of the molecule, therefore we expected no significant modification in optical properties or in electrochemical characterization. In the case of the glycolic chain the electrochemical compatibility is quite sure since this group has already been reported in many articles for water DSSC as well.[50] The inertia of the sugar derivative upon oxidation and reduction cycling is trickier. We decided to block the anomeric carbon to prevent

reductive behaviour of the glucose and in principle no other parts of the sugar should interfere with electrochemical behaviour of the dye. For the glycolic chain we selected tris(ethylene glycol) monomethyl ether (TEG) group and the corresponding glycolic dye has been nominated **PTZ7**, while **PTZ8** is the derivative bearing the glucose unit, the structures are depicted in Figure 3.17.

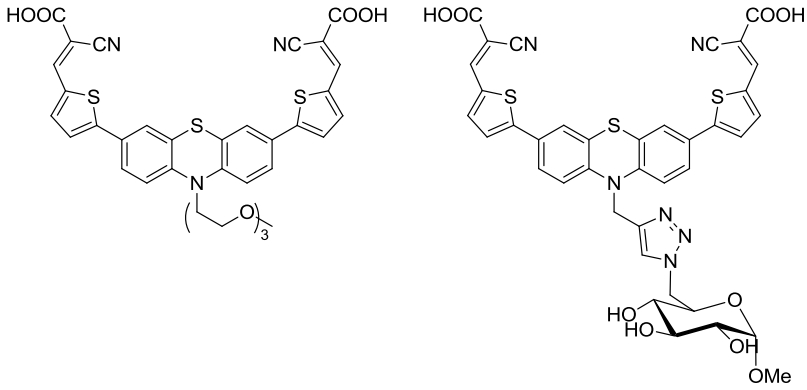

PTZ7 **PTZ8**

Figure 3.17: Designed dyes with improved hydrophilicity.

Apart from optical and electrochemical characterization, we performed DSSC in organic electrolyte (standard devices already illustrated in paragraph 3.2.3) to evaluate efficiencies that we do not expect to be very high since the developed dyes are not optimized to work in organic media. We evaluated the hydrophilicity of the new dyes by mean of contact angles measurements, and then we performed hydrogen production tests.

3.3.1 Synthetic Strategy

The synthetic routes to achieve **PTZ7** and **PTZ8** are depicted in Scheme 3.4. The synthetic strategy to afford **PTZ7** has followed an analogous route as for **PTZ2** since the glycolic chain is expected not to interfere with any synthetic step. Bromination reaction has been anticipated before alkylation since it worked without problems on 10*H*-phenothiazine with the same reaction conditions as the ones reported for molecule **1**. In this case we preferred to anticipate bromination since it is the shared intermediate between the synthesis of **PTZ7** and **PTZ8**. The synthetic procedure has been adapted from the one used in paragraph 3.2 with Br_2.[51] The alkylating reagent for glycolic chain introduction has been prepared according to the literature procedure starting from triethylene glycol monomethyl ether and treatment with *p*-

TsOH for the introduction of a good leaving group.[52] Alkylation has been performed in the same conditions as previously reported: deprotonation of the phenothiazine nitrogen occurred with NaH and subsequent addition of the tosylate reagent allowed to achieve intermediate **16**. Microwave assisted Suzuki-Miyaura cross-coupling with 5-formyl-2-thienylboronic acid was selected as reaction to introduce the π-spacer, while Knoevenagel condensation in basic conditions was used to transform the aldehyde in the cyanoacrylic acid. The synthetic approach to achieve **PTZ8** has been less straightforward and it has been developed in collaboration with the group of Prof. Peri. The first reaction considered for the introduction of the sugar moiety has been glycosilation, thus appropriate intermediate has been prepared, the alkylation on phenothiazine was done using a protected alcohol that was the deprotected in the terminal OH to run glycosilation. Unfortunately the reaction did not work and we decided to change approach and to introduce the sugar moiety in a more general way, using Cu-assisted azide-alkyne cycloaddition (CuAAC) "click" reaction (catalytic cycle in Annexes).[53,54] In this way a triazole ring is introduced between the dye and the sugar moiety; saturated alkyl spacers ensure no electronic contribution to the conjugation pathway in the dye. Glycosilation would have been able to introduce the sugar without ring linker, thus in a simpler way from the molecular design point of view, while the "click" approach is better to eventually develop a library of sugar conjugated dyes since the "click" reaction is perfect for a modular approach. Another advantage of azide–alkyne cycloadditions is their high chemoselectivity, which makes these reactions particularly attractive to conjugate highly functional molecules as for example carbohydrates.[55] We decided to introduce the triple bond in the phenothiazine residue through the alkylation step. The first attempt with butynyl bromide failed with likely side-reactions occurring at the triple bond in strong basic conditions because of NaH. The use of shorter alkylating agent such as propargyl bromide avoid such detrimental side-reactions and allowed the isolation of the desired intermediate **18**. Azide group has been therefore introduced on the sugar moiety according to a reported procedure,[56] after having the anomeric carbon blocked as α-methyl glucopyranoside and the three hydroxyl groups protected as acetyl. Standard conditions for cycloaddition, using sodium ascorbate as reducing agent to generate the catalytic Cu(I) species, allowed to achieve intermediate **19**. The shorter chain of the propargyl bromide allowed less flexibility of the sugar moiety but from the electronic point of view the presence of a sp^3 carbon atom ensures no conjugation between the phenothiazine and the triazole ring.

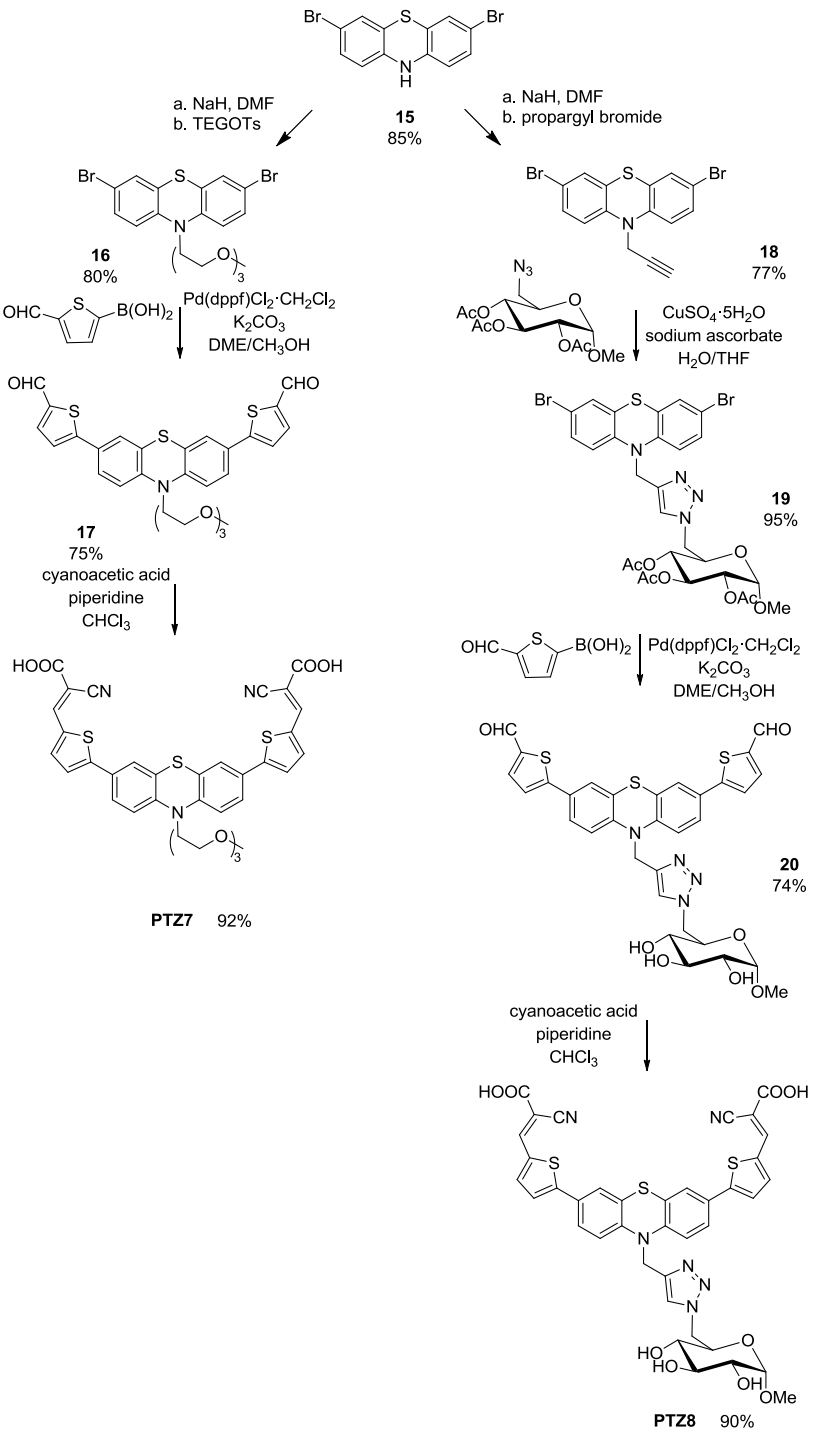

*Scheme 3.4: Synthetic routes for **PTZ7-8**.*

The π-spacer has been introduced through microwaves assisted Suzuki-Miyaura cross-coupling in the same conditions as for **PTZ7**. During the reaction the cleavage of all acetate groups occurs and free OH have been found in the product. Apart from purification problems, free hydroxyl groups are not problematic for the following and last step, the Knoevenagel condensation in basic media, since protections were introduced in order to perform previous metal catalyzed reactions. The experimental details of the synthesis are reported in paragraph 3.5.

3.3.2 Optical and Electrochemical Characterization

Optical and electrochemical characterizations have been run to ensure our hypothesis of no contribution from glycolic and sugar chains to the electronic properties of the new designed dyes. For comparison **PTZ2** values are reported as well. As for the other dyes, absorption spectra have been measured from 10^{-5} M solutions in THF and no fluorescence spectra have been used to determine the optical band gap since Tauc plot analysis was considered more reliable for these dyes as in the case of **PTZ1-6**. Absorption spectra of dyes **PTZ2**, **PTZ7-8** normalized to molar extinction coefficients are shown in Figure 3.18, while optical characterization parameters are reported in Table 3.5.

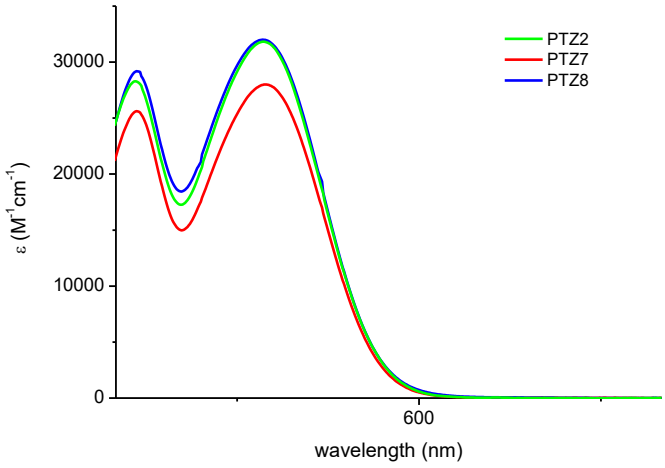

*Figure 3.18: Absorption spectra of dyes **PTZ2** and **PTZ7-8** in 10^{-5} M solutions of THF normalized to ε.*

It is evident that there is no influence of the molecular modification on the optical properties, maximum of absorption wavelengths are the same while slight differences are found in the ε value with a small decrease for **PTZ7**, though the

overall values are very similar. The shape of the absorption peaks are typical of dipolar molecules with an intense absorption band in the Vis region that can be attributed to an intramolecular charge-transfer (ICT) transition as for **PTZ1-6** dyes and a shorter wavelength peak due to local π-π* thiophene transitions.

Table 3.5: Optical parameters.

Dye	λ_{max} (nm)	ε (M^{-1} cm^{-1})	λ_{onset} (nm)	E_{gap}^{opt} (eV)
PTZ2	471	34000 ± 1800	608	2.04
PTZ7	470	28000 ± 1000	611	2.03
PTZ8	471	32000 ± 1000	617	2.01

Electrochemical characterization has been performed in the same way as in the case of **PTZ1-6** dyes series. $6x10^{-4}$ M solutions of **PTZ7** and **PT8** in DMSO and the supporting electrolyte (0. 1 M $TBAClO_4$) have been tested in cyclovoltammetric measurements (CV) with a scan rate of 50 mV/s.

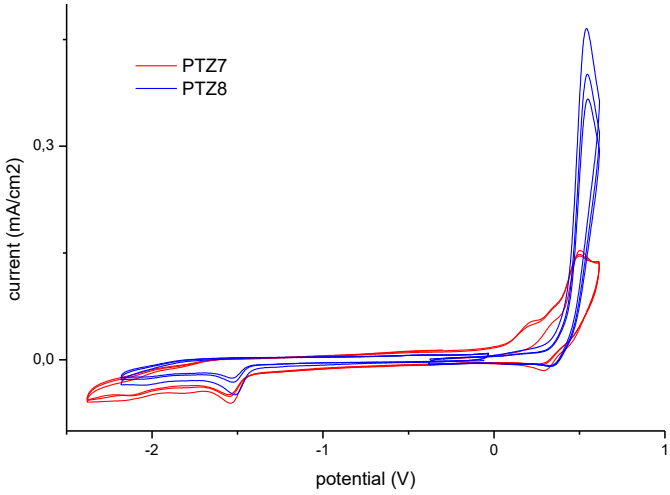

*Figure 3.19: CV traces for **PTZ7-8**.*

As in the case of **PTZ1-6** series, CV analysis was not able to distinguish and make deconvolution of the two oxidation processes, thus DPV (Figure 3.20) has been used to have clearer interpretation. In such a technique easier evaluation of the oxidation and reduction potentials can be done. In the case of **PTZ7** oxidation scan is characterized by two quasi-reversible processes, while one irreversible peak is present in the cathodic scan. **PTZ8** is instead characterized by two irreversible processes in both anodic and cathodic scans as can be easily seen from Figure 3.19, while calculated parameters are listed in Table 3.6. Therefore optical and electrochemical analyses showed a similar behavior for dyes **PTZ2**, **PTZ7-8** confirming our hypothesis of little contribution of the kind of modification in the redox properties of the dyes.

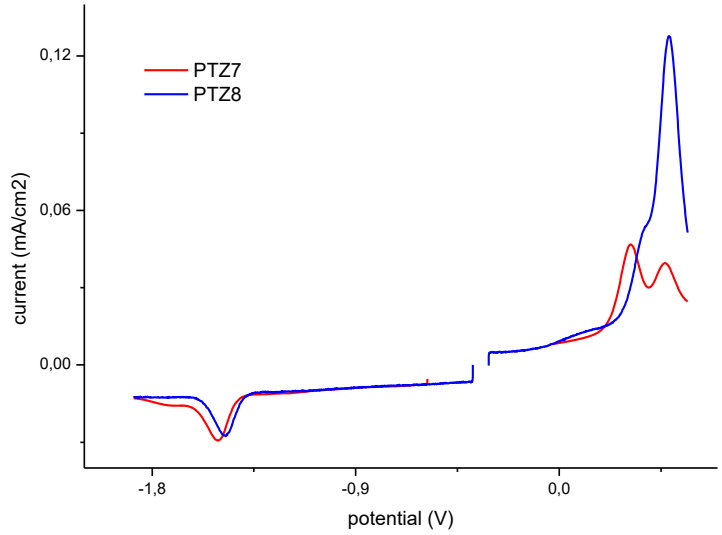

*Figure 3.20: DPV traces fot **PTZ7-8**.*

Table 3.6: Electrochemical data for hydrophilic dyes.

Dye	E_{ox} (V) ± 10 mV	HOMO (eV)[a] ± 0.1 eV	E_{red} (V) ± 10 mV	LUMO (eV) ± 0.1 eV
PTZ7	0.33	-5.5	−1.52	−3.7
PTZ8	0.30	-5.5	−1.49	−3.7

[a] Vacuum potential = Fc/Fc^+ + 5.2 V.

3.3.3 Enhancing Surface Wettability: Contact Angles

In order to investigate surface interaction properties in aqueous media of the new designed dyes, contact angles measurements have been done. Contact angles measurements consist in the evaluation of the angle that is formed by the surface of the investigated material and a drop of deionized water that is present on the surface. In our case bare unsensitized TiO_2 films made of sintered nanoparticles have been taken as reference. A high contact angle (> 90°) indicates a hydrophobic surface while little contact angles (< 90°) are typical of hydrophilic surfaces. Measurements of bare TiO_2 sintered films and the ones sensitized with **PTZ2**, **PTZ7-8** have been performed. The images of water droplets on TiO_2 surface are depicted in Figure 3.21. It is clear that bare TiO_2 is highly hydrophilic thanks to the hydroxyl groups on the surface, while when it is sensitized with **PTZ2**, bearing octyl chain, the contact angle raises to almost 120° indicating a hydrophobic nature of the film. We suppose that this could be a limitation for hydrogen production since water needs to reach TiO_2 surface in order for catalysis to occur. In the case of **PTZ7** we can see that hydrophilicity is recovered in great extent, even though lower than bare TiO_2, and the effect is more pronounced in the case of **PTZ8** with a contact angle of less than 27° that is closer to the bare TiO_2 film behavior. Contact angles are listed in Table 3.7.

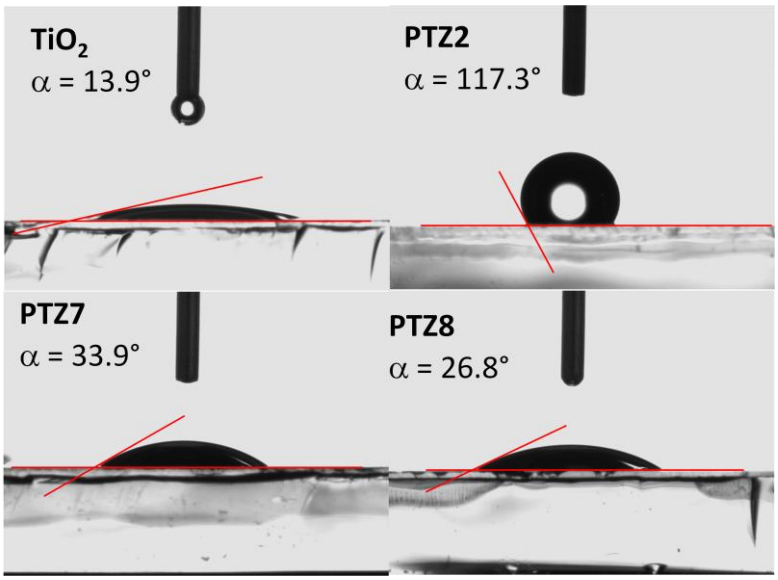

*Figure 3.21: Contact angles images, a) bare TiO_2 ; TiO_2 sensitized with b) **PTZ2**; c) **PTZ7**; d) **PTZ8**.*

Table 3.7: Contact angles.

Sample	Contact angle (ϑ_c/°)
Bare TiO_2	13.9
PTZ2	117.3
PTZ7	33.9
PTZ7	26.8

3.3.4 DSSC Performances

The new hydrophilic dyes have been tested in DSSC devices in standard conditions to see if the efficiency in solar energy conversion was modified by chains introduction. Even though we did not suppose any electronic contribution from the modification, as outlined by optical and electrochemical characterization, hydrophilic chains could have a detrimental effect in DSSC performances since the used electrolyte is in organic solvent. Thus we expect that the modification that might be positive for hydrogen production could have an opposite effect in DSSC performances. We decided to test them anyway to see the extent of such influence. A shorter photovoltaic characterization than in the case of **PTZ1-6** has been done, we were not interested in IPCE curves since no light harvesting modification on the dye has been made, and no EIS has been performed as well since we already knew that the organic media was not the best condition to compare **PTZ2** and **PTZ7-8**. Aqueous DSSC[57] could have given a better idea to fairly compare performances especially between **PTZ7** and **PTZ8** to see if a different behavior could be ascribed to the presence of the sugar moiety. We decided not to perform such tests since DSSC in organic electrolyte are well developed and standard conditions are reported, while aqueous DSSC performances are still low and an optimization in building cells would have been necessary. That would have implied strong efforts in devices optimization that is not the final goal of the research thus it goes beyond the role of "routine" screening as in the case of organic DSSC. We decided to directly test the dyes in photocatalytic hydrogen production to see any performance difference between **PTZ7** and **PTZ8**. The new dyes tested in organic DSSC showed lower performances but still remarkable efficiencies considering that the environment is not the optimal one for their test. **PTZ8** showed better performances compared to **PTZ7** and efficiencies that

are similar to the ones of **PTZ2**. Very interestingly the presence of the sugar moiety did not interfere with the photo-induced electron injection and the corresponding dye regeneration, meaning that all the properties evidenced by electrochemical measurements and our starting suppositions were true. J/V curves are represented in Figure 3.22, while performances characteristics are listed in Table 3.8.

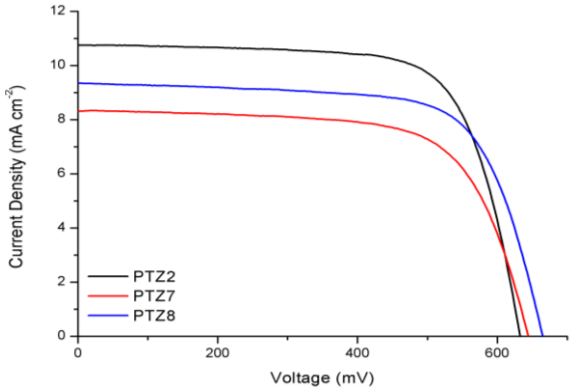

*Figure 3.22: J/V curves for DSSCs containing **PTZ2** and **PTZ7-8** dyes (AM 1.5 solar light).*

*Table 3.8: Photovoltaic characteristics of DSSCs containing **PTZ2** and **PTZ7-8** dyes (AM 1.5 solar light).*[a]

Dye[b]	J_{sc} (mA)	V_{oc} (mV)	ff (%)	PCE (%)
PTZ2	10.8 (13.4)	632 (649)	72 (70)	4.9 (6.1)
PTZ7	8.3 (11.0)	644 (653)	68 (68)	3.6 (4.9)
PTZ8	9.4 (11.8)	664 (672)	70 (69)	4.3 (5.5)
N719[c]	14.7 (17.4)	768 (753)	73 (71)	8.3 (9.3)

[a] Values without a black mask on the top of the cell are listed in brackets.
[b] Dye solution of 2 x 10^{-4} M in EtOH solution with 1:1 CDCA; electrolyte Z960 (1.0 M dimethyl imidazolium iodide, 0.03 M I_2, 0.05 M LiI, 0.1 M guanidinium thiocyanate and 0.5 M 4-*t*-butylpyridine in acetonitrile/valeronitrile 85/15), single TiO_2 layer (10 µm); surface area 0.20 cm^2
[c] Dye solution of 5 x 10^{-4} M in EtOH solution with 1:1 CDCA; electrolyte A6141 (0.6 M *N*-butyl-*N*-methyl imidazolium iodide, 0.03 M I_2, 0.10 M guanidinium thiocyanate, and 0.5 M 4-*t*-butylpyridine in acetonitrile/valeronitrile 85:15).

3.3.5 Dye-Sensitized Hydrogen Production

Photocatalytic hydrogen production tests have been performed in a similar manner as already reported in paragraph 3.2.4. Pt/TiO_2 composite has been used as support material to compare sensitization ability of **PTZ7** and **8** under visible light irradiation ($\lambda > 420$ nm). Pt nanoparticles have been photodeposited on TiO_2 surface using the same procedure illustrated in paragraph 3.2.4. Characterization of the Pt/TiO_2 support has been performed through textural analysis that showed a surface area of 55 m^2/g with pores diameters around 48 nm and a pore volume of 0.242 mL/g. Dimensional characterization through HAADF-STEM showed that TiO_2 nanoparticles have an irregular shape (12 – 45 nm), while homogeneously deposited Pt nanoparticles have a mean size of 2.4 nm (Figure 3.23).

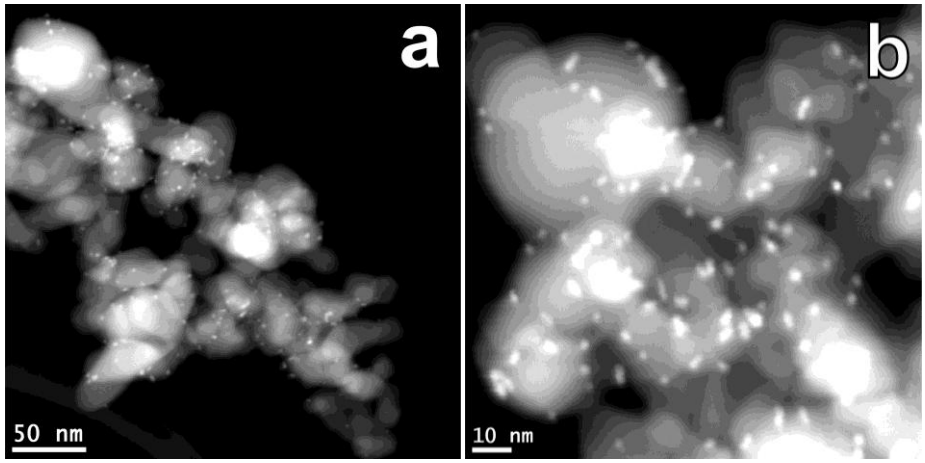

Figure 3.23: Representative HAADF-STEM images of the Pt/TiO_2 nanocomposite.

PTZ7 and **PTZ8** have been anchored on Pt/TiO_2 composite suspending such a powder in ethanol solutions of the corresponding dye. Dye loading was complete (30 μmol/g) as confirmed by the absence of visible peaks in the UV/Vis spectra of the remaining solutions. An analogous procedure as described in paragraph 3.2.4 has been followed, adapting Kitch and Bahnenmann practice.[46] First of all dye sensitization is responsible for hydrogen production since bare Pt/TiO_2 under the same conditions showed no catalytic activity. A scan on the photocatalytic performances at variation of the suspension concentration has been done for **PTZ8**, with 60 mg (in 60 mL of suspension volume) being the optimized concentration then used to evaluate photocatalytic efficiency for **PTZ7** (Figure 3.24). Dependence of the photocatalytic activity on suspension concentration has already been presented in paragraph 2.2.3.

The typical behavior is a first increment due to the increase of the amount of active material in the photoreactor, then, after having reached a maximum, there is a slight decrease (e.g. 80 and 100 mg) likely due to scattering effects of the incoming photons on the concentrated nanoparticles.

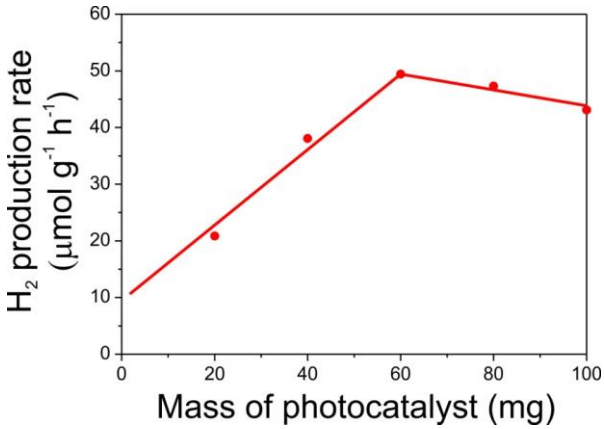

*Figure 3.24: Optimization of the suspension concentration for **PTZ8**.*

Hydrogen production curves are illustrated in Figure 3.25 while the TON and LFE_{20} values are listed in Table 3.9. The behaviour of both dyes is similar to the one highlighted for **PTZ2-6**. There is an initial induction period before achieving complete activation of the catalyst that in the case of **PTZ7-8** is of about 8 hours. This is quite a long period and it could be due to the combination of two effects. The first one is that there is a progressive increase of H_2 concentration in the gaseous effluent because of diffusion in the dead volume of the photo-reactor that takes around 1-2 h. The second one is probably due to passivation of Pt nanoparticles because of surface oxygen adsorption. Indeed this hypothesis is highly probable since Pt/TiO_2 composite is stored in air. Thus activation of the photocatalyst takes place in each experiment. When the system reaches a steady state it is evident that performances of **PTZ8** are double than the ones of **PTZ7**, hinting that surface wettability could be not the only phenomenon that influences activity. Since the difference in contact angles measurements are not able to explain such a big divergence in activity, we suggest that an additional beneficial effect is arising in the case of carbohydrate derivative that might be ascribed to self assembly properties induced by the sugar unit. Further future investigations are necessary to confirm such hypothesis and are briefly described in the following paragraph. Moreover both dyes seems to be stable

over the whole irradiation period as **PTZ2-6** series, confirming the superior photo-stability of thiophene spacer derivatives.

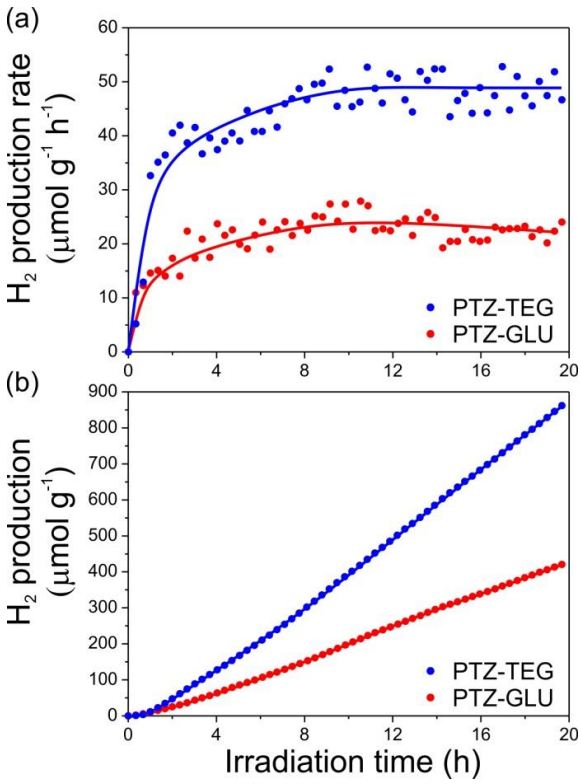

*Figure 3.25: Production rates (a) and overall productivities (b) in H_2 evolution from TEOA 10% v/v solution at pH = 7.0 under irradiation with visible light (λ > 420 nm) using the Pt/TiO_2 composite sensitized with **PTZ7** and **PTZ8.***

Table 3.9: Photocatalytic performance of the dye/Pt/TiO_2 materials in H_2 production from TEOA 10% v/v solution at pH = 7.0 under irradiation with visible light (λ > 420 nm)

Sample	Dye loading (μmol/g)	H_2 amount[a] (μmol/g)	TON[b]	LFE_{20}[c]
PTZ7	30.0	421	14.4	0.012
PTZ8	30.1	862	29.6	0.027

[a] Overall H_2 amount produced after 20 h of irradiation.
[b] TON = (2 x H_2 amount)/(dye loading).
[c] Light-to-Fuel Efficiency calculated after 20 h of irradiation.

3.3.6 Carbohydrates as Surface Spacers to Study Self-Assembly Properties: Brief Future Developments

The results of hydrogen production measurements pointed out the superior activity of the sugar derivative **PTZ8** compared to the glycolic one **PTZ7**. To explain higher efficiency we suggested an active role of carbohydrate units, that are able to interact through directional hydrogen bonds, in assembly dye molecules on TiO_2 surface. Alternatively, carbohydrates units could have a de-aggregating effect in keeping dye molecules separated thanks to a steric hindrance of the quite bulky glucose unit (compared to the glycolic one). To discern between these two hypotheses we planned to introduce spacing molecules as co-adsorbents during staining of the dye on TiO_2 surface. In DSSC field it is very well documented the beneficial effect of co-adsorbent molecules, e.g. chenodeoxycholic acid, that are able to keep dye molecules separated and prevent detrimental π-stacking phenomena.[58,59,60] We can imagine an analogous role for the sugar moiety in **PTZ8** that could in some way have a de-aggregating effect due to steric hindrance. Through the test of carbohydrates and spacers of other nature, such as chenodeoxycholic acid, we should discern between de-aggregating effects and self-assembly. For this reason we decided to test as spacer two different carbohydrate units that differ for the presence of a chain between the sugar unit and the carboxylic anchoring ending (Figure 3.26), thus resulting in different distances of the sugar moiety from the catalyst surface. Moreover we decided to test different ratios of the concentration of the dye and the co-adsorbent in the staining solution (1:1 and 1:10).

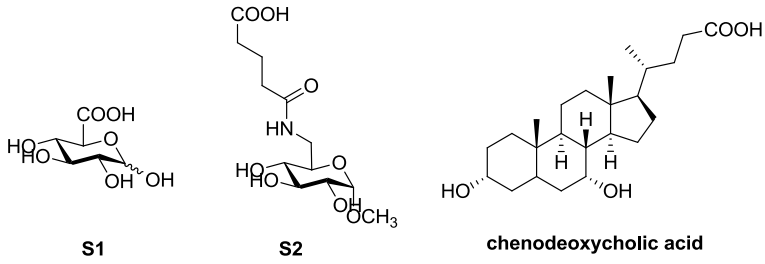

*Figure 3.26: Carbohydrate spacers **S0-1** and chenodeoxycholic acid.*

The synthesis of **S2** has been done in collaboration with the group of Professor Peri, while **S1** and chenodeoxycholic acid are commercially available and measurements on photocatalytic hydrogen production are currently in progress.

3.3.7 Conclusions

Hydrophilic dyes **PTZ7** and **PTZ8** have been successfully synthetized and characterized, a "click chemistry" approach allowed the introduction of the carbohydrate moiety in **PTZ8**. Using a easily scalable reaction such as the Cu-assisted azide-alkyne cycloaddition (CuAAC) a dye library with different carbohydrates could be straightforwardly designed and synthetized. Optical and electrochemical characterization have been performed to confirm that modification on the **PTZ2** structure with the two other chains was not affecting the conjugated skeleton of the dyes or their redox properties. DSSC characterization has been performed in organic electrolyte to evaluate the extent of the modification on efficiency. We expected that the introduction of two hydrophilic chains could have an opposite and detrimental effect than the hydrophobic chain in standard DSSC. The PCE of **PTZ7** and **PTZ8** have been slightly lower than **PTZ2** but still promising especially for an eventual test in aqueous DSSC. Hydrogen production experiments have been run to evaluate the photocatalytic efficiency of **PTZ7-8** in sensitizing Pt/TiO_2 composite, as already explained in paragraph 3.2.4. The results are very promising with **PTZ8** having double TON than **PTZ7**, hinting that surface wettability is probably only one of the characteristics that the sugar moiety is able to modify. It has been the first time that a sugar derivative has been tested both in DSSC and in hydrogen production and this first attempt paves the way to many research projects. We demonstrated that linking a carbohydrate moiety on a dye could result in promising performances that could be ascribed to both de-aggregating effect and/or self-assembly. If the second phenomenon takes place and it is verified by the efficiency tests, that are currently in progress, that would confirm the great contribution that sugar chemistry could give to photocatalytic hydrogen production field.

3.4 HYDROXAMIC ACIDS AS ANCHORING GROUPS TO PREVENT DYE DESORPTION

After the improvement of the light harvesting properties through spacer tuning as illustrated in paragraph 3.2 and the investigations on the effect of hydrophilic chains on the donor core as described in paragraph 3.3, the third kind of modification was dealing with the part of dye that is directly connected to TiO_2 surface. Anchoring/accepting moiety is strongly involved both in electron injection and in dye stability on the semiconductor surface. As already described in the introduction to anchoring groups in DSSC (paragraph 2.1.2), the cyanoacrylic acid is the most common choice as anchoring group in many sensitizers. The good compromise between the electron-withdrawing ability, due to the nitrile group, and the anchoring stability of the carboxylic acid, led to establish the leadership of this moiety over many other groups. However, besides all these advantages, cyanoacrylic acids suffer from some limitations, especially related to stability issues of the ester bond that is formed between the dye and the TiO_2 surface. Many anchoring geometries (illustrated in paragraph 2.1.2) have been proposed and all of them are probably contributing to the real way of interaction of the dye on the surface of the semiconductor, even though with different extents. All the interactions are labile to hydrolysis, thus this drawback is expected to be critical in the case of aqueous DSSC and in photocatalytic hydrogen production, where water is the working medium of the device.[61] Amongst the alternative anchoring units, the main limitation seems to be that groups that are responsible for strong bonds on TiO_2 do not ensure a good electronic communication thus hampering performances (e.g. phosphonic acids compared to carboxylic acids). An overview on the literature on metallorganic complexes and their *ad hoc* modification for use in aqueous medium, shows that phosphonic acids are the preferred ones for replacing carboxylic moieties.[62,63] Electronic communications is often limited by this group because of tetrahedral phosphorous, thus original solution of asymmetric anchors have been proposed where the electronic communication is ensured by carboxylic end while strong binding is done by phosphonic acid.[64] In the case of organic dyes for photo-catalytic hydrogen production, all the tested sensitizers have cyanoacrylic acid as A group with the only exception of a malononitrile end that has been tested in order to improve electron withdrawing character of the acceptor unit (paragraph 2.3).[65] In this last example the interaction of the dye with the semiconductor surface is not ensured by any covalent bond and it is probably weaker than the usual ester bond even though higher efficiencies have been recorded thanks to the better light harvesting properties. As already pointed out in paragraph 3.2, stability is an important issue to

be solved to have practical application in devices. There are two aspects in durability: stability of the dyes upon irradiation (photostability) and towards hydrolysis (strength of the connection between dye and semiconductor surface). The first kind of stability have been reached through modification of the spacer unit, thanks to the peculiar behaviour of thiophene derivatives, as already illustrated in paragraph 3.2. Attention has thus been focused in the development of more stable covalent attachment of dye on TiO_2 surface. Hydroxamic acids have been chosen as promising candidates since they should ensure a similar electronic communication as carboxylic acids, while the strength of the covalent bond with TiO_2 surface has been calculated to be 33% more stable upon hydrolysis reaction.[66,67] Few examples have been reported in the literature so far concerning this anchoring group for application in organic dyes in DSSC,[68,69] while there is no investigation in the field of hydrogen production. The ideal acceptor candidate to be tested would then be a cyano-hydroxamic acid where both the electron-withdrawing ability of the nitrile group and the stability of the hydroxamic acid would be cooperating. The anchoring geometry of this group could be alternative to the carboxylic one having both nitrogen and oxygen able to interact with the hydroxyl groups of TiO_2, and if nitrogen is linked on the surface, an amide-type bond is formed in contrast with the weaker ester bond. In this research **PTZ1** structure has been modified in order to test the advantages of such anchoring modification in a very simple molecule. During the writing of this thesis such a project is still under development thus no hydrogen tests are available and a partial characterization of the product will be presented. After having been synthesized, **PTZ1-HA** (Figure 3.27), has been tested in DSSC and in desorbing tests together with **PTZ1** as a comparison and with the mono-branched system of **PTZ1** (**PTZ1M**) to compare stability results (Figure 3.27).

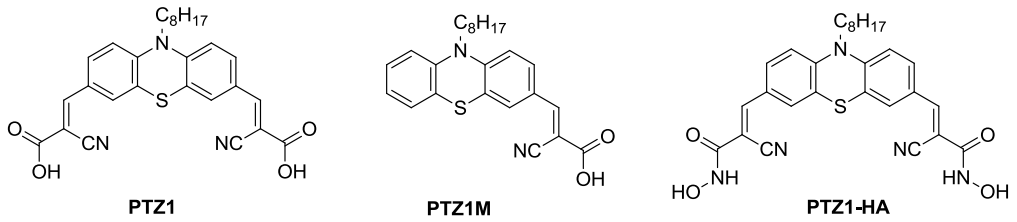

*Figure 3.27: **PTZ1** as reference dye, the corresponding mono-branched **PTZ1M**, and the hydroxamic acid derivative **PTZ1-HA**.*

In parallel with this characterization, two other dyes, **PTZ2-HA** and **PTZ5-HA**, designed as an analogous modification of dye **PTZ2** and **PTZ5**, have been synthesized and their characterization is still in progress.

3.4.1 Synthetic Strategy

The synthetic strategy has been adapted from the thesis work of Dr. Ottavia Bettucci.[70] There are many synthetic approaches to transform a carboxylic into a hydroxamic acid; the selected one has already been successfully employed in the laboratory where the synthesis was performed. The carboxylic precursor has been treated with an activating agent for peptide coupling as 4-(4,6-dimethoxy-1,3,5-triazin-2-yl)-4-methylmorpholinium chloride (DMTMM) in the presence of a base such as N-methyl morpholine (NMM). The resulting activated intermediate is illustrated in Figure 3.28.

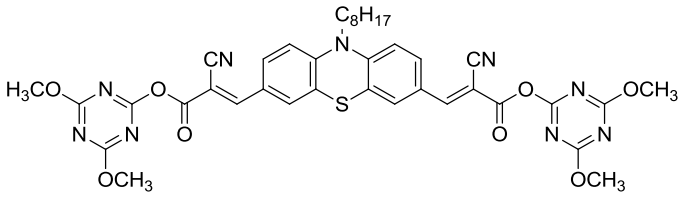

Figure 3.28: Activated carboxylic acid through DMTMM.

Such intermediate was not isolated but its formation could be monitored through TLC and through the darkening of the reaction mixture (from red to dark red, because of the high electron withdrawing ability of triazine cores). The hydroxamic moiety was then introduced in the THP protected form (tetrahydropyranyl). Protection allowed purification through column chromatography that would not have been possible if the hydroxamic ends were free. A partial problem arising from the use of THP has been the formation of two stereogenic centers in the intermediate that complicated the purification, but which are of course lost during deprotection in acidic conditions. The overall reaction is illustrated in Scheme 3.5. A side reaction that may occur during the deprotection step is the transformation of the hydroxamic group into the starting carboxylic acid, moreover the reaction conversion is not easily followed through TLC since the partial deprotection of one out of two endings brings to two red spots with similar behaviour, difficult to be distinguished, on TLC. The isolated crude product has been simply washed with AcOEt for purification, avoiding further manipulations which could promote hydrolysis.

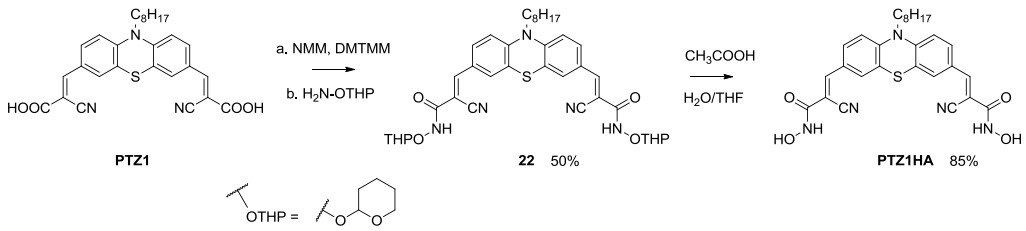

*Scheme 3.5: Synthetic routes for **PTZ1-HA**.*

The synthetic scheme has been then extended to synthesize the hydroxamic acids of **PTZ2** and **PTZ5**. The first step on the carboxylic acids gave similar results to the test done on **PTZ1**, while the deprotection step has presented some problems during the purification step. Solvent washings or crystallizations did not allow to get cleaner products, while column chromatography has not been performed because the desired product stuck on silica gel. Further approaches will be necessary for isolation of clean **PTZ2-HA** and **PTZ5-HA**, thus characterization of **PTZ1-HA** only will be presented in the next paragraph**.**

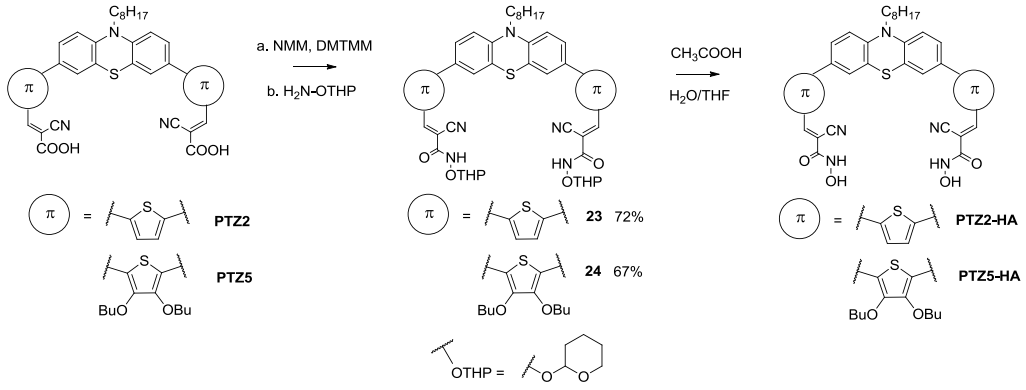

*Scheme 3.6: Synthetic routes for **PTZ2-HA** and **PTZ5-HA**.*

3.4.2 Optical Characterization

Optical characterization of **PTZ1-HA** has been done to compare the results with **PTZ1** and is illustrated in Figure 3.29. 10^{-5} M solutions of each dye in THF have been used to measure the maximum of absorption and the molar extinction coefficient applying the Lambert Beer law. The shape of the absorption band for **PTZ1-HA** is less pronounced than **PTZ1**, hinting that at least two bands are contributing to that shape. **PTZ1** shows an intense ICT peak at 460 nm but there is a second peak around 400 nm that is much more evident in the case of **PTZ1-HA**. The molar extinction coefficient is lower and the maximum of absorption is shifted towards higher energy

by 12 nm. This behaviour was not expected since hydroxamic acid was not supposed to modify optical properties, as illustrated in the case of the dye reported in the literature.[68] It has to be pointed out that this is the first time that two anchoring hydroxamic acids are used and that the molecular structure of **PTZ1-HA** is much simpler than **MK2-HA** that has been tested in the literature. The replacement of the carboxylic acids with the hydroxamic moieties can possibly have a more noticeable effect in a simple structure such as **PTZ1** with respect to **MK2** where the light harvesting properties are mainly due to the rather complex spacer structure that is illustrated in Figure 2.7 (paragraph 2.1.2). Anyway the shape of the absorption peak could be assigned to an ICT process as in the other dyes since **PTZ1-HA** is a dipolar molecule. Tauc plots have been used to evaluate E_{gap}^{opt} as reported for the other illustrated dyes. All the optical parameters are listed in Table 3.10.

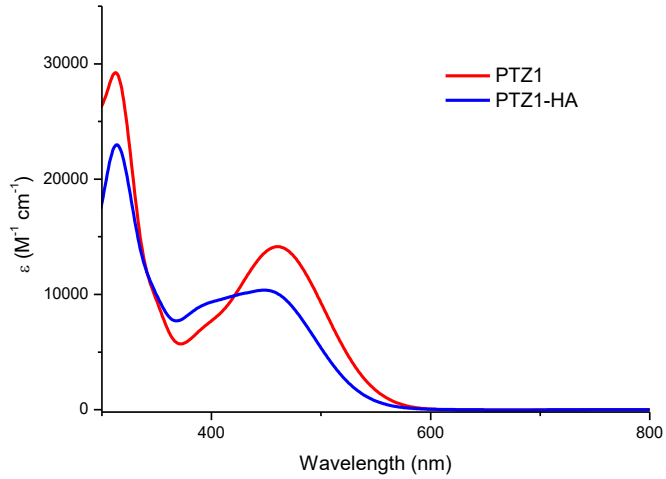

*Figure 3.29: UV/Vis absorption spectra of **PTZ1** and **PTZ1-HA**.*

*Table 3.10: Optical parameters for **PTZ1** and **PTZ1-HA**.*

Dye	λ_{max} (nm)	ε ($M^{-1}cm^{-1}$)	λ_{onset} (nm)	E_{gap}^{opt} (eV)
PTZ1	460	14100 ±100	590	2.10
PTZ1HA	448	10500 ± 450	579	2.14

3.4.3 DSSC Performances

DSSC performances have been investigated to compare activities of **PTZ1** and **PTZ1-HA** before testing them in photocatalytic hydrogen production tests. Moreover, since there are few examples of dyes bearing hydroxamic acids in the DSSC literature, while there are no examples aimed at the modification of the anchoring unit for hydrogen production purposes, a careful screening of the photovoltaic performances is thus essential. In particular the working medium could strongly interfere with the activity of the devices when passing from the organic medium of DSSC to the aqueous one for hydrogen production. For that reason it is even more relevant the comparison between the efficiencies in DSSC and in the hydrogen production. Photovoltaic performances have been evaluated in the same conditions as **PTZ1-6** in order to directly compare results. The efficiency of the dye containing the hydroxamic acid is globally the half of the carboxylic acid containing counterpart as illustrated in Figure 3.30. While fill factor and photo-voltage are comparable, there is a strong loss in photo-current for **PTZ1-HA** that is the main responsible for the total decrease in PCE (Table 3.11).

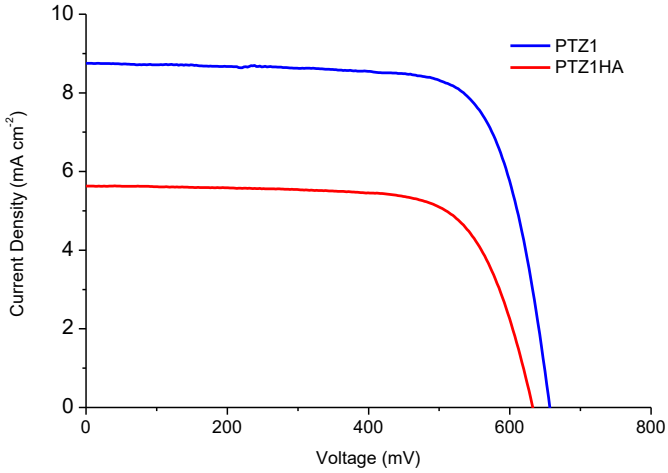

*Figure 3.30: J/V curves for **PTZ1** and **PTZ1-HA**.*

Lower photo-current could be ascribed to a lower dye loading or to a less efficient electron injection. It should be considered that optical characterization has outlined a lower light harvesting efficiency for **PTZ1-HA** that could be responsible for this lower PCE value. This result is in contrast with efficiency reported for the hydroxamic derivative of **MK2**, where analogous performances were registered for the two dyes.

As already illustrated in paragraph 3.4.2 **MK2** and **PTZ1** are very different in the molecular structure, since the second one has no spacer unit and two anchoring points. It could be that possible limitations of hydroxamic end are partially overcome in the case of **MK2** with the fine tuning of the spacer structure.

*Table 3.11: Photovoltaic characteristics of **PTZ1** and the hydroxamic acid **PTZ1-HA.***

Dye[a]	J_{sc} ($mAcm^{-2}$)	V_{oc} (mV)	ff (%)	PCE (%)
PTZ1	8.76 (11.1)	656 (667)	74 (74)	4.3 (5.5)
PTZ1-HA	5.01 (5.63)	627 (618)	66 (65)	2.1 (1.9)

3.4.4 Desorption Kinetics

Desorption kinetics are important experiments to evaluate the strength of the bond that is formed between the dye and the semiconductor surface. The experiment is done through acceleration of the desorption process through the help of a basic solution. There are some examples in the literature in which kinetic studies of this type have been performed with THF:EtOH - 5:1 with KOH 0.1 M solutions.[71,72] Thus the same desorbing mixture has been first selected. The strength of the bond in the case of the investigated dyes has revealed to be stronger than the one reported in the literature, thus no detachment is noticeable in the medium-long term. For long desorption times the reproducibility is low because of degradation of the TiO_2 film, thus stronger desorption solutions have been used. Starting from the literature one, THF:EtOH - 5:1 with KOH 0.1 M, the strength of the basis is enforced by the introduction of water in the mixture at increasing concentrations. The best option seemed to be EtOH:H_2O - 15:1 with KOH 0.1 M. The investigated samples are composed of commercial TiO_2 films, sensitized with **PTZ1M**, **PTZ1** and **PTZ1-HA**. In the case of the mono-branched dye the selected desorbing solution was too strong and the desorption was immediate, thus EtOH:H_2O – 30:1 with KOH 0.1 M has been used. In the reference articles[71,72] a kinetic model for desorption has been proposed, in the case of di-branched structures such a model is no more valid since there are

[a] Dye solution of 2 x 10^{-4} M in EtOH solution with 1:1 CDCA; electrolyte Z960 (1.0 M dimethyl imidazolium iodide, 0.03 M I_2, 0.05 M LiI, 0.1 M guanidinium thiocyanate and 0.5 M 4-*t*-butilpiridine in acetonitrile/valeronitrile 85/15), single TiO_2 layer (10 µm); surface area 0.20 cm^2. Parameters without black mask are reported in parenthesis.

two anchoring points and a pseudo-first order kinetics will probably be no more valid. Moreover since a different solution has been used in the case of **PTZ1M**, there is not any possibility to make data comparison in terms of kinetic constants between **PTZ1** and **PTZ1M**. A second issue that has occurred was that the high binding stability generates problems in the measurement of UV/Vis spectra of the desorbing solution. Side reactions occurred thus the visible peak corresponding to the desorbed dye increased in intensity in the first moments but decreased for longer times giving very broad bands. One of the possible side reactions is the retro-Knoevenagel that brings to the aldehyde intermediate in the case of **PTZ1** tests. There is no evidence of which is the reaction responsible for dye detachment, if hydrolysis or retro-Knoevenagel, as hinted by a study of Sun *et al*.,[73] thus reference to the overall survived dye amount of TiO_2 surface will be given, without any further investigation on the instability reason. Since the monitoring of the ICT peak in solution of the detached dye was no more reliable, an alternative approach has been used. Instead of measuring the amount of dye in solution, the survived dye on TiO_2 film could be measured through UV/Vis spectroscopy in transmittance mode. To perform such analysis the TiO_2 films could not be the one used for the DSSC tests (opaque paste) but they must be transparent. Moreover, because of surface roughness, many spectra have been registered in different points of the films to calculate a mean value and a standard deviation. The results are illustrated in Figure 3.31.

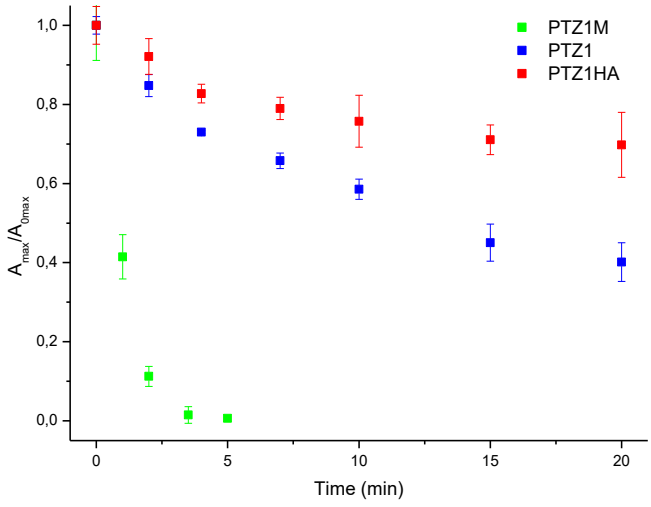

*Figure 3.31: Desorption kinetic graphs for **PTZ1M**, **PTZ1**, and **PTZ1-HA**.*

It is evident that there is a great effect on stability going from a mono- to a di-branched structure as already suggested in the literature.[74] Moreover the hydroxamic derivative showed an increase of stability that is qualitatively evident. Application of the pseudo-first order model to these curves failed since the exponential correlation does not go to zero. Therefore, to try to quantitatively evaluate the stability of the system upon hydrolysis, the amounts of desorbed dye after 2, 10, and 20 minutes have been calculated and reported in Table 3.12. All the numeric evaluation has been done with extension of the Lambert Beer law to the solid state of dyes attached on TiO_2 surface, even though molar absorption coefficients have not been used to evaluate the amount of dye since they should be different. It is anyway likely to assume a linear correlation between dye molecules concentration on the surface and intensity of the resulting absorption spectrum, thus values in Table 3.12 could be considered a reliable estimation.

Table 3.12: Percentage of dye anchored on TiO_2 surface after different irradiation times.

Dye	2 min	10 min	20 min
PTZ1M	10%	-	-
PTZ1	85%	59%	40%
PTZ1HA	92%	76%	70%

3.4.5 Conclusions

Hydroxamic acids have been introduced in di-branched phenothiazine dyes through peptide coupling. **PTZ1** has been modified in order to get **PTZ1-HA** that has been characterized in optical properties, DSSC performances and stability in anchoring TiO_2 surface in comparison with **PTZ1**. DSSC performances have been considerably lower because of halving in the photo-current, perhaps due to a different and less efficient photo-injection mechanism than the carboxylic counterpart. Alternatively the low light harvesting properties of **PTZ1-HA** could be responsible for lower photovoltaic performances, thus the development of more sophisticated dyes could be a promising solution. **PTZ2** and **PTZ5** have been modified to introduce the hydroxamic moiety in order to have enhanced optical properties. Unfortunately the purification step of these dyes is not straightforward and it is still in progress. Despite the lower photovoltaic performances, the enhancement in stability of dyes anchoring upon hydrolysis has been found to be considerable with 70% of the dye survived on TiO_2

surface at 20 min of dipping compared to 40% of the carboxylic **PTZ1**. This result confirmed the hypothesis of a stronger binding of hydroxamic acids compared to carboxylic acids that is a remarkable beneficial effect since dye hydrolysis could be one of the major limiting factors in the case of hydrogen production. Therefore efforts will now be given in the purification of **PTZ2-HA** and **PTZ5-HA**, in order to have dyes that should better harvest light and in the design and synthesis of more conjugated spacers to have dyes to be fairly compared to **MK2-HA** performances. The di-branched structure has been confirmed to be highly stable, as established by desorption tests of **PTZ1M** and **PTZ1**, suggesting that new stable sensitizers for hydrogen production should have a di-branched structure because of their superior stability. Hydrogen production tests are now in progress with **PTZ1-HA** and it is not unlikely that **PTZ1-HA** could overcome performances of **PTZ1**. DSSC performances have not been translated in analogous hydrogen production efficiencies in the case of **PTZ1-6**, with **PTZ1** that was almost the lowest performer in DSSC and the best one for short irradiation time in hydrogen production application. For that reason it is not excluded that **PTZ1-HA** could over-perform **PTZ1**; an even better result could be if the deactivation in hydrogen production that characterized **PTZ1** after 2-3 hours of irradiation will be partially hampered thanks to the new anchoring unit. That result would hint that hydroxamic acids could enhance overall durability of the device, both in terms of photo-stability of dyes and in stability upon hydrolysis in basic media without strong irradiation.

3.5 SYNTHETIC PROCEDURES

NMR spectra have been recorded with Bruker AMX-500 spectrometer operating at 500.13 MHz (^{1}H) and 125.77 MHz (^{13}C), Varian Gemini 200 spectrophotometer operating at 200 MHz (^{1}H) and 50.4 MHz (^{13}C), and Varian Mercury 400 spectrometer operating at 400 MHZ (^{1}H) and 100.8 MHz (^{13}C). Chemical shift values are expressed in ppm on the δ scale and referred to the residual solvent ($CDCl_3$, δ 7.26 ppm for ^{1}H and δ 77.16 ppm for ^{13}C; DMSO-d_6, δ 2.50 ppm for ^{1}H and 39.51 ppm for ^{13}C; THF-d_8 δ 1.72 and 3.58 ppm for ^{1}H, δ 67.21 and 25.31 ppm for ^{13}C). Coupling constants (J) are expressed in Hz, while the used abbreviations are s (singlet), d (doublet), dd (doublet of doublets), t (triplet), td (triplet of doublets), and m (multiplet). Multiplets are indicated as chemical shift interval.

ESI-MS analyses have been performer through a Thermo Scientific LCQ − FLEET with infusion technique.

Absorption spectra were recorded with a V-570 Jasco spectrophotometer and a Varian Cary 4000 spectrophotometer.

Infrared spectra (IR) were recorded with an ATR-FTIR Perkin–ElmerSpectrum100 spectrometer.

Flash chromatography was performed with Merck grade 9385 silica gel 230–400 mesh (60Å). Conversion was monitored by thin-layer chromatography by using UV light (254 and 365 nm) as visualizing agent. Reactions performed under inert atmosphere were done in flame- or oven-dried glassware and a nitrogen atmosphere was generated with Schlenk technique.[75] All reagents were obtained from commercial suppliers at the highest purity grade and used without further purification. Anhydrous solvents were purchased from Sigma-Aldrich and used without further purification. Extracts were dried with Na_2SO_4 and filtered before removal of the solvent by evaporation.

Low temperature conditions have been achieved through acetone and liquid N_2 mixture for -78 °C, ice/NaCl bath to reach till -10 °C, and water and ice to reach 0 °C.

Molecules **1,**[6] **2,**[6] **3**,[23,24] **7**,[29] **8**,[31] **10**,[30] **15**,[51] **21**,[6] **PTZ1**,[6] and **PTZ1M**[6] have been synthesized adapting known procedures from the literature.

General Procedure A for Suzuki-Miyaura Cross-Coupling: Product **1** (1 eq.) and Pd(dppf)Cl_2·CH_2Cl_2 (10% eq.) were dissolved in dimethoxyethane (DME, 0.1 M) and stirred for 15 minutes under nitrogen atmosphere. Then boronic acid/ester

derivative (2.4 eq.) and K_2CO_3 (10 eq.) were added as suspension in oxygen-free methanol (0.1 M). The reaction was performed with microwave irradiation (100 °C, 200 W, 90 minutes) and then quenched by pouring into a saturated solution of NH_4Cl (50 mL). Filtration on Celite and extractions with organic solvent allowed to isolate the crude product, then purified through column chromatography on silica gel.

General Procedure B for Suzuki-Miyaura Cross-Coupling: Bromo-derivative (2.2 eq.) and Pd(dppf)Cl_2·CH_2Cl_2 (10% eq.) were dissolved in dimethoxyethane (DME, 0.1 M) and stirred for 15 minutes under nitrogen atmosphere. Then product **11** (1 eq. of crude product) and K_2CO_3 (10 eq.) were added as suspension in oxygen-free methanol (0.1 M). The reaction was performed with microwave irradiation (100 °C, 200 W, 90 minutes) and then quenched by pouring into a saturated solution of NH_4Cl (50 mL). Filtration on Celite and extractions with organic solvent allowed to isolate the crude product, then purified through column chromatography on silica gel.

General Procedure C for Knoevenagel Condensation: Aldehyde precursor (1 eq.), cyanoacetic acid (10 eq.) and piperidine (10 eq. + catalytic) were dissolved in $CHCl_3$ (0.02 M) and heated to reflux for 5 h. After having the solvent evaporated, a solution of HCl 1 M (~50 mL) was added and the mixture was left under magnetic stirring for 5 h at rt. The dark red solid that precipitated was filtered and washed with water (3x30 mL), PE (2x30 mL) and Et_2O (1x10 mL).

General Procedure D for Alkylation: Product **15** (1 eq.) was dissolved in dry DMF under N_2 atmosphere, then the solution was cooled to 0°C using an ice bath and NaH 60% (2 eq.) was slowly added. After stirring at 0 °C for 1 h, the appropriate tosylate or bromide (2 eq.) was added and the solution was stirred at rt for 4 h, when TLC revealed the complete conversion. The reaction mixture was quenched with iced water, then extracted with Et_2O and the organic phase was dried with $NaSO_4$ and concentrated. The crude was purified using flash column chromatography on silica gel.

General Procedure E for Hydroxylamination Reaction: N-Methylmorpholine (NMM, 3 eq) and 4-(4,6-Dimethoxy-1,3,5-triazin-2-yl)-4-methylmorpholinium chloride (DMTMM, 2.4 eq) were added to a solution of the appropriate cyanoacrylic intermediate in THF. After 1 h under magnetic stirring at rt the solution color is darker than the starting one and the TLC shows the presence of an additional spot with respect to the starting material. *O*-(Tetrahydro-2*H*-pyran-2-yl)hydroxylamine (H_2N-OTHP, 5 eq) is added and the solution recovers the starting color. After 3 h under magnetic stirring at rt the TLC shows no more starting material and a series of

red spots. THF was evaporated and water was added to the mixture, extractions with AcOEt (2 x 30 mL) were performed and then the combined organic phases were washed with HCl 1 M and water. Anhydrification with Na_2SO_4 and concentration of the solvent gave the crude product that has been purified through flash column chromatography on silica gel.

General Procedure F for THP cleavage: protected hydroxamic acid compound (1 eq.) was solubilized in THF and a mixture of water and acetic acid is then added (overall ratio THF: H_2O:AcOH – 7:2:1). The mixture is heated to 60 °C for 24 h protected from light through Al foils. The solvent mixture is then evaporated and water is added, the dark red solid was separated through filtration.

10-octyl-10*H*-phenothiazine (1)

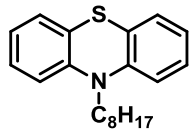

10*H*-phenothiazine (2.0 g, 10 mmol) was dissolved in DMF (30 mL) under N_2 atmosphere. The reaction mixture was cooled down to 0 °C and NaH (60% mixture with paraffin oil, 1.2 g, 50 mmol) was slowly added to the solution. The solution changed aspect from transparent yellow to an orange suspension. After 1 h of stirring at 0 °C, 1-bromooctane was added and temperature allowed to reach rt. The mixture was stirred overnight and then quenched through pouring on ice. The aqueous phase was extracted with Et_2O (3 x 200 mL), and the organic phases were combined and dried. Product **1** was obtained as a colorless liquid in >95% yield (3.10 g, 10 mmol) and used without any further purification for next step.

^{1}H NMR (500 MHz, $CDCl_3$) δ 7.23 – 7.15 (m, 4H), 6.96 (td, *J* = 7.5, 1.0 Hz, 2H), 6.91 (dd, *J* = 8.5, 0.8 Hz, 2H), 3.88 (t, *J* = 7.2 Hz, 2H), 1.86 (m, 2H), 1.53 – 1.45 (m, 2H), 1.42 – 1.28 (m, 8H), 0.95 (t, *J* = 6.9 Hz, 3H).

10-octyl-10*H*-phenothiazine-3,7-dicarbaldehyde (2)

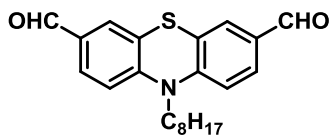

$POCl_3$ (21.5 g, 140 mmol) was added dropwise to DMF (10.2 g, 140 mmol) at -15 °C under N_2 atmosphere; at the end of the addition a white solid formed, that, after 50

minutes, was dissolved in DMF (30 mL). Product **1** (3.10 g, 10 mmol) was added and the mixture heated at 70 °C for 24 h. Then a saturated solution of NaOAc (50 mL) was added dropwise and the mixture stirred for 2 h at 100 °C. The mixture was extracted with Et_2O (3 x 100 mL), the organic phases were combined and dried. Purification through column chromatography on silica gel, using a mixture 3:1 of PE and AcOEt, gave the product **2** as orange oil in 18% yield (670 mg, 1.8 mmol).

^{1}H NMR (500 MHz, $CDCl_3$) δ 9.81 (s, 2H), 7.65 (dd, *J* = 8.4, 1.7 Hz, 2H), 7.56 (d, *J* = 1.2 Hz, 2H), 6.94 (d, *J* = 8.5 Hz, 2H), 3.92 (t, *J* = 7.2 Hz 2H), 1.86 – 1.74 (m, 2H), 1.49 – 1.34 (m, 2H), 1.36 – 1.18 (m, 8H), 0.86 (t, *J* = 6.9 Hz, 3H).

3,3'-(10-octyl-10*H*-phenothiazine-3,7-diyl)bis(2-cyanoacrylic acid) (PTZ1)

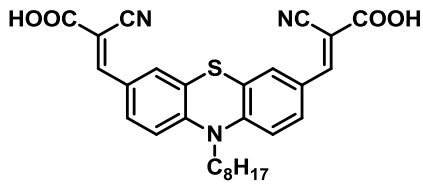

PTZ1 was synthesized according to general procedure C for Knoevenagel condensation using product **2** (650 mg, 1.77 mmol), cyanoacetic acid (1.50 g, 17.7 mmol), piperidine (1.80 g, 17.7 mmol + cat) and $CHCl_3$ (15 mL). A dark red solid has been isolated as the product (800 mg, 1.59 mmol) with 84% of yield.

^{1}H NMR (500 MHz, DMSO-d_6) δ 8.14 (s, 2H), 7.94 (dd, *J* = 8.8, 2.0 Hz, 2H), 7.80 (d, *J* = 2.1 Hz, 2H), 7.24 (d, *J* = 8.9 Hz, 2H), 4.00 (t, *J* = 7.0 Hz, 2H), 1.74 – 1.61 (m, 2H), 1.43 – 1.34 (m, 2H), 1.31 – 1.15 (m, 8H), 0.83 (t, *J* = 6.8 Hz, 3H).

^{13}C NMR (126 MHz, DMSO-d_6) δ 164.0, 151.9, 147. 1, 131.6, 129.7, 127.3, 122.7 (x 2), 117.4, 116.9, 44.1, 31.5, 29.0, 28.9, 26.3, 22.7, 22.5, 14.4.

3,7-dibromo-10-octyl-10*H*-phenothiazine (3)

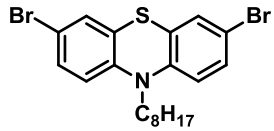

To a solution of **1** (1.00 g, 3.2 mmol) in acetic acid (10 mL), bromine (0.6 g, 3.2 mmol) was added dropwise. The mixture was left under magnetic stirring for 1 h and then a second portion of bromine (0.6 g, 3.2 mmol) was added giving a black mixture that was left under stirring overnight. The mixture was then quenched with a saturated

solution of Na_2SO_3 (50 mL) and left under magnetic stirring for 1 h. Extractions with Et_2O (3x100 mL) and anhydrification on Na_2SO_4 gave **3** as a crude product. Purification through column chromatography using PE as eluent allowed to afford **3** as a pale yellow oil in 96% of yield (1.42 g).

^{1}H NMR (500 MHz, $CDCl_3$) δ 7.26 – 7.20 (m, 4H), 6.68 (d, *J* = 8.5 Hz, 2H), 3.75 (t, *J* = 7.1 Hz, 2H), 1.79 – 1.69 (m, 2H), 1.42 – 1.34 (m, 2H), 1.33 – 1.19 (m, 8H), 0.87 (t, *J* = 6.8 Hz, 3H).

5,5'-(10-octyl-10*H*-phenothiazine-3,7-diyl)dithiophene-2-carbaldehyde (4)

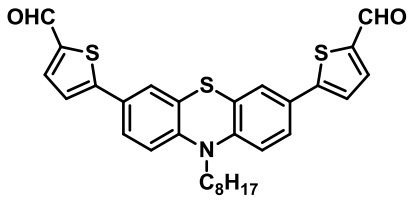

Product **4** was synthesized according to general procedure A for Suzuki-Miyaura cross-coupling, using product **3** (200 mg, 0.43 mmol), $Pd(dppf)Cl_2{\cdot}CH_2Cl_2$ (35 mg, 0.043 mmol), 5-formyl-2-thienylboronic acid (160 mg, 1.03 mmol), K_2CO_3 (600 mg, 4.3 mmol), DME (3 mL) and methanol (3 mL). Extractions were performed with AcOEt (3 x 50 mL) and a mixture of PE:AcOEt - 3:1 was used as eluent for purification. The desired product was isolated as a red solid (200 mg) in 87% of yield.

^{1}H NMR (500 MHz, $CDCl_3$): δ 9.82 (s, 2H), 7.65 (d, *J* = 3.9 Hz, 2H), 7.38 (dd, *J* = 8.5, 2.0 Hz, 2H), 7.31 (d, *J* = 2.0 Hz, 2H), 7.24 (d, *J* = 3.9 Hz, 2H), 6.79 (d, *J* = 8.5 Hz, 2H), 3.79 (t, *J* = 7.2 Hz, 2H), 1.81 – 1.71 (m, 2H), 1.44 – 1.34 (m, 2H), 1.34 – 1.18 (m, 8H), 0.84 (t, *J* = 6.9 Hz, 3H).

^{13}C NMR (126 MHz, $CDCl_3$): δ 182.5, 153.1, 145.1, 141.7, 137.6, 127.7, 125.7, 124.8, 124.4, 123.2, 115.6, 47.8, 31.7, 29.2, 29.1, 26.8, 26.6, 22.6, 14.1.

Anal. Calcd for $C_{30}H_{29}NO_2S_3$: C, 67.76; H, 5.50; N, 2.63. Found: C, 67.69; H, 5.59; N, 2.72.

IR: cm^{-1} 2924, 2851, 1654, 1580, 1429, 1220, 1053, 792.

3,3'-(5,5'-(10-octyl-10*H*-phenothiazine-3,7-diyl)bis(thiophene-5,2-diyl))bis(2-cyanoacrylic acid) (PTZ2)

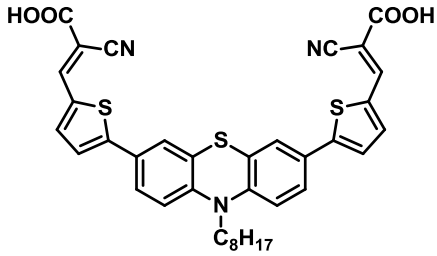

PTZ2 was synthesized according to general procedure C for Knoevenagel condensation using product **4** (140 mg, 0.26 mmol), cyanoacetic acid (220 mg, 2.6 mmol), piperidine (270 mg, 2.6 mmol + cat) and $CHCl_3$ (5 mL). A dark red solid (150 mg) has been isolated as the product with 87% of yield.

^{1}H NMR (500 MHz, DMSO-d_6): δ 8.48 (s, 2H), 8.00 (d, *J* = 4.2 Hz, 2H), 7.72 (d, *J* = 4.0 Hz, 2H), 7.64 – 7.56 (m, 4H), 7.14 (d, *J* = 8.4 Hz, 2H), 3.95 (t, *J* = 6.7 Hz, 2H), 1.76 – 1.62 (m, 2H), 1.45 – 1.37 (m, 2H), 1.34 – 1.16 (m, 8H), 0.82 (t, *J* = 6.7 Hz, 3H).

^{13}C NMR (126 MHz, DMSO-d_6): δ 164.1, 152.3, 147.0, 145.2, 142.0, 134.4, 127.6, 126.6, 125.0, 124.9, 124.0, 117.1, 117.0, 98.4, 63.3, 44.2, 31.5, 29.1, 28.9, 22.7, 22.5, 14.4.

Anal. Calcd $C_{36}H_{31}N_3O_4S_3$: C, 64.94; H, 4.69; N, 6.31. Found: C, 64.71; H, 5.13; N, 6.26.

IR: cm^{-1} 2921, 2846, 2218, 1678, 1559, 1479, 1393, 1355, 1250, 1212, 1061, 788.

10-octyl-3,7-di(thieno[3,2-b]thiophen-2-yl)-10*H*-phenothiazine (5)

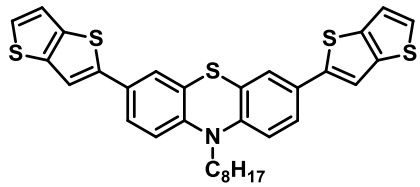

Product **5** was synthesized according to general procedure A for Suzuki-Miyaura cross-coupling using product **3** (500 mg, 1.07 mmol), $Pd(dppf)Cl_2 \cdot CH_2Cl_2$ (90 mg, 0.107 mmol), 4,4,5,5-tetramethyl-2-(thieno(3,2-b)thiophen-2-yl)-1,3,2-dioxaborolane (660 mg, 2.46 mmol), K_2CO_3 (1.50 g, 10.7 mmol), DME (7 mL) and methanol (7 mL).

Extractions with AcOEt and purification with PE:CH_2Cl_2 - 8:1 as eluent gave product **5** as a yellow solid in 84% yield (530 mg).

^{1}H NMR (500 MHz, $CDCl_3$): δ 7.39 – 7.34 (m, 6H), 7.33 (d, *J* = 5.2 Hz, 2H), 7.23 (d, *J* = 5.2 Hz, 2H), 6.81 (d, *J* = 9.1 Hz, 2H), 3.81 (t, *J* = 7.2 Hz, 2H), 1.85 – 1.76 (m, 2H), 1.48 – 1.39 (m, 2H), 1.38 – 1.21 (m, 8H), 0.90 (t, *J* = 6.9 Hz, 3H).

^{13}C NMR (126 MHz, $CDCl_3$): δ 145.3, 144.2, 140.1, 138.0, 129.4, 126.5, 124.9, 124.6, 124.5, 119.6, 115.5, 114.4, 47.6, 31.8, 29.3, 29.2, 26.9, 26.8, 22.7, 14.2.

Anal. Calcd for $C_{32}H_{29}NS_5$: C, 65.37; H, 4.97; N, 2.38. Found: C, 65.35; H, 4.83; N, 2.54.

IR: cm^{-1} 2923, 2849, 1467, 1451, 1329, 1243, 1155, 807.

5,5'-(10-octyl-10*H*-phenothiazine-3,7-diyl)dithieno[3,2-b]thiophene-2-carbaldehyde (6)

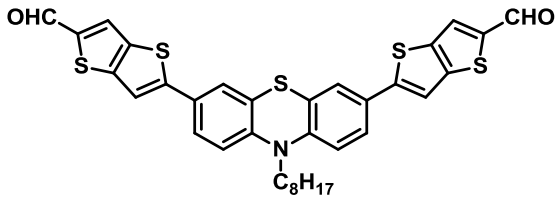

Distilled $POCl_3$ (250 mg, 1.63 mmol) was added dropwise to DMF (120 mg, 1.63 mmol) at -15 °C under N_2 atmosphere; at the end of the addition a white solid formed, that, after 60 minutes, was dissolved in DMF (15 mL). Product **5** (320 mg, 0.54 mmol) was added and the mixture heated at 80 °C for 8 h. Then a saturated solution of NaOAc (30 mL) was added dropwise and the mixture was extracted with CH_2Cl_2 (3 x 50 mL), the organic phases were combined and dried. Purification through column chromatography on silica gel, with PE:AcOEt - 3:1 as eluent, gave the product **6** as orange solid in 65% yield (225 mg, 0.35 mmol).

^{1}H NMR (500 MHz, $CDCl_3$): δ 9.93 (s, 2H), 7.88 (s, 2H), 7.44 – 7.39 (m, 4H), 7.37 (d, *J* = 2.1 Hz, 2H), 6.87 (d, *J* = 8.5 Hz, 2H), 3.87 (t, *J* = 7.2 Hz, 2H), 1.88 – 1.79 (m, 2H), 1.50 – 1.42 (m, 2H), 1.37 – 1.22 (m, 8H), 0.87 (t, *J* = 6.9 Hz, 3H).

^{13}C NMR (126 MHz, $CDCl_3$): δ 183.0, 151.8, 146.9, 145.0, 144.3, 137.7, 129.1, 128.5, 125.5, 124.8, 124.6, 115.7, 114.9, 47.8, 31.7, 29.2, 29.2, 26.8, 26.7, 22.6, 14.1.

Anal. Calcd. For $C_{34}H_{29}NO_2S_5$: C, 63.42; H, 4.54; N, 2.18. Found: C, 63.41; H, 4.50; N, 1.83.

IR: cm^{-1} 2875, 1565, 1498, 1452, 1351, 1201, 1100, 1027, 920, 854, 729.

3,3'-(5,5'-(10-octyl-10*H*-phenothiazine-3,7-diyl)bis(thieno[3,2-b]thiophene-5,2-diyl))bis(2-cyanoacrylic acid) (PTZ3)

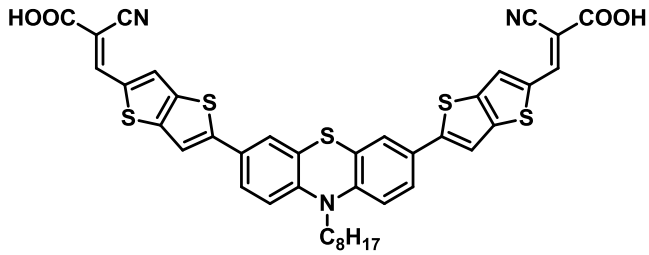

PTZ3 was synthesized according to general procedure C for Knoevenagel condensation using product **6** (200 mg, 0.31 mmol), cyanoacetic acid (270 mg, 3.10 mmol), piperidine (320 mg, 3.10 mmol + cat) and $CHCl_3$ (10 mL). A dark red solid (200 mg) has been isolated as the product in 83% of yield.

^{1}H NMR (500 MHz, DMSO-d_6): δ 8.55 (s, 2H), 8.29 (s, 2H), 7.96 (s, 2H), 7.63 – 7.44 (m, 4H), 7.10 (d, *J* = 8.4 Hz, 2H), 4.05 – 3.72 (m, 2H), 1.78 – 1.59 (m, 2H), 1.50 – 1.32 (m, 2H), 1.32 – 1.10 (m, 8H), 0.82 (t, *J* = 9.7 Hz, 3H).

^{13}C NMR (126 MHz, DMSO-d_6): δ 164.2, 151.6, 147.9, 147.8, 144.8, 137.9, 137.1, 132.8, 128.4, 126.1, 124.5, 123.8, 117.0, 116.8, 116.5, 98.0, 63.3, 31.6, 29.1, 28.9, 26.5, 22.5, 14.4.

Anal. Calcd. For $C_{40}H_{31}N_3O_4S_5$: C, 61.75; H, 4.02; N, 5.40. Found: C, 61.59; H, 4.29; N, 5.81.

IR: cm^{-1} 2920, 2850, 2216, 1678, 1565, 1454, 1396, 1236, 1158, 1132, 796.

5'-bromo-[2,2'-bithiophene]-5-carbaldehyde (7)

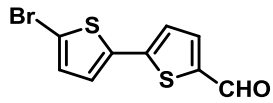

5,5'-dibromo-2,2'-bithiophene (650 mg, 2.00 mmol) was dissolved in THF (15 mL) under inert atmosphere and the solution cooled down to -78 °C. *n*BuLi (1.6 M solution in hexane, 1.4 mL, 2.20 mmol) was then added dropwise and the mixture was left under magnetic stirring for 60 min. Then DMF (190 mg, 2.60 mmol) was added and the mixture was left under magnetic stirring for 15 h at rt. The quench

was performed by pouring a saturated solution of NH_4Cl and extractions with CH_2Cl_2 were performed, followed by anhydrification. Purification through column chromatography on silica gel, using a mixture 5:1 of PE and AcOEt, led to the desired product (310 mg, 1.13 mmol) a light yellow solid in 57% yield.

^{1}H NMR (500 MHz, $CDCl_3$) δ 9.87 (s, 1H), 7.66 (d, *J* = 3.9 Hz, 1H), 7.18 (d, *J* = 3.9 Hz, 1H), 7.11 (d, *J* = 3.9 Hz, 1H), 7.04 (d, *J* = 3.9 Hz, 1H).

3,4-dibutoxythiophene (8)

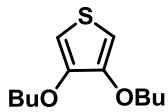

To a solution of 3,4-dimethoxythiophene (1.50 g, 10.4 mmol) in dry toluene (120 mL), *p*-TsOH (200 mg) and butanol (3.1 g, 42 mmol) were added under nitrogen atmosphere. The mixture was warmed to reflux for 24 h and then quenched with water (50 mL). Extractions with CH_2Cl_2 (3x50 mL) and anhydrification allowed to isolate a crude product that was purified through column chromatography on silica gel using CH_2Cl_2 as eluent. The desired product is a light yellow liquid and it was isolated in yield >95%.

^{1}H NMR (500 MHz, $CDCl_3$) δ 6.17 (s, 2H), 3.99 (t, *J* = 6.7 Hz, 4H), 1.86 – 1.75 (m, 4H), 1.54 – 1.44 (m, 4H), 0.98 (t, *J* = 7.4 Hz, 6H).

5-bromo-3,4-dibutoxythiophene-2-carbaldehyde (9)

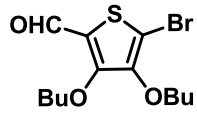

Product **8** (1.25 g, 5.47 mmol) was solubilized in dry THF (30 mL) under nitrogen atmosphere. The mixture was cooled to -78 °C and *n*-BuLi (3.76 mL, 6.02 mmol) was added dropwise. After having stirred the mixture for 60 min, DMF (480 mg, 6.57 mmol) was added and the mixture was stirred at rt for 15 h. Then the solvent was evaporated and the mixture was quenched with 50 mL of a saturated solution of NH_4Cl**,** extracted with Et_2O (3x50 mL), and dried. The isolated product (850 mg, 3.32 mmol) was solubilized in DMF (7 mL), temperature was lowered to -5 °C and NBS (710 mg, 3.97 mmol) was added dropwise as DMF solution (7 mL). The color changed from yellow to brown-green. After 7 h of stirring at rt, 50 mL of water were added and Et_2O extractions performed (3x50 mL). Anhydrification and purification through

column chromatography (mixture of PE:AcOEt – 10:1 as eluent) allowed isolation of the desired product (1.06 g, 3.16 mmol) as yellow oil with an overall yield of 58%. The product has been used without any further purification for the following step.

^{1}H NMR (500 MHz, $CDCl_3$): δ 9.85 (s, 1H), 4.27 (t, *J* = 6.5 Hz, 2H), 4.03 (t, *J* = 6.5 Hz, 2H), 1.78 – 1.67 (m, 4H), 1.52 – 1.42 (m, 4H), 1.00 – 0.90 (m, 6H).

^{13}C NMR (126 MHz, $CDCl_3$): δ 180.0, 155.7, 147.5, 124.3, 112.1, 74.5, 73.9, 31.9, 31.8, 19.0, 18.9, 13.7, 13.6.

7-bromo-2,3-dihydrothieno[3,4-b][1,4]dioxine-5-carbaldehyde (10)

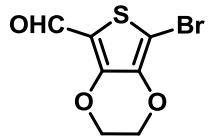

2,3-dihydrothieno[3,4-b][1,4]dioxine-5-carbaldehyde (500 mg, 2.94 mmol) was solubilized in DMF (5 mL), temperature was lowered to -5 °C and NBS (580 mg, 3.26 mmol) was added dropwise as DMF solution (5 mL). The color changed from grey to violet. After 15 h of stirring at rt, 50 mL of water was added and a white solid precipitated, that was isolated as the desired product with an overall yield of 77%.

^{1}H NMR (500 MHz, $CDCl_3$) δ 9.82 (s, 1H), 4.44 – 4.30 (m, 4H).

10-octyl-3,7-bis(4,4,5,5-tetramethyl-1,3,2-dioxaborolan-2-yl)-10*H*-phenothiazine (11)

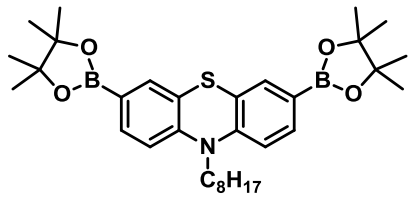

Product **3** (1.00 g, 2.14 mmol) was dissolved in THF (30 mL) under inert atmosphere and the solution cooled down to -78 °C. *n*BuLi (1.6 M solution in hexane, 3.4 mL, 5.36 mmol) was then added dropwise and the mixture was left under magnetic stirring for 60 min. Then 2-isopropoxy-4,4,5,5-tetramethyl-1,3,2-dioxaborolane (1.00 g, 5.36 mmol) was added at -78 °C and the mixture was left under magnetic stirring for 48 h at rt. The quench was performed by pouring into 50 mL of a saturated solution of NH_4Cl and extractions with Et_2O were performed, followed by anhydrification. The

crude product was a sticky liquid that was used for cross-coupling step without any further purification.

^{1}H NMR (500 MHz, $CDCl_3$): δ 7.55 (dd, *J* = 8.1, 1.3 Hz, 2H), 7.51 (d, *J* = 1.3 Hz, 2H), 6.80 (d, *J* = 8.2 Hz, 2H), 3.84 (t, *J* = 7.2 Hz, 2H), 1.81 – 1.73 (m, 2H), 1.42 – 1.35 (m, 2H), 1.31 (s, 24H), 1.28 – 1.19 (m, 8H), 0.88 (t, *J* = 7.2 Hz, 3H).

5',5'''-(10-octyl-10H-phenothiazine-3,7-diyl)bis((2,2'-bithiophene)-5-carbaldehyde) (12)

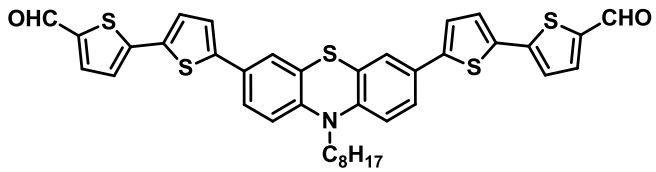

Product **12** was synthesized according to general procedure B for Suzuki-Miyaura cross-coupling using product **11** (115 mg, 0.20 mmol), $Pd(dppf)Cl_2 \cdot CH_2Cl_2$ (17 mg, 0.020 mmol), product **7** (120 mg, 0.44 mmol), K_2CO_3 (280mg, 2.0 mmol), DME (3 mL) and methanol (3 mL). Extractions with AcOEt and purification with CH_2Cl_2 as eluent, gave product **12** as an orange solid in 64% yield (90 mg).

^{1}H NMR (500 MHz, $CDCl_3$): δ 9.86 (s, 2H), 7.67 (d, *J* = 4.0 Hz, 2H), 7.39 (dd, *J* = 8.4, 2.2 Hz, 2H), 7.36 (d, *J* = 2.1 Hz, 2H), 7.31 (d, *J* = 3.8 Hz, 2H), 7.25 (d, *J* = 3.9 Hz, 2H), 7.17 (d, *J* = 3.8 Hz, 2H), 6.86 (d, *J* = 8.5 Hz, 2H), 3.87 (t, *J* = 7.2 Hz, 2H), 1.93 – 1.73 (m, 2H), 1.48 – 1.40 (m, 2H), 1.40 – 1.17 (m, 8H), 0.87 (t, *J* = 6.9 Hz, 3H).

^{13}C NMR (126 MHz, $CDCl_3$): δ 182.4, 147.2, 145.1, 144.5, 141.5, 137.3, 134.4, 128.2, 127.2, 125.0, 124.7, 124.5, 123.8, 123.4, 115.6, 47.8, 31.7, 29.2, 26.9, 26.8, 22.6, 14.0.

Anal. Calcd. For $C_{38}H_{33}NO_2S_5$: C, 65.58; H, 4.78; N, 2.01. Found: C, 65.38; H, 4.51; N, 1.28.

IR: cm^{-1} 2920, 2851, 1649, 1442, 1367, 1223, 1047, 791.

3,3'-(5',5'''-(10-octyl-10*H*-phenothiazine-3,7-diyl)bis([2,2'-bithiophene]-5',5-diyl))bis(2-cyanoacrylic acid) (PTZ4)

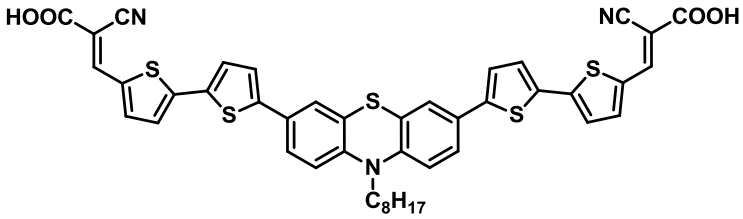

PTZ4 was synthesized according to general procedure C for Knoevenagel condensation using product **12** (60 mg, 0.086 mmol), cyanoacetic acid (75 mg, 0.86 mmol), piperidine (100 mg, 0.86 mmol + cat) and $CHCl_3$ (3 mL). A dark red solid (60 mg) has been isolated as the product in 86% of yield.

^{1}H NMR (500 MHz, DMSO-d_6): δ 8.46 (s, 2H), 7.97 (d, *J* = 4.1 Hz, 2H), 7.61 (d, *J* = 3.9 Hz, 2H), 7.58 (d, *J* = 3.9 Hz, 2H), 7.57 – 7.50 (m, 6H), 7.06 (d, *J* = 8.3 Hz, 2H), 3.92 (t, *J* = 6.5 Hz, 2H), 1.75 – 1.60 (m, 2H), 1.45 – 1.35 (m, 2H), 1.33 – 1.06 (m, 8H), 0.82 (t, *J* = 6.6 Hz, 3H).

^{13}C NMR (126 MHz,DMSO-d_6): δ 164.9, 147.3, 147.2, 146.8, 145.7, 145.3, 142.6, 135.3, 134.7, 129.7, 128.8, 126.5, 126.1, 125.1, 124.9, 118.1, 117.6, 99.9, 32.4, 30.0, 29.8, 27.4, 27.3, 23.6, 23.4, 15.3.

Anal. Calcd. For $6C_{38}H_{33}NO_2S_5 \cdot H_2O$: C, 63.41; H, 4.64; N, 5.04. Found: C, 62.81; H, 4.87; N, 5.35.

IR: cm^{-1} 2925, 2215, 1686, 1570, 1400, 1254, 1207, 1155, 1052, 788.

5,5'-(10-octyl-10*H*-phenothiazine-3,7-diyl)bis(3,4-dibutoxythiophene-2-carbaldehyde) (13)

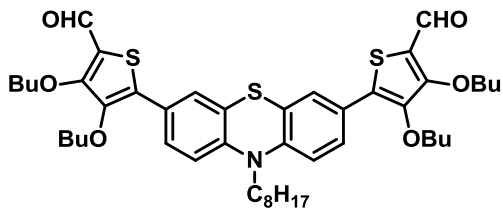

Product **13** was synthesized according to general procedure B for Suzuki-Miyaura cross-coupling using product **11** (200 mg, 0.35 mmol), $Pd(dppf)Cl_2 \cdot CH_2Cl_2$ (30 mg, 0.035 mmol), product **9** (200 mg, 0.71 mmol), K_2CO_3 (500mg, 3.5 mmol), DME (5 mL)

and methanol (5 mL). Purification with PE:AcOEt - 10:1 as eluent gave product **13** as an orange solid in 45% yield (130 mg).

^{1}H NMR (500 MHz, $CDCl_3$): δ 9.98 (s, 2H), 7.61 (d, *J* = 2.1 Hz, 2H), 7.53 (dd, *J* = 8.6, 2.1 Hz, 2H), 6.85 (d, *J* = 8.6 Hz, 2H), 4.34 (t, *J* = 6.5 Hz, 4H), 3.91 (t, *J* = 6.5 Hz, 4H), 3.87 (t, *J* = 7.2,2H), 1.87 – 1.76 (m, 6H), 1.72 – 1.63 (m, 4H), 1.57 – 1.41 (m, 10H), 1.38 – 1.20 (m, 8H), 1.00 (t, *J* = 7.4 Hz, 6H), 0.94 (t, *J* = 7.4 Hz, 6H), 0.87 (t, *J* = 6.9 Hz, 3H).

^{13}C NMR (126 MHz, $CDCl_3$): δ 180.7, 157.4, 144.9, 144.7, 136.3, 126.7, 126.4, 125.9, 124.3, 121.3, 115.3, 74.5, 73.3, 47.8, 32.1, 32.0, 31.7, 29.2, 29.1, 26.8, 26.7, 22.6, 19.2, 19.0, 14.0, 13.8, 13.8.

Anal. Calcd. For $C_{46}H_{61}NO_6S_3$: C, 67.36; H, 7.50; N, 1.71. Found: C, 67.69; H, 7.23; N, 2.00.

IR: cm^{-1} 2956, 2927, 2871, 1647, 1578, 1459, 1417, 1401, 1350, 1254, 1105, 1062, 1029, 811.

3,3'-(5,5'-(10-octyl-10*H*-phenothiazine-3,7-diyl)bis(3,4-dibutoxythiophene-5,2-diyl))bis(2-cyanoacrylic acid) (PTZ5)

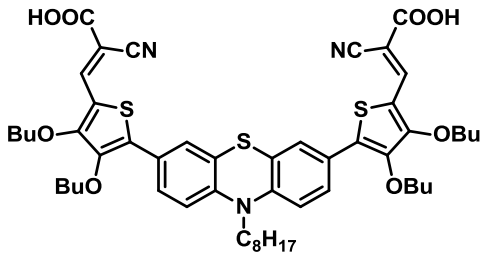

PTZ5 was synthesized according to general procedure C for Knoevenagel condensation using product **13** (200 mg, 0.23 mmol), cyanoacetic acid (200 mg, 2.32 mmol), piperidine (240 mg, 2.32 mmol + cat) and $CHCl_3$ (10 mL). A dark red solid (200 mg) has been isolated as the product in a 90% of yield.

^{1}H NMR (500 MHz, DMSO-d_6): δ 8.26 (s, 2H), 7.59 – 7.47 (m, 4H), 7.16 – 7.02 (m, 2H), 4.28 (t, *J* = 6.4 Hz, 6H), 3.95 – 3.85 (m, 8H), 1.78 – 1.67 (m, 6H), 1.67 – 1.55 (m, 4H), 1.52 – 1.44 (m, 4H), 1.44 – 1.35 (m, 6H), 1.32 – 1.15 (m, 8H), 0.95 (t, *J* = 7.4 Hz, 6H), 0.87 (t, *J* = 7.4 Hz, 6H), 0.82 (t, *J* = 6.8 Hz, 3H).

^{13}C NMR (126 MHz, DMSO-d_6): δ 164.2, 157.1, 145.4, 144.9, 141.4, 134.6, 127.0, 126.2, 125.5, 123.5, 117.1, 116.8, 116.0, 96.2, 74.4, 73.4, 31.9, 31.5, 29.0, 28.9, 26.4, 22.5, 19.2, 19.0, 14.4, 14.0.

Anal. Calcd. For $C_{52}H_{63}N_3O_8S_3$: C, 65.45; H, 6.65; N, 4.40. Found: C, 65.85; H, 6.06; N, 4.96.

IR: cm^{-1} 2927, 2871, 2214, 1683, 1555, 1457, 1394, 1362, 1230, 1172, 1027, 794.

7,7'-(10-octyl-10H-phenothiazine-3,7-diyl)bis(2,3-dihydrothieno[3,4-b][1,4]dioxine-5-carbaldehyde) (14)

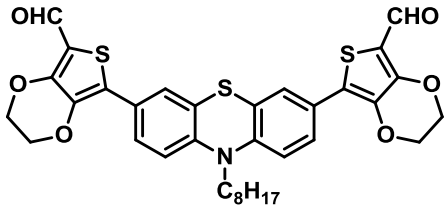

Product **14** was synthesized according to general procedure B for Suzuki-Miyaura cross-coupling using product **11** (400 mg, 0.71 mmol), Pd(dppf)Cl_2·CH_2Cl_2 (58 mg, 0.071 mmol), product **10** (400 mg, 1.56 mmol), K_2CO_3 (1.00 g, 7.10 mmol), DME (7 mL) and methanol (7 mL). Purification with CH_2Cl_2:Et_2O – 100:1 as eluent gave product **14** as an orange solid in 40% yield (185 mg).

^{1}H NMR (500 MHz, $CDCl_3$): δ 9.90 (s, 2H), 7.57 (d, *J* = 2.1 Hz, 2H), 7.52 (dd, *J* = 8.6, 2.2 Hz, 2H), 6.82 (d, *J* = 8.6 Hz, 2H), 4.44 – 4.35 (m, 8H), 3.83 (t, *J* = 7.0 Hz, 2H), 1.80 – 1.75 (m, 2H), 1.47 – 1.06 (m, 10H), 0.86 (t, *J* = 6.5 Hz, 3H).

^{13}C NMR (126 MHz, $CDCl_3$): δ 179.4, 149.0, 144.6, 137.2, 128.0, 126.4, 126.0, 125.5, 124.1, 115.3, 115.0, 65.1, 64.5, 47.7, 31.7, 29.2, 29.1, 26.8, 26.7, 22.6, 14.1.

Anal. Calcd. For $C_{34}H_{33}NO_6S_3$: C, 63.04; H, 5.13; N, 2.16. Found: C, 63.12; H, 4.96; N, 2.40.

IR: cm^{-1} 2926, 2851, 1638, 1438, 1357, 1254, 1217, 1080, 805.

3,3'-(7,7'-(10-octyl-10*H*-phenothiazine-3,7-diyl)bis(2,3-dihydrothieno[3,4-b][1,4]dioxine-7,5-diyl))bis(2-cyanoacrylic acid) (PTZ6)

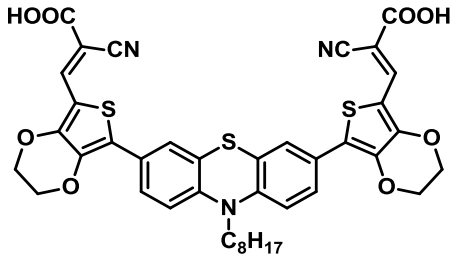

PTZ6 was synthesized according to general procedure C for Knoevenagel condensation using product **14** (90 mg, 0.14 mmol), cyanoacetic acid (120 mg, 1.40 mmol), piperidine (140 mg, 1.40 mmol + cat) and $CHCl_3$ (5 mL). A dark red solid (88 mg) has been isolated as the product in 80% yield.

^{1}H NMR (500 MHz, DMSO-d_6): δ 8.14 (s, 2H), 7.48 (dd, *J* = 8.6, 1.7 Hz, 2H), 7.41 (d, *J* = 1.9 Hz, 2H), 6.97 (d, *J* = 8.8 Hz, 2H), 4.60 – 4.30 (m, 8H), 3.90 – 3.60 (m, 2H), 1.70 – 1.60 (m, 2H), 1.45 – 1.14 (m, 10H), 0.82 (t, *J* = 6.7 Hz, 3H).

^{13}C NMR (126 MHz, DMSO-d_6): δ 164.5, 149.6, 144.2, 140.2, 138.2, 126.6, 126.2, 126.1, 124.9, 123.0, 117.5, 116.4, 108.8, 94.4, 66.1, 65.2, 47.4, 31.6, 29.1, 29.0, 26.5, 26.3, 22.5, 14.4.

Anal. Calcd. For $C_{40}H_{35}N_3O_8S_3$: C, 61.44; H, 4.51; N, 5.37. Found: C, 61.48; H, 4.77; N, 5.47.

IR: cm^{-1} 2924, 2210, 1676, 1561, 1545, 1438, 1396, 1356, 1225, 1069, 1024, 760.

3,7-dibromo-10*H*-phenothiazine (15)

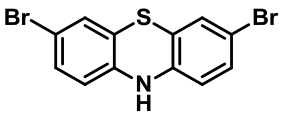

To a solution of 10*H*-phenothiazine (2.00 g, 10 mmol) in acetic acid (20 mL), bromine (1.88 g, 10 mmol) was added dropwise. The mixture was left under magnetic stirring for 1 h and then a second portion of bromine (1.88 g, 10 mmol) was added giving a black mixture that was left under stirring overnight. The mixture was then quenched with a saturated solution of Na_2SO_3 (100 mL) and left under magnetic stirring for 2 h. Extractions with Et_2O (2 x 100 mL) and anhydrification on Na_2SO_4 allowed the

isolation of a brownish solid that has been washed with cold CH_2Cl_2 affording the desired product in 85% yield (3.05 g).

^{1}H NMR (500 MHz, DMSO-d_6) δ 9.02 (s, 1H), 7.15 (dd, *J* = 8.4, 2.3 Hz, 2H), 7.12 (d, *J* = 2.2 Hz, 2H), 6.62 (d, *J* = 8.4 Hz, 2H).

3,7-dibromo-10-(2-(2-(2-methoxyethoxy)ethoxy)ethyl)-10*H*-phenothiazine (16)

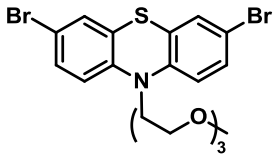

Compound **16** was synthesized according to general procedure D for alkylation using product **15** (200 mg, 0.56 mmol), NaH 60% (0.13 g, 1.12 mmol), TEG-OTs (350 mg, 1.12 mmol) in 5 mL of dry DMF. Extractions with Et_2O and purification with PE/AcOEt 5:1 as eluent, gave product **16** as pale yellow oil in 80% yield (700 mg).

^{1}H NMR (500 MHz, $CDCl_3$) δ 7.21 (dd, *J* = 8.6, 2.2 Hz, 2H), 7.17 (d, *J* = 1.7 Hz, 2H), 6.73 (d, *J* = 8.7 Hz, 2H), 3.99 (t, *J* = 6.1 Hz, 2H), 3.78 (t, *J* = 6.1 Hz, 2H), 3.67 – 3.57 (m, 6H), 3.55 – 3.48 (m, 2H), 3.35 (s, 3H).

^{13}C NMR (126 MHz, $CDCl_3$) δ 143.7, 130.2, 129.6, 126.0, 116.6, 115.0, 71.9, 70.7, 70.6 (x3), 68.1, 59.0, 47.9.

5,5'-(10-(2-(2-(2-methoxyethoxy)ethoxy)ethyl)-10*H*-phenothiazine-3,7-diyl)bis(thiophene-2-carbaldehyde) (17)

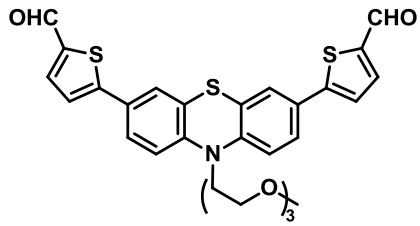

Compound **17** was synthesized according to general procedure A for Suzuki-Miyaura cross-coupling using product **16** (240 m g, 0.48 mmol), Pd(dppf)Cl_2·CH_2Cl_2 (40 mg, 0.05 mmol), 5-formyl-2-thienylboronic acid (210 mg, 1.15 mmol), K_2CO_3 (660 mg, 4.80 mmol), DME (5 mL) and methanol (5 mL). Extractions with AcOEt and

purification with PE/AcOEt 2:1 as eluent, gave product **17** as an orange solid in 75% yield (190 mg).

^{1}H NMR (500 MHz, DMSO-d_6) δ 9.76 (s, 2H), 7.60 (d, *J* = 3.9 Hz, 2H), 7.31 (dd, *J* = 8.5, 2.1 Hz, 2H), 7.22 (d, *J* = 2.2 Hz, 2H), 7.19 (d, *J* = 3.9 Hz, 2H), 6.81 (d, *J* = 8.6 Hz, 2H), 3.99 (t, *J* = 6.0 Hz, 2H), 3.78 (t, *J* = 6.0 Hz, 2H), 3.71 – 3.51 (m, 6H), 3.50 – 3.45 (m, 2H), 3.29 (s, 3H).

^{13}C NMR (126 MHz, DMSO-d_6) δ 182.4, 152.7, 144.6, 141.6, 137.5, 127.8, 125.7, 124.6, 123.9, 123.2, 115.5, 71.8, 70.7, 70.5, 70.4(x2), 67.9, 58.9, 47.9.

3,3'-(5,5'-(10-(2-(2-(2-methoxyethoxy)ethoxy)ethyl)-10*H*-phenothiazine-3,7-diyl)bis(thiophene-5,2-diyl))bis(2-cyanoacrylic acid) (PTZ7)

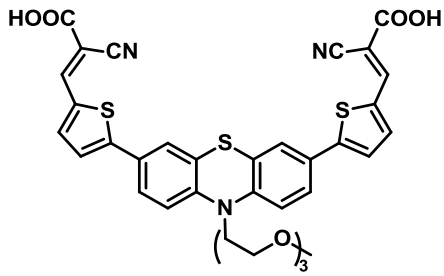

Compound **PTZ7** was synthesized according to general procedure C for Knoevenagel condensation using product **17** (190 mg, 0.34 mmol), cyanoacetic acid (190 mg, 3.4 mmol), piperidine (340 mg, 3.4 mmol + cat) and $CHCl_3$ (6 mL). A dark red solid (220 mg) has been isolated as the product in 92% yield.

^{1}H NMR (500 MHz, DMSO-d_6) δ 8.45 (s, 2H), 7.98 (d, *J* = 3.8 Hz, 2H), 7.71 (d, *J* = 3.8 Hz, 2H), 7.57 (m, 4H), 7.16 (d, *J* = 9.1 Hz, 2H), 4.13 (t, *J* = 5.3 Hz, 2H), 3.79 (t, *J* = 5.3 Hz, 2H), 3.66 – 3.43 (m, 6H), 3.43 – 3.29 (m, 2H), 3.20 (s, 3H).

^{13}C NMR (126 MHz, DMSO-d_6) δ 164.2, 152.0, 146.0, 145.0, 141.0, 134.5, 127.7, 126.5 125.0, 124.8, 123.8, 117.2, 116.9, 98.8, 71.7, 70.4, 70.2, 70.1, 67.8, 58.5, 44.1.

Anal. Calcd. For $C_{35}H_{29}N_3O_7S_3$, 60.70; H, 4.18; N, 6.00. Found: C, 60,21; H, 4.12; N, 5.46.

3,7-dibromo-10-(prop-2-yn-1-yl)-10*H*-phenothiazine (18)

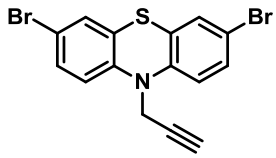

Compound **18** was synthesized according to general procedure D for alkylation using product **15** (200 mg, 0.56 mmol), NaH 60% (130 mg, 1.12 mmol), and propargyl bromide (0.04 g, 1.12 mmol) in 5 mL of dry DMF. Extractions with Et_2O and purification with PE/AcOEt 20:1 as eluent, gave product **18** as pale yellow solid in 77% yield (170 mg).

^{1}H NMR (400 MHz, $CDCl_3$) δ 7.28 (dd, *J* = 8.6, 2.2 Hz, 2H), 7.22 (d, *J* = 2.2 Hz, 2H), 7.04 (d, *J* = 8.6 Hz, 2H), 4.43 (d, *J* = 2.3 Hz, 2H), 2.47 (t, *J* = 2.3 Hz, 1H).

^{13}C NMR (101 MHz, $CDCl_3$) δ 143.1, 130.5, 129.5, 125.1, 116.1, 115.8, 78.2, 75.2, 38.8.

(2R,3R,4S,5R)-2-((4-((3,7-dibromo-10H-phenothiazin-10-yl)methyl)-1H-1,2,3-triazol-1-yl)methyl)-6-methoxytetrahydro-2H-pyran-3,4,5-triyl triacetate (19)

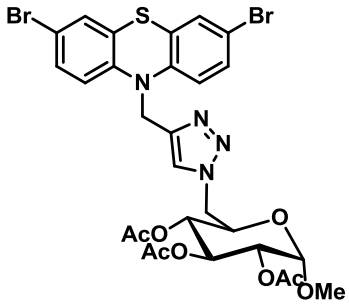

Compound **19** was synthesized by mixing compound **18** (120 mg, 0.30 mmol) and methyl 2,3,4-tri-*O*-acetyl-6-azido-6-deoxy-α-D-glucopyranoside (90 mg, 0.27 mmol) in THF (6 mL), and adding a second solution of $CuSO_4 \cdot 5H_2O$ (0.08 g, 0.33 mmol) and sodium ascorbate (80 mg, 0.41 mmol) in H_2O (2.5 mL), then the reaction mixture was stirred at rt in the dark for 4 h. TLC (PE/AcOEt 1:1) revealed the complete consumption of compound **18**, then the solvents were evaporated and the crude washed with HCl 5% solution and brine. The crude was purified using flash chromatography (PE/AcOEt 8:2 then 4:6) affording compound **19** (190 mg, 95%) as an oil.

^{1}H NMR (500 MHz, $CDCl_3$) δ 7.48 (s, 1H), 7.23 (d, *J* = 2.2 Hz, 2H), 7.15 (dd, *J* = 8.7, 2.3 Hz, 2H), 6.65 (d, *J* = 8.7 Hz, 2H), 5.42 (t, *J* = 10.0 Hz, 1H), 5.12 (s, 2H), 4.79 (d, *J* = 3.6 Hz, 1H), 4.67 – 4.58 (m, 2H), 4.51 (dd, *J* = 14.5, 2.1 Hz, 1H), 4.37 – 4.31 (m, 1H), 4.07 (td, *J* = 8.2, 4.1 Hz, 1H), 2.91 (s, 3H), 2.08 (s, 3H), 2.06 (s, 3H), 2.00 (s, 3H).

^{13}C NMR (101 MHz, $CDCl_3$) δ 170.1, 169.9, 169.7, 144.1, 143.2, 130.2, 129.6, 125.7, 123.8, 116.6, 115.5, 96.5, 70.6, 69.5, 69.4, 67.6, 55.2, 50.8, 44.6, 20.7 (x3).

5,5'-(10-((1-(((2R,3S,4S,5R,6S)-3,4,5-trihydroxy-6-methoxytetrahydro-2H-pyran-2-yl)methyl)-1H-1,2,3-triazol-4-yl)methyl)-10*H*-phenothiazine-3,7-diyl)bis(thiophene-2-carbaldehyde) (20)

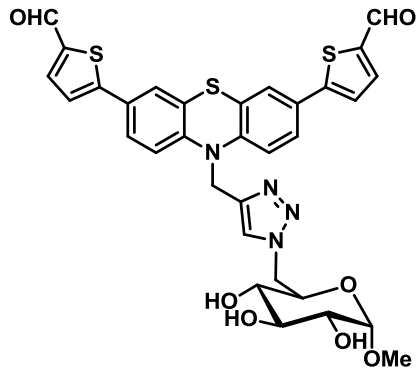

Compound **20** was synthesized according to general procedure A for Suzuki-Miyaura cross-coupling using product **19** (100 mg, 0.13 mmol), $Pd(dppf)Cl_2 \cdot CH_2Cl_2$ (10 mg, 0.010 mmol), 5-formyl-2-thienylboronic acid (50 mg, 0.31 mmol), K_2CO_3 (180 mg, 1.35 mmol), DME (3 mL) and methanol (3 mL). Extractions with AcOEt and purification with AcOEt/iPrOH 10:1 as eluent, gave product **20** as an orange solid in 74% yield (70 mg).

^{1}H NMR (500 MHz, DMSO-d_6) δ 9.88 (s, 2H), 8.01 (d, *J* = 3.8 Hz, 2H), 7.97 (s, 1H), 7.69 (d, *J* = 3.6 Hz, 2H), 7.61 (s, 2H), 7.53 (d, *J* = 8.5 Hz, 2H), 7.02 (d, *J* = 8.6 Hz, 2H), 5.33 (d, *J* = 5.8 Hz, 1H), 5.24 (s, 2H), 4.93 (d, *J* = 4.7 Hz, 1H), 4.77 (d, *J* = 6.5 Hz, 1H), 4.71 (d, *J* = 14.0 Hz, 1H), 4.46 – 4.29 (m, 2H), 3.61 (t, *J* = 9.2 Hz, 1H), 3.23 – 3.11 (m, 1H), 3.02 – 2.93 (m, 1H), 2.73 (s, 3H).

^{1}H NMR (500 MHz, DMSO-d_6 + D_2O) δ 9.83 (s, 2H), 7.96 (d, *J* = 3.8 Hz, 2H), 7.92 (s, 1H), 7.61 (d, *J* = 3.8 Hz, 2H), 7.55 (s, 2H), 7.49 (d, *J* = 8.2 Hz, 2H), 6.99 (d, *J* = 8.6 Hz, 2H), 5.20 (s, 2H), 4.68 (d, *J* = 13.4 Hz, 1H), 4.35 (d, *J* = 3.6 Hz, 2H), 3.56 (s, 1H), 3.32 (s, 1H), 3.15 (dd, *J* = 9.5, 3.6 Hz, 1H), 2.97 (s, 1H), 2.70 (d, *J* = 24.2 Hz, 3H).

^{13}C NMR (126 MHz, DMSO) δ 184.1, 152.0, 144.5, 143.1, 141.8, 139.8, 127.9, 126.3, 125.1, 124.6, 123.1, 116.7, 100.1, 73.5, 72.2, 72.2, 71.0, 54.4, 51.6, 44.5.

3,3'-(5,5'-(10-((1-(((2R,3S,4S,5R,6S)-3,4,5-trihydroxy-6-methoxytetrahydro-2H-pyran-2-yl)methyl)-1H-1,2,3-triazol-4-yl)methyl)-10*H*-phenothiazine-3,7-diyl)bis(thiophene-5,2-diyl))bis(2-cyanoacrylic acid) (PTZ8)

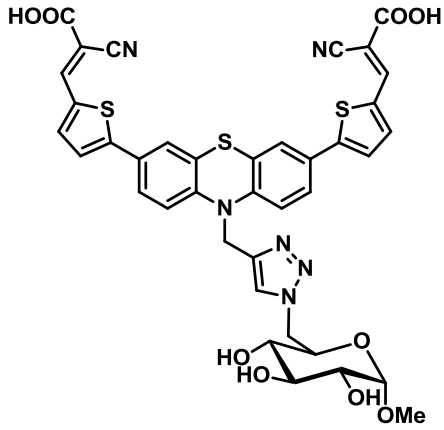

Compound **PTZ8** was synthesized according to general procedure C for Knoevenagel condensation using product **20** (180 mg, 0.27 mmol), cyanoacetic acid (110 mg, 2.7 mmol), piperidine (220 mg, 2.7 mmol + cat) and $CHCl_3$ (5 mL). A dark red solid (190 mg) has been isolated as the product in 90% of yield.

^{1}H NMR (500 MHz, DMSO-d_6) δ 8.47 (s, 2H), 7.99 (m, 3H), 7.71 (d, *J* = 4.0 Hz, 2H), 7.57 (d, *J* = 2.1 Hz, 2H), 7.50 (dd, *J* = 8.5, 2.0 Hz, 2H), 7.05 (d, *J* = 8.7 Hz, 2H), 5.24 (s, 2H), 4.71 (d, *J* = 12.9 Hz, 1H), 4.46 – 4.29 (m, 2H), 3.61 (t, *J* = 9.5 Hz, 1H), 3.36 (t, *J* = 9.1 Hz, 1H), 3.17 (dd, *J* = 9.6, 3.6 Hz, 1H), 2.98 (t, *J* = 9.2 Hz, 1H), 2.74 (s, 3H).

^{13}C NMR (126 MHz, DMSO-d_6) δ 164.1, 152.2, 147.0, 144.6, 143.0, 142.0, 134.4, 127.7, 126.3, 125.1, 124.6, 123.1, 117.0, 116.8, 100.1, 98.2, 73.5, 72.2, 72.1, 71.0, 54.4, 51.6, 44.4.

10-octyl-10H-phenothiazine-3-carbaldehyde (21)

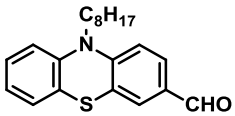

Product **21** has been obtained as a side product in the synthesis of product **2** in 74% yield (2.5 g).

^{1}H NMR (500 MHz, $CDCl_3$) δ 9.75 (s, 1H), 7.59 (d, *J* = 8.4 Hz, 1H), 7.53 (d, *J* = 1.8 Hz, 1H), 7.13 (dd, *J* = 8.0, 7.5 Hz, 1H), 7.07 (d, *J* = 7.6 Hz, 1H), 6.93 (t, *J* = 7.5 Hz, 1H), 6.85 (d, *J* = 8.3 Hz, 2H), 3.84 (t, *J* = 7.1 Hz, 2H), 1.84 – 1.72 (m, 2H), 1.47 – 1.35 (m, 2H), 1.35 – 1.17 (m, 8H), 0.85 (t, *J* = 6.9 Hz, 3H).

2-cyano-3-(10-octyl-10H-phenothiazin-3-yl)acrylic acid (PTZ1M)

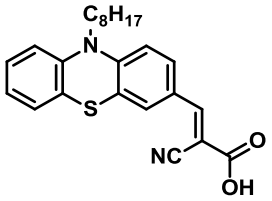

PTZ1M was synthesized according to general procedure C for Knoevenagel condensation using product **21** (750 mg, 2.21 mmol), cyanoacetic acid (1.50 g, 21.1 mmol), piperidine (1.80 g, 21.2 mmol + cat) and $CHCl_3$ (25 mL). A dark red solid has been isolated as the product (760 mg, 1.88 mmol) with 85% of yield.

^{1}H NMR (200 MHz, DMSO) δ 8.21 (s, 1H), 7.97 (d, *J* = 8.7 Hz, 1H), 7.87 (s, 1H), 7.42 – 6.93 (m, 5H), 3.99 (s, 2H), 1.73 (s, 2H), 1.59 – 0.99 (m, 10H), 0.85 (t, *J* = 6.5 Hz, 3H).

3,3'-(10-octyl-10H-phenothiazine-3,7-diyl)bis(2-cyano-N-((tetrahydro-2H-pyran-2-yl)oxy)acrylamide) (22)

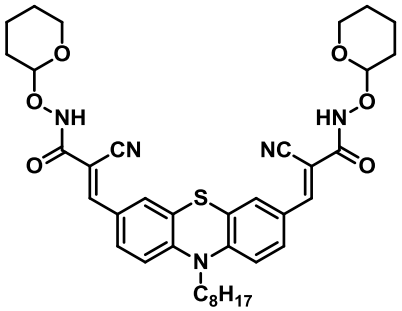

Product **22** was synthesized according to general procedure E for hydroxylamination using **PTZ1** (75 mg, 0.15 mmol), NMM (46 mg, 0.45 mmol), DMTMM (100 mg, 0.36 mmol) and H_2N-OTHP (87 mg, 0.75 mmol) in 20 mL of THF. A mixture of CH_2Cl_2:AcOEt - 7:1 was used as eluent for purification and the desired product has been isolated in 50% yield (53 mg).

^{1}H NMR (400 MHz, $CDCl_3$) δ 8.99 (s, 2H), 8.13 (s, 2H), 7.80 (dd, *J* = 8.7, 2.1 Hz, 2H), 7.59 (d, *J* = 2.2 Hz, 2H), 6.89 (d, *J* = 8.7 Hz, 2H), 5.11 – 5.03 (m, 2H), 4.01 (t, *J* = 10.3 Hz, 2H), 3.92 – 3.81 (m, 2H), 3.76 – 3.64 (m, 2H), 1.96 – 1.75 (m, 4H), 1.75 – 1.50 (m, 138H), 1.50 – 1.38 (m, 2H), 1.38 – 1.16 (m, 10H), 0.93 – 0.81 (m, 3H).

^{13}C NMR (101 MHz, $CDCl_3$) δ 151.49, 147.28, 131.12, 129.73, 126.98, 123.88, 116.40, 115.54, 102.92, 98.26, 62.68, 48.43, 31.66, 29.67, 29.14, 29.07, 27.88, 26.72, 26.57, 24.89, 22.56, 18.41, 14.04.

ESI-MS: *m/z* 698.74 (100%) $[M-1]^-$.

3,3'-(5,5'-(10-octyl-10H-phenothiazine-3,7-diyl)bis(thiophene-5,2-diyl))bis(2-cyano-N-((tetrahydro-2H-pyran-2-yl)oxy)acrylamide) (23)

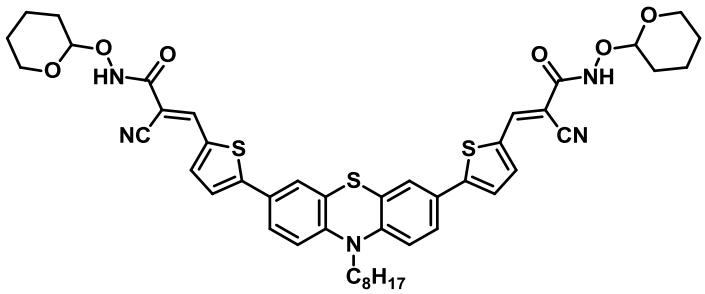

Product **23** was synthesized according to general procedure E for hydroxylamination using **PTZ2** (100 mg, 0.15 mmol), NMM (46 mg, 0.45 mmol), DMTMM (100 mg, 0.36 mmol) and H_2N-OTHP (87 mg, 0.75 mmol) in 20 mL of THF. A mixture of CH_2Cl_2:AcOEt - 5:1 was used as eluent for purification and the desired product has been isolated in 72% yield (93 mg).

^{1}H NMR (400 MHz, $CDCl_3$) δ 9.02 (s, 2H), 8.35 (s, 2H), 7.65 (d, *J* = 4.2 Hz, 2H), 7.44 (dd, *J* = 8.5, 2.1 Hz, 2H), 7.27 (d, *J* = 5.0 Hz, 2H), 6.82 (d, *J* = 8.6 Hz, 2H), 5.08 (s, 2H), 4.02 (t, *J* = 10.2 Hz, 2H), 3.83 (d, *J* = 5.9 Hz, 2H), 3.70 (dd, *J* = 7.1, 5.2 Hz, 2H), 2.01 – 1.13 (m, 24H), 0.86 t, *J* = 9.6, 3H).

^{13}C NMR (101 MHz, $CDCl_3$) δ 159.3, 152.9, 145.3, 145.2, 139.2, 134.5, 127.5, 125.9, 124.9, 124.5, 123.4, 116.4, 115.6, 102.9, 95.6, 62.7, 47.9, 31.9, 31.7, 29.7, 29.3, 29.2, 29.1, 27.9, 26.8, 26.7, 25.2, 24.9, 22.7, 22.6, 20.2, 18.5, 14.1.

ESI-MS: *m/z* 862.51 (100%) $[M-1]^-$.

3,3'-(5,5'-(10-octyl-10H-phenothiazine-3,7-diyl)bis(3,4-dibutoxythiophene-5,2-diyl))bis(2-cyano-N-((tetrahydro-2H-pyran-2-yl)oxy)acrylamide) (24)

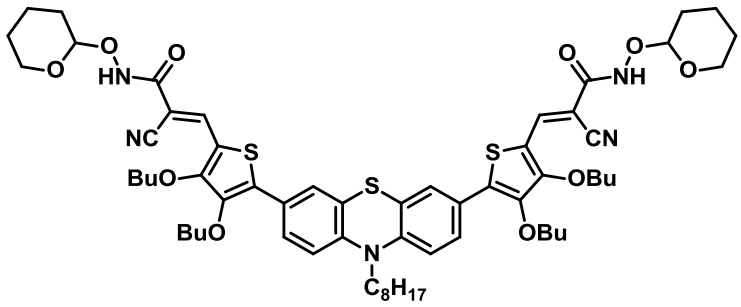

Product **24** was synthesized according to general procedure E for hydroxylamination using **PTZ5** (75 mg, 0.079 mmol), NMM (24 mg, 0.24 mmol), DMTMM (52 mg, 0.19 mmol) and H_2N-OTHP (46 mg, 0.40 mmol) in 20 mL of THF. A mixture of CH_2Cl_2:AcOEt - 15:1 was used as eluent for purification and the desired product has been isolated in 67% yield (50 mg).

^{1}H NMR (400 MHz, $CDCl_3$) δ 8.85 (s, 2H), 8.53 (s, 2H), 7.63 (d, *J* = 2.1 Hz, 2H), 7.57 (dd, *J* = 8.6, 2.1 Hz, 2H), 6.84 (d, *J* = 8.7 Hz, 2H), 5.06 (s, 2H), 4.26 (t, *J* = 6.7 Hz, 4H), 4.06 – 3.95 (m, 2H), 3.95 – 3.82 (m, 6H), 3.73 – 3.64 (m, 2H), 1.99 – 1.06 (m, 24H), 0.98 (t, *J* = 7.4 Hz, 6H), 0.94 (t, *J* = 7.4 Hz, 6H), 0.87 (t, *J* = 6.8 Hz, 3H).

^{13}C NMR (101 MHz, $CDCl_3$) δ 157.5, 145.2, 144.9, 141.6, 135.6, 126.5, 126.4, 125.8, 124.3, 116.7, 115.3, 102.9, 92.4, 74.4, 73.4, 62.6, 47.8, 32.0, 32.0, 31.7, 29.7, 29.2, 29.2, 27.9, 26.8, 26.7, 24.9, 22.6, 19.4, 19.2, 19.0, 18.5, 14.1, 13.8, 13.8.

ESI-MS: *m/z* 1150.83 (100%) $[M-1]^-$.

3,3'-(10-octyl-10H-phenothiazine-3,7-diyl)bis(2-cyano-N-hydroxyacrylamide) (PTZ1-HA)

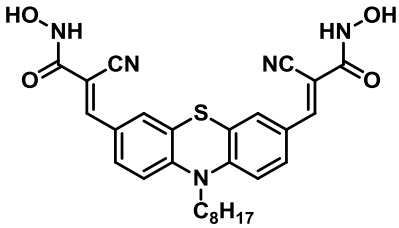

Product **PTZ1-HA** was synthesized according to general procedure F for deprotection of THP group starting from product **22** (70 mg, 0.1 mmol). The recovered red solid has been washed with H_2O, PE, Et_2O, and AcOEt affording the desired product in 85% yield.

^{1}H NMR (400 MHz, THF-d_8) δ 9.92 (s, 2H), 9.75 (dd, *J* = 8.5, 1.4 Hz, 2H), 9.58 (d, *J* = 1.8 Hz, 2H), 8.96 (d, *J* = 8.8 Hz, 2H), 5.86 (t, *J* = 8.5Hz, 2H), 4.36 (s, 7H), 3.75 – 3.63 (m, 2H), 3.40 – 3.27 (m, 3H), 3.27 – 3.00 (m, 11H), 2.73 (t, J = 6.8 Hz, 4H).

^{13}C NMR (101 MHz, THF-d_8) δ 148.7, 132.1, 130.9, 129.4, 125.5, 117.5 (x 2), 101.9, 49.5, 33.5, 31.0, 30.9, 28.4, 28.3, 24.3, 15.2.

ESI-MS: *m*/*z* 530.31 (100%) $[M-1]^-$.

3,3'-(5,5'-(10-octyl-10H-phenothiazine-3,7-diyl)bis(thiophene-5,2-diyl))bis(2-cyano-N-hydroxyacrylamide) (PTZ2-HA)

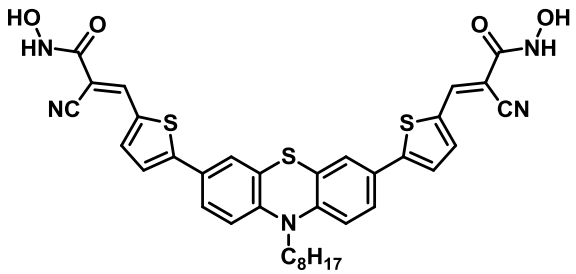

Product **PTZ2-HA** was synthesized according to general procedure F for deprotection of THP group starting from product **23** (80 mg, 0.092 mmol). The recovered solid has been washed with H_2O, PE, Et_2O, and AcOEt. Further purification methodology is under evaluation, but the product presence has been assessed through ESI-MS.

ESI-MS: *m*/*z* 964.50 (100%) $[M-1]^-$.

3,3'-(5,5'-(10-octyl-10H-phenothiazine-3,7-diyl)bis(3,4-dibutoxythiophene-5,2-diyl))bis(2-cyano-N-hydroxyacrylamide) (PTZ5-HA)

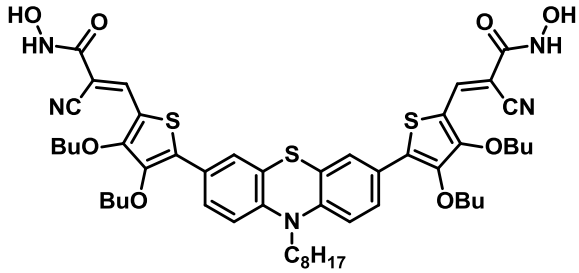

Product **PTZ5-HA** was synthesized according to general procedure F for deprotection of THP group starting from product **24** (90 mg, 0.079 mmol). The recovered solid has been washed with H_2O, PE, Et_2O, and AcOEt. Further purification methodology is under evaluation, but the product presence has been assessed through ESI-MS.

ESI-MS: *m/z* 982.44 (100%) $[M-1]^-$.

3.6 OTHER EXPERIMENTAL DETAILS

DSSC Fabrication

DSSCs have been prepared adapting a procedure reported in literature.[76] In order to exclude metal contamination, all of the containers were in glass or Teflon and were treated with EtOH and 10% HCl prior to use. Plastic spatulas and tweezers have been used throughout the procedure. FTO glass plates were cleaned in a detergent solution for 15 min using an ultrasonic bath, rinsed with pure water and EtOH. After treatment in a UVO_3 system for 18 min, the FTO plates were treated with a freshly prepared 40 mM aqueous solution of $TiCl_4$ for 30 min at 70 °C and then rinsed with water and EtOH. An opaque active layer of 0.20 cm^2 was screen-printed using Dyesol 18NR-AO active opaque TiO_2 paste. The coated films were thermally treated at 125 °C for 6 min, 325 °C for 10 min, 450 °C for 15 min, and 500 °C for 15 min. The heating ramp rate was 5-10 °C/min. The sintered layer was treated again with 40 mM aqueous $TiCl_4$ (70 °C for 30 min), rinsed with EtOH and heated at 500 °C for 30 min. After cooling down to 80 °C the TiO_2 coated plates were immersed into a solution of the dye for 20 h at room temperature in the dark. Counter electrodes were prepared according to the following procedure: a 1-mm hole was made in a FTO plate, using diamond drill bits. The electrodes were then cleaned with a detergent solution for 15 min using an ultrasonic bath, 10% HCl, and finally acetone for 15 min using an ultrasonic bath. After thermal treatment at 500 °C for 30 min, 15 µL of a 5 mM solution of H_2PtCl_6 in EtOH was added and the thermal treatment at 500 °C for 30 min repeated. The dye adsorbed TiO_2 electrode and Pt-counter electrode were assembled into a sealed sandwich-type cell by heating with a hot-melt ionomer-class resin (Surlyn 30-µm thickness) as a spacer between the electrodes. A drop of the electrolyte solution was added to the hole and introduced inside the cell by vacuum backfilling. Finally, the hole was sealed with a sheet of Surlyn and a cover glass. A reflective foil at the back side of the counter electrode was taped to reflect unabsorbed light back to the photoanode.

Photovoltaic and Photoelectric Characterization

Photovoltaic measurements of DSSCs were carried out with an antireflective layer and with or without black mask on top of the photoanode of 0.38 cm^2 surface area under a 500 W Xenon light source (ABET Technologies Sun 2000 class ABA Solar Simulator). The power of the simulated light was calibrated to AM 1.5 (100 mW cm^{-2}) using a reference Si cell photodiode equipped with an IR-cutoff filter (KG-5, Schott) to reduce the mismatch in the region of 350-750 nm between the simulated light and

the AM 1.5 spectrum. J/V curves were obtained by applying an external bias to the cell and measuring the generated photocurrent with a Keithley model 2400 digital source meter. Incident photon-to-current conversion efficiencies (IPCE) were recorded as a function of excitation wavelength by using a monochromator (Omni 300 LOT ORIEL) with single grating in Czerny-Turner optical design, in AC mode with a chopping frequency of 1 Hz and a bias of blue light (0.3 sun). EIS spectra were obtained using an Eg&G PARSTAT 2263 galvanostat potentiostat. The analysis of the impedance spectra has been performed in terms of Nyquist plots. In this experiment a small sinusoidal voltage stimulus of a fixed frequency is applied to an electrochemical cell and its current response measured. The measurements have been performed in the frequency range from 100 kHz to 100 mHz under ac stimulus with 10 mV of amplitude and no applied voltage bias. The obtained Nyquist plots have been fitted via a non-linear least square procedure using the equivalent circuit model.

Electrochemical Characterization

DPV and CV were carried out using a PARSTA2273 potentiostat in a two-compartment, 3-electrode electrochemical cell in a glove box filled with N_2 ($[O_2]$ and $[H_2O] \leq 0.1$ ppm). The working, counter, and the pseudo-reference electrodes were a glassy carbon pin, a Pt flag and an Ag/AgCl wire, respectively. The working electrodes discs were well polished with alumina 0.1 μm suspension, sonicated for 15 min in deionized water, washed with 2-propanol, and cycled for 50 times in 0.5 M H_2SO_4 before use. The Ag/AgCl pseudo-reference electrode was calibrated, by adding ferrocene (10^{-4} M) to the test solution after each measurement. Energy levels were calculated using the absolute value of 5.2 V vs. vacuum for the ferrocene reference couple.

Dye absorption on Pt/TiO_2 composite

Dye staining was done by suspending 200 mg of Pt/TiO_2 nanopowders in 20 mL of dye solution (0.3 mM in ethanol) for 24 h in the dark. Then nanopowders were separated through centrifugation, washed twice with ethanol, and dried under vacuum at room temperature overnight.

Hydrogen Production Measurements

The required amount of the photocatalyst was suspended into 60 mL of 10% v/v aqueous solution of triethanolamine (TEOA) previously neutralized with HCl. After purging with Ar (15 mL min^{-1}) for 30 min, the suspension was

irradiated using a 150 W Xe lamp with a cut-off filter at 420 nm. Irradiance was ~ 6 x 10^{-3} W m^{-2} in the UV-A range and ~ 1080 W m^{-2} in the visible range (400 – 1000 nm). The concentration of H_2 in gas stream coming from the reactor has been quantified using a Agilent 7890 gaschromatograph equipped with a TCD detector, connected to a Carboxen 1010 column (Supelco, 30 m x 0.53 mm ID, 30 μm film) using Ar as carrier.

Desorption Studies

Commercially available transparent TiO_2 coated glass electrodes have been used for desorption studies (Dyesol MS001630). Electrodes heated at 70 °C have been dipped in 2 x 10^{-5} M dye solutions in EtOH and left overnight in the dark. They have been rinsed with EtOH and dried under N_2 flux. Each electrode has been dipped in 10 mL of desorbing solution, then rinsed with ethanol and dried at the corresponding time. UV/Vis transmittance spectra have been measured with a Shimadzu UV-2600 spectrophotometer using the integrating sphere apparatus.

3.7 BIBLIOGRAPHY

1. Y. Hua, S. Chang, D. Huang, X. Zhou, X. Zhu, J. Zhao, T. Chen, W.-Y. Wong, W.-K. Wong, *Chem. Mater.*, **2013**, *25*, 2146.
2. S. H. Kim, H. W. Kim, C. Sakong, J. Namgoong, S. W. Park, M. J. Ko, C. H. Lee, W. I. Lee, J. P. Kim, *Org. Lett.*, **2011**, *13*, 5784.
3. M. Cheng, X. Yang, J. Zhao, C. Chen, Q. Tan, F. Zhang, L. Sun, *ChemSusChem*, **2013**, *6*, 2322.
4. W.-I. Hung, Y.-Y. Liao, C.-Y. Hsu, H.-H. Chou, T.-H. Lee, W.-S. Kao, J. T. Lin, *Chem. Asian J.*, **2014**, *9*, 357.
5. D. Cummins, G. Boschloo, M. Ryan, D. Corr, S. N. Rao, D. Fitzmaurice, *J. Phys. Chem. B*, **2000**, *104*, 11449.
6. J. Lee, J. Kwak, K. C. Ko, J. H. Park, J. H. Ko, N. Park, E. Kim, D. H. Ryu, T. K. Ahn, J. Y. Lee, S. U. Son, *Chem. Commun.*, **2012**, *48*, 11431.
7. R. Abe, K. Shinmei, K. Hara, B. Ohtani, *Chem. Commun.*, **2009**, 3577.
8. A. Albert, Heterocyclic Chemistry, Oxford University Press, New York, 1968.
9. P.J. Skabara, Fused Oligothiophenes. In *Handbook of Thiophene-Based Materials*; John Wiley & Sons, Ltd.: Chichester, UK, **2009**, 219.
10. L. Yu, X. Zhang, C. Zhuang, L. Lin, R. Li, T. Peng, Phys. Chem. Chem. Phys., 2014, 16, 4106.
11. S.-H. Lee, Y. Park, K.-R. Wee, H.-J. Son, D. W. Cho, C. Pac, W. Choi, S. O. Kang, *Org. Lett*. **2010**, *12,* 460.
12. R. Abe, K. Shinmei, N. Koumura, K. Hara, B. Ohtani, *J. Am. Chem. Soc*., **2013**, *135,* 16872.
13. X. Li, S. Cui, D. Wang, Y. Zhou, H. Zhou, Y. Hu, J.-G. Liu, Y. Long, W. Wu, J. Hua, H. Tian, *ChemSusChem*, **2014**, *7,* 2879.
14. W.-S. Han, K.-R. Wee, H.-Y. Kim, C. Pac, Y. Nabetani, D. Yamamoto, T. Shimada, H. Inoue, H. Choi, K. Cho, S. O. Kang, *Chem. Eur. J.*, **2012**, *18,* 15368.
15. J. Li, Y. E, L. Lian, W. Ma, *Int. J. Hydrogen Energy*, **2013**, *38,* 10746.
16. M. Watanabe, H. Hagiwara, A. Iribe, Y. Ogata, K. Shiomi, A. Staykov, S. Ida, K. Tanakaab, T. Ishihara, *J. Mater. Chem. A*, **2014**, *2*, 12952.
17. P. Kumaresan, S. Vegiraju, Y. Ezhumalai, S. L. Yau, C. Kim, W.-H.Lee, M.-C. Chen, *Polymers,* **2014**, *6*, 2645.
18. A. Mishra, C.-Q Ma, P. Bäuerle, *Chem. Rev.,* **2009**, *109*, 1141.
19. G. Zhang, Y. Bai, R. Li, D. Shi, S. Wenger, S. M. Zakeeruddin, M. Gratzel, P. Wang, *Energy Environ. Sci.,* **2009**, *2*, 92.
20. S. Paek, H. Choi, H. Choi, C. W. Lee, M. S. Kang, K. Song, M. K. Nazeeruddin, J. Ko, *J. Phys. Chem. C,* **2010**, *114*, 14646.

21. G. A. Sewvandi, C. Chen, T. Ishii, T. Kusunose, Y. Tanaka, S. Nakanishi, Q. Feng*, J. Phys. Chem. C*, **2014**, *118,* 20184.
22. M. W. Lee, J Y. Kim, D. H. Lee, M. J. Ko, *ACS Appl. Mater. Interfaces,* **2014**, *6*, 4102.
23. M. Sailer, A. W. Franz, T. J. J. Müller, *Chem. Eur. J.*, **2008**, 14, 2602.
24. Z. B. Tang, X. X. Sun, P. L. Zhang, in *Advanced Materials Research*, **2014**, vol. 1061-1062, pp. 307–310.
25. A. M. Echavarren, D. J. Cárdenas, *in Metal-Catalyzed Cross-Coupling Reactions*, Wiley-VCH Verlag GmbH, **2008**, pp. 1-40.
26. N. Miyaura, in *Metal-Catalyzed Cross-Coupling Reactions*, Wiley-VCH Verlag GmbH, **2008**, pp. 41-123.
27. S. Alesi, F. Di Maria, M. Melucci, D. J. Macquarrie, R. Luque, G. Barbarella, *Green Chem.*, **2008**, *10*, 517.
28. C. S. Krämer, T. J. Zimmermann, M. Sailer, T. J. J. Müller, *Synthesis*, **2002**, 1163.
29. C.-Y. Kuo, Y.-C. Huang, C.-Y. Hsiow, Y.-W. Yang, C.-I. Huang, S.-P. Rwei, H.-L. Wang, L. Wang, *Macromolecules*, **2013**, *46*, 5985.
30. W.-H. Liu, I.-C. Wu, C.-H. Lai, C.-H. Lai, P.-T. Chou, Y.-T. Li, C.-L. Chen, Y.-Y. Hsu, Y. Chi, *Chem. Commun.*, **2008**, 5152.
31. N. Agarwal, C.-H. Hung, M. Ravikanth, *Tetrahedron*, **2004**, *60*, 1067.
32. P. Chen, J. H. Yum, F. De Angelis, E. Mosconi, S. Fantacci, S.-J. Moon, R. H. Baker, J. Ko, M. K. Nazeeruddin, M. Gr_tzel, *Nano Lett.*, **2009**, *9*, 2487.
33. P. Docampo, S. Guldin, T. Leijtens, N. K. Noel, U. Steiner, H. J. Snaith, *Adv. Mater.*, **2014**, *26*, 4013.
34. J. Tauc, *Mater. Res. Bull.*, **1968**, *3*, 37.
35. W.-I Hung, Y.-Y. Liao, T.-H. Lee, Y.-C. Ting, J.-S Ni, W.-S. Kao, J. T. Lin, .T.-C. Wei, Y.-S. Yen, *Chem. Commun*., **2015**, *51*, 2152.
36. C. Barolo, M. K. Nazeeruddin, S. Fantacci, D. Di Censo, P. Comte, P. Liska, G. Viscardi, P. Quagliotto, F. De Angelis, S. Ito, M. Grätzel, *Inorg. Chem.,* **2006**, *45*, 4642.
37. W. Zeng, Y. Cao, Y. Bai, Y. Wang, Y. Shi, M. Zhang, F. Wang, C. Pan, P. Wang, *Chem. Mater.*, **2010**, *22*, 1915.
38. W. H. Nguyen, C. D. Bailie, J. Burschka, T. Moehl, M. Grätzel, M. D. McGehee, A. Sellinger, *Chem. Mater.*, **2013**, *25*, 1519.
39. Y. Wu, X. Zhang, W. Li, Z.-S. Wang, H. Tian, W. Zhu, *Adv. Energy Mater.*, **2012**, *2*, 149.
40. S. Qu, C. Qin, A. Islam, Y. Wu, W. Zhu, J. Hua, H. Tian, L. Han, *Chem.Commun.*, **2012**, *48*, 6972.
41. J. Liu, J. Zhang, M. Xu, D. Zhou, X. Jing, P. Wang, *Energy Environ. Sci.*, **2011**, *4*, 3021.
42. P. Ganesan, A. Chandiran, P. Gao, R. Rajalingam, M. Grätzel, M. K. Nazeeruddin, *J. Phys. Chem. C*, **2014**, *118*, 16896.

43. B. Cecconi, N. Manfredi, R. Ruffo, T. Montini, I. Romero Ocaña, P. Fornasiero, A. Abbotto, *ChemSusChem*, **2015**, *8*, 4216.
44. D. Y. C. Leung, X. Fu, C. Wang, M. Ni, M. K. H. Leung, X. Wang, X. Fu, *ChemSusChem*, **2010**, *3*, 681.
45. X. Zhang, L. Yu, C. Zhuang, T. Peng, R. Li, X. Li, *RSC Adv.*, **2013**, *3*, 14363.
46. H. Kisch, D. Bahnemann, *J. Phys. Chem. Lett.*, **2015**, *6*, 1907.
47. R. Y.-Y. Lin, F.-L. Wu, C.-T. Li, P.-Y. Chen, K.-C. Ho, J. T. Lin, *ChemSusChem*, **2015**, *8*, 2503.
48. v. authors, in *Engineered Carbohydrate-Based Materials for Biomedical Applications*, John Wiley & Sons, Inc., 2011.
49. G. Pescitelli, O. H. Omar, A. Operamolla, G. M. Farinola, L. Di Bari, *Macromolecules*, 2012, **45**, 9626.
50. V. Leandri, H. Ellis, E. Gabrielsson, L. Sun, G. Boschloo, A. Hagfeldt, *Phys. Chem. Chem. Phys.*, 2014, **16**, 19964.
51. A. Deronzier et al. PCT Int. Appl., 2012066048, 24 May **2012**.
52. H. Brunner, N. Gruber, *Inorg. Chim. Acta*, **2004**, *357*, 4423.
53. V. V. Rostovtsev, L. G. Green, V. V. Fokin, K. B. Sharpless, *Angew. Chem. Int. Ed.*, **2002**, *41*, 2596.
54. C. W. Tornøe, C. Christensen, M. Meldal, *J.f Org. Chem.*, **2002**, *67*, 3057.
55. A. J. Dirks, J. J. L. M. Cornelissen, F. L. van Delft, J. C. M. van Hest, R. J. M. Nolte, A. E. Rowan, F. P. J. T. Rutjes, *QSAR & Combinatorial Science*, **2007**, *26*, 1200.
56. S. P. Chakrabarty, R. Ramapanicker, R. Mishra, S. Chandrasekaran, H. Balaram, *Biorg. Med. Chem.*, **2009**, *17*, 8060.
57. F. Bella, C. Gerbaldi, C. Barolo, M. Grätzel, *Chem. Soc. Rev.*, **2015**, *44*, 3431.
58. P. Salvatori, G. Marotta, A. Cinti, C. Anselmi,E. Mosconi, F. De Angelis, *J. Phys. Chem. C*, **2013**, *117*, 3874.
59. T. Daeneke, T.-H. Kwon ,A. B. Holmes, N. W.Duffy, U. Bach, L. Spiccia, *Nature Chem.*, **2011**, *3*, 211.
60. S. Ito, H. Miura, S. Uchida, M. Takata, K. Sumioka, P. Liska, P. Comte, P. Péchy, M. Grätzel, *Chem. Commun.*, **2008**, 5194.
61. R. Harikisun, H. Desilvestro, *Solar Energy*, **2011**, *85*, 1179.
62. W. J. Youngblood, S.-H. A. Lee, Y. Kobayashi, E. A. Hernandez-Pagan, P. G. Hoertz, T. A. Moore, A. L. Moore, D. Gust, T. E. Mallouk, *J. Am. Chem. Soc.*, **2009**, *131*, 926.
63. E. Bae, W. Choi, J. Park, H. Suk Shin, S. Bin Kim, J. Sung Lee, *J. Phys. Chem. B*, **2004**, *108*, 14093
64. D. G. Brown, P. A. Schauer, J. Borau-Garcia, B. R. Fancy, C. P. Berlinguette, *J. Am. Chem. Soc.*, **2013**, *135*, 1692.

65. K. Narayanaswamy, A. Tiwari, I. Mondal, U. Pal, S. Niveditha, K. Bhanuprakash, S. P. Singh, *Phys. Chem. Chem. Phys.*, **2015**, *17*, 13710.

66. W. R. McNamara, R. C. Snoeberger III, G. Li, C. Richter, L. J. Allen, R. L. Milot, C. A. Schmuttenmaer, R. H. Crabtree, G. W. Brudvig, V. S. Batista, *Energy Environ. Sci*., **2009**, *2*, 1173.

67. W. Li, L. G. C. Rego, F.-Q. Bai, J. Wang, R. Jia, L.-M. Xie, H.-X. Zhang, *J. Phys. Chem. Lett*., **2014**, *5*, 3992.

68. C. Koenigsmann, T. S. Ripolles, B. J. Brennan, C. F. A. Negre, M. Koepf, A. C. Durrell, R. L. Milot, J. A. Torre, R. H. Crabtree, V. S. Batista, G. W. Brudvig, J. Bisquert, C. A. Schmuttenmaer, *Phys. Chem. Chem. Phys.*, **2014**, *16*, 16629.

69. W. R. McNamara, R. L. Milot, H.-E. Song, R. C. Snoeberger III, V. S. Batista, C. A. Schmuttenmaer, G. W. Brudvig, R. H. Crabtree, *Energy Environ. Sci*.**, 2010**, *3*, 917.

70. O. Bettucci, Master Degree Thesis, Progettazione e sintesi di fotosensibilizzatori organici per celle solari di terza generazione con gruppi ancoranti solforati, April **2015**.

71. D. Franchi, M. Calamante, G. Reginato, L. Zani, M. Peruzzini, M. Taddei, F. Fabrizi de Biani, R. Basosi, A. Sincropi, D. Colonna, A. Di Carlo, A. Mordini, *Tetrahedron*, **2014**, *70*, 6285.

72. B. Cecconi, A. Mordini, G. Reginato, L. Zani, M. Taddei, F. Fabrizi de Biani, F. De Angelis, G. Marotta, P. Salvatori, M. Calamante, *Asian J. Org. Chem.,* **2014**, *3*, 140.

73. C. Chen, X. Yang, M. Cheng, F. Zhang, L. Sun, *ChemSusChem*, **2013**, *6*, 1270.

74. N. Manfredi, B. Cecconi, A. Abbotto, *Eur. J. Org. Chem.* **2014**, 7069 *and references therein*.

75. Shriver D. F., Drezdzon M. A. "The Manipulation of Air-Sensitive Compounds", John Wiley & Sons, Hoboken, **1986**.

76. S. Ito, T. N. Murakami, P. Comte, P. Liska, C. Grätzel, M. K. Nazeeruddin, M. Grätzel, *Thin Solid Films*, **2008**, *516*, 4613.

Chapter 4

MOLECULAR APPROACH FOR H_2 EVOLUTION CATALYSIS: COBALOXIMES

Experimental Studies for Co(I) Intermediate Characterization

Before my world turned blue

Turn blue

The Black Keys

4.1 INTRODUCTION

During the last decades attention has been focused not only on the development of light-harvesting systems, but also on catalytic centers with high turnover number (high durability), high turnover frequency (near thermodynamic equilibrium, thus high activity) and low cost. Nowadays the most effective catalysts able to perform water splitting rely on noble metal, as it has been described in paragraph 2.2.4, with platinum as the most successful catalyst to perform proton reduction. This is a huge limitation to develop simple, cheap and viable water splitting systems. That is the reason why a considerable part of the scientific world is focusing efforts on trying to reduce the amount of active material in devices, on the development of alternative noble-metal free catalysts to drive the desired reactions, and on the recovery or recycling of the precious elements.[1] Natural photosynthesis gave many ideas in the development of well-working antenna systems, therefore the same may be done for the building of new catalysts. This paragraph will be focused on the reduction semi-reaction, therefore mainly catalysts for hydrogen evolution will be presented.

Nature usually does not produce hydrogen, but the "reducing equivalents" coming from the light-induced charge separation are used in photosystem I for the reduction of $NADH^+$ into NADPH (that then enters the Calvin cycle). Naturally there are some enzymes, hydrogenases, that are able to drive protons reduction to give molecular hydrogen; the active core of such macromolecules is composed of earth abundant metals such as iron or nickel.[2,3] That is the reason why many efforts have been done in developing artificial catalysts that mimic the natural active sites of hydrogenases.[4] Most of the iron-containing catalysts are directly inspired by the shape and atoms disposition in active sites of hydrogenases with two bridged iron centers, as well as in other catalysts containing iron-nickel.[5,6] DuBois and co-workers gave a great contribution in developing nickel catalysts for electrochemical hydrogen generation.[7] An example of a DuBois's catalyst is represented in Figure 4.1, it should be pointed out the smart role of the pendant amine, fundamental for proper protonation at Ni atom when it is at the reduced state.

In addition to those metals, a great attention has been given to a third earth copious metal that is cobalt,[8,9,10] even though no biological example is known for water splitting. Cobalt's abundance on earth is 20-30 ppm, so it is rarer than iron (6.3%), manganese (0.1%) or nickel (90 ppm), but it could still be considered abundant and there are promising results for its complexes in both water splitting semi-reactions.

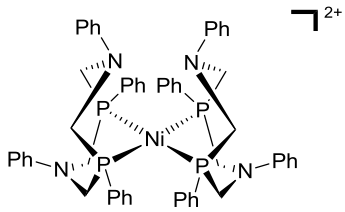

$[Ni(P^{Ph}_2N^{Ph}_2)]^{2+}$

Figure 4.1: DuBois's catalyst.

In this dissertation, attention will be centered on molecular approaches that have many advantages compared to other systems, i.e. fine tunability, high control of purity (there is not the problem of surface defects control as in material synthesis) and a potential good understanding of cause and effect relationships between structural differences and activities (or other properties) when comparison between different molecular catalysts is made.

4.2 COBALT COMPLEXES FOR PHOTOCATALYTIC PROTON REDUCTION

The molecular approach in building cobalt complexes differs mainly in the kind of ligand that is employed. In most of the cases they are square-planar macrocyclic or pseudo macrocyclic complexes, such as the examples reported in Figure 4.2 (left),[11] water soluble porphyrin derivatives as the examples reported in Figure 4.2 (right),[12] cobaloximes, or the water stable analogues such as diimine-dioxime complexes,[13] shown in Figure 4.3. In all these complexes, the coordination sphere of cobalt is not complete, at least in the Co(II)/Co(I) states, so that there is a axial-free or labile position for the coordination of the proton necessary for catalysis. There are other families of complexes with saturated coordination sphere. In those cases the catalytic cycle requests a labile ligand to dissociate, as in the cases of complexes of cobalt with polypyridine ligands (Figure 4.4 top),[14] hexaamino complexes (Figure 4.4 bottom) such as sepulchrate and clathrochelate trisdioxime compounds (Figure 4.4 bottom).[15,16] In the last complexes where no labile ligand is present, the actual mechanisms could interest the outer-sphere or activity could be due to degradation to nanoparticles.[17]

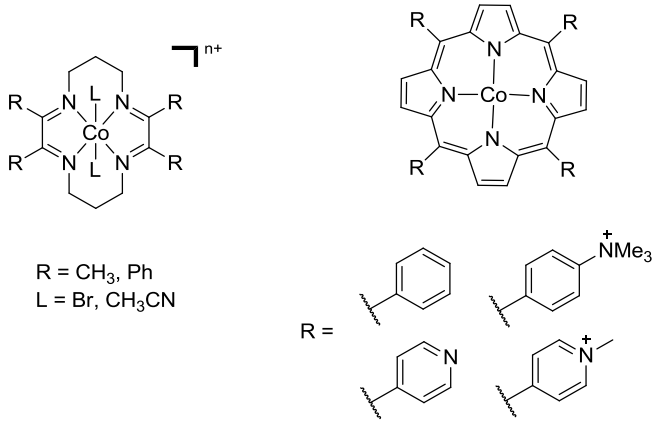

Figure 4.2: Cobalt macrocyclic complexes.

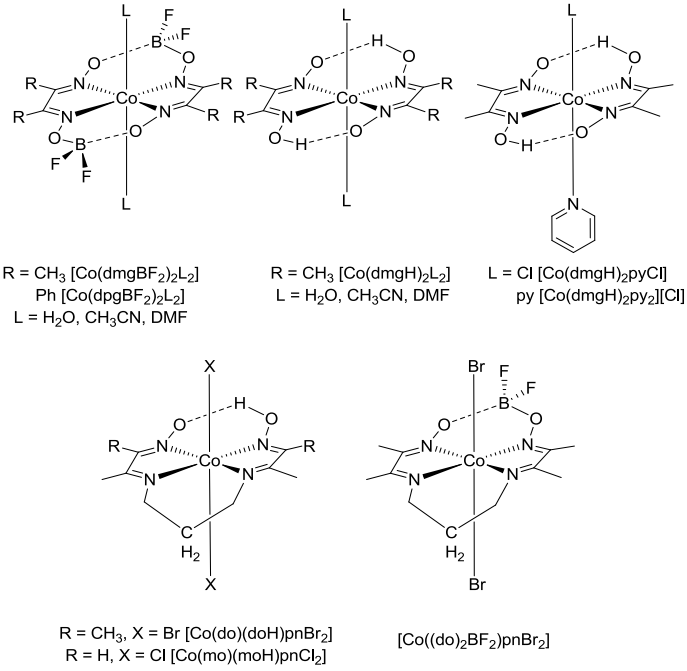

Figure 4.3: Cobaloximes and diimine-dioximes Cobalt complexes.

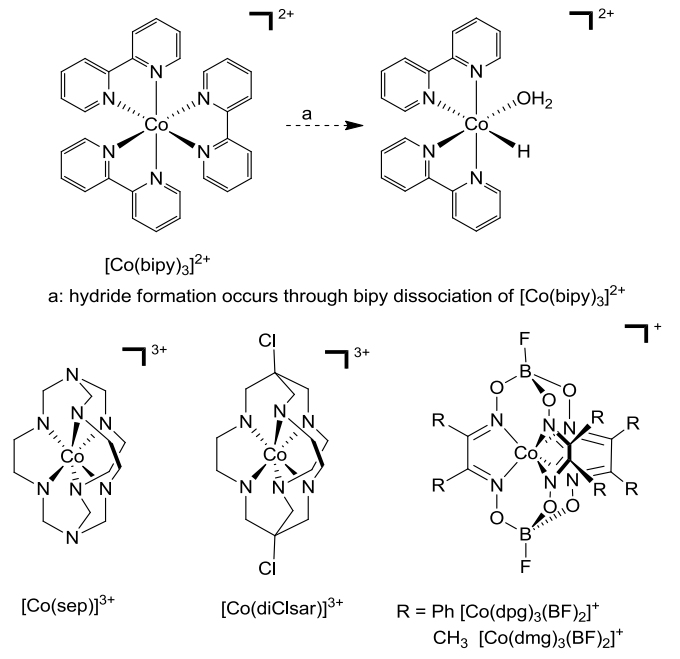

Figure 4.4: Polypyridine ligands (top), hexaamino complexes, sepulchrate and clathrochelate trisdioxime compounds (bottom).

Electrocatalysis is a very useful instrument to start studying the potentialities of new catalysts. Nevertheless electrocatalytic performances of catalysts are generally not perfectly transferred to their activities in photocatalytic processes, when electrons availability is related to the activities of photosensitizers and sacrificial electron donors. Usually electrochemical measurements are performed in organic solvents, using added acid at different concentrations and strength to protonate the reduced form of the catalyst, moreover the electrons are supplied by an electrode at the desired potential and with the right "timing". That means that all the critical steps of the cycles rely on the catalyst only, the kinetics and thermodynamics involved in the electron transfer are not an issue. When the tests shift to the photocatalytic ones more variables are present: the photosensitizer, the sacrificial electron donor, an electron mediator (not always present), and generally an aqueous mixed solvent that could give rise to stability issues. Apart from those limitations, electrocatalytic experiments are fundamental to screen catalysts and to try to rationalize advantages and disadvantages connected to a specific modification; such experiments are indeed supported by electrochemical simulations and computational methods that simplify the interpretation and comparison between analyzed systems.[18,19] One of the most important parameter in electrocatalysis is the overpotential; such requirement is the most reliable parameter for comparison of performances. Overpotential is the difference between the potential applied to the system to have hydrogen evolution and the standard potential of the redox couple H^+/H_2 in the same operating conditions.[20] When the overpotential required to observe a significant current, i.e. a significant reaction rate, is about 200 mV the catalyst could be a good candidate for photocatalytic tests. Definitely most of the cobaloximes and diimine-dioximes catalysts shows an overpotential requirements in the range of 200-300 mV, that is the reason why they are considered promising catalysts. A second important parameter is the turnover frequency (TOF) that is connected to the number of electrons exchanged between the electrode and the redox couple per time unit. However the catalytic current (measured from the voltammogram) is related to the TOF only if the catalytic mechanism, so the rate determining step, is known. The turnover number (TON) is instead measured in conditions of bulk electrolysis till the almost complete deactivation of the system, thus it gives information about the thermodynamic and kinetic stability of the catalyst. For molecular systems in solution the TON is quite low, reaching some hundreds for the best ones; this is not the best condition, but surely the transition from homogeneous to heterogeneous catalysis

(needed for engineering requirements) will improve stability deleting some of the degradation pathways.[21,22,23]

Lastly Faradaic yield is a parameter that gives an idea of the selectivity of the catalyst, if it is close to 1 it means that the selectivity of the catalyst towards proton reduction is very high, if it is close to 0 it means that there are many other detrimental pathways that waste electrons.

In the following paragraph, a detailed description of the components of a photocatalytic test will be presented with special attention to the cobaloximes catalysts as they have been the investigated complexes during this research period.

4.3 COMPONENTS OF PHOTOCATALYTIC EXPERIMENTS

In the first examples of photocatalytic experiments, the system was made of a catalyst, a photosensitizer (PS), a sacrificial electron donor (SED), and an electron relay. Lehn *et al.* were amongst the first researchers that tested a cobaloxime together with a PS and an SED avoiding the need for the electron relay.[24,25]

The attention will be now focused on this kind of systems, the ones related to Lehn approach, because the elimination of the electron relay simplifies the method.

4.3.1 Photosensitizer

Concerning the photosensitizers, there are two possible pathways responsible for electron transfer: oxidative or reductive quenching. Figure 4.5 shows these two possibilities, in both cases the PS absorbs a photon and passes to the excited state PS*, which could transfer an electron to the oxidized catalyst and be transformed to PS^+ that is then reduced by the electron donor (oxidative quenching), or could be directly reduced by the electron donor giving PS^- that is then responsible for electron transfer with the catalyst (reductive quenching). A brief description of the photosensitizers used in photocatalytic tests in the presence cobalt catalyst will now be given.

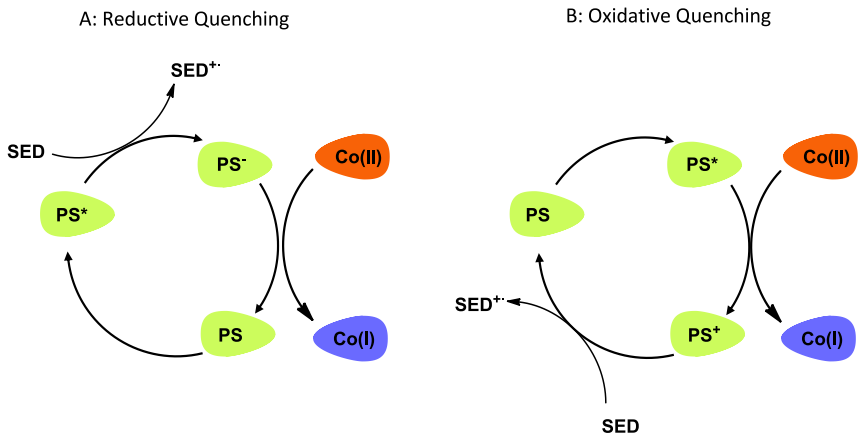

Figure 4.5: Possible pathways for photosensitizers: Reductive Quenching (left) and Oxidative Quenching (right).

In most of the cases both pathways are possible and working, depending on the conditions of the system, meaning the redox properties of all the couples involved

PS^+/PS^*, PS^*/PS^-, Co(III)/Co(II), Co(II)/Co(I), $SED^{+\cdot}/SED$ and the relative concentrations of all the components. For example $[Ru(bpy)_3]^{2+}$ (Figure 4.6-left)[26] is one of the most widespread sensitizer and the quenching pathway strongly depends on the kind of electron donor used: when the Ru chromophore absorbs a photon and passes to the excited state, an intersystem crossing that involves a spin-orbit coupling yields to the transition from a singlet state (S=0) to a triplet state (S=1) that is described as a Ru(III) with an anionic ligand. Therefore there is an electron in the π* orbital of the bipy ligand with a standard potential of -0.86 V (powerful reductant) and an empty d orbital on the metal at a standard potential of 0.84 V vs. NHE (powerful oxidant). The selected pathway depends on the operating conditions. When ascorbic acid is used, the reductive quench occurs, but with TEOA only the oxidative quenching occurs since TEOA has a thermodynamically unfavorable potential to reduce the photosensitizer.[27] Other versatile sensitizers are the cyclometalated iridium chromophores (Figure 4.6-right) that have similar quenching rates with TEOA (10^6-10^9 $M^{-1}s^{-1}$) or with cobalt complexes (10^8 $M^{-1}s^{-1}$), so the pathway depends on their relative concentrations.[28] Those sensitizers have relative low extinction coefficients (<600 $M^{-1}cm^{-1}$) but excitation generates a long-lived triplet state that is able to efficiently mediate electrons transfers.

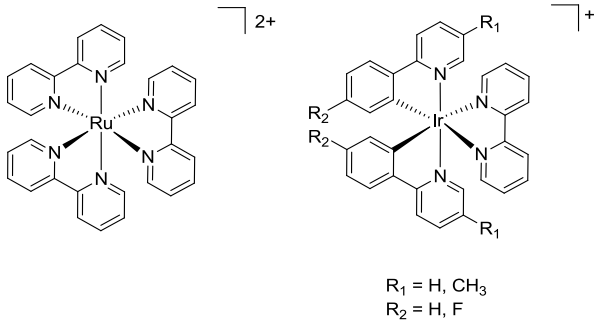

Figure 4.6: Ruthenium complex (left) and Iridium chromophores (right).

A third class of chromophores are the platinum terpyridylacetylide complexes for which both pathways are possible,[29,30] while for a fourth class of rhenium tricarbonyl-diimine complexes[31,32] the only possible quenching using TEOA is the reductive one (examples of Pt and Re photosensitizers are illustrated in Figure 4.7). The reduced diimine ligand of these photosensitizers has a fundamental role in stabilizing the triplet state arising from excitation.

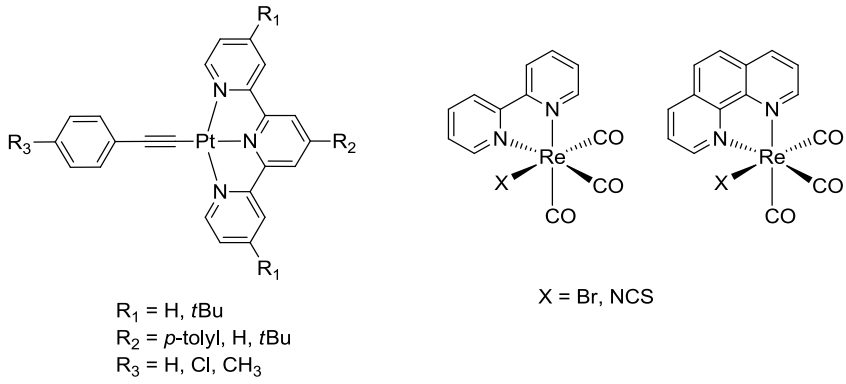

Figure 4.7: Platinum terpyridylacetylide complexes (left) and Rhenium chromophores (right).

Since the aim of developing cobalt catalysts is to eliminate noble metal it is clear that chromophores based on Ru, Ir, Pt, or Re do not have a bright future for application. A large interest is therefore given to the organic sensitizers (Figure 4.8). Amongst the organic dyes, the family of fluoresceins and rhodamines are the most used. Not all the xanthenes work in electron transfer to cobalt catalyst, the best ones are Eosin Y[33,34] and Rose Bengal,[35] instead most of all the other ones are not working at all or with few complexes. The reason for this different behavior was found in the presence of heavy halogen atoms like Br (Eosin Y) or I (Rose Bengal) that facilitate intersystem crossing, producing a long-lived triplet state necessary for the suitable electron transfer to the catalyst. Usually rhodamine dyes give good performances and even in this case the activity could be related to the presence of heavy atoms (S or Se instead of O).[36]

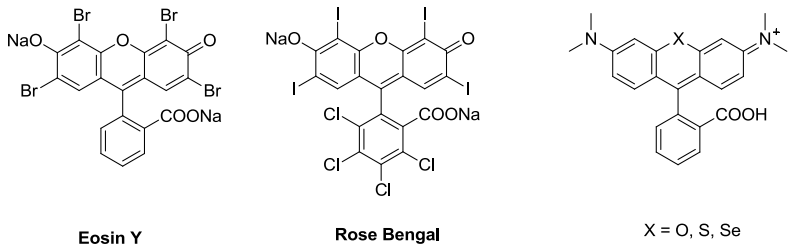

Figure 4.8: Xanthene dyes.

In conclusion the stability of the photosensitizer strongly depends on the quenching pathway, since radical cations or anions that form will have different properties, so

there are conditions in which organic dyes are highly stable and other ones in which they are subject to fast degradation, thus limiting the activity.

4.3.2 Sacrificial Electron Donor

Concerning the sacrificial electron donor, the basic requirement is that it undergoes an irreversible decomposition path upon oxidation so that back electron transfer is inhibited. A second requirement to correctly analyze the data from the tests is that the sacrificial electron donor itself is not able to drive the direct transfer of the electron to the cobalt complex, otherwise the studied reaction is a simple thermal redox process. Amongst the most common sacrificial electron donors there are ascorbic acid,[26] triethanolamine (TEOA),[37] triethylamine (TEA), and most of them can transfer/give two electrons, the second reaction taking place via a dark process.[38]

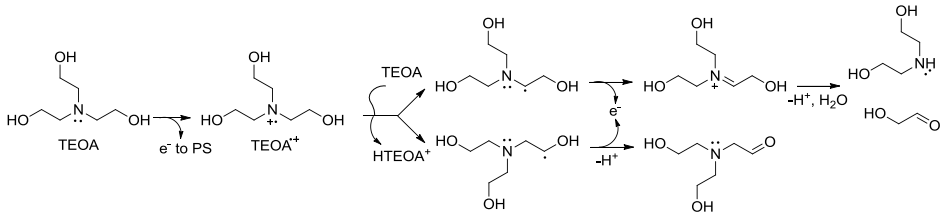

Figure 4.9: TEOA decomposition pathway upon interaction with the photosensitizer.

Figure 4.9 illustrates the decomposition pathway proposed by Alberto *et al.* for TEOA.[38] The radical cation $NR_3^{+\cdot}$, that forms after electron transfer to the chromophore, is highly unstable and it undergoes to a series of protons and electrons transfers till the breaking of the C-N bond and/or the formation of stable intermediates (two possible pathways on Figure 4.9-right).[39] One of the decomposition intermediate is deprotonated at α-carbon position, such radical is highly reactive and is a reductant for cobalt catalyst, for this reason usually for each excited PS molecule (i.e. for each photon) two electrons are generated in the case of TEOA. However, this is not always true and it depends on the used solvent, for example it is highly marked in DMF but less evident in aqueous solvents, meaning that alternative decomposition pathways occur.[38] Irreversible decomposition pathways for common electron donors are well established.[40,41] Depending on the chosen electron donor many other parameters should be adjusted, for example ascorbic acid usually works in a pH range of 4-5, while the amine donors are more active in the 8-9 range of pH. The pH range is important since the basic form only of those molecules is able to act as sacrificial electron donor. To better understand the

reason of the pH range requirements, TEOA may be taken as example: as the pH goes down the amine function is increasingly protonated, which affects the capability of electron transfer to the chromophore, at the same time as the pH goes more basic the availability of protons necessary for the cobalt catalytic cycle are too low in concentration. The pH should be chosen as the best compromise between two divergent aspects. As pH is a fundamental parameter that must be controlled during experiments, problems arise when the medium used is an aqueous mixture with almost half of it as organic solvent. The glassy electrode used to measure the pH is calibrated in aqueous media and its response could be altered.[25] Thus the pH can be measured before mixing the aqueous medium (even if the acidity of protons is influenced by the organic medium that will be added in a second moment) with the organic one, but the literature data can only be compared with identical or similar experimental conditions.[33,42]

4.3.3 Catalysts

One of the main issues in the development of new catalysts is the deep understanding of all the intermediates formed during the catalytic cycle, so that rational optimization of the complex can be made. Regarding the cobalt catalysts, in particular the cobaloxime complexes, many catalytic cycles have been proposed in the last decade. Apparently there is not an exclusive solution to the catalytic cycle, but many possible pathways can be envisaged and the success of one over the other may also depend on the photocatalytic conditions used.[43,44]

The pathways can be divided into two main categories: the homolytic and the heterolytic routes, the former is a bimetallic kinetics, while the latter is a monometallic one.[45,46] Figure **4.10** represents schematically the two alternative paths with the relative subdivisions.

Kinetic studies on a stabilized [Co(III)-H] species, such as [$HCo(dmgH)_2(PBu_3)$], revealed both a first and second-order dependence of the reaction rate with respect to proton concentration, supporting that both the pathways are possible and they occur in parallel.[47] This is true if catalysis is the slow process, meaning that electron transfer from the PS to the catalyst should not be the rate determining step. Usually homolytic pathway is predominant with a higher kinetic constant, while the heterolytic one is competitive for low catalyst concentration or high acid/proton concentration. In the electrocatalytic tests the proton source is responsible for the kind of pathway:[11,48] if the acid is strong enough to protonate both the Co(I)

intermediate and Co(III)-H, the heterolytic way is preferred. On the contrary a weak acid able to protonate Co(I) only but not the Co(III)-H, will force the system to follow the bimetallic route with coupling of the two hydrides.

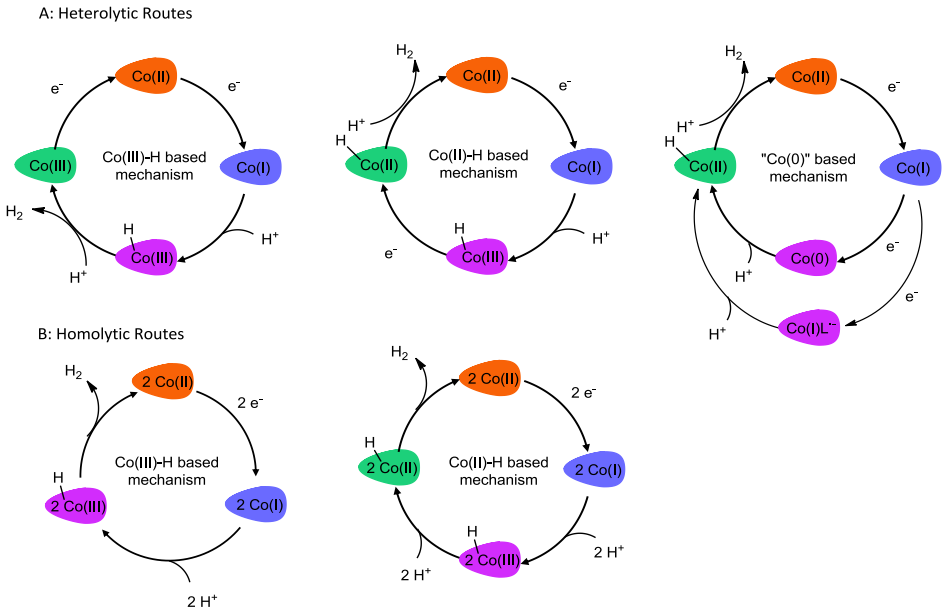

Figure 4.10: ***Proposed catalytic cycles for cobaloximes, heterolytic (top) and homolytic routes (bottom).***

Alternatively in the literature of cobaloximes and diimine-dioxime complexes it has been proposed that if the acid is not strong enough to protonate Co(III)-H species, for example if the pH of the solution is neutral or basic, another intermediate, the Co(II)-H species (Figure 4.10A), could form by reduction of Co(III)-H, which is definitively more reactive towards protonation and can support the heterolytic route.[48,49] There is an extreme hypothesis considering weak acids for which even the first protonation at Co(I) is inhibited and the reduction occurs first giving a Co(0) complex that then is protonated two times (heterolytic route) or once (homolytic route).[43]

Almost all the paths predict the formation of a key intermediate that is Co(III)-H starting from a Co(I) species formed through reduction; that intermediate has been isolated chemically or electrochemically for “special” complexes ideated with unique ligands able to stabilize it, lowering the hydrogen production kinetics. That necessity arises from the difficulty of analyzing the eventual Co(III)-H that forms transiently, but such modification is supposed to slow down the kinetics only and not to modify

the catalytic cycle. Apart from some experimental results reported by Peters *et al.*[50] that have challenged the nature of the Co(III)-H in the chemical preparations, hinting that the real studied species is an inactive Co(II) dimer, most of the data reported on the literature highlighted the presence of a Co(III)-H species. The most used ligands for Co(III)-H stabilization are phosphines that only interact with Co(I) intermediates and could prevent them from decomposition, or they are able to stabilize the hydride intermediate as in the case of $[HCo(dmgH)_2(PBu_3)]$.[42,51,52] Modification of the coordination sphere of catalyst may modulate the activities and stability, for example in the case of cobaloximes the equatorial plane may be modified to lower the overpotential, whereas the modification of the *trans* axial ligand influences the pK_a of protonation at the Co(III) centre, or the stability and reactivity of the hydride Co(III)-H intermediate, but has no effect in the Co(II)/Co(I) redox potential. That statement is highlighted in the screening of various pyridine ligands for the cobaloxime $[Co(dmgH)_2pyCl]$, where pyridine is substituted with different electronic groups (electron-withdrawing or electron-donating) in the *para* position: that modification influences the pK_a of the corresponding Co(III)-H.[53] Wang *et al.* investigated a series of cobaloximes bearing pyridine rings with carboxylic acids or esters in *meta*- and *para*- positions studying the relationship between the kind of substituent and the ring position in efficiencies in photocatalytic experiments.[54] They found out that the best performing catalyst is the one bearing a carboxylic acid in *meta*- position linked through an alkyl chain to the pyridine core, hinting a possible role of the pendant moiety in proton relay to the dmgH bridge. The main limitation in the ligand manipulation is that each modification does not only affect the redox properties of the complexes but also the protonation constants and those two effects are opposite, in particular hard ligands give easier protonation and enhance the hydridicity of the Co(III)-H intermediate. An important observation must be done when the catalytic cycles are studied: the final aim of the investigation of new catalytic complexes is to build devices, and engineering needs catalysts immobilized on supports. Indeed heterogenization of catalyst is a common route to scale up devices, for that reason the heterolytic route must be favored, and the conditions that are the best for the monometallic path must be very clear because once the catalyst is fixed on a surface the bimetallic route is almost completely suppressed, thus activity is only due to heterolytic catalysis.[55,56]

Stability issues on cobaloximes

A great topic in the development of new catalysts is not only the research for higher activity but also a great stability and durability in time. From that point of view cobaloximes have various limitations, since it has been demonstrated that most of the axial ligands present in the starting complex may have no role in the catalytic cycle meaning that probably they are lost during catalysis. For example pyridine ligand was supposed to be unstable in the catalytic conditions and the confirmation came from tests regarding linked systems (paragraph 4.3.4) where pyridine was used to link the photosensitizer to the catalyst resulting in a supramolecular unity. Such systems were not stable in photocatalytic tests and the instability was found in the weakness of the coordination of pyridine to the Co centre. Secondly the need of free dmg ligand addition to recover activity is a clear evidence of ligand leakage or decomposition.[24,31,33,36,38] It has been demonstrated that if dmg^{2-} ligands are partially hydrogenated or lost during catalysis (detrimental routes) the catalyst looses activity and the decomposition of the photosensitizer starts. The reason is that with the decreasing of the catalyst concentration the reduced photosensitizer decomposes because no more electron transfer occurs (Figure 4.11). [31,32,38]

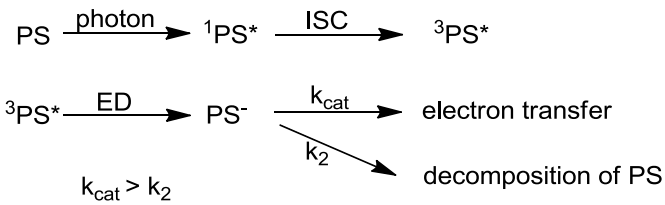

Figure 4.11: Excitation of the photosensitizer and possible pathways.

During photocatalytic tests, even if they are not hydrogenated during catalysis, the dmg^{2-} ligands could decoordinate, an evidence of that phenomenon is that the addition of fresh ligand at the solution, when hydrogen production rate is low, restores the initial rate. Moreover comparing the activities of $[Co(dpgH)_2pyCl]$ and $[Co(dmgH)_2pyCl]$, it turns out that the former is much less active than the second one, but if 2 equivalents of dmg^{2-} are added to the solution the hydrogen rate production increases reaching an intermediate rate and the ending reaction mixture contains both the catalysts and the mixed form [Co(dmgH)(dpgH)pyCl], that is a clear proof of ligands exchange.[57]

4.3.4 Linked Supramolecular Assemblies

A clever way to enhance electron transfer efficiency from the photosensitizer to the catalyst is to link the two moieties together. This approach is called the supramolecular assembly and has first been introduced by Artero *et al.* in 2008 in the case of cobaloximes.[58,59] The first example is represented by a dyad composed of a Ru sensitizer and a cobaloxime (Figure 4.12), the supramolecular architecture gives efficiencies that can be tuned manipulating the coordination sphere of the Co center. The efficiencies are slightly higher than the separated counterparts even if they are not so markedly different. This can be attributed to two different reasons: the first one is that the electron transfer from the sensitizer to the catalyst is not the rate-determining step of the whole mechanism thus enhancing that step does not increase the overall rate; the second interpretation is that as the direct electron transfer is facilitated, the back electron transfer can also be easier if the two parts are linked, so that the overall transfer rate is unmodified. The second purpose of the supramolecular approach is to increase stability of the system upon irradiation, that is partially verified if the two moieties are covalently linked, on the contrary supramolecular coordination is found not so robust; some exceptions are known, for example in the case of the linked system depicted in Figure 4.12-top-left a high stability is verified. Usually the two systems are linked through coordination of a pyridine-substituted sensitizer as axial ligand of the Co center. It has been demonstrated that many Co centers are prone to pyridine detachment if water is present in the solution, which is a strong limitation of this method,[60] that anyway has put the basis for the supramolecular approach. The major limitation is that the extent of the detachment depends on the particular system taken into consideration and some pyridines detach very easily while other ones are more stable, depending on the structure of the rest of the molecule. Porphyrins as well have been linked to cobaloximes and the efficiencies depend on the metal center used, with the most promising results with Zn (Figure 4.12).[61] Some Ir sensitizers have been linked to Co catalyst through covalent bond of alkyl chains that are enough to guarantee a good electronic communication, pointing out the hypothesis that there is no need for a total conjugated system, even though such systems have not been characterized in hydrogen production yet (Figure 4.12).[62, 63]

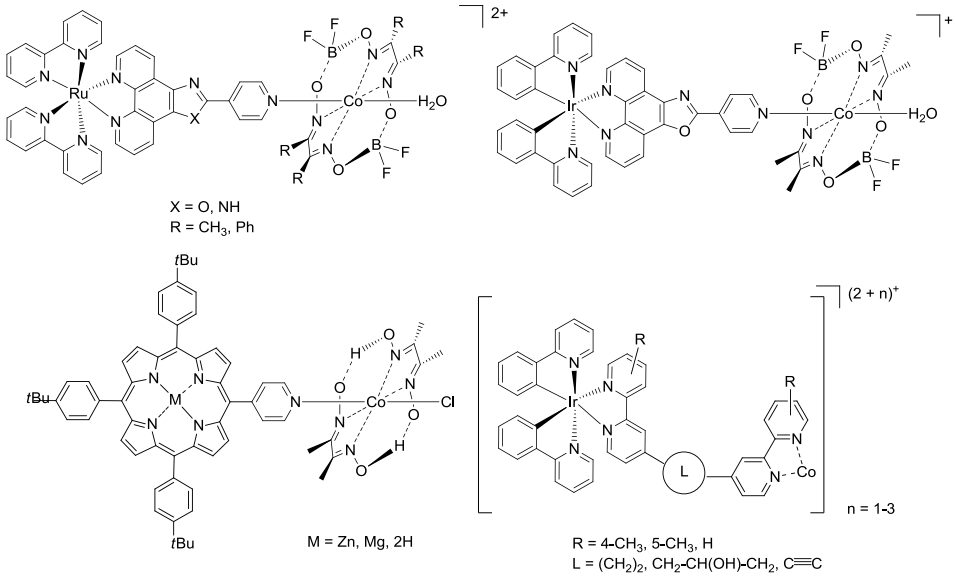

Figure 4.12: Supramolecular structures.

4.4 OBJECTIVES OF THE STUDY

As it has been illustrated in paragraph 4.3.3, all the catalytic cycles proposed for cobaloximes involve the formation of a Co(I) species as key intermediate. To better understand the potentialities of cobaloximes and to optimize their performances it is necessary to deeply understand the characteristics of all the intermediates involved in the catalytic cycle. Only in that way it is possible to tune and modulate the coordination sphere of the Co center to improve efficiency or stability. The stabilization of the more reactive intermediates through ligand tuning is fundamental, but at the same time it is very difficult to have a structural characterization of such intermediates, since they are intrinsically the more reactive ones. During the catalytic cycle the Co center changes oxidation number and that might imply different coordination geometries, different acidities of all the basic sites, and different strengths of interactions with the coordination sphere. This is the reason why in recent years many efforts have been dedicated to the determination of the intermediates' properties. Hypothesized Co(I) species are probably slightly different from precursors in the catalytic cycles in the geometry of the equatorial and axial ligands, meaning the eventual displacement, reinforcement or weakening of those groups.

The problem of investigating Co(I) species formed in photocatalytic reactions is that there is generally a high number of variable factors, many other chemical species involved and the Co(I) forms transiently, thus an isolation of the intermediate is quite impossible. For this reason most of the strategies involve a modification of the system towards a chemical instead of a photocatalytic reaction. That means that Co(I) species forms from reaction with a reductant, such as $NaBH_4$, and not from electron transfer from a sensitizer; that greatly simplifies the study of the system. Moreover, since Co(I) species are unstable and difficult to be isolated, modification of the coordination sphere, for example introducing phosphines, is a further way to stabilize and isolate the intermediate. All that methods have a fundamental problem, which is the modification of the real experimental conditions that operate in photocatalysis, e.g. the introduction of a phosphine could modify the catalytic cycle and could give mistaken information about the geometry of the intermediate. The same problem is present if a chemical reductant or an electrode is used to transfer electrons: the kinetics and thermodynamics of such transfer are not the same as if the electron is given by a transient and unstable species such as the excited

sensitizer, so those experiments could give interesting information but are likely incomplete.

The aim of my research might be divided in two phases: a first part in which a library of cobaloximes has been tested for photocatalytic tests in homogeneous conditions so to have a trend in activity depending on the species, and a second part in which photo-accumulation tests to try to characterize Co(I) species have been performed. The second part has been performed in parallel with the studies of Dr. Grigory Smolentsev at the University of Villigen in Switzerland who has developed a time-resolved X-Ray Spectroscopic technique to investigate transient Co(I) species. The mini-library of cobaloximes that has been investigated is depicted in Figure 4.13.

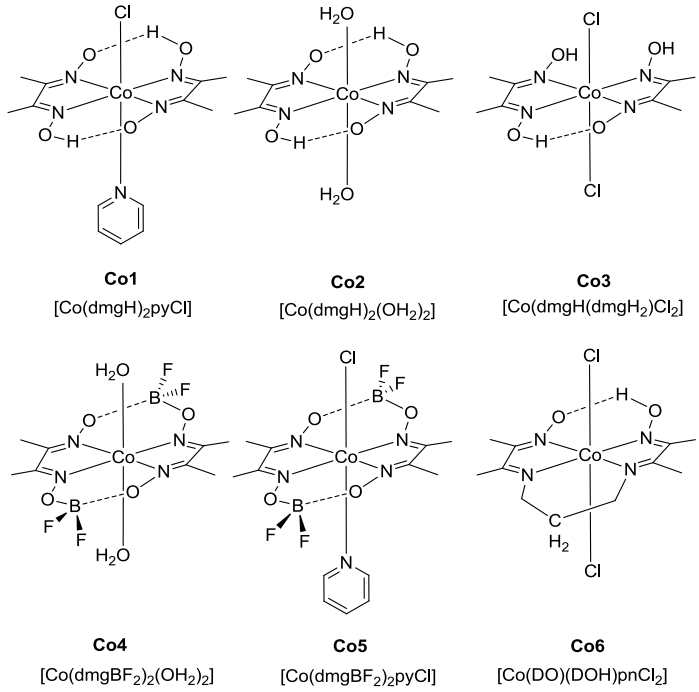

*Figure 4.13: Mini-library of cobaloximes (and a diimine-dioxime cobalt complex **Co6**) investigated.*

The main parameters that have been varied are the following ones:

- the equatorial coordination sphere that sweeps from the H-bridged glyoximate (**Co1**, **Co2**, **Co3**), to the BF_2-bridged systems (**Co4**, **Co5**) and propylene linker that transforms the cobaloxime into a diimine-dioxime

cobalt complex (**Co6**). Diimine-dioxime complexes are different macrocycles but they might give insights on the catalytic activity, especially in explaining comparisons between the other catalysts, moreover they are known to be more stable in aqueous mixture over a large pH range and they are considered the "evolution" of cobaloxime catalysts since they can be easily functionalized to attach them on surfaces and proceed to heterogenization necessary for future application;[13]

- the axial ligands that vary from solvent molecules (**Co2**, **Co4**) to anions such as chloride (**Co1**, **Co3**, **Co5**, **Co6**) and to π-ligand as pyridine (**Co1**, **Co5**);
- different oxidation states in cobalt center of the starting complex, varying from +2 (**Co2**, **Co4**) to +3 (**Co1**, **Co3**, **Co5**, **Co6**).

The development of the topics will be structured in a first illustration of photocatalytic hydrogen production tests in homogeneous solution, followed by a brief introduction of the apparatus for the microseconds X-Rays absorption spectroscopy and the results from Dr. Grigory Smolentsev that have been the basis to run the photo-accumulation tests, and finally a screening of the UV/Vis behavior of the complexes and the comparison with the results from Switzerland.

4.5 PHOTOCATALYTIC TESTS

The initial screening was performed following a classical photocatalytic hydrogen production procedure in the presence of TEOA as sacrificial electron donor at pH 7. Many articles reported this kind of analysis but all the data have never been collected and run together for the complexes **Co1-Co6**. The aim of the screening was the comparison between different molecular catalysts so the most common conditions have been chosen to run the tests. The chosen photosensitizer is eosin Y since it shows a good activity (in electron releasing) with all the complexes, while other sensitizers, such as $[Ir(ppy)_2(bpy)](PF_6)$, could not be able to drive the reduction step from the potential point of view for all the investigated cobaloximes. The main drawback in the use of eosin Y is that its stability in photocatalytic tests is quite low, it suffers from de-bromination of the core that transforms it into fluorescein (that is no more active in the reduction of many cobaloximes) and it might be partially hydrogenated. [33,64] We confirmed this instability since the photocatalytic reactions were run over a period of 5 h and after that all the reaction mixtures were almost colorless indicating the decomposition of the dye. Even though the photocatalytic tests were run in a quite short period, the aim of the screening was to compare activities and interesting results have been collected (Figure 4.14).

Turnover Numbers (TON) with respect to the cobaloxime concentration have been calculated and the major insight that comes out from that tests is that activity seems to be only dependent on the equatorial coordination sphere (Table 4.1). Looking in details, the TON of **Co1**, **Co2**, and **Co3** are comparable even though the complexes differ in the starting oxidation state and axial ligands, moreover the presence of the axial pyridine that is supposed to influence activity, is surprisingly irrelevant. The counterparts **Co4** and **Co5** that are the BF_2-bridged systems showed very limited or no activity and an intense blue coloration of the solution is observed during the irradiation tests. The diimine-dioxime **Co6** has an activity that is in between the other two equatorial systems. Thus the main statement that comes out from this test is a strong correlation between the equatorial coordination sphere and the efficiency, pointing out that maybe the real active catalytic species of **Co1**, **Co2**, and **Co3** is the same or at least that the axial ligands do not influence the catalytic cycle in the rate-determining step. The starting oxidation state seems to be irrelevant as well, since, apart from the first cycle, the real catalytic cycle probably passes through the same oxidation state intermediates.

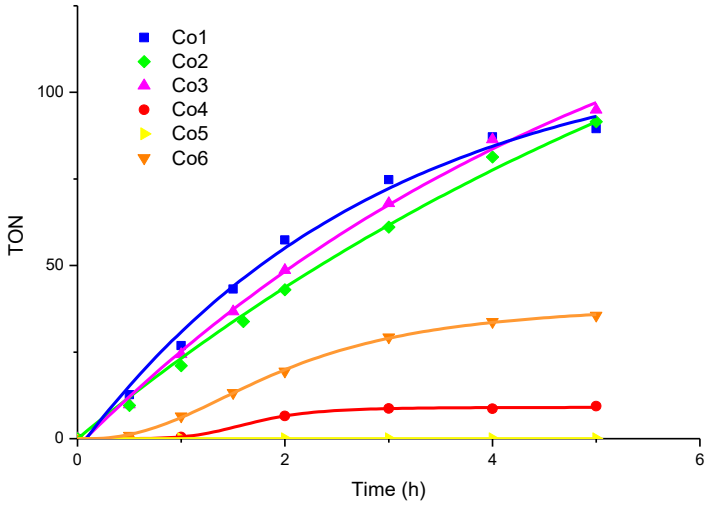

*Figure 4.14: Photocatalytic hydrogen production curves for cobaloximes **Co1-Co6** at pH 7.*

Table 4.1: TON values for 5 h of irradiation for the 6 complexes.

Complex	TON (5 h)
Co1	89
Co2	91
Co3	95
Co4	9
Co5	0
Co6	36

Further investigations have been done varying the pH conditions and the catalyst/sensitizer ratio, picking **Co6** as reference since its efficiency was in between the other ones. As it is reported in many articles, screening the pH of the medium is important to evaluate the efficiency of the system,[35,65] thus the pH was varied to pH 8 and 9 that are supposed to be better conditions for the use of TEOA. Results are illustrated in Figure 4.15 and TON values are reported in Table 4.2. The results

showed that pH 7 seems to be the best choice together with pH 8 that has probably the best starting efficiency having a very short induction period, as it can be seen from the shape of the curves in Figure 4.15 for the first irradiation times. After the first hour of irradiation the hydrogen produced at pH 8 is higher in amount compared to the pH 7 reaction mixture, but additional irradiation till 3 h showed a higher stability of the pH 7 mixture compared to the more basic one, while pH 9 is the lowest performing during the whole period. This is a good result since most of the catalysts for hydrogen production are tested and work well in slightly basic or acid conditions and the final goal of the water splitting system will need the integration of oxidation catalysts, thus the neutral condition will be the best choice even from the engineering point of view.

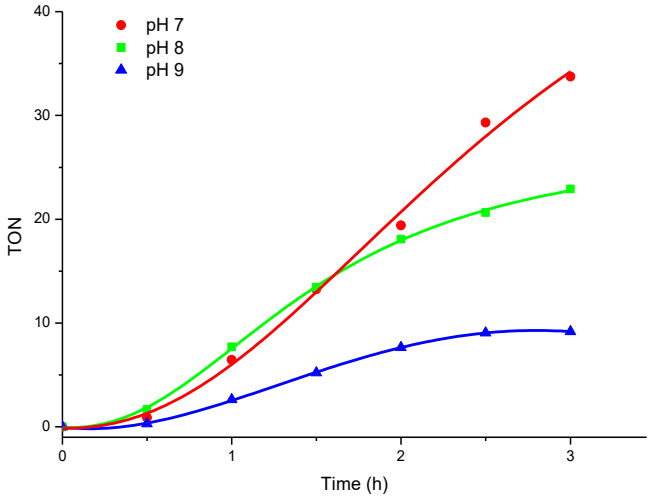

*Figure 4.15: Photocatalytic hydrogen production curves for **Co6** at various pH.*

*Table 4.2: TON values for **Co6** at different pH.*

Conditions	TON (3 h)
pH 7	34
pH 8	23
pH 9	9

A second kind of screening was performed in order to understand the optimal ratio between the photosensitizer and the catalyst concentrations. The ratio used in the other tests was 1:1 but ideally two molecules of eosin Y should be excited to have one molecule of catalyst performing a complete cycle, since the stoichiometry of the reaction is of 2 electrons. Anyway such an assumption is valid if the rates of electron injection and catalytic cycle are the same while generally the second one is rate determining in the whole process. Moreover such a stoichiometric assumption does not consider the electrons that could be transferred directly by TEOA when it is in the form of radical cation as it is known from decomposition pathways (see Figure 4.9). Thus the first modification has been the duplication of the amount of eosin Y in order to test the performances in case of stoichiometric amount of the components, but the activity has been found lower. A second test keeping the same ratio but half of the amount of total eosin Y and **Co6** has been performed to verify that the high amount of the dye in the second test was not interfering with the light harvesting efficiency. The total TON was found lower indicating that the best conditions were the starting ones. Finally the opposite ratio has been tested with double amount of catalyst compared to the photosensitizer and very low activity has been registered, probably because the amount of photo-generated electrons is not enough to bring all the cobalt centers to the most reduced species of the catalytic cycle.

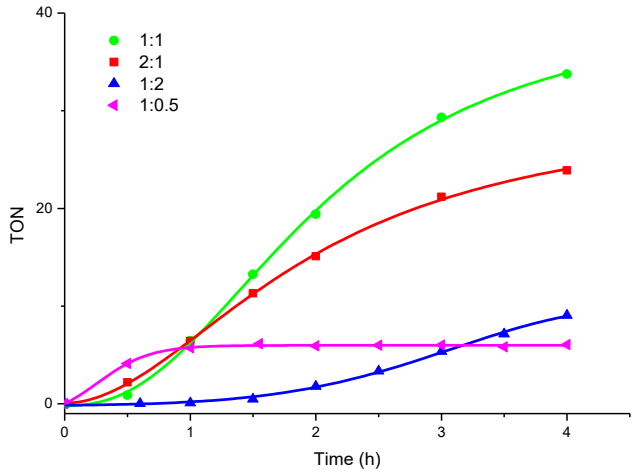

*Figure 4.16: Photocatalytic hydrogen production curves for **Co6** at various eosin Y/catalyst ratios.*

*Table 4.3: TON values for **Co6** at different photosensitizer/catalyst ratios.*

Eosin Y/catalyst ratio	TON (4 h)
1:1	34
2:1	24
1:0.5	6
1:2	9

Other two tests have been run on **Co6**: the first one aimed at seeing if it was possible to have hydrogen production under acidic conditions, so ascorbic acid was selected to replace TEOA (that is not active as sacrificial electron donor at acidic pH due to protonation), but no hydrogen evolution was measured at pH 4. The second test was performed by adding PPh_3 to the solution to see if it had some effect, as already illustrated in the literature,[52] on the stabilization of the Co(I) species that is supposed to be at the basis of the catalytic cycle. No hydrogen has been measured in these conditions and the color of solution was darkly blue[66] during all the experiment, probably hinting a very stable Co(I) species that is not protonated to go further in the catalytic cycle. As a matter of fact, the stabilization of the Co(I) intermediates by mean of phosphines is a known method in the literature.[52,67]

Conclusions

The efficiency tests allowed the evaluation of some trends in terms of molecular structure/activity. Even though the efficiency tests are not considering all the possible conditions, some general information could be outlined. The major consideration regards the activity role of the ligands of the coordination sphere. Equatorial plane seems to be fundamental in determining the efficiency in photocatalytic tests, with the H-bridged complexes being highly more active than the BF_2-bridged cobaloximes. The diimine-dioxime complex is in the middle in terms of efficiency as already reported in the literature. Such complexes are expected to be more stable than the H-bridged ones, but such an advantage has not been screened in these tests with short irradiation times and no characterization of the resulting solutions.[13] BF_2-bridged complexes have a strong blue coloration during all the

irradiation period hinting that protonation of the Co(I) species[66] could be the rate-determining step of the catalytic cycle, probably due to the different pKa of a BF_2-bridged compared to a H-bridged system. The axial ligands are found less effective in affecting activities, opening a series of questions, i.e. if axial ligands are kept in the coordination sphere during the whole catalytic cycle or if the same catalytic species could be envisaged for all the complexes with the same equatorial bridge. Moreover a little screen of the photocatalytic conditions has been done for the diimine-dioxime complex, since its activity is in between all the other catalysts. The pH screening pointed out that pH 7 is the best condition that is an interesting result compared to other tests where basic conditions are generally best performing. Neutral solution is the best choice for industrial application by far, thus confirming cobaloximes as promising candidates for protons reduction. Concerning photosensitizer/catalyst ratios the best test has been with 1:1 ratio even though an induction period in the curve is present for the first irradiation phase.

4.6 PHOTO-ACCUMULATION TESTS

4.6.1 Microseconds X-Rays Absorption Spectroscopy

Labile and reactive intermediates are difficult to be isolated with classical techniques, while time-resolved spectroscopy could give a help in studying transient states of catalytic cycles. Laser-initiated time-resolved X-rays absorption measurements are techniques in which the arrival time, related to the laser impulse, of all the photons and their energies can be measured, thus both structural and kinetic information might be collected. Since all the X-rays that strike the detector are revealed, the technique has high resolution, and more importantly lower power X-rays beams can be used so that the eventual damage of the sample is minimized. The peculiarities of this microseconds X-rays absorption technique is that the timescale of the measurements is raised from the picoseconds to the microseconds range. Compared to other time-resolved techniques in the optical or IR regions, X-ray absorption spectroscopies are element-specific and the XANES (X-rays near-edge structure) spectra could give information about the local arrangement around the metal center (shape of the signal) and its oxidation number (position in energy of the absorption edge and EXAFS that provides insights of the local structure around cobalt). The sample is in solution and it is forced to circulate in a reactor with a constant flux (some meters per second) and it is continually irradiated by pulses since there is no need to wait the decay of the excitation (it needs just to wait the refresh of the solution in the laser spot thanks to the motion of the liquid). This trick allows reduced experiment times and a reduction of the eventual damaging of the species because of the X-rays, since fresh solution is always irradiated. This technique has not only the right time range and appropriate resolution but a high sensitivity in electronic changes of the metal center (fundamental to study catalytic cycles in which the metal center changes oxidation state) and high selectivity towards the species even in high complicated matrix as the one needed for photocatalytic tests. Detailed information about the experimental apparatus and simulation instruments used to assist the experimental data are reported in the two papers by Smolentsev *et al.* where the technique is introduced and applied to the study of cobaloximes.[68,69]

The tested cobaloximes are **Co4** and **Co1**, the solution contained a ruthenium complex as photosensitizer and methyl viologen (MV^{2+}) as electron relay. In the experimental conditions, both Co(I) and Co(III) species could form, as illustrated by reactions 2), 3) and 4) in Figure 4.17, and other eventual deactivation species.

$$[Ru(bpy)_3]^{2+*} + MV^{2+} \longrightarrow [Ru(bpy)_3]^{3+} + MV^{+} \quad 1)$$

$$[Ru(bpy)_3]^{2+*} + Co(II) \longrightarrow [Ru(bpy)_3]^{3+} + Co(I) \quad 2)$$

$$MV^{+} + Co(II) \longrightarrow MV^{2+} + Co(I) \quad 3)$$

$$[Ru(bpy)_3]^{3+} + Co(II) \longrightarrow [Ru(bpy)_3]^{2+} + Co(III) \quad 4)$$

Figure 4.17: Possible electron transfers.

The aim of the experiment was to determine the number of species and their nature; the results showed no presence of Co(III) and of a single Co(I) species for the sample containing **Co4**. The graph in Figure 4.18 reports the obtained signal in parallel with the signal prior to irradiation (black curve).

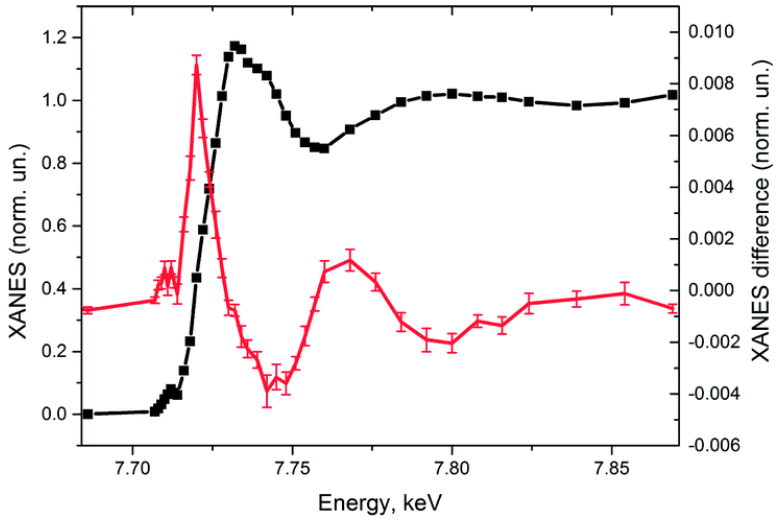

*Figure 4.18: Co K-edge XANES of the multi-component photocatalytic system with **Co4** catalyst in the ground state (black line, left scale) and transient X-ray absorption spectrum (red line, right scale) that corresponds to 10 µs time window after the laser pulse.*

The information that can be extrapolated from that graph is not only the oxidation number of the metal center (since in such a case the edge is at lower energies compared to the starting signal indicating a lower oxidation number), but also the modification of the coordination sphere of the intermediate. Indeed it is likely that the ligand distances to the metal center are different in the Co(I) species; the XRD studies of crystalline complexes or DFT vacuum simulation could give interesting results, but the behavior of the system in solution might be completely different,

especially with regards to the labile axial ligands. Thus simulations of the XANES spectra starting from the XRD and DFT data and modifying the Co-ligand distances in the hypothetical structure of the cobaloximes both in the +2 and +1 oxidation states have been run. The second article by Smolentsev *et al.*[69] focused on the comparison between cobaloximes with different coordination spheres, dealing with both the nature of the Co(I) intermediate transiently formed and the stability of the photo-accumulated species in the presence of TEOA. Concerning the results for the transiently-formed Co(I) species from **Co4** using a ruthenium sensitizer and methyl viologen as electron relay, the results confirmed the data previously reported[68] and the UV-Vis photo-accumulation spectra (illustrated in paragraph 4.6.2). But in the simulations of the experimental shape of the XANES spectra different results have been obtained compared to the previous studies: the coordination sphere in solution is still octahedral and not penta-coordinated[70] as identified by XRD for an analogous complex,[11] or tetra-coordinated[71] as indicated in other DFT simulations. There is a distortion of the structure in one axial acetonitrile molecule compared to the starting complex, while the other one is at the same distance in Co(I) as in starting Co(II), and the metal center is out of plane of about 0.08 Å.

In studying the **Co1** complex, different conditions were chosen, since TEOA was used as sacrificial electron donor and eosin Y replaced the ruthenium photosensitizer. The starting oxidation state of the metal center is now +3, thus in the first moments after laser irradiation a signal corresponding to Co(II) species can be collected; irradiating further, the Co(II) signal disappears and another signal becomes visible that is assigned to a Co(I) species, but quite different from the other one collected for **Co4**. The interpretation of this unforeseen XANES spectrum is not straightforward. The replacement of pyridine by TEOA or its decomposition side-products has been first ruled out: the interaction of TEOA and **Co4** complex exists (no pyridine is present) but without such a big difference in the XANES spectrum. The different behavior has thus been ascribed to a distinct reactivity of the Co(I) species; the H-bridged species has a cathodic shift of 500 mV[49] in the reduction potential of $Co^{II/I}$ and the corresponding Co(III)-H is supposed to be more hydridic at the ligand.[72] Therefore it is expected that the Co(I) species of **Co1** is highly reactive with protons and so it is the Co(III)-H species under these anhydrous conditions, it might undergo to a degradation pathway with hydride transfer to the ligand that brings to an inactive species. A feasible alternative interpretation is that the highly reactive species Co(I) could react with the radical cation of TEOA giving an inactive Co(III)-alkyl species further

photocatalytically reduced to form a Co(I)-alkyl species as already reported in the literature.[73]

In order to validate the results highlighted by X-rays absorption spectroscopic tests, UV/Vis photo-accumulation analyses have been performed trying to reproduce the same experimental conditions. These parallel analyses (illustrated in the next paragraph) come from the necessity of comparison of the data coming from a technique that is new in the field with a more widespread approach already reported in the literature for this class of complexes.

4.6.2 Photo-Accumulation Tests in Anhydrous Conditions

In situ UV/Vis spectroscopy has been largely employed for the identification of some metal complexes intermediates.[74,75] It is largely limited by the nature of the species under investigation, but if such key molecule exhibits an absorption in the UV/Vis range this spectroscopic method is quite simple, inexpensive, compared to other complicated techniques (such as the X-rays spectroscopy illustrated in paragraph 4.6.1), and largely diffused. Indeed in almost all the experimental laboratories, or at least departments, a UV/Vis spectrophotometer is available. As illustrated by many reports,[42,49,76,77] Co(I) species of cobaloximes are characterized by an intense blue peak with two components that has been theoretically assigned to a Co(I) state as supported by *ab initio* calculations.[78] The aim of this research has been the supporting of the X-Ray absorption spectroscopic studies, especially in the comparison of the two cobaloximes **Co1** and **Co4**. X-rays apparatus is quite complicated and expensive, with long waiting times to have a short time-slot at the instruments, and moreover it is a new technique applied to the field, thus a check with a well known apparatus is necessary.

Co(I) species forms in solution under photo-accumulation conditions; even though the used conditions should resemble as much as possible the ones used in the X-rays analysis, there are some limitations when passing to the UV/Vis spectroscopy. The first limitation is in the absorption maxima that can be revealed that should lie below 1, while the concentrations reported for the previous tests are in the order of 10^{-3} M that is too high to be analyzed through UV/Vis spectroscopy. Thus lower concentrations for the eosin Y samples have been chosen till 10^{-5} M. A second limitation is in the use of the electron relay, methyl viologen assumes a strong blue coloration upon reduction with a typical structured peak that would cover the eventual peak belonging to Co(I).[79] Some trials in making difference spectra between

a background composed of all the components apart from the cobaloxime and the real sample have been performed without a positive check, especially because the concentration of methyl viologen is high, in the order of 10^{-2} M and its peak covers all the visible range. So methyl viologen has been eliminated from the mixture but the result is that ruthenium dye $[Ru(bpy)_3](PF_6)_2$ is not able to directly transfer electrons to the cobalt complex under photo-excitation. Thus the sensitizer has been replaced by $[Ir(ppy)_2(bpy)](PF_6)$ that has been chosen because of its low absorption in the visible range so that the interference could be limited especially in the blue region. In the cases, in which the Ir complex was not reducing enough to reach Co(I) species, eosin Y has been selected. Eosin Y is a good photosensitizer, able to transfer electrons to almost all the cobaloximes catalysts, but it has been taken as last choice since it has a strong absorption band nearby the blue region (at around 520 nm with $\varepsilon > 10^5$ M $^{-1}$cm^{-1}) that could hamper the detected Co(I) peak.

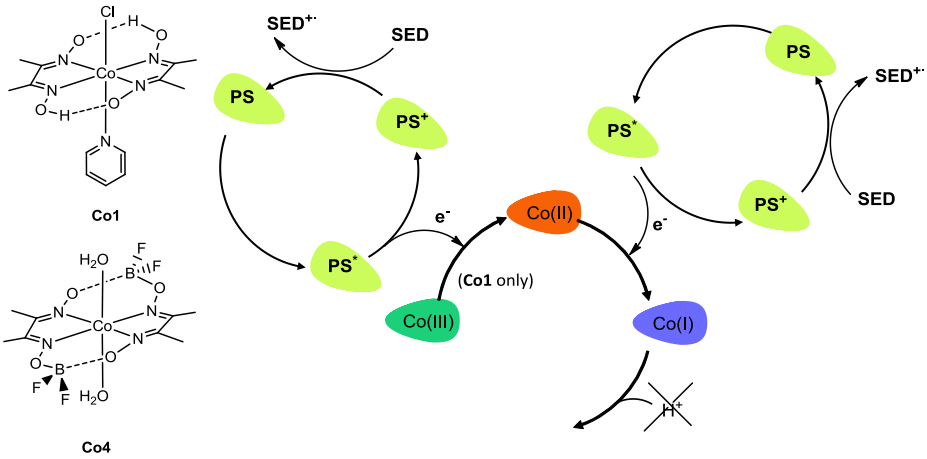

Figure 4.19: Photo-accumulation of Co(I) species is done avoiding the presence of protons, ***Co1*** *and* ***Co4*** *structures are illustrated on the left.*

Photo-accumulation of Co(I) is achieved with irradiation of the sample in the absence of protons that could form Co(III)-H species that is able to close the catalytic cycle (Figure 4.19). The absence of protons might be obtained with two alternative techniques: the use of anhydrous conditions and the use of aqueous media at very high pH.

The first tests have been run with Ir sensitizer and **Co4** as cobaloxime. The starting UV/Vis spectrum is, as expected, the sum of the two components from the Ir catalyst

and Co(II) species that are known to absorb around 400 nm, indicating that no fast degradation or rearrangement of the structures occurs without irradiation. The spectrum of the starting degassed solution is depicted in Figure 4.20. The solutions suffered from fast aging (observed when performing the starting spectrum) so they were freshly prepared for each test and checked.

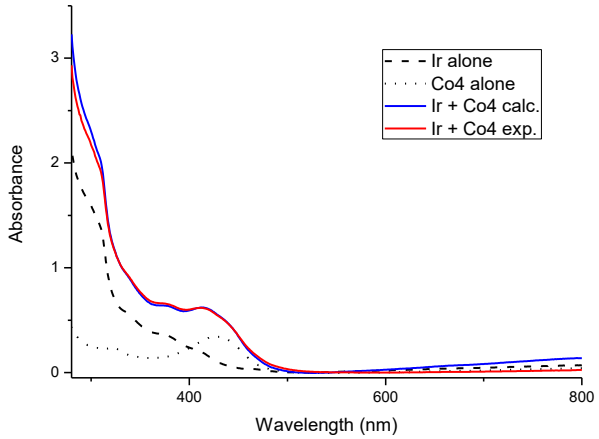

Figure 4.20: UV/Vis spectrum prior to irradiation.

Irradiation was performed with visible light (> 400 nm) and UV/Vis spectra were recorded for different irradiation times. The blue color that initially appears lasts for a few minutes so careful transfer of the cuvette from the light source holder to the spectrometer has to be done. The results were satisfactory for the first minutes of irradiation because the two components peak was observed with an increasing intensity as it was described elsewhere in the literature.[42,49,76,77] The results reported in the literature were rarely obtained through photo-accumulation reactions, but with electrochemical setup or chemical conditions: Norton *et al.* saw the blue color maintaining the **Co4** catalyst in an atmosphere of hydrogen at 70 atm;[76] Peter *et al.* isolated the Co(I) species running electrolysis, so giving electrons through an electrode;[11] Pantani *et al.* recorded UV/Vis spectra during spectro-electrochemical experiments;[80] Gray *et al.* isolated the blue coloration using Na amalgam as reducing agent;[77] Bakac *et al.* used $NaBH_4$ to chemically reduce the Co(II) catalyst;[81] while only Eisenberg *et al.* reported the photo-accumulation of Co(I) species in the presence of a photosensitizer and a sacrificial electron donor.[42,65]

The recorded spectra for early irradiation time of **Co4** are depicted in Figure 4.21: the graph represents the first 5 minutes of irradiation and the disappearance of the Co(II) species can be easily seen by the decrease of the peak at around 420 nm, while the blue peak with the two maxima at 556 nm and 627 nm increases.

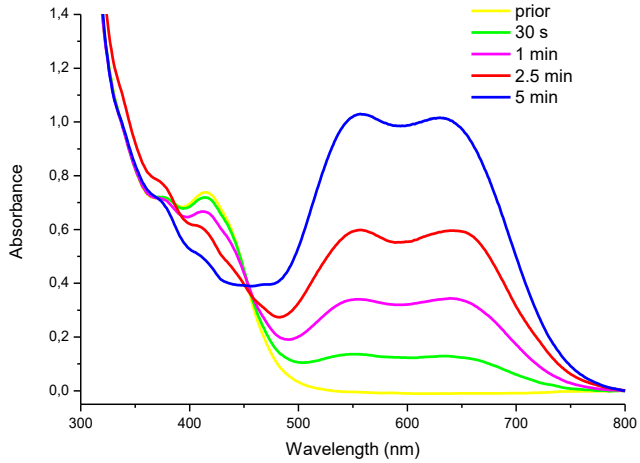

*Figure 4.21: Photo-accumulation spectra of **Co4** in the presence of Ir sensitizer for 0-5 min of irradiation.*

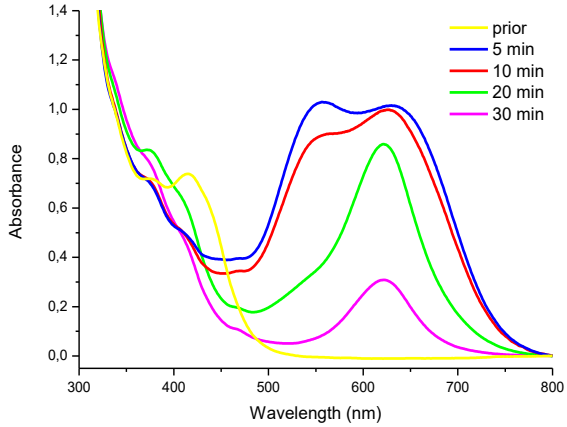

*Figure 4.22: Photo-accumulation spectra of **Co4** in the presence of Ir sensitizer for 5-30 min of irradiation.*

Larger irradiation times gave surprising results: the two components peak disappeared while a second blue peak with only one component arose in the irradiation ranges of 5 – 20 minutes. Further irradiation made the second peak disappear and the solution became colorless. Figure 4.22 shows the disappearance of the typical Co(I) peak and the appearance of the new peak still centered in the blue zone of the spectrum. The color difference is qualitatively appreciable even with unaided eye as can be seen from Figure 4.23.

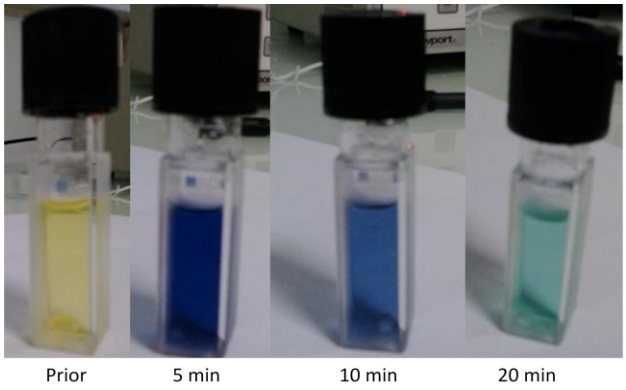

Figure 4.23: Different colors of the solution in the cuvette for different irradiation times.

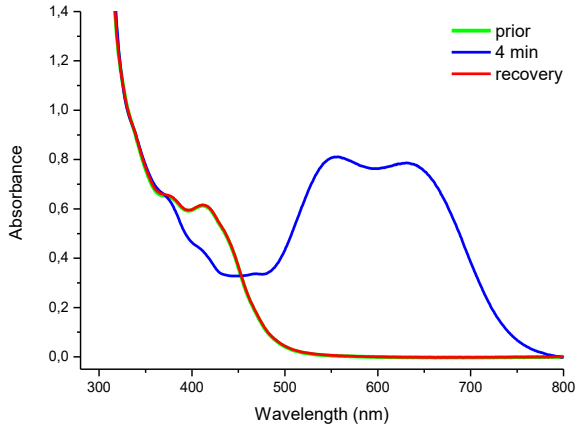

Figure 4.24: Prior to irradiation, 4 minutes of irradiation and recovery spectra.

We decided to investigate further the nature of the second blue intermediate that forms for long irradiation times by measuring the recovery spectra of the solutions

after irradiation. After having the UV/Vis spectrum measured, the cuvette was opened so that oxygen could regenerate the oxidized form of the catalyst. The results showed that with short irradiation times, typically within 5 minutes, the recovery spectrum resembles the starting one (Figure 4.24), while for longer irradiation time the peak belonging to Co(II) is not recovered (Figure 4.25).

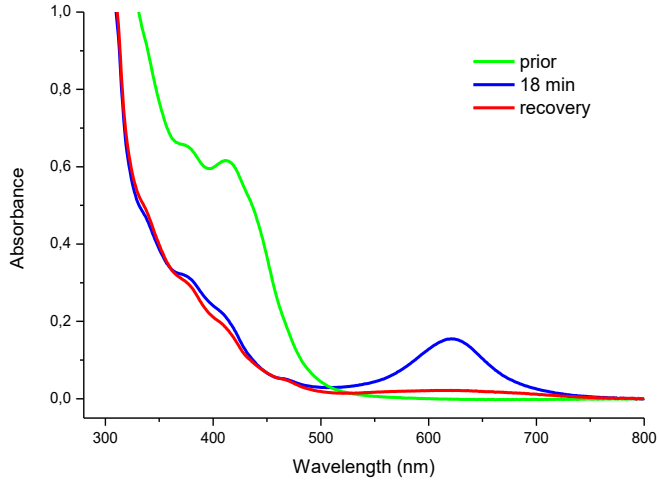

Figure 4.25: Prior to irradiation, 18 minutes of irradiation and recovery spectra.

That indicates that a further evolution of the catalyst takes place that might be the evolution towards a Co(III)-H or the formation of an inactive species. To discriminate between this two hypotheses, few drops of HCl 0.05 M have been added at the sample irradiated longer than 30 minutes and a peak corresponding to H_2 has been detected at the GC, hinting that the system is still catalytically active. We hypothesize that the second blue intermediate might be a protonated form of the Co(I) species different from Co(III)-H, in that way we are able to explain the blue coloration that should not be typical of the Co(III)-H species. Even though we worked in an anhydrous medium, the presence of protons could not be excluded because of the decomposition pathways of TEOA that produce electrons and protons (as illustrated in Figure 4.9).[33] During the research period, a paper by Norton *et al.* presented the same hypothesis on the basis of NMR spectroscopy.[76] In particular the protonation on the BF_2-bridged of their catalyst is discussed. In our case we might ascribe the intermediate to a Co(I) species with the same kind of protonation at the bridge as it is illustrated in Figure 4.26.

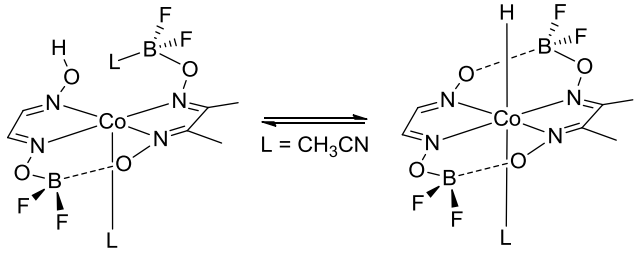

Figure 4.26: Protonation equilibrium hypothesized by Norton et al.[76]

Conversely Peters *et al.* investigated the putative Co(III)-H that is supposed to be formed by chemical reduction of a cobaloxime by $NaBH_4$ in the presence of the phosphine ligand as stabilizer and they found out that the assumed hydride species is likely to decompose and transform into a dimer between two Co(II) species $[P\text{-}Co(II)]_2$.[50] Such a dimer formation could not be excluded in our case as well, since Co(I) transiently forms as evidenced from the UV/Vis traces, probable protonation at the ligand then occurs, but no information about eventual Co(II) dimer formation could be deduced from this kind of study. Moreover the investigated cobaloxime by Peter *et al.* is a H-bridged species with Co(III) as starting oxidation number, so an early reduction step Co(III)→Co(II) must be included before getting the Co(I) species. They observed the immediate transformation of the Co(II) species into the dimer without going through the Co(I). The dimer has a one component peak at 570 nm at very low temperature while at rt the evidence is much lower. This is in contrast with our results, thus for our system the dimer formation could be considered less likely than the protonation equilibrium presented by Norton *et al*.

We then tried to repeat the same kind of experiment with **Co1** species to see if the presence of a different coordination sphere and pyridine as axial ligand changed the situation. Unfortunately in the case of the H-bridged systems, Ir sensitizer is reducing enough to transform Co(III) to Co(II) but not to obtain the Co(I) species. We decided to shift to eosin Y as sensitizer and we repeated the same experiments with **Co4** to see if there was an influence on the nature of the photosensitizer on the results. Unfortunately, eosin Y strongly interferes with the identification of the evolution of the blue peaks, because it partially covers the first component of the eventual peak and it decomposes during irradiation[33] so that the peak lowers in absorbance but shifts as well to lower wavelength (because of de-bromination of the eosin Y that brings to the ineffective fluorescein, as already reported in the literature).[33] Moreover the concentration used of eosin Y was 5 times lower than the Ir complex

one, and, to keep the same ratio between the photosensitizer and the catalyst, the cobalt concentration was lowered as well, thus the relative intensity of the eventual blue peak would be ⅕ of the other experiments. In addition an unforeseen influence of the presence of NBu_4PF_6 has been highlighted. The salt has been kept in the photo-accumulation tests since it was present in the X-ray investigations; in the case of the Ir complex the presence or not of the salt did not affect the evolution of the UV/Vis spectra but in the case of eosin Y a different behavior is verified. In the absence of the salt it seems that the "one component" blue peak is directly formed (Figure 4.27), while with the salt the two component blue peak is highly persistent and the degradation of eosin Y occurs faster than the eventual transition.

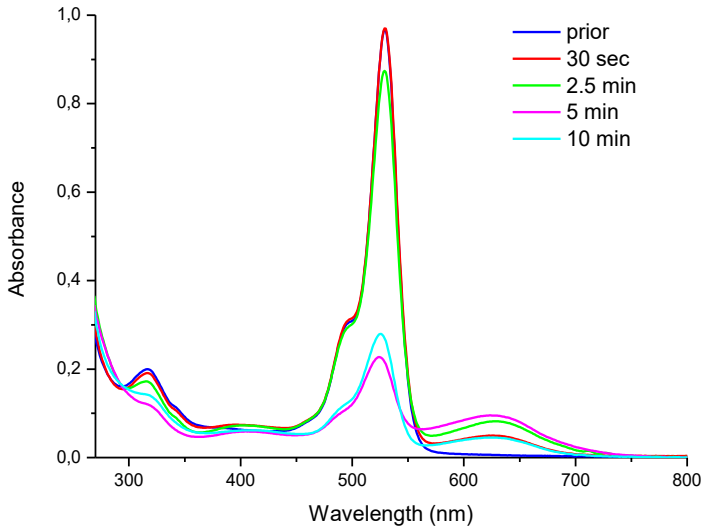

*Figure 4.27: Photo-accumulation spectra of **Co4** in the presence of eosin Y and in the absence of NBu_4PF_6.*

We could ascribe this behavior to the eventual availability of protons, in such a situation the salt could speed up or down the protonation step. Overlapping the traces of the one- and two-components peaks obtained with the iridium photosensitizer with the trace obtained in the absence of salt, it seems that the detected peak is more similar to the one-component peak than the other, even though the shape of the peaks are not exactly superimposable (Figure 4.28). The absence of the salt does not limit the availability of some protons, e.g. coming from

TEOA decomposition, while in the presence of the salt proton transfer is slowed down.

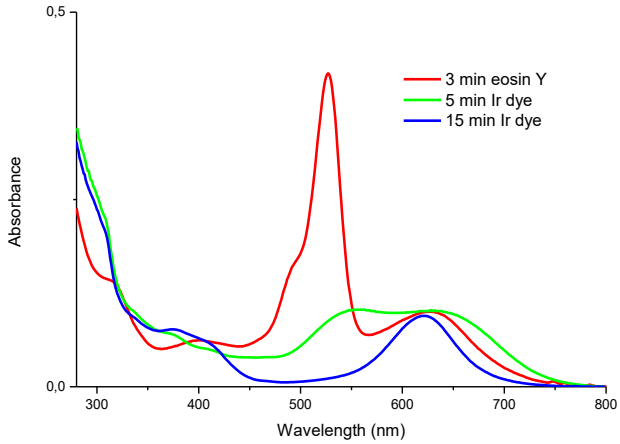

*Figure 4.28: Comparison between photo-accumulation spectra of **Co4** with Ir sensitizer and eosin Y in the absence of NBu_4PF_6.*

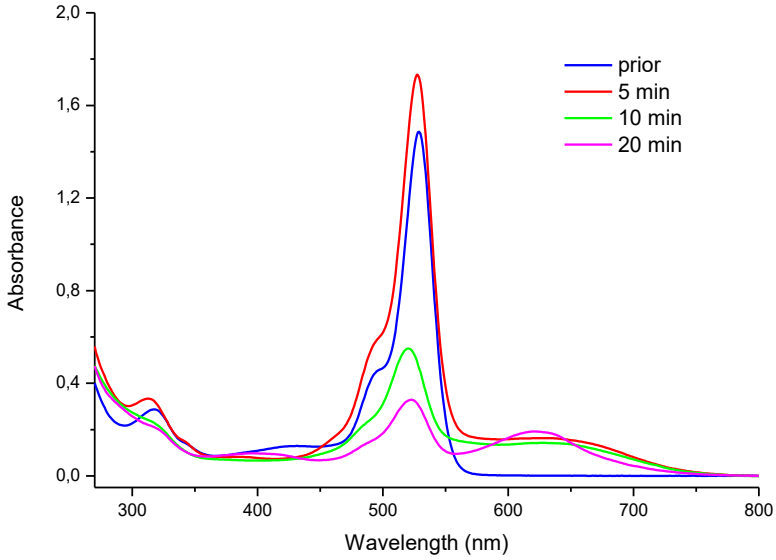

*Figure 4.29: Photo-accumulation spectra of **Co4** in the presence of eosin Y, NBu_4PF_6, and water.*

By adding 25 µL of water to the cuvette before irradiation, the transition from the two-components peak to the one-component signal is observed as could be seen in Figure 4.29. On the other hand these results are less clear than the other ones obtained with the iridium photosensitizer and the transition in this case could not be surely validated. Figure 4.30 reports the absorption traces in the case of the iridium photosensitizer in parallel with the eosin Y + salt + water sample and it is clear that the "20 min" trace is the corresponding one to the one-component band in the case of iridium photosensitizer; while it seems that for short irradiation times (5 min) the trace is similar to the two-components one in the case of iridium. The identification could not be completely confirmed since the eosin Y peak partially covers the first component of the investigated peak so it cannot be distinguished from the convolution of the sensitizer and the catalyst peaks.

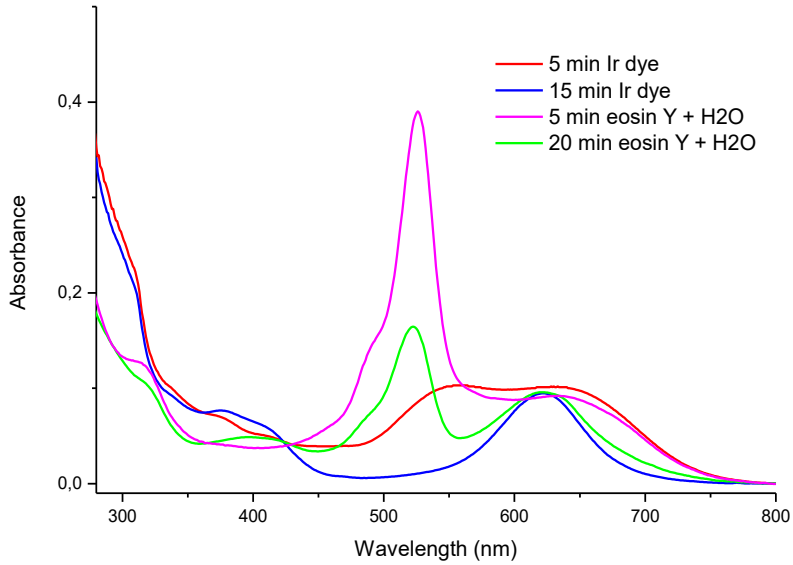

*Figure 4.30: Comparison between photo-accumulation spectra of **Co4** with Ir sensitizer and eosin Y in the presence of NBu_4PF_6 and water.*

Any attempt to repeat those experiments on **Co1** catalyst did not give any useful result, the transition Co(III) to Co(II) is seen around 420 nm (Figure 4.31), but the system seems unable to go further in reduction. A slight component in the blue region seems to be present for the sample containing 25% of water as solvent, but

the decomposition of eosin Y is too fast to irradiate further. We can see that the blue zone is not flat, but nothing can be said about the shape of the peak (Figure 4.31). Higher concentration of cobalt has been tested as well to see if the signal was a little bit higher in intensity but no change in the spectrum is seen, likely because the limitation in here is given by the eosin Y sensitizer.

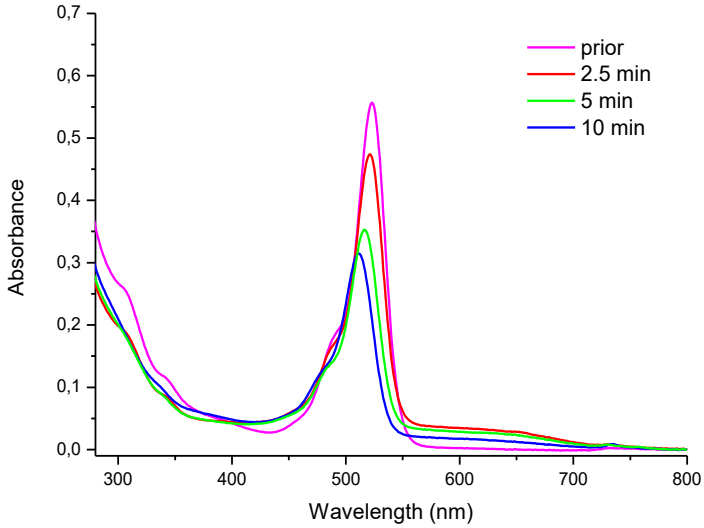

*Figure 4.31: Photo-accumulation spectra of **Co1** in the presence of eosin Y, NBu_4PF_6, and water.*

We decided to test **Co5** because its structure is in between the one of **Co1** and **Co4**, having pyridine as axial ligand but a BF_2-bridged system in the equatorial plane. In the case of **Co5** Ir photosensitizer could be used to reach Co(I) even though we expected a longer timescale for the spectrum evolution since the starting species is a Co(III), moreover a mixture of Co(III), Co(II) and Co(I) had to be forecasted so the manipulation of the spectrum was expected to be more complicated. We performed experiments in the same conditions as for **Co4** and Figure 4.32 represents the results we got for this sample. It is clear that the transition between the two blue peaks occurs in that case as well as for **Co4**. To highlight the presence of the one-component peak a spectra difference must be performed since not all the Co(II) is converted into Co(I) while some of it is already transformed into the other

intermediate. An asymmetrization of the peak is anyway quite visible and becomes clearer when spectra difference is run.

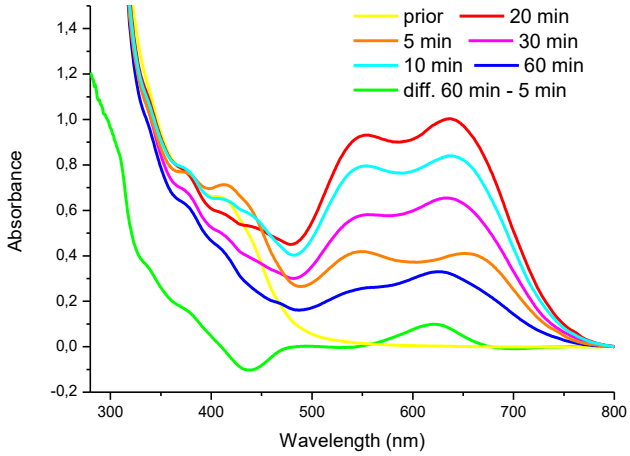

*Figure 4.32: Photo-accumulation spectra of **Co5** in the presence of Ir sensitizer.*

That confirmed our hypothesis of the protonation kinetics since the H-bridged systems are known to be protonated faster than the BF_2 couterparts.[70] This could be used to explain efficiency tests paragraph 4.5) as well in which the two BF_2 systems are the worst performing ones and they keep a strong blue coloration for all the experiment indicating that the protonation is slow enough to be seen even at the UV/Vis spectroscopy timescales. The results obtained by these experiments are interesting especially because of the insights of the transformation of the blue peak in the case of **Co4** and **Co5**, paving the way of new hypothesis in the Co(I) evolution to the Co(III)-H species. That is anyway a lateral result to the main objective of the research since the limitation in the use of the Ir sensitizer first and the eosin Y lately denied the possibility of comparing the behavior of all the catalysts.

Starting from the interesting results of photo-accumulation tests with **Co4** and Ir photosensitizer, a further investigation employing EPR spectroscopy has been done to evaluate the photo-conversion efficiency to Co(I) species. Co(II) has a d^7 configuration that tends to give high spin complexes with the use of non-macrocyclic ligands with five- or six-coordination number.[82] In the case of cobaloximes the behavior is instead more similar to macrocyclic systems where the stabilization

coming from the high ligand field is responsible for low spin complexes with an unpaired electron in the d_{z^2} orbital (S = ½). This unpaired electron results in a non-null spectrum at the EPR, as it has already been reported in the literature.[83,84,85] We registered the EPR spectrum of the same mixture used in the photo-accumulation experiments before irradiation, for 5 and 20 minutes that correspond to the observed color transitions (Figure 4.33). Due to the use of acetonitrile as solvent and the need of fast freezing of the solutions to avoid bleaching, the glass of the frozen solution is not perfect and the hyperfine structure of the spectrum is not available. **Co4** has been already investigated through EPR in acetonitrile solution and the main components of the X-band have been reproduced in our sample. The EPR spectrum of **Co4** was found to be strongly dependent on the solvent that is axially-coordinated to the Co center. The EPR spectrum clearly indicates two coordinated acetonitrile molecules resulting in the observation of the superhyperfine structure of the $g_{\|}$ because of the presence of axially linked ^{14}N (S = 1) coming from acetonitrile molecules, as it has already been reported in the literature.[83]

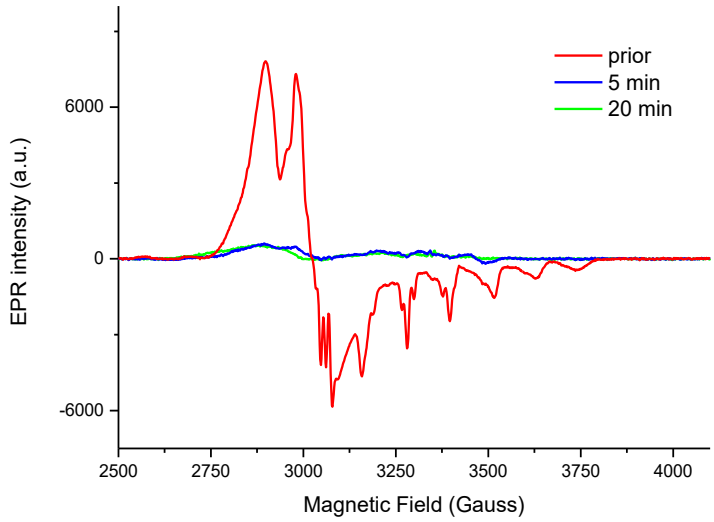

*Figure 4.33: EPR spectra for **Co4** before irradiation, after 5 and 20 minutes.*

Upon irradiation we assisted at the complete disappearance of the EPR signal coming from the Co(II) species and we interpreted such a modification as the complete conversion of the Co(II) into Co(I). The latter intermediate will have a d^8 configuration

that will have all paired electrons giving rise to a null EPR spectrum as observed. A total 95% suppression of the signal indicated that the photo-transformation is quantitative and very fast (in 5 minutes of irradiation). Concerning the other photo-accumulated species no other information could be extrapolated from the spectrum, apart that it is still an EPR silent species and, even though the spectrum is not perfectly overlapping on the 5 minutes one (indicating the presence of a second species), the differences are not so evident and could not be clearly caught from the background noise.

The EPR spectrum enabled us to analyze in a more accurate way the UV/Vis photo-accumulation experiments, since knowing that almost all the Co(II) is converted into Co(I), a rough estimation of the molar extinction coefficient of the Co(I) could be run. Applying the Lambert-Beer law to our system we got $\varepsilon = 4500\ M^{-1}cm^{-1}$ for the Co(II) signal (the maximum is at 415 nm) while for the two component peak ε are around $6000\ M^{-1}cm^{-1}$ for both the components.

4.6.3 Photo-Accumulation Tests In Aqueous Conditions

Owing to the limited applicability of the photo-accumulation tests in anhydrous conditions, we decided to test the second possibility to achieve photo-accumulation of Co(I) species by the use of aqueous solution at high pH. In this case the observation of the Co(I) species for all the catalysts has been possible. The presence of water partially suppresses the degradation pathway of eosin Y, even though a shift of the eosin Y peak is still observed, indicative for probable de-bromination reaction of the aromatic core leading to the inactive fluorescein.[33] No transition occurs in the case of **Co4** and **Co5** species corroborating the hypothesis of the Co(I) species protonated at the ligand, since under those conditions protons are present but their activity is low thanks to the high pH. While an eventual deactivation pathway (as firstly hypothesized) should be possible anyway, the absence of the transition could indicated that the previous results were not coming from a decomposition pathway. The results are shown in Figure 4.34 and it is immediately evident that the shape of the blue peak, meaning the relative intensity of the two components and their positions, is strongly dependent on the equatorial ligands and uninfluenced by the axial ligands, validating the results from the activity tests in hydrogen production. Wavelengths of the absorption maxima are listed in Table 4.4.

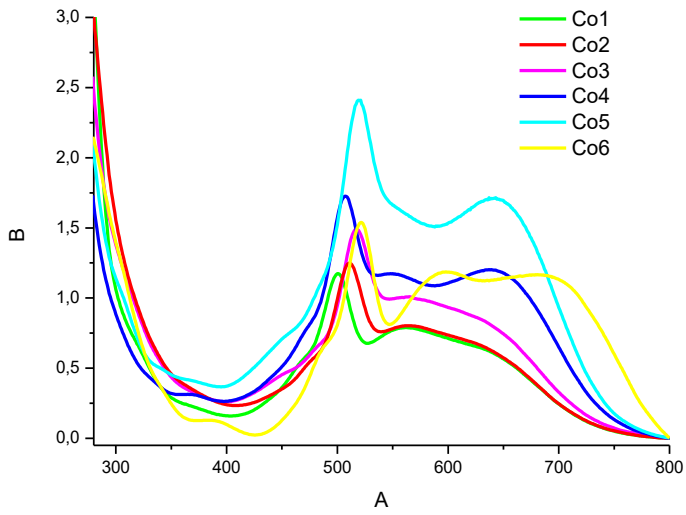

*Figure 4.34: Photo-accumulation for **Co1-Co6** at basic pH in mixed aqueous media for 10 min of irradiation.*

*Table 4.4: Wavelength maxima for **Co1-Co6** under photo-accumulation tests in aqueous media.*

Complex	λ_1 (nm)	λ_2 (nm)
Co1	563	~630
Co2	565	~630
Co3	564	~630
Co4	548	639
Co5	~550	639
Co6	600	679

4.7 CONCLUSIONS AND OUTLOOKS

A mini-library of cobaloximes catalysts has been screened in photocatalytic hydrogen production and in photo-accumulation tests. Differences amongst catalysts regarded the starting oxidation state, the kind of bridge at the macrocyclic equatorial ligand and the type of axial ligands. H-bridged catalysts are more efficient in hydrogen production under investigated conditions and their activities are comparable, suggesting a probable common catalytic pathway characterized by the same intermediates regardless from the starting complex. Diimine-dioxime cobalt catalyst showed an intermediate activity, while the BF_2-bridged systems were almost or completely inactive. The blue color of the solution could hint that the limiting step is the protonation at the BF_2-bridged that is known to be less easily protonated that the H-bridged counterpart. The limitation in stability for the hydrogen tests seems to be eosin Y since after 5 hours of irradiation the solutions are almost colorless and it is known that the photostability of eosin Y is limited. In further experiments, an alternative photosensitizer could be tested to screen the photo-durability of the cobalt catalysts. The photo-accumulation tests in basic aqueous media confirmed the photocatalytic tests since the position of the Co(I) absorption band is influenced more by the equatorial plane than the starting oxidation state or the axial ligands. It is known that when solvent molecules are present as axial ligands a spontaneous exchange takes place (e.g. water molecules with acetonitrile), but less investigation is known for the strength of the bond between pyridine or anionic ligands. Future investigations will necessarily need to elucidate the stability of the catalysts and molecular investigation on the real catalytic species should be done to clarify if the axial ligands are retained during the catalytic cycle or not. Photo-accumulation tests of **Co4** and **Co5** in anhydrous conditions pointed out unexpected results with the appearance of two hypothetical species that might be ascribed to Co(I). It is the first time that such transition has been seen and further investigation should clarify if the second intermediate is a further step in the catalytic cycle or if it is a bottomless side-reaction that brings to deactivation species. Moreover a proper photosensitizer should be found to see if the same behavior is reproducible for the H-bridged species or if it is peculiar of the BF_2-bridged systems. The EPR spectra highlight an almost quantitative photo-reduction of the cobalt catalyst to a Co(I) state. Further investigation in the protonation step must be done to see if the Co(III)-H formation is, as expected, mediated by the bridge or it occurs directly on the metal center. Since the Co(III)-H intermediate is forecast to be colorless in the Vis range an alternative *in situ* technique should be found to validate the microseconds X-ray experiments.

4.8 EXPERIMENTAL DETAILS

4.8.1 Photocatalytic Tests

Eosin Y (2',4',5',7'-Tetrabromofluorescein), acetonitrile, and triethanolamine (TEOA) were purchased from Sigma-Aldrich and used without further purification. The catalysts $[Co(dmgH)_2pyCl]$ (**Co1**),[86] $[Co(dmgH)_2(OH_2)_2]$ (**Co2**),[86] $[Co(dmgH)(dmgH_2)Cl_2]$ (**Co3**),[87] $[Co(dmgBF_2)_2(OH_2)_2]$ (**Co4**),[88] $[Co(dmgBF_2)_2(py)Cl]$ (**Co5**),[69] and $[Co(DO)(DOH)pnCl_2]$ (**Co6**)[89] were synthesized according to literature procedures.

Samples have been prepared in a Schlenk tube by solubilization of the catalyst (0.3 mM) and eosin Y (0.3 mM) in 5 mL of a mixture of acetonitrile and water (1:1) with 5% TEOA at pH 7. pH has been previously adjusted by adding diluted HCl to the TEOA solution. The Schlenk vial has been degassed with 10 minutes of nitrogen bubbling and irradiated with a 300 W Xenon lamp (Oriel, ozone free), operating at 280 W coupled with a water filter (Spectra Physics 6123NS liquid filter) and a UV filter (Spectra Physics 59472 UV cutoff filter >400 nm). The power intensity was set to 50 mW/cm^2. Every hour 50 µL of the gaseous phase above the photocatalytic solution has been injected in the gas chromatographer for hydrogen determination by mean of a gas tight syringe and the missing volume in the reactor has been replaced with 50 µL of nitrogen.

Hydrogen evolution was monitored with a Perkin-Elmer Clarus 500 gas chromatographer equipped with a porapack Q 80/100 column (6' 1/8") thermostated at 40 °C and a TCD detector thermostated at 100 °C.

4.8.2 Photo-accumulation tests

$Ir(ppy)_2(bpy)](PF_6)$ has been synthesized according to literature procedure.[90] All the other chemicals have been purchased or synthesized as illustrated in paragraph 4.8.1. NBu_4PF_6 was purchased from Sigma-Aldrich. Acetonitrile was purchased from Sigma-Aldrich, distillated and stored over activated molecular sieves for experiments in anhydrous conditions.

The *in situ* UV-Vis experiments consist in the measurement of UV-Vis absorption spectra with different photo-accumulation times. Samples have been irradiated with a 300 W Xenon lamp (Oriel, ozone free), operating at 280 W coupled with a water filter (Spectra Physics 6123NS liquid filter) and a UV filter (Spectra Physics 59472 UV cutoff filter >400 nm). The power intensity was set to 50 mW/cm^2. Different times of

irradiation have been set and then UV-visible spectra have been recorded with a Agilent Cary 60 UV-Vis Spectrophotometer.

For the anhydrous photo-accumulation tests with $[Ir(ppy)_2(bpy)](PF_6)$, the dye (0.08 mM) is dissolved together with $[Co(dmgBF_2)_2(OH_2)_2]$ (0.16 mM), or $[Co(dmgBF_2)_2pyCl]$ (0.16 mM), or $[Co(dmgH)_2pyCl]$ (0.16 mM) in acetonitrile with 5% of TEOA. The solutions have been degassed with 5 minutes of nitrogen bubbling before performing the experiments.

For the anhydrous photo-accumulation tests with eosin Y, the dye (0.016 mM) is solubilized together with $[Co(dmgBF_2)_2(OH_2)_2]$ (0.032 mM), or $[Co(dmgBF_2)_2pyCl]$ (0.032 mM), in acetonitrile with 5% of TEOA. Water as been added according to the test conditions and the solutions have been degassed with 5 minutes of nitrogen bubbling before performing the experiments.

For the aqueous photo-accumulation tests eosin Y (0.0125 mM) with the corresponding cobaloxime (0.25 mM) were solubilized in a solvent mixture composed of acetonitrile and water with 1.25% of TEOA. pH was adjusted to 13 by addition of a diluted solution of NaOH, irradiation for 10 minutes was performed for all the samples before analyzing at UV/Vis spectrophotometer.

4.8.3 EPR

$[Ir(ppy)_2(bpy)](PF_6)$ (0.08 mM), $[Co(dmgBF_2)_2(OH_2)_2]$ (0.16 mM), were solubilized in acetonitrile and TEOA 5% in the same way as for the photo-accumulation tests in dry solutions, but irradiation was performed in ERP tubes. The degassed solution was transferred in the tubes in a glove box, and after irradiation all the samples were frozen with liquid nitrogen. Data (X-band) were collected at 25 K, in a Bruker EMX spectrometer equipped with a Oxford ESR 910 cryostat for low temperature studies. The microwave frequency was calibrated with a frequency counter and the magnetic field with an NMR gaussmeter.

4.9 BIBLIOGRAPHY

1. T. R. Cook, D. K. Dogutan, S. Y. Reece, Y. Surendranath, T. S. Teets, D. G. Nocera, *Chem. Rev*., **2010**, *110*, 6474.
2. J. C. Fontecilla-Camps, A. Volbeda, C. Cavazza, Y. Nicolet, *Chem. Rev.*, **2007**, *107*, 4273.
3. E. Bouwman, J. Reedijk, *Chem. Coord. Rev.*, **2005**, *249*, 1555.
4. F. Gloaguen, T. B. Rauchfuss, *Chem. Soc. Rev.*, **2009**, *38*, 100.
5. C. Tard, C. J. Pickett, *Chem. Rev.*, **2009**, *109*, 2245.
6. S. Canaguier, V. Artero, M. Fontecave, *Dalton Trans.*, **2008**, 315.
7. M. L. Helm, M. P. Stewart, R. M. Bullock, M. R. DuBois, D. L. DuBois, *Science*, **2011**, *333*, 863.
8. V. Artero, M. Chavarot-Kerlidou, M. Fontecave, *Angew. Chem. Int. Ed.*, **2011**, *50*, 7238.
9. W. T. Eckenhoff, R. Eisenberg, *Dalton Trans.*, **2012**, *41*, 13004.
10. W. T. Eckenhoff, W. R. McNamara, P. Du, R. Eisenberg, *Biochim. Biophys. Acta*, **2013**, *1827*, 958.
11. X. Hu, B. S. Brunschwig, J. C. Peters, *J. Am. Chem. Soc.*, **2007**, *129*, 8988.
12. R. M. Kellett, T. G. Spiro, *Inorg. Chem.*, **1985**, *24*, 2373.
13. N. Kaeffer, M. Chavarot-Kerlidou, V. Artero, *Acc. Chem. Res.*, **2015**, *48*, 1286.
14. N. Queyriaux, R. T. Jane, J. Massin, V. Artero, M. Chavarot-Kerlidou, *Coord. Chem. Rev.*, **2015**, *304–305*, 3.
15. P.V. Bernhardt, L. A. Jones, *Inorg. Chem.*, **1999**, *38*, 5086.
16. O. Pantani, S: Naskar, R. Guillot, P. Millet, E. Anxolabéhère-Mallart, A. Aukauloo, *Angew. Chem. Int. Ed.,* **2008**, *47*, 9948.
17. E. Anxolabéhère-Mallart, C. Costentin, M. Fournier, S. Nowak, R. Marc, J.-M. Savéant, *J. Am. Chem. Soc.*, **2012**, *134*, 6104.
18. M. Rudolph, *J. Electroanal. Chem.*, **2003**, *543*, 23.
19. M. Rudolph, *J. Comput. Chem.*, **2005**, *26*, 1193.
20. V. Fourmond, P.-A. Jacques, M. Fontecave, V. Artero, *Inorg. Chem.*, **2010**, *49*, 10338.
21. A. Le Goff, V. Artero, B. Jousselme, P. D. Tran, N. Guillet, R. Metaye, A. Fihri, S. Palacin, M. Fontecave, *Science*, **2009**, *326*, 1384.

22 P. D. Tran, A. Le Goff, J. Heidkamp, B. Jousselme, N. Guillet, S. Palacin, H. Dau, M. Fontecave, V. Artero, *Angew. Chem.*, **2011**, *123*, 1407; *Angew. Chem. Int. Ed.*, **2011**, *50*, 1371.

23. E. S. Andreiadis, P.-A. Jacques, P. D. Tran, A. Leyris, M. Chavarot-Kerlidou, B. Jousselme, M. Matheron, J. Pécaut, S. Palacin, M. Fontecave, V. Artero, *Nature Chem.*, **2012**, *5*, 48.
24. J. Hawecker, J. M. Lehn, R. Ziessel, *Nouv. J. Chim.*, **1983**, *7*, 271.

25. J. M. Lehn, R. Ziessel, *Proc. Natl. Acad. Sci. USA*, **1982**, *79*, 701.
26. C. V. Krishnan, N. Sutin, *J. Am. Chem. Soc.*, **1981**, *103*, 2141.
27. A. Juris, V. Balzani, F. Barigelletti, S. Campagna, P. Belser, A. Vonzelewsky, *Coord. Chem. Rev.* **1988**, *84*, 85.
28. J. I. Goldsmith, W. R. Hudson, M. S. Lowry, T. H. Anderson, S. Bernhard, *J. Am. Chem. Soc.*, **2005**, *127*, 7502.
29. P. Du, J. Schneider, P. Jarosz, R. Eisenberg, *J. Am. Chem. Soc.*, **2006**, *128*, 7726.
30. P. Du, J. Schneider, P. Jarosz, J. Zhang, W. W. Brennessel, R. Eisenberg, *J. Phys. Chem. B*, **2007**, *111*, 6887.
31. B. Probs, C. Kolano, P. Hamm, R. Alberto, *Inorg. Chem.*, **2009**, *48*, 1836.
32. B. Probs, M. Guttentag, A. Rodenberg, P. Hamm, R. Alberto, *Inorg. Chem.*, **2011**, *50*, 3404.
33. T. Lazarides, T. McCormick, P. Du, G. Luo, B. Lindley, R. Eisenberg, *J. Am. Chem. Soc.*, **2009**, *131*, 9192.
34. M. Yin, S. Ma, C. Wu, Y. Fan, *RSC Adv*., **2015**, *5*, 1852.
35. P. Zhang, M. Wang, J. Dong, X. Li, F. Wang, L. Wu, L. Sun, *J. Phys. Chem. C*, **2010**, *114*, 15868.
36. T. M. McCormick, B. D. Calitree, A. Orchard, N. D. Kraut, F. V. Bright, M. R. Detty, R. Eisenberg, *J. Am. Chem. Soc,* **2010**, *132*, 15480.
37. C. Creutz, N. Sutin, *Coord. Chem. Rev.,* **1985**, *64*, 321.
38. B. Probst, A. Rodenberg, M. Guttentag, P. Hamm, R. Alberto, *Inorg. Chem.*, **2010**, *49*, 6453.
39. P. J. DeLaive, T. K. Foreman, C. Giannotti, D. G. Whitten, *J. Am. Chem. Soc.*, **1980**, *102*, 5627.
40. S.F. Chan, M. Chou, C. Creutz, T. Matsubara, N. Sutin, *J. Am. Chem. Soc.*, **1981**, *103*, 369.
41. J. F. Kennedy, C. A. White, F. P. Warner, L. L. Lloyd, Z. S. Rivera *J. Micronut. Anal.,* **1989**, 5, 91.
42. P. Du, J. Schneider, G. Luo, W. W. Brennessel, R. Eisenberg, *Inorg. Chem.*, **2009**, *48*, 4952.
43. J. L. Dempsey, B. S. Brunschwig, J. R. Winkler, H. B. Gray, *Acc. Chem. Res*., **2009**, *42*, 1995.
44. J. L. Dempsey, J. R. Winkler, H. B. Gray, *J. Am. Chem. Soc.*, **2010**, *132*, 1060.
45. I. Bhugun, D. Lexa, J. M. Saveant, , *J. Am. Chem. Soc.*, **1996**, *118*, 3982.
46. M. Besora, A. Lledó, F. Maseras, Chem. Soc. Rev., 2009, 38, 957.
47. T.-H. Chao, J. H. Esperson, *J. Am. Chem. Soc.*, **1978**, *100*, 129.
48. P.A. Jacques, V. Artero, J. Pecaut, M. Fontecave, *Proc. Natl. Acad. Sci. USA,* **2009**, *106*, 20627.

49. C. Baffert, V. Artero, M. Fontecave, *Inorg. Chem.*, **2007**, *46*, 1817.
50. D. C. Lacy, G. M. Roberts, J C. Peters, *J. Am. Chem. Soc.*, **2015**, *137*, 4860.
51. G. N. Schrauzer, R. J. Holland, *J. Am. Chem. Soc*., **1971**, *93*, 1505.
52. P. Zhang, P. A. Jacques, M. Chavarot-Kerlidou, M. Wang, L. Sun, M. Fontecave, V. Artero, *Inorg. Chem.*, **2012**, *51*, 2115.
53. M. Razavet, V. Artero, M. Fontecave, *Inorg. Chem.*, **2005**, *44*, 4786.
54. J. Wang, C. Li, Q. Zhou, W. Wang, Y. Hou, B. Zhang, X. Wang, *Dalton Trans*., **2015**, *44*, 17704.
55. V. Artero, M. Fontecave, *Coord. Chem. Rev.*, **2005**, *249*, 1518.
56. L. A. Berben, J. C. Peters, *Chem. Commun.*, **2010**, *46*, 398.
57. T. M. McCormick, Z. Han, D. J. Weinberg, W. W. Brennessel, P. L. Holland, R. Eisenberg, *Inorg. Chem*., **2011**, *50*, 10660.
58. A. Fihri, V. Artero, M. Razavet, C. Baffert, W. Leil, M. Fontecave, *Angew. Chem. Int. Ed.*, **2008**, *47*, 564.
59. A. Fihri, V. Artero, A. Pereira, M. Fontecave, *Dalton Trans.*, **2008**, 5567.
60. K. L. Mulfort, D. M. Tiede, *J. Phys. Chem. B,* **2010**, *114*, 14572.
61. P. Zhang, M. Wang, C. Li, X. Li, J. Dong, L. Sun, *Chem. Commun.*, **2010**, *46*, 8806.
62. C. Li, M. Wang, J. X. Pan, P. Zhang, R. Zhang, L. C. Sun, *J. Organomet. Chem.*, **2009**, *694*, 2814.
63. S. Jasimuddin, T. Yamada, K. Fukuju, J. Otsuki, K. Sakai, *Chem. Commun.*, **2010**, *39*, 8466.
64. Z.-Y. Wang, H. Rao, M.-F. Deng, Y.-T. Fan, H.-W- Hou, *Phys. Chem. Chem. Phys.*, **2013**, *15*, 16665.
65. P. Du, K. Knowles, R. Eisenberg, *J. Am. Chem. Soc.,* **2008**, *130*, 12576.
66. Co(I) species are characterized by an intense blue color.
67. G. Li, D. P. Estes, J. R. Norton, S. Ruccolo, A. Sattler, W. Sattler, *Inorg. Chem.*, **2014**, *53*, 10743.
68. G. Smolentsev, A. Guda, M., Janousch, C. Frieh, G. Jud, F. Zamponi, M. Chavarot-Kerlidou, V. Artero, J. A. van Bokhoven, M. Nachtegaal, *Faraday Discuss.*, **2014**, *171*, 259.
69. G. Smolentsev, B. Cecconi, A. Guda, M. Chavarot-Kerlidou, J. A. van Bokhoven, M. Nachtegaal, V. Artero, *Chem. Eur. J.*, **2015**, *21*, 15158.
70. B. H. Solis, S. Hammes-Schiffer, *Inorg. Chem.*, **2011**, *50*, 11252.
71. J. T. Muckermann, E. Fujita, *Chem. Commun.*, **2001**, *47*, 12456.
72. B. H. Solis, Y. Yu, S. Hammer-Schiffer, *Inorg. Chem.*, **2013**, *52*, 6994.
73. A. Rodenberg, M. Orazietti, B. Probst, C. Bachmann, R. Alberto, K. K. Baldridge, P. Hamm, *Inorg. Chem.*, **2014**, *53*, 646.

74. C. Fischer, T. Beweries, A. Preetz, H.-J. Drexler, W. Baumann, S. Peitz, U. Rosenthal, D. Heller, *Catal. Today*, **2010**, *155*, 282.
75. M. Dooshaye, "Spectroscopic Characterization of the Water-Oxidation Intermediates in the Ru-Based Catalysts for Artificial Photosynthesis" *Open Access Dissertations*, **2013**, Paper 101.
76. D. P. Estes, D. C. Grills, J. R. Norton, *J. Am. Chem. Soc.*, **2014**, *136*, 17362.
77. J. L. Dempsey, J. R. Winkler, H. B. Gray, *J. Am. Chem. Soc.*, **2010**, *132*, 16774.
78. A. Bhattacharjee, M. Chavarot-Kerlidou, J. L. Dempsey, H. B. Gray, E. Fujita, J. T. Muckerman, M. Fontecave, V. Artero, G. M. Arantes, M. J. Field, *ChemPhysChem,* **2014**, *15*, 2951.
79. T. M. Bockman, J. K. Kochi*, J. Org. Chem.*, **1990**, *55*, 4127.
80. O. Pantani, E. Anxolabéhère-Mallart, A. Aukauloo, P . Millet, *Electrochem. Commun.*, **2007**, *9*, 54.
81. E. Szajna-Fuller, A. Bakac, *Eur. J. Inorg. Chem.*, **2010**, 2488.
82. G. W. Roberts, S. C. Cummings, J. A. Cunningham, *Inorg. Chem.*, **1976**, *12*, 2503.
83. A. Bakac, M. E. Brynildson, J. H. Espenson, *Inorg. Chem.*, **1986**, *25*, 4108.
84. J. Niklas, K. L. Madis, R. R. Rakhimov, K. L. Mulfort, D. M. Tiede, O. G. Poluektov, *J. Phys. Chem. B*, **2012**, *116*, 2943.
85. M. Bacchi, G. Berggren, J. Niklas, E. Veinberg, M. W. Mara, M. L. Shelby, O. K. Poluektov, L. X. Chen, D. M. Tiede, C. Cavazza, M. J. Field, M. Fontecave, V. Artero, *Inorg. Chem.*, **2014**, *53*, 8071.
86. G. N. Schrauzer, G. W. Parshall, E. R. Wonchoba, *Inorg. Synth.* (Ed.: W.L. Jolly), John Wiley & Sons, Inc., **1968**, *11*, 61.
87. W. C. Trogler, R. C. Stewart, L. A. Epps, L. G. Marzilli, *Inorg. Chem.*, **1974**, *13*, 1564.
88. A. Bakac, J. H. Espenson, *J. Am. Chem. Soc.* **1984**, *106*, 5197.
89. G. Costa, G. Mestroni, E. de Savorgnani, *Inorg. Chim. Acta*, **1969**, *3*, 323.
90. M. S. Lowry, W. R. Hudson, R. A. Pascal, S. Bernhard, *J. Am. Chem. Soc.,* **2004**, *126*, 14129.

ANNEXES: LIST OF ABBREVIATIONS

AcOEt Ethyl Acetate

AcOH Acetic acid

APCE Absorbed Photon To Current Efficiency

AQY Apparent Quantum Yield

BET Brunauer-Emmett-Teller Theory

BJH Barrett-Joyner-Halenda Analysis

bpy bipyridyl

CB Conduction Band

CDCA Chenodeoxycholic Acid

CV Cyclic Voltammetry

C_μ Chemical Capacitance

DME Dimethoxyethane

DMF N-N-Dimethylformamide

DMSO Dimethylsulfoxide

DMTMM 4-(4,6-Dimethoxy-1,3,5-Triazin-2-Yl)-4-Methylmorpholinium Chloride

dmg dimethylglyoxymate

dpg diphenylglyoxymate

dppf (diphenylphosphino)Ferrocene

DPV Differential Pulse Voltammetry

DSSC Dye-Sensitized Solar Cells

EDOT 3,4-Ethylenedioxythiophene

EDTA Ethylenediaminetetraacetic Acid

EIS Electrochemical Impedance Spectroscopy

ff Fill Factor

FTO Fluorine-Doped Tin Oxide

HOMO Highest Occupied Molecular Orbital

ICT Intramolecular Charge Transfer

IPCE Incident Photon To Current Efficiency

IQY Internal Quantum Yield

J_{sc} Short-Circuit Photocurrent

LFE Light-To-Fuel Efficiency

LH Light Harvesting Complex

LHE Light Harvesting Efficiency

LMCT Ligand To Metal Charge Transfer

LUMO Lowest Unoccupied Molecular Orbital

MeOH Metanol

MLCT Metal To Ligand Charge Transfer

MV Methyl Viologen

NaOAc Sodium Acetate

NBS N-Bromosuccinimide

NHE Normal Hydrogen Electrode

***n*BuLi** Normal-Butyllithium

NIR Near-Infrared

NMM N-Methylmorpholine

OTs Tosylate

PE Petroleum Ether

P_{in} Power Of Incident Light

PS Photosensitizer

PSC Perovskite Solar Cells

PTZ Phenothiazine

PXRD X-Ray Diffraction

RC Reaction Centre

R_{rec} Recombination Resistance

SED Sacrificial Electron Donor

STH Solar-To-Hydrogen Efficiency

$TBAClO_4$ Tetrabutylammonium Perchlorate

TEG Tris(Ethylene Glycol) Monomethyl Ether Group

TEM Transmission Electron Microscopy

TEA Triethylamine

TEOA Triethanolamine

THF Tetrahydrofuran

THP Tetrahydropyrane

TOF Turnover Frequency

TON Turnover Number

TPA Triphenylamine

VB Valence Band

XANES X-Rays Near-Edge Structure

V_{oc} Open-Circuit Voltage

ε Molar Extinction Coefficient

λ Wavelength

τ_n Electron Lifetime

ANNEXES: CATALYTIC CYCLES

SUZUKI-MIYAURA CROSS COUPLING - MECHANISM

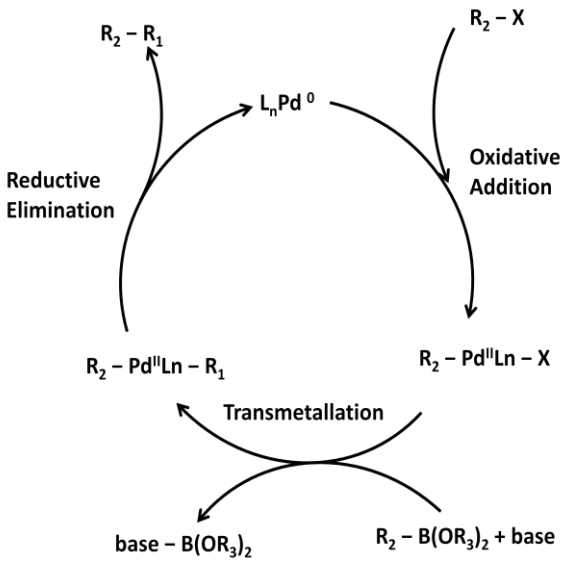

CUAAC COPPER CATALYZED COUPLING (CLICK CHEMISTRY) – MECHANISM